UNIVERSITAT DE BARCELONA

Modeling Neurofibromatosis type1 neurofibroma composition and formation

Helena Mazuelas Gallego

Modeling Neurofibromatosis type 1 neurofibroma composition and formation

Memòria presentada per

Helena Mazuelas Gallego

per optar al grau de

Doctora per la Universitat de Barcelona

Programa de Genètica

Tesi realitzada a l'Institut d'Investigació Germans Trias i Pujol

sota la direcció de la Dra. **Meritxell Carrió Llach** i el Dr. **Eduard Serra Arenas**

i tutoritzada pel Dr. Daniel Raúl Grinberg Vaisman

Dra. Meritxell Carrió Llach

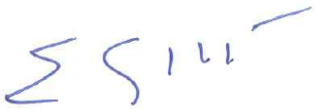

Dr. Eduard Serra Arenas

Dr. Daniel Grinberg Vaisman

Helena Mazuelas Gallego

Barcelona 2020

A mis padres

Acknowledgments

I ara que això ja s'acaba només queda una cosa pendent: agrair. Agrair a tota la gent que d'una manera o d'una altra ha contribuït a que aquesta tesi s'hagi pogut materialitzar.

Primer de tot vull agrair als meus directors: Dra. Meritxell Carrió i Dr. Eduard Serra. Gràcies Edu per donar-me l'oportunitat de quedar-me al teu laboratori a fer aquesta tesi, per ensenyar-me, per corregir-me cada paraula que he escrit durant tots aquests anys. He après molt. Gràcies! I gràcies Meri per tot el teu suport científic i moral, pel teu optimisme, per les teves paraules "dona de poca fe" quan jo no les tenia totes amb algun experiment i per ajudar-me a materialitzar algunes de les tantíssimes idees de l'Edu (que en té moltes), però sempre tocant de peus a terra. Gràcies als dos! Ha estat un gran plaer que m'hagueu co-dirigit la tesis.

Segon, vull agrair a tothom del laboratori. Aquesta feina no hagués estat possible sense la implicació més directa, o menys, de molta gent. Vull donar les gràcies explícitament a la Míriam: per la teva implicació, motivació i, sobretot, per fer-nos la feina més fàcil. Al Bernat per aportar sempre noves idees i noves formes de visualitzar les dades. A la Itziar per l'aportació d'una línia cel·lular tant necessària per les conclusions d'aquesta tesi. També vull donar les gràcies a la resta de companyes del laboratori: José Marcos, Eli, Imma, Àlex i Núria. En especial als tres últims, pel seu suport moral i, en moltes ocasions, consells tècnics molt útils i necessaris. Gràcies! A la resta del grup de NF de Barcelona per riures, coneixement i l'oportunitat de conèixer la NF1 des d'un altre punt de vista: Conxi, Juani, Edgar, Ignacio, Andrea, Belén, Héctor, Alba i Federico. Explícitament a la Conxi i a la Juani per la seva participació en els experiments d'"engraftment" i a l'Héctor per donar-me l'oportunitat de participar com a voluntària en les primeres colònies de NF1. Per tu també Ernest, per ser el meu primer mestre dins d'un laboratori i ensenyar-me què era fer ciència; va ser amb tu que vaig veure clar que volia fer la tesi.

Tercer m'agradaria donar les gràcies al meu cercle més proper pel seu suport, amor i consell en tot aquest procés: Garazi, Itziar, Ainoa, Jonatan, Andrea, Anna, Pau, Marc, Nàdia, etc. Especialment a tu Garazi per estar, escoltar i aportar noves visions i maneres d'encarar la tesi, i la vida. De ben segur que m'estic deixant a molta gent; així que gràcies a totes les que al llarg de la vida ens hem trobat i hagueu contribuït d'alguna manera o d'una altra a seguir caminant el meu camí.

I per anar acabant gràcies a tu Xavi, pel teu suport tècnic (al connectar-te remotament al meu ordinador mentre jo estava de congrés a París i a San Francisco i arreglar el que calgués), per les teves abraçades de "ja ho tens això", i per ser-hi. Això només és un capítol més de la vida. Però gràcies per haver-hi format part!

Y por último gracias a mis padres. A ti mama por el amor al conocimiento y las palabras, por enseñarme desde bien pequeña que lo que uno quiere requiere esfuerzo, dedicación y horas de estudio. Y a ti papa por el entusiasmo por la vida y por las cosas, y por no olvidarnos de reír. Gracias a los dos por estar siempre, sin vosotros esta tesis sí que no se hubiera realizado.

Abstract

Neurofibromatosis type 1 (NF1) is a genetic disease caused by inherited mutations in the *NF1* gene. NF1 is a cancer predisposition syndrome, and the disease's hallmark is the appearance of tumors of the peripheral nervous system called neurofibromas. Neurofibromas are mainly composed of Schwann cells (SCs) and endoneurial fibroblasts (eFbs) and also contain infiltrating immune cells and other cell types. Neurofibromas appear after the complete inactivation of the *NF1* gene in SCs or their precursors. Almost all NF1 patients (>99%) develop cutaneous neurofibromas (cNFs), small benign tumors that appear in the skin around puberty and continue appearing throughout the patient's life. Although cNFs have no risk of becoming malignant, they significantly impact the quality of life of NF1 patients. The only current treatment is surgical removal. Around 50% of patients develop plexiform neurofibromas (PNFs). PNFs form during development and are generally diagnosed either at birth or in early childhood when they grow most rapidly. Some PNFs can progress towards a malignant peripheral nerve sheath tumor, the leading cause of death in NF1.

The three main objectives of this thesis were: (i) to develop an imperishable cell-based model system to study PNFs, (ii) to study the identity of the cells composing PNFs, and (iii) to study the signaling between SCs and Fb concerning cNF growth.

To establish an imperishable cell-based PNF model system, we generated *NF1*(-/-) and *NF1*(+/-) induced pluripotent stem cell (iPSC) lines from PNF-derived cells. Then, we set up protocols to differentiate iPSCs into Neural Crest (NC) cells and from them further to SCs, providing a robust NC-SC *in vitro* differentiation system. We identified differentially expressed genes in stages and timepoints along the *in vitro* NC-SC lineage that were grouped to establish a NC-SC expression roadmap. Altogether, it provided a framework for analyzing the role of the *NF1* gene during SC differentiation. *NF1*(-/-) differentiating SCs in 2D cultures did not constitute an adequate system due to a high proliferation capacity but poor homogeneous differentiation ability towards SCs. However, using the natural tendency of *NF1*(-/-) differentiating SCs to form spheres, different 3D models were developed in a multiplexed format. The engraftment of heterotypic spheroids, composed of *NF1*(-/-) differentiating SC and primary eFbs, represented the most efficient and consistent way of producing human neurofibroma-like tumors in mice.

In addition to being composed of different cell types, we identified the existence of different SC subpopulations within PNFs, by using flow cytometry and single-cell RNA-seq analysis. We characterized at least two distinct SC subpopulations, one expressing markers appearing early in the NC-SC axis, suggesting a precursor-like identity, and another subpopulation expressing both early and late markers along the NC-SC lineage, suggesting a singular committed SC. This heterogeneity may change the current view of PNF development and progression.

We identified differentially upregulated genes produced by the interaction between cNF-derived SCs and eFbs, expressed in both cell types. Analyzing these genes, we identified several enriched signaling pathways potentially participating in SC-Fb crosstalk. Those involved in the infiltration of immune cells were significantly represented and were confirmed by a secretion profile analysis of SC-eFb co-cultures.

In conclusion, in the present work, an imperishable iPSC-based *in vitro*/*in vivo* PNF model system has been developed, allowing the generation of human neurofibroma-like tumors in mice for the first time. We discovered the presence of different subpopulations of SCs within PNFs that may change the view of how they develop and grow. Finally, we found different promising signaling pathways triggered by the heterotypic interaction between SCs and eFbs that could be relevant for cNF growth.

Table of contents

List of Figures and Tables

1. Figures

Figure D1. Schematic representation of the potential uses of the iPSC-based 3D plexiform neurofibroma model.

2. Tables

Table I1: Frequency of the main clinical manifestations of NF1 patients.

Table I2: The 1987 NIH NF1 Diagnostic Criteria with newly proposed changes (in blue) from SF American NF conference 2019.

Table I3: Neural crest derivatives.

Table I4. List of different publications using differentiation of neural crest cells and Schwann cells from pluripotent stem cells.

Table M1: Schwann cell media composition

Table M2: Neural crest media composition.

Table M3: Schwann cell differentiation media composition.

Table M4: Primers for RT-qPCR.

Table M5: Antibody list.

Table R1. Clinical data from Neurofibromatosis type 1 patients, plexiform neurofibromas, and iPSC lines generated.

Table R2. Plexiform neurofibromas used in each reprogramming strategy, either through direct reprogramming or establishment of primary Schwann cell cultures, endoneurial fibroblast cultures, or skin fibroblast cultures.

Table R3. Simplified version of current iPSC lines nomenclature.

Table R4. Summary of tumor masses formed *in vivo* after engraftment of *NF1*(+/+) and *NF1*(-/-) cells at neural crest stage, and at 7 and 14 days of Schwann cell differentiation.

Table R5. Table summarizing the specific cell lines that composed homotypic and heterotypic spheroids.

Table R6. Summary table showing the results of the second engraftment experiment.

Table R7. Clinical data of the 5 plexiform neurofibromas from independent NF1 patients used in flow cytometry analysis.

Table R8. Summary table showing all cutaneous neurofibromas analyzed.

Table R9. Patient and neurofibroma data from the 4 selected cutaneous neurofibromas.

Table R10. Simplified nomenclature for cutaneous neurofibroma-derived Schwann cell and endoneurial fibroblast cultures.

3. Appendixes: figures and tables

Abbreviations

2D two dimensional

3D three dimensional

ADHD attention-deficit/hyperactivity disorder

aNF(s) atypical neurofibroma(s)

ASD autism spectrum disorder

ATP adenosine triphosphate

BC Boundary Cap

BMP bone morphogenetic protein

BSA Bovine Serum Albumin

CA(s) Choroidal abnormalities(s)

CALMs café-au-lait macules

cAMP cyclic adenosine monophosphate

Cas9 CRISPR associated protein 9

CMRB Centre de Medicina Regenerativa de Barcelona

CN copy neutral

CNAG Centre Nacional d'Anàlisis Genòmics

cNF(s) Cutaneous neurofibroma(s)

CN-LOH copy neutral loss of heterozygosity

CNS central nervous system

CREB cAMP-response element binding protein

CRISPR clustered regularly interspaced short palindromic repeats

DEG differentially expressed genes

dpc days post conception

DRG dorsal root ganglia

ECM extracellular matrix

EDTA Ethylenediaminetetraacetic acid

eFb(s) endoneurial fibroblast(s)

EGF epidermal growth factor

EMT epithelial-mesenchymal transition

ES4 Embryonic stem cell 4

ESC(s) embryonic stem cell(s)

FACS Fluorescent Activated Cell Sorting

Fb(s) fibroblast(s)

FGF fibroblast growth factor

FiPS fibroblast induced pluripotent stem cells

GAP GTPase activating protein

GC Gastrocnemius muscle

GDP guanosine diphosphate

GEMMs genetically engineered mouse models

GIST gastrointestinal stromal tumors

GO Gene Ontology

GPCR G protein-coupled receptor

GRD GAP related domain

gRNA guided RNA

GTEx Genotype-Tissue Expression

GTP Guanosine 5' triphosphate

H&E Hematoxylin & Eosin

HDAC histone deacetylases

HFF human foreskin fibroblasts

HUGTP Hospital Universitari Germans Trias i Pujol

ICC: immunocytochemistry

ICO Institut Català d'Oncologia

IDIBELL Institut d'Investivació Biomèdica de Bellvitge

IGTP Research Institute Germans Trias i Pujol

IHC: immunohistochemistry

iPSC(s) Induced pluripotent stem cell(s)

IQ intelligence quotient

iSC(s) immature Schwann cell(s)

LOH loss of heterozygosity

MAPK mitogen-activated protein kinase

MPNSTs Malignant peripheral nerve sheath tumors

MRI magnetic resonance image

mSC myelinating Schwann cells

mTOR mammalian target of the rapamaycin

NC Neural crest

NC-SC Neural crest- Schwann cell

NF1 Neurofibromatosis type 1

NGFR nerve growth factor receptor

NIH National Institutes of Health

nmSC non-myelinating Schwann cells

NPC(s) neural progenitor cell(s)

NRE normalized relative expression

NRG1 neuregulin 1

OCT optimal cutting temperature

OPC optic pathway glioma

PAM protospacer adjacent motif

PBS phosphate buffered saline

PC Principal Component

PCA Principal Component Analysis

PET positron emission tomography

PFA paraformaldehyde

PNFs Plexiform neurofibromas

PNS peripheral nervous system

PRC2 polycomb repressive complex 2

PSC(s) pluripotent stem cell(s)

QoL quality of life

RA retinoic acid

RNP ribonucleoprotein

RT-qPCR qualitative reverse transcription polymerase chain reaction

SC(s) Schwann cell(s)

SCP(s) Schwann cell precursor(s)

SNP Single Nucleotide Polymorphism

SNV single nucleotide variant

SOX10 SRY box 10

SRY sex determining region Y

SUV standardized uptake values

TFAP2α transcription factor AP2α

TGFβ transforming growth factor β

UPL Universal Probe Library

WES Whole exome sequencing

WT wild type

Introduction

Neurofibromatosis type 1 (NF1) is a genetic disease caused by inherited mutations in the *NF1* tumor suppressor gene. NF1 is a cancer predisposition syndrome since people suffering from this disease have a much higher risk than the general population to develop tumors. In particular, the disease's hallmark is the appearance of tumors of the peripheral nervous system, like cutaneous and plexiform neurofibromas. This introduction focuses on this type of tumors; in the cells composing them, like Schwann cells, their development, and differentiation; in the cells originating neurofibromas; in the different models; and in particular, in induced pluripotent stem cells (iPSCs) as a model system.

1. Neurofibromatosis type 1

1.1. Clinical features of Neurofibromatosis type 1

1.1.1. Epidemiology and genetics of Neurofibromatosis type 1

Neurofibromatosis type 1 (NF1) is an autosomal dominant genetic condition (OMIM 162200, https://www.omim.org/entry/162200). NF1 is caused by the inheritance of a pathogenic variant in the *NF1* gene, located on chromosome 17. Almost 50% of cases are familial and 50% as a result of *de novo* mutations (DeBella, Szudek, and Friedman 2000). The penetrance is almost 100% at 8 years of age. The main feature of NF1 is the appearance of benign tumors of the peripheral nervous system (PNS) called neurofibromas.

Different epidemiological studies estimated the prevalence between 1/3,000 to 1/6,000 and the birth incidence between 1/2,558 to1/4,436 (Huson et al. 1989; Poyhonent, Kytola, and Leisti 2000; Lammert et al. 2005; and Evans et al. 2010). Recent studies in the Finnish population have estimated the prevalence in 1:4,000 (Kallionpää et al. 2018) and the birth incidence around 1:2,000 (Uusitalo et al. 2015), a little higher than previously reported. Nevertheless, despite the little differences in the birth incidence reported in different studies, NF1 is still one of the most common inherited conditions.

1.1.2. Clinical features and diagnostic criteria

NF1 is a highly heterogeneous disease affecting different tissues and showing a high phenotypic variability among NF1 patients; even affected individuals from the same family may present different manifestations. Skin, bones, central, and peripheral nervous system are the main tissues implicated.

NF1 patients might present cutaneous signs as the café-au-lait macules (CALMs), Lisch nodules (iris hamartomas), and axillary or inguinal freckling (skin-fold freckling) (**Figure I1**). These patients may also have skeletal and structural abnormalities like tibial dysplasia or scoliosis (**Figure I1**). Some neurological manifestations have also been reported as

learning and cognitive deficits, a higher incidence of attention-deficit/hyperactivity disorder (ADHD), or autism spectrum disorder (ASD).

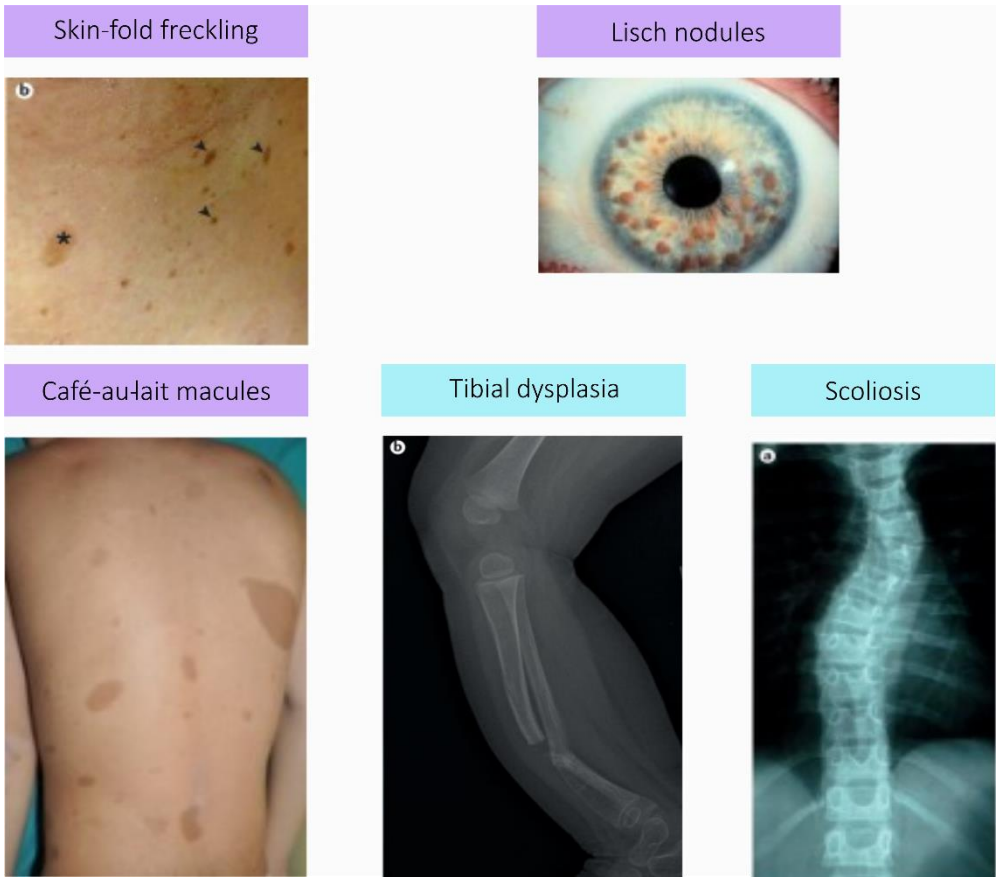

Figure I1. Pigmentary manifestations and skeletal abnormalities characteristic of NF1 patients. In purple, pigmentary manifestations are shown as skin-fold freckling extracted from (Gutmann et al. 2017), Lisch nodules extracted from (Costa, Tojal, and Valverde 2012), and café-au-lait macules extracted from (Hernández-Martín and Duat-Rodríguez 2016). In blue, skeletal abnormalities as tibial dysplasia and scoliosis extracted from (Gutmann et al. 2017).

The hallmark of the disease is the appearance of benign tumors from the PNS called neurofibromas. An entire section will be dedicated exclusively to them.

There exists a high variability on the onset of the clinical manifestations (**Figure I2**). At birth or very early in life, NF1 patients may present CALMs, some skeletal abnormalities, Lisch nodules and/or a plexiform neurofibroma. During childhood, other neurological manifestations as learning deficits, ADHD, or ASD might appear, as well as optic pathway glioma (OPG). In the adolescence period, more cutaneous signs as skin-fold freckling might appear in a high frequency. In this period, some patients may develop scoliosis and many cutaneous neurofibromas. In **Table I1**, the frequency of the most common or relevant clinical symptoms is shown. In adulthood, NF1 patients have a higher predisposition to develop cancer-related features than the general population (Uusitalo et al. 2016) as Malignant Peripheral Nerve Sheath Tumors (MPNSTs) (2-5%), gastrointestinal stromal tumors (GIST), breast cancer, pheochromocytomas, duodenal carcinoids, glomus tumor, juvenile xanthogranuloma, and rhabdomyosarcomas (Upadhyaya and Cooper 2012).

The overall survival of NF1 patients is reduced compared to the general population (Kallionpää et al. 2018), mainly due to the increased risk of developing cancer-related features.

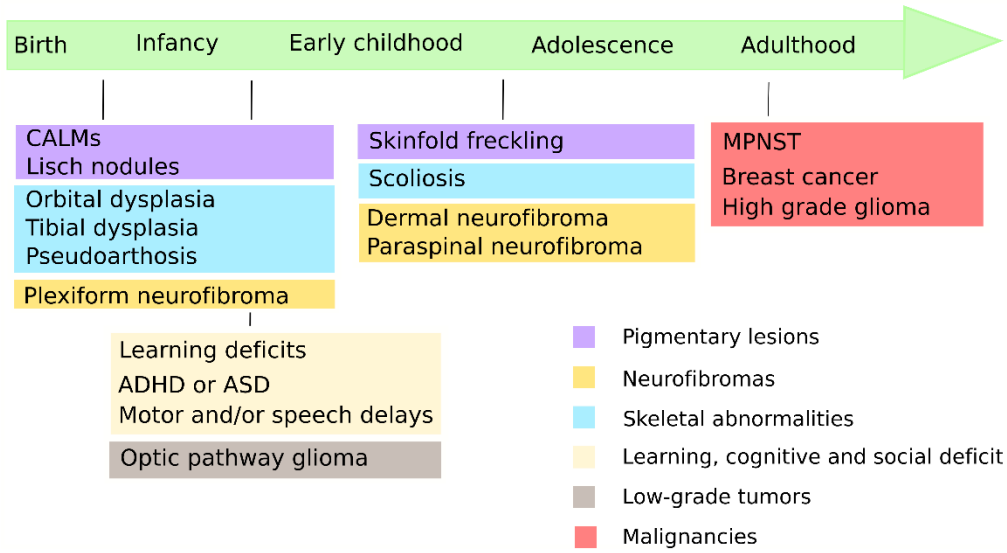

Figure I2. Clinical features of NF1 have different onsets. CALMs: café-au-lait macules. ADHD: attention deficit hyperactivity disorder. ASD: autism spectrum disorder. MPNST. Malignant peripheral nerve sheath tumor. Adapted from (Gutmann et al. 2017).

Clinical manifestation	Frequency (%)
Café-au-lait macules	>99
Skin-fold freckling	85
Lisch nodules	90-95
Cutaneous neurofibromas	>99
Plexiform neurofibromas	30 (visible) – 50 (on imaging)
Disfiguring facial plexiform neurofibromas	3-5
Malignant peripheral nerve sheath tumor	2-5
Scoliosis	10
Scoliosis requiring surgery	5
Pseudoarthrosis of tibia	2
Renal artery stenosis	2
Phaeochromocytoma	2
Severe cognitive impairment (IQ<70)	4-8
Learning problems	30-60
Epilepsy	6-7
Optic pathway glioma	15 (only 5% symptomatic)
Cerebral gliomas	2-3
Sphenoid wing dysplasia	<1
Aqueduct stenosis	1.5

Table I1: Frequency of the main clinical manifestations of NF1 patients. In yellow, cutaneous neurofibroma, plexiform neurofibroma, and disfiguring facial plexiform neurofibroma are highlighted.IQ: intelligence quotient. Extracted and adapted from (Ferner et al. 2007).

In the 1987 National Institutes of Health (NIH) meeting, an established consensus for NF1 diagnosis was established. Almost all NF1 patients (97%) meet NIH Diagnostic Criteria by eight years old, and at the age of 20 years, all do so (DeBella, Szudek, and Friedman 2000)). Some recommended changes have been proposed to update the diagnostic criteria for NF1 (shown in blue in **Table I2**) in the 2019 San Francisco American NF Conference. Thus, NF1 clinical diagnosis is established if two or more of the following manifestations are present in the patient:

1987 NIH NF1 Diagnostic Criteria with recommended changes

Two or more of the following:
• Six or more café-au-lait macules, bilaterally localized (clarification of existing criterion)
  • ≥ 5mm diameter in prepubertal children
  • ≥ 15 mm in postpubertal children
• Bilateral freckles in axilla or groin * (clarification of existing criterion)
• Two or more neurofibromas of any type or one plexiform neurofibroma
• Two or more iris Lisch nodules (iris hamartomas) or two or more choroidal abnormalities (CA) (addition to existing criteria)
• Optic pathway glioma
• A distinctive osseous lesion such as sphenoid wing dysplasia **; anterolateral bowing of tibia (tibial dysplasia); or pseudarthrosis of a long bone (clarification of existing criterion)
• A pathogenic *NF1* variant (addition to existing criteria)
• A parent with NF1 by the above criteria (clarification of existing criterion)

Table I2: The 1987 NIH NF1 Diagnostic Criteria with newly proposed changes (in blue) from SF American NF conference 2019. *: If only CALM and freckling are present, the diagnosis is most likely NF1, but exceptionally, the person might have another diagnosis such as Legius syndrome. **: Spheroid wing dysplasia is not a different criterion in the case of an ipsilateral orbital plexiform neurofibroma.

1.2. Molecular features of Neurofibromatosis type 1

1.2.1. The *NF1* gene

The *NF1* gene (GeneID:4763) is located in chromosome 17q11.2 and expands approximately 280kb of genomic DNA. (Wallace et al. 1990; Li et al. 1995). It is composed of 60 exons, three of which are alternatively spliced exons: 9br, 23a, and 48a (Shen, Harper, and Upadhyaya 1996). The exclusion or inclusion of one of these alternatively spliced exons generates different *NF1* isoforms with other signaling activity and tissue specificity (Barron and Lou 2012). Although Type I and Type II isoforms, generated by the alternative splicing of exon 23a, are the most commonly expressed *NF1* isoforms (Nishi et al. 1991).

The *NF1* gene is a tumor suppressor gene, and the majority of pathogenic variants lead to loss-of-function alleles. Accordingly, based on Knudson's two-hit hypothesis (Knudson 1971), all cells in the NF1 patient harbor the "first-hit", the pathogenic constitutional variant. When a "second-hit" pathogenic variant, the somatic variant, occurs in the remaining wild-type allele in specific somatic cells, these cells acquire a greater proliferation capacity, and a tumor may be initiated. Somatic pathogenic variants have

been found in NF1 associated tumors, including cutaneous and plexiform neurofibromas, glomus tumors, gastrointestinal stromal tumors, pheochromocytomas, juvenile myelomonocytic leukemia and astrocytomas (reviewed by De Raedt et al. 2008) as well as non-tumor lesions like pseudoarthrosis of a long bone (Stevenson et al. 2006) and CALMs (De Schepper et al. 2008).

NF1 syndrome is due to a pathogenic constitutional variant in the *NF1* gene, and NF1 patients may exhibit a wide range of different pathogenic constitutional variants (Ludwine M. Messiaen et al. 2000). In a comprehensive multistep genetic diagnostic approach, the mutational spectrum of 1770 unrelated patients was identified (L. M. Messiaen and Wimmer 2008). In such study, 18% of mutations were due to a missense or 1-multi amino acid deletion or duplication, 27% to splice mutations, 5% to total gene deletions, 2% to deep intronic alterations, 21% to nonsense mutations, 26% to frameshift mutations, and 1% to other complex alterations. Although the majority of mutations are located in exonic regions, some are located inside introns or in flanking intronic sequences affecting the proper splicing of exons.

Current molecular diagnostics (summarized by L. M. Messiaen 2020) are based on multistep approaches based on genomic DNA sequence analysis either by Sanger sequencing or by Next Generation Sequencing (NGS) of all exons and flanking intronic sequence; on cDNA analysis to seek mutations located inside introns or complex splicing mutations (L. M. Messiaen and Wimmer 2008); and on copy number analysis like Multiplex Ligation-dependent probe analysis (MLPA), array-based or bioinformatic analysis of NGS data (Moreno-Cabrera et al. 2020). The detection of the pathogenic variants in the *NF1* gene is challenging since it is a large gene, without specific hotspots, and with a diverse spectrum of pathogenic variants.

Despite the wide range of pathogenic variants, only a few have been correlated with a specific phenotype. For instance, 5% of NF1 patients harbor microdeletions that encompass the *NF1* gene and a variable number of surrounding genes. These *NF1* patients have been associated with a more severe phenotype: an increased risk for MPNST (De Raedt et al. 2003), facial abnormalities, and early onset of neurofibromas (Leppig et al. 1997). Currently, a genotype-phenotype correlation has been established for several missense mutations (Koczkowska et al. 2020)

1.2.2. Neurofibromin

The *NF1* gene encodes for a protein called neurofibromin, a 2818 amino acid protein with a molecular weight of approximately 280 kDa (Declue, Cohen, and Lowy 1991). Neurofibromin is ubiquitously expressed but with the highest levels in neurons, Schwann cells (SCs), and oligodendrocytes (Daston and Ratner 1992). It was also found to be expressed in keratinocytes and melanocytes (Malhotra and Ratner 1994). Data from the Genotype-Tissue Expression (GTEx) project shows the highest *NF1* expression in human adult tissues at the cerebellar hemisphere, the cerebellum, and in the tibial nerve (GTEx Analysis Release V8).

Although being a massive protein with different domains, its structure and function are still largely unknown. The best-characterized domain is the GTP-ase-Activating-Protein (GAP)-related domain (GRD). Neurofibromin, through the GRD, down-regulates the activity of Ras (Martin et al. 1990; Ballester et al. 1990). Neurofibromin increases the intrinsic GTP hydrolysis activity of Ras, facilitating a switch from an active form of Ras bound to GTP into an inactive Ras form bound to GDP. Active Ras interacts with several downstream effectors such as the mitogen-activated protein kinase (MAPK) pathway or the phosphoinositol 3 kinase/AKT signaling, which in turn activates the mammalian target of the rapamycin (mTOR), among others (reviewed in Walker and Upadhyaya 2018). Through these different signaling pathways, various biological processes might be regulated such as proliferation, cell growth, differentiation, etc.

Neurofibromin is also known to influence cAMP-dependent signaling through the regulation of adenylate cyclase (Guo et al. 1997; Tong et al. 2002). In astrocytes, neurofibromin regulates positively cAMP levels through adenylate cyclase stimulation, at least partially by the GRD (Dasgupta, Dugan, and Gutmann 2003).

In addition to GRD, several other domains have been described for neurofibromin, such as the cysteine-serine-rich domain (CSRD), a tubulin-binding domain (TBD), a SEC14 domain, a pleckstrin homology (PH) domain, a carboxy-terminal domain (CTD), and a syndecan-binding domain (SBD). However, the partners and functions of these domains remain to be elucidated. Recently, neurofibromin regions interacting with Spred1 have been identified (Hirata et al. 2016; Dunzendorfer-matt et al. 2016). Mutations in *SPRED1* cause Legius syndrome, a RASopathy that, at an early age, has clinical overlap with NF1.

2. Neurofibromas

As explained before, almost all NF1 patients (>99%) develop cutaneous neurofibromas, and up to 50% develop plexiform neurofibromas (Figure I3).

Neurofibromas are benign (WHO grade I) tumors that can appear in virtually any nerve of the body. There are different types of neurofibromas, and different classifications have also been proposed. Recently, French national NF1 guidelines were published based on an extensive literature review (Bergqvist et al. 2020). The suggested classification for neurofibromas was the following:

- Cutaneous neurofibromas (or dermal): small neurofibromas that appear and are limited to the skin.
- Subcutaneous neurofibromas (or peripheral nodular neurofibromas): palpable discrete neurofibromas that lie more profound in the skin (Ortonne et al. 2018).
- Internal (nodular) neurofibromas: these neurofibromas cannot be detected by physical examination.
- Plexiform neurofibromas: thought to be congenital, arise in deeper and bigger nerves or nerve plexus.

This thesis will be focused on the study of cutaneous and plexiform neurofibromas.

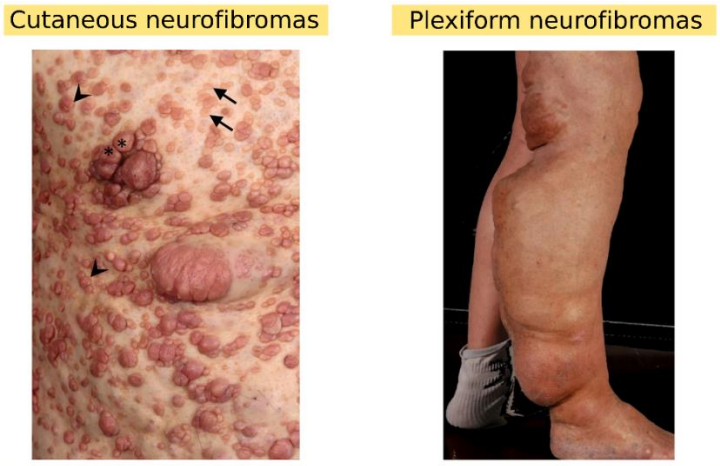

Figure I3. Cutaneous and plexiform neurofibromas have different onsets. Images extracted from (Ortonne et al. 2018) and (Ferner 2007).

Neurofibromas are composed of mainly SCs, endoneurial fibroblasts (eFbs), infiltrating immune cells like mast cells, macrophages, T lymphocytes, and other cell types characteristically of the nerves like perineurial cells. Neurofibromas are hypocellular tumors embedded in a highly collagenous extracellular matrix (ECM) (Peltonen et al. 1981).

Neurofibromas appear when the "second-hit mutation", the somatic mutation, occurs in the remaining wild type allele of the *NF1* gene in SCs or their precursors (Kluwe, Friedrich, and Mautner 1999; Serra et al. 2000; **Figure I4**), triggering *NF1*(-/-) cells proliferation and, leading to the loss of the standard nerve structure. SCs are the principal glial cells from the peripheral nervous system derived from neural crest stem cells (see section 3), and they wrap axons producing the myelin sheath to allow the rapid propagation of action potentials.

In normal nerves, each axon is surrounded by the endoneurium, and a group of unsheathed axons is surrounded by a perineurium, forming a fascicle. A group of fascicles surrounded by the epineurium constitutes a nerve. Inside the perineurium, besides the unsheathed nerve fibers, nonmyelinated SCs are enveloping multiple small axons (also known as Remak bundles), and other cell types reside in this space as fibroblasts and mast cells. This highly organized structure is completely lost when a neurofibroma is formed (**Figure I4**).

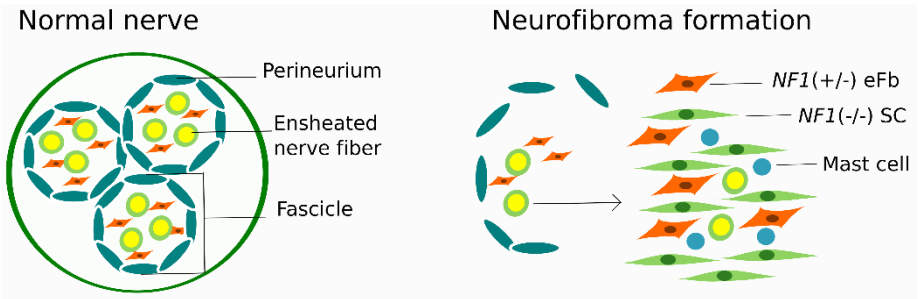

Figure I4. Neurofibromas arise through the double inactivation of the *NF1* gene in Schwann cells or their precursors. In normal nerves, axons are surrounded by myelinating SCs, forming

unsheathed nerve fibers. When a "second-hit" mutation occurs in the remaining wild-type allele of the *NF1* gene in SCs or their precursors, cells start proliferating, and the nerve structure is lost. Adapted from Cichowski and Jacks 2001.

2.1. Cutaneous neurofibromas

Cutaneous neurofibromas (cNFs) are small benign tumors that appear in the skin for the first time around puberty and continue appearing throughout the patient's life (Ortonne et al. 2018; Figure I5).

Almost all adults with NF1 have cNFs (99%). Although some patients with mild phenotype present only a few tens, others show a more severe phenotype with thousands of them (Duong et al. 2011).

Virtually all NF1 patients show an increased number of cNFs during life (Duong, 2011) and pregnancy. NF1 female patients commonly report an increased number of new cNFs and the growth of existing ones during gestation (Dugoff and Sujansky 1996). Indeed, recent studies in cNF-derived *NF1*(-/-) SCs showed an increased proliferation rate under estradiol, testosterone, and human chorionic gonadotropin than in cNF-derived *NF1*(+/-) SCs (Pennanen et al. 2018).

In approximately 25% of cNFs, the "second-hit" is identified by a loss of heterozygosity (LOH) analysis (Colman, Williams, and Wallace 1995; Serra et al. 1997), while in the remaining 75%, a small pathogenic variant is identified (Maertens et al. 2006). The primary cause of LOH is homologous recombination, which happens in 60% of LOH-bearing cNFs (Garcia-Linares et al. 2011), reducing the constitutional *NF1* mutation to homozygosity (Serra et al. 2001). The other 40% of LOH-bearing cNFs carry deletions of various sizes (80Kb-8Mb) involving the *NF1* gene (Garcia-Linares et al. 2011). Patients with *NF1* microdeletions as a pathogenic constitutional variant do not present LOH as a "second-hit" (Maertens et al. 2006).

Although cNFs are benign and have no risk of becoming malignant, they significantly impact the quality of life (QoL) and self-esteem of adult NF1 patients (Granstörm et al. 2012). These tumors can cause severe disfigurement and discomfort, and the only current treatment is surgical removal or physical destruction (Moreno, 2001). Some patients undergo surgery on a regular basis to excise some of them and reduce the tumor burden mass.

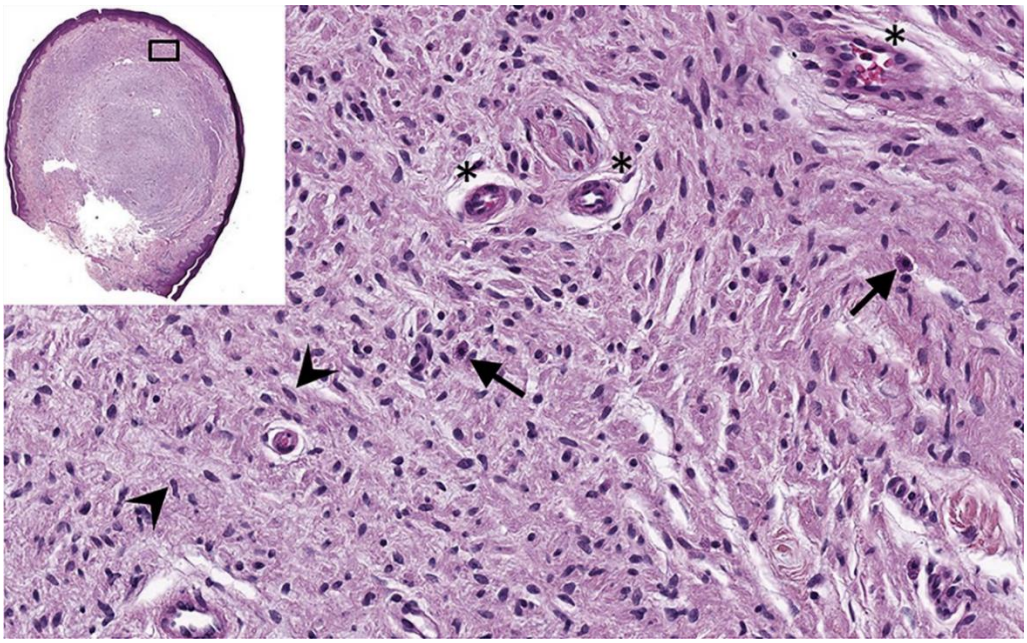

Figure I5. Morphological and histological appearance of cutaneous neurofibromas. The scattered spindle SCs (arrowheads) and eFbs compose the cNFs, as well as the numerous capillaries and veins (asterisks) and mast cells (arrows). Hematoxylin & Eosin, staining. An x400 magnification, and inset x25. Extracted from Ortonne et al. 2018.

2.2. Plexiform neurofibromas

Plexiform neurofibromas (PNFs) are benign tumors that arise in deeper nerves, being more prominent and more heterogeneous than cNFs (**Figure I6**). PNFs might become large and compress other structures causing disfigurement and pain. PNFs are thought to be congenital and generally diagnosed either at birth or in early childhood when they grow most rapidly. Around 30-50% of NF1 individuals present PNFs.

As PNF may be visible or may lie internally, they are diagnosed by physical examination or magnetic resonance imaging (MRI). Depending on the size and location, surgical removal might be sometimes recommended. Unfortunately, when tumors are giant with high vascular content or compressing other vital structures, this might not be possible, and these tumors become inoperable. The MEK inhibitor Selumetinib has been used in children with inoperable PNFs in Phase 1 (Dombi et al. 2016) and Phase 2 (Gross et al. 2020) trials showing tumor volume decrease in about 70% of the cases, most of them with a durable response, lowering pain and improving their quality of life. The FDA has recently approved Selumitinib as the first-ever treatment for NF1.

In contrast to cNFs that never become malignant, some PNFs might progress towards a malignant peripheral nerve sheath tumor (MPNST). MPNSTs are soft tissue sarcomas with limited sensitivity to chemotherapy and radiation. NF1 patients have an 8-13% lifetime risk of developing an MPNST. The prognosis of MPNST associated with NF1 is worse than sporadic cases with a five-year survival of 21% compared to the 42% for sporadic cases (Evans et al. 2010; Uusitalo et al. 2016).

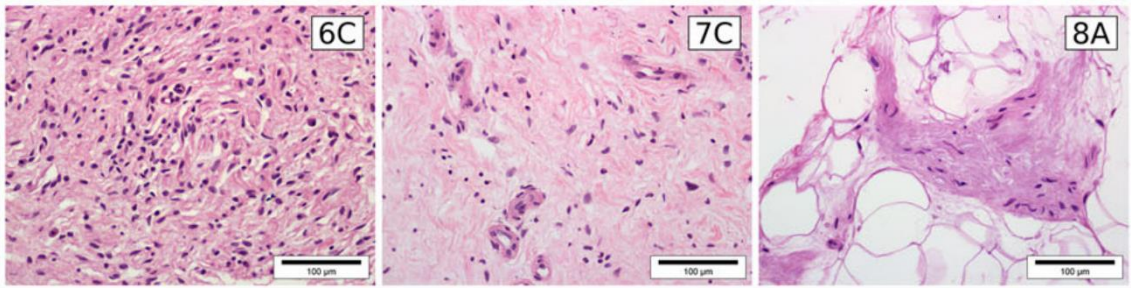

Figure I6. Hematoxylin & eosin staining of three independents plexiform neurofibromas showing heterogeneity among them. The PNF 6C shows the presence of plexiform areas with high cellular density and the PNF 7C with low cellular density. In the third image, the PNF 8A shows a very low cellular density with tumor-infiltrating fat. Picture extracted from Carrió et al. 2018.

2.2.1. From plexiform neurofibromas to malignant peripheral nerve sheath tumor

The generation of an MPNST from a PNF commonly involves developing a pre-malignant lesion called atypical neurofibroma (aNF). aNFs show atypical histological features such as hypercellularity and hyperchromatic nuclei, generally in the absence of mitosis (Beert et al. 2011; Miettinen et al. 2017; Higham et al. 2018). aNFs concentrating many atypical features have also been termed atypical neurofibromatous neoplasms of uncertain biologic potential (ANNUBP). When growing inside a PNF, aNF exhibit a more rapid growth pattern than its surrounding PNF, generating a typical distinctive nodular lesion that may be positron emission tomography (PET) positive with lower standardized uptake values (SUVs) compared to MPNSTs (Beert et al. 2011; Miettinen et al. 2017; Higham et al. 2018).

In addition to the biallelic *NF1* inactivation, loss of the *CDKN2A/B* locus drive aNF formation (Beert et al. 2011; Carrió et al. 2018; Pemov et al. 2019). aNFs may or may not progress towards malignancy, and there is no marker to predict progression from aNF to MPNST, but surgery is recommended when possible. On top of these two molecular events, MPNSTs frequently exhibit mutations in genes of polycomb repressive complex *2* (PRC2) (*SUZ12*, *EED*) and, although more controversial, also in *TP53* (W. Lee et al. 2014). Another distinctive characteristic is that MPNSTs show hyperploid and highly rearranged genomes but with a low mutation burden, like other soft tissue sarcomas (Abeshouse et al. 2017). MPNST cell lines do not express markers from the NC-SC lineage (see section 3.2), like neurofibroma-derived SCs (Miller et al. 2009).

2.3. Neurofibroma microenvironment

The neurofibroma microenvironment is composed of both ECM, rich in collagens, and different types of *NF1*(+/-) cells such as SCs, eFbs, mast cells, macrophages, leukocytes, perineurial cells, and vascular elements (reviewed in Walker and Upadhyaya 2018).

Although *NF1*(-/-) cells are the tumor-initiating cells, it is believed that *NF1*(+/-) cells present in neurofibromas also contribute to tumor growth.

For example, from studies performed in mice, we know that *Nf1(-/-)* SCs secrete elevated levels of the growth factor Kit ligand (KitL; also known as Stem Cell Factor (SCF)). KitL acts as a potent migratory stimulus for mast cells(Yang et al. 2003). These *Nf1*(+/-) mast cells secrete high concentrations of the transforming growth factor-beta (TGF-β), which in turn activates the proliferation of *Nf1*(+/-) eFbs.

Active eFbs, that account for approximately 30% of cells in a neurofibroma, synthesize the high rich collagen matrix (Peltonen et al. 1981). The extracellular matrix is enriched in collagen type I, III, IV, and fibronectin (Peltonen et al. 1986). One of the classical markers to study eFbs is CD34 (Hirose et al. 2003). Although being the second most representative cell type in the neurofibroma, there is no much information available about these cells and their specific signaling pathways in neurofibroma development (reviewed in (Richard, Topilko, Magy, and Charnay 2012)).

In normal nerve, perineurial cells form a layer around groups of axon-SC units delineating nerve fascicles. In neurofibromas, perineurial cells are present and may account for up to 10% of the cell population, depending on the tumor (Carrió et al. 2018). Perineurial cells have a basement membrane, while eFbs do not. This characteristic can be used to distinguish them in pathological sections. Other markers that can be used to identify perineurial cells in neurofibromas are glucose transporter 1 (Glut1), epithelial membrane antigen (EMA), type IV collagen, and claudin-1 (Jaakkola, Chu, and Uitto 1989; Hirose et al. 2003; and Pummi et al. 2006).

Mast cells, macrophages, T cells, and dendritic cells are also recruited into neurofibromas (Prada et al. 2013; and reviewed in Fletcher, Pundavela, and Ratner 2019). *Nf1*(*-/-*) SCs secrete growth factors as the KitL (explained before) and chemokines as CXCL10. A conditional mice strain was generated to study the implication of dendritic and T cells on neurofibroma formation. In such mice, the *Nf1* was deleted in *Dhh* expressing cells, and there was no expression of *CXCR3*, the receptor of CXCL10. Although the mice strain in which the *Nf1* gene was deleted in *Dhh* expressing cells formed neurofibromas, the mice strain that did not express *CXCR3* in any cell did not develop PNFs (Fletcher et al. 2019). These results highlight the importance of the tumor microenvironment in tumor formation and development.

3. Schwann cell development: the neural crest-Schwann cell lineage

As explained above, SCs are the principal glial cells from the PNS. They wrap peripheral neurons and produce the myelin sheath to allow the rapid propagation of the action potentials.

SCs are formed during embryonic development from a specific cell population called the neural crest cells through a multistep differentiation process

3.1. Neural crest cells

3.1.1. The neural crest development

The neural crest (NC) is a highly migrating population in the developmental embryo that can give rise to many different cell types. NC is unique to vertebrates (reviewed in (York and McCauley 2020)).

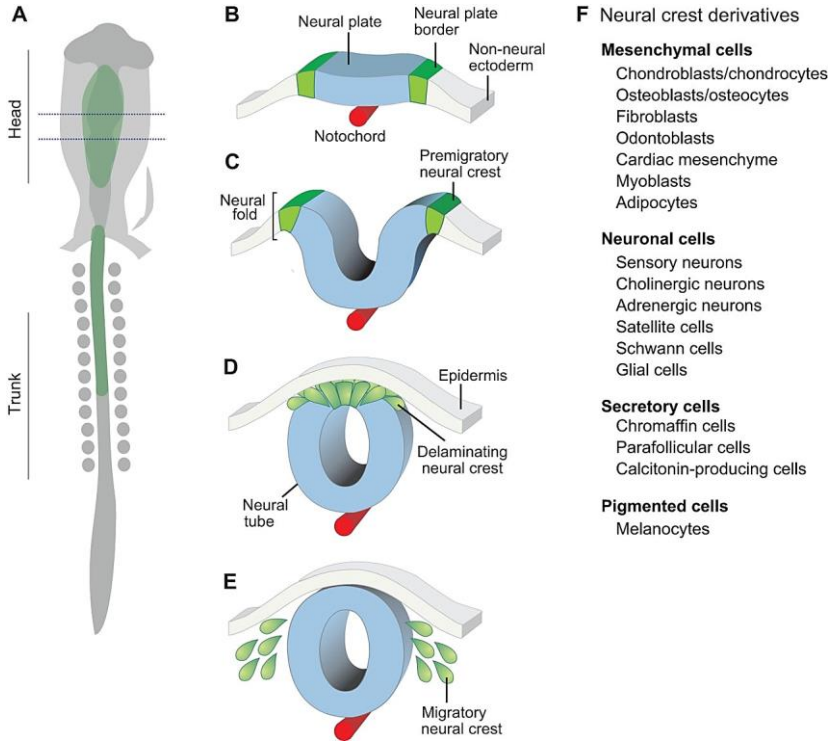

Figure I7. The neural crest cells are formed while the neural tube is closing. Extracted from Simões-Costa and Bronner 2015.

After neural induction is produced in the developing embryo, a subgroup of cells in the ectoderm differentiates to produce the neuroectoderm (**Figure I7**). At the neural plate, the neuroectoderm is found in the middle, surrounded by the neural plate border at each site, and next to it, the non-neural ectoderm. Afterward, the neuroectoderm starts to form the neural groove in a process called neurulation. The neural plate borders transform into the neural folds. Thus, while the neural tube is closing, the neural folds get

closer until the presumptive NC cells remain between the dorsal neural tube and the epidermis. At this moment, the NC cells separate from the surrounding tissues through an epithelial-mesenchymal transition (EMT) in a process called delamination. The NC cells migrate through the entire embryo to lately settle and differentiate into all the different specific cell types (Theveneau and Mayor 2012; Green, Simoes-Costa, and Bronner 2015). Depending on the rostrocaudal axis where the NC settle, they can give rise to different cell types: ranging from SCs and neurons of the PNS, to fibroblasts, and chondrocytes from the head, myoblasts, and cardiac cells (Petersen et al. 2015; Monk, Feltri, and Taveggia 2015; see Table I3).

The specification of the neural fold, the NC induction, comes from specific inductive molecules: the bone morphogenetic proteins (BMPs) and their antagonists, like noggin and chordin; several fibroblast growth factors (FGF); retinoic acid (RA); different Wnt molecules and Notch/Delta (Mayor and Theveneau 2013).

	Cell types			
	Neurons and glial cells	Pigment cells	Endocrine cells	Mesenchymal cells
Trunk NC	Sensory ganglia (DRG) Sympathetic ganglia Parasympathetic ganglia SCs along PNS nerves	Skin melanocytes	Adrenal medullary cells	Endoneurial fibroblasts (mouse sciatic nerve)
Cranial NC	Sensory cranial ganglia Parasympathetic (ciliary) ganglia Enteric ganglia Satellite glial cells in ganglia Enteric glia SCs along PNS nerves Ensheating Olfactory Cells lining the olfactory nerve	Skin melanocytes Pigment cells of the inner ear	Carotid body cells C cells of the ultimobranchial body and thyroid	Cranio-facial skeleton Dermal bone-forming cells Endochondral osteocytes Chondrocytes Other cells in the head and neck Myofibroblasts/Smooth muscle cells (conotroncus and aortic arch-derived arteries) Pericytes in brain Meninges (forebrain) Odontoblasts, cells in periodontal ligament and tooth papillae Adipocytes Dermal cells of the face Connective cells of glands, muscle, and tendons Corneal cells in endothelium and stroma Ciliary muscles

Table I3: Neural crest derivatives. Adapted from Dupin and Sommer 2012.

3.1.2. The signaling pathways in neural crest formation

One known mechanism of the NC specification is the establishment of a BMP gradient. At the median part of the neural plate border, the antagonistic BMPs are secreted, as noggin and chordin, and from the lateral part, BMPs are secreted, establishing a BMP gradient. Thus, NC cells are induced in the middle, in the neural plate border, where intermediate levels of BMPs are found (Theveneau and Mayor 2012).

Another signaling pathway involved in NC cell development *in vivo* is the canonical Wnt signaling (García-Castro, Marcelle, and Bronner-Fraser 2002). The activation of Wnt redirects the neural progenitor towards a NC fate. Wnt regulates temporal control of BMP exposure. Concomitant exposure to both Wnt and BMP generates epidermal cells. In contrast, the exposure of Wnt in an early phase and a concomitant exposure of Wnt and BMP specifies NC cells in the neural plate border (Patthey, Edlund, and Gunhaga 2009).

3.2. The boundary cap cells

A population of NC-derived cells, known as the boundary cap (BC), are formed at the boundary between the central nervous system (CNS) and the PNS. This cell population has been related with the neurofibroma cell of origin (explained in section 3.4).

The BC cells are a highly proliferative cell population transiently localized at the dorsal root entry zone (sensory) and ventral exit points (motor) of all cranial and spinal nerves at E10.5 in the developing mouse embryo (Niederländer and Lumsden 1996; Radomska and Topilko 2017).

Some of the specific BC markers are *Krox-20* (also known as *Egr2*), *Prss56* (previously described as L20), Hey2, and *Wif1* (Wnt inhibitory factor-1 gene) (Topilko et al. 1994; Coulpier et al. 2009). The Krox20-expressing BC cells and the Prss56-expressing BC produce Schwann cell precursors (SCP) in the dorsal and ventral nerve roots, which will give rise to primarily SC (Aquino et al. 2006) and a small fraction to eFbs (Gresset et al. 2015), also a subgroup of sensory neurons (Hjerling-Leffler et al. 2005) and satellite glia in the dorsal root ganglia (DRG) (Marol et al. 2004). A small portion of these cells migrates along the nerves to the skin. However, there is a slight difference in the differentiating cells from the Krox20-expressing BC cells and the Prss56-expressing BC cells at around E13.5. The Krox20-expressing BC cells delaminate from nerves and integrate into the cutaneous vascular plexus like pericytes. In contrast, the Prss56-expressing BC cells remain in close contact with cutaneous nerves and differentiate into mature SCs (Figure I8).

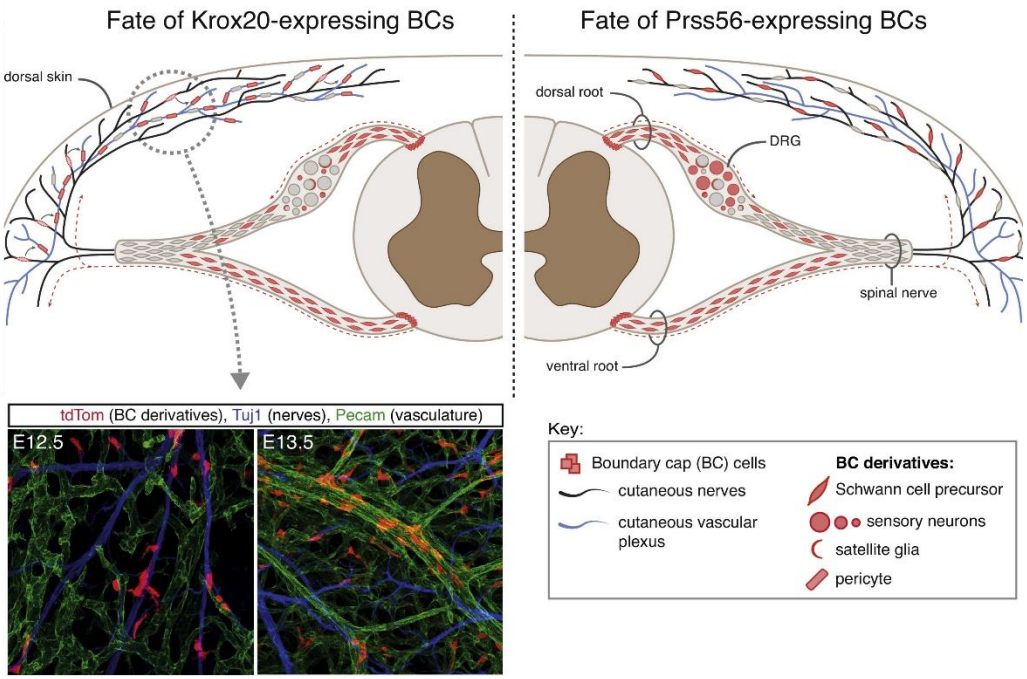

Figure I8. Scheme of the Krox20- and Prss56- expressing boundary cap cell fates. The Krox20-expressing BC cells delaminate from nerves and integrate into the cutaneous vascular plexus (left). In contrast, the Prss56-expressing BC cells remain in close contact with cutaneous nerves and differentiate into mature SCs (right). Extracted from Radomska and Topilko 2017.

3.3. Neural crest-Schwann cell differentiation axis: stages and markers

SCs are the main glial cell of the PNS. Glial cells can provide growth support, structural support, and/or insulation. The PNS is composed mainly of peripheral neurons, SCs, and fibroblasts.

SCs are a very specialized cell type that wraps around peripheral axons generating insulation and allowing the rapid propagation of the electric impulses transmitted between neurons, the action potentials, like the wires in electrical systems. The concentrical membrane layers to insulate axons that SCs generate are called the myelin sheaths.

There can be myelinated or non-myelinated axons. Bigger-caliber axons are myelinated, while small-caliber axons are non-myelinated axons. Myelination generally occurs around axons that are equal or bigger than 1 µm in diameter (Salzer 2015). There is a correlation between the caliber of the axons and the thickness of the myelin sheath: bigger-caliber axons have thicker myelin, and vice versa (reviewed in Sherman and Brophy 2005).

The myelinating SC-axon unit is covered with a basal lamina that is generated during development. The basal lamina is essential for SC differentiation and myelination since it radially polarizes the cells in the inner, adaxonal, membrane and outer, abaxonal membrane. In between these two membranes is the myelin lamellae, the concentrical layers of SC plasma membrane. The nucleus of the cell is localized in the abaxonal compartment.

Different molecules signal differently in each membrane. In the adaxonal membrane, SC-axon interaction occurs with, for instance, the activation of the ErbB2-ErbB3 receptors through the type III neuregulin in the axonal membrane. In the abaxonal membrane, the SC plasma membrane interacts with proteins from the basal lamina as laminins.

During development, NC differentiate into SCs in a multistep process (Kristjan R. Jessen and Mirsky 2005a). NC cells first differentiate (i) into an intermediate cell population called Schwann cell precursor (SCP), then (ii) into immature Schwann cells (iSC) and last (iii) into myelinating (mSC) or non-myelinating Schwann cells (nmSC) (Figure I9).

Thus, NC cells differentiate into SCPs at around day 12-13 during mouse embryonic development. SCPs can migrate and are dependent on axonal factors to survive. SCPs have been recently proposed to be a multipotent stem cell population cells (Kristjan R. Jessen and Mirsky 2019) able to produce different cell types as melanocytes, endoneurial fibroblasts (Morrison et al. 1999; Joseph 2004) parasympathetic/enteric neurons, Chromaffin cells, and tooth pulp.

In developing mice nerves, SCPs differentiate into iSCs at E15/16 or early postnatally. The iSCs stop migrating, become dependent on autocrine factors, not axonal, to survive and deposit ECM components, and organize them to produce the basal lamina. This basal lamina consists of laminins, like laminin 211, and laminin 411; collagens like collagen IV and XV (Carey et al. 1983; Rasi et al. 2010) and heparin sulfate proteoglycans including glypican and perlecan.

At this stage, iSCs undergo radial sorting. This process consists of ensheathing either one bigger caliber peripheral axon to become myelinating SC (mSC) or multiple smaller caliber axons to become non-myelinating SC (nmSC). During this process, a proper polarization must occur since one cytoplasmic membrane, the abaxonal, will be in contact with the basal lamina while the other will be in direct contact with the axonal membrane, the adaxonal (Salzer 2015; Laura, Yannick, and Carlo 2016).

Promyelinating SC spirally and gradually compacts around the axon in a 1:1 ratio to produce the thick protective layer of myelin. Hence, myelinating SCs myelinate only a single portion of one axon, unlike oligodendrocytes in the CNS that myelinate various parts of different axons.

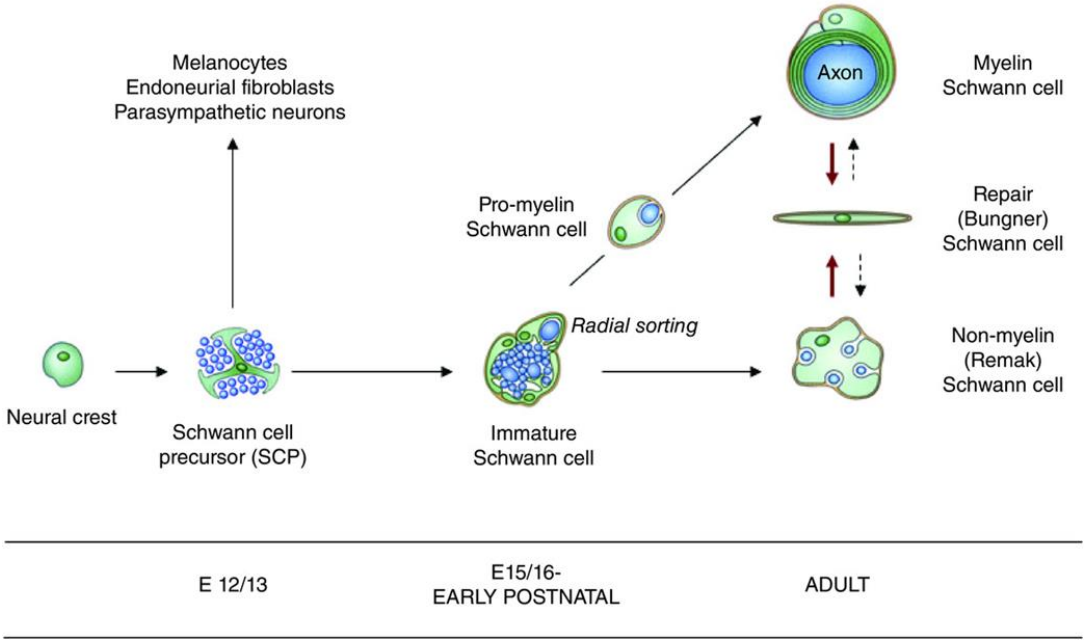

Figure I9. Schematic representation of *in vivo* Schwann cell differentiation in mice. NC cells first differentiate into an intermediate cell population called Schwann cell precursor (SCP), then into immature Schwann cells (iSC), and last into myelinating (mSC) or non-myelinating Schwann cells (nmSC). Extracted from (K R Jessen, Mirsky, and Lloyd 2015).

The specific molecular mechanisms that control the development SCP from NC are not entirely understood. However, some contributing actors are known as well as some particular markers (**Figure I9**)

The essential master transcription factor for the specification of NC-SC lineage is SRY (sex-determining region Y) box 10 (***SOX10***). SOX10 is expressed in all migrating NC and maintained in BC cells, satellite cells, and in nerve roots and distal nerve SCPs, and among other derivatives from NC cells as melanocytes (Sauka-Spengler and Bronner-Fraser 2008; Jacob 2015). Although SOX10 is necessary for SC specification, it is not sufficient (K. R. Monk, Feltri, and Taveggia 2015).

The nerve growth factor receptor (*NGFR*) or **p75** is a well-established marker of NC cells. Stemple and Anderson (1992) first isolated mammalian NC cells using a monoclonal antibody to the low-affinity p75 (Stemple and Anderson 1992). The p75 is a neurotrophin receptor, a member of the tumor necrosis receptor superfamily. This receptor binds with low-affinity to nerve growth factor (NGF), but also other neurotrophins as a brain-derived neurotrophic factor (BDNF), neurotrophin-3 (NT-3), and neurotrophin-4 (NT-4) (Reichardt, 2006). In the developing human embryo, p75 is mainly expressed, although not exclusively, in migrating NC cells (Betters et al. 2010). Moreover, p75 is needed for axonal growth and for SC migration in mice. Knockout mice embryos for p75, p75(-/-), showed an impaired limb innervation from stages E11.5 to E14.5 and a decreased S100B immunoreactivity (see below) in the developing axons (Bentley and Lee 2000). In the human adult, it is primarily expressed in SCs from peripheral nerves (GTEx Analysis Release V8).

Other significant markers are the transcription factor AP2α (*TFAP2α*), needed for SC development, the CD57 antigen or HNK1, and the early growth response-2 (Egr2), or *Krox20*. The transcription factor *Krox20* expressed along the NC-SC lineage, also a marker of boundary cap cells. In embryonic nerve roots, Krox20 positive cells colocalize with PLP positive cells (Chen et al. 2014).

The ErbB3 or Tyrosine Kinase-Type Cell Surface Receptor HER3 is a member of the epidermal growth factor (EGF) receptor family. This tyrosine kinase receptor has a neuregulin binding domain but not an active kinase domain. Hence, this receptor forms heterodimers with other EGF receptor family members, as ErbB2 (HER2), which do have kinase activity leading to the activation of the pathway. Neuregulin 1 (NRG1) binds to the heterodimer ErbB2/ErbB3 and activates it. NRG1 is a membrane glycoprotein, and a wide range of different isoforms are produced from the *NRG1* gene by alternative splicing and the use of alternative promoters (Douglas, 2003). The NRG1 type III (also known as Heregulin) is expressed on the axonal membrane of neurons and is essential for SCP survival and SC differentiation (Z. Ma 2011) and myelinization (Michailov et al. 2004; (Taveggia et al. 2005).

Cadherin 19, Cad19 (*CDH19* gene), and Alpha4 integrin (*ITGA4*) are two specific factors of the SCP stage.

The GPCRs are a family of membrane receptors with seven conserved transmembrane domains that signal through the heterotrimeric G proteins. The GPR126 (also known as *ADGRG6*) was discovered to be necessary for SC development in zebrafish (Kelly R Monk et al. 2009), and, a few years later, it was confirmed to be also essential for SC myelinization in mammals (Mogha et al. 2013). Collagen IV and laminin 211 bind to the GPR126 to perform the radial sorting (Paavola et al. 2014; (Petersen et al. 2015b). Upon GPR126 activation, a $G_{\alpha s}$ subunit stimulates the adenylate cyclase to produce cAMP from ATP, which in turn activates the PKA that phosphorylates the cAMP-response element-binding protein (CREB) and the NFκB. Ultimately, these effectors activate the expression of key transcription factors for myelinization as OCT6 (also known as Poue3f1) or Krox20.

GPR56 (ADGRG1) is another GPCR involved in the SC development (Ackerman et al. 2018). In this case, the GPR56 is necessary for timely radial sorting through the RhoA signaling pathway. In addition, this receptor may also be relevant for myelin maintenance and stability in the adult.

Another mechanism involved in SC development is the epigenetic regulation of histone acetylation or deacetylation. The acetylation mechanism, when the acetyl groups are transferred into the amino groups of Lysine residues in the tails of histone cores, the overall chromatin structure is altered. The different conformation of chromatin, relaxed or closed, has different functional implications. Thus, histone acetylation has been functionally associated with active transcription while histone deacetylation with transcription repression. In fact, the histone deacetylases 1 and 2 (HDAC1/2) have been shown to be necessary for NC specification and for the establishment of SC lineage *in vivo*

(Jacob et al. 2014). Specifically, HDAC1 and HDAC2, together with SOX10, upregulate the expression of Pax3.

The Growth Associated Protein 43 (GAP43) is a marker of SC development, and it is associated with nerve growth. Proteolipid Protein 1 (PLP1) is one of the principal components of myelin. This transmembrane protein may play a role in the compaction, stabilization, and maintenance of myelin. Other significant components of myelin are the Peripheral Myelin Protein 22 (PMP22) and the Myelin Protein Zero (Po or MPZ). The Charcot-Marie-Tooth disease is a group of hereditary conditions where the peripheral nervous system is damaged. Two different types of this disease, type 1A and type 1B, are caused by mutations in the *PMP22* gene and *MPZ* gene, respectively. These three myelin proteins, PLP1, PMP22, and MPZ, as well as GAP43, start to appear at the SCP stage (Kristjan R. Jessen and Mirsky 2005b).

The Glial Fibrillary Acidic Protein (GFAP) is a filament protein and a classical marker of SCs.

One of the most used markers for SC identification is S100B. This protein contains a conserved calcium-binding motif termed the EF-hand and belongs to the 24 members of the S100 family of proteins. S100B is also expressed by chondrocytes, adipocytes, melanocytes, astrocytes, maturing oligodendrocytes, certain neuronal populations, skeletal myofibers, myoblasts, muscle satellite cells (Rosario Donato et al. 2009; R Donato et al. 2013). The role of S100B in SCs is not entirely understood. During SC differentiation, the expression of S100B starts in the immature SC stage (Kristjan R. Jessen and Mirsky 2005) and persists in myelinating and non-myelinating SCs. Sox10 has been shown to activate the expression of S100B in rat SC differentiation, and Sox10 insufficiency suppressed S100B and Mpz expression (Fujiwara et al. 2014).

The expression of some of these markers along the NC-SC differentiation axis is summarized in Figure I10.

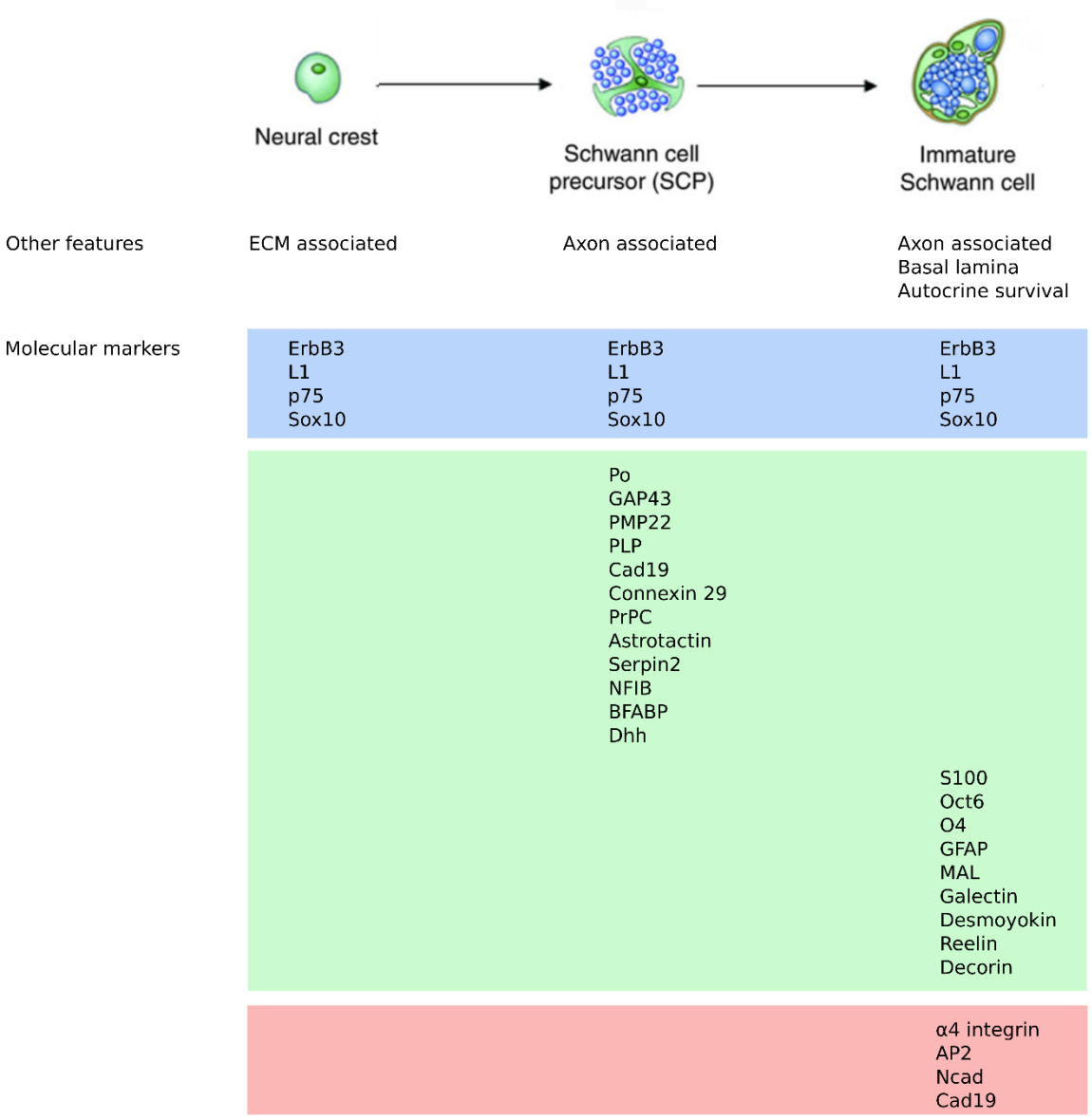

Figure I10. Schematic representation of the main features and molecular markers during *in vivo* Schwann cell differentiation. The stages of NC, SCP, and iSC are shown. The molecular markers highlighted in blue are expressed along all NC-SC lineage, although may be expressed at different levels depending on the cell stage; in green, the ones that are up-regulated in that stage; and in red, the ones that are down-regulated in that stage. Adapted from(K R Jessen, Mirsky, and Lloyd 2015).

3.4. Neurofibroma cell of origin

To study the cell of origin of neurofibromas, different genetically engineered mouse models (GEMMs) have been developed (reviewed in (Brossier and Carroll 2012).

The first knockout mouse models were developed in 1994 by Copeland and Weinberg labs independently (Brannan et al. 1994; Jacks et al. 1994). Both groups generated KO mice with a null mutation in the *Nf1* gene. The homozygous mutant embryos died *in utero* due to a severe malformation of the heart, indicating that the homozygous mutant is

lethal at 14.5 days post conception. This lethality seems to be related to the NC-derivatives that generate the aortic arch-derived arteries (see section 3.1) and not with the formation of neurofibromas. The heterozygous mutant mice did not exhibit any apparent neurofibroma after ten months of age. All these results suggested that the "second-hit" mutation in the wild-type allele had to occur in one or more cell types in peripheral nerves. To experimentally address this question, chimeric mice composed in part of *Nf1*(-/-) cells were generated (Cichowski et al. 1999). All mice that exhibited a moderate degree of chimerism presented PNFs resembling the human tumors. However, cNFs were not observed.

To identify whether the specific cell type receiving the second-hit mutation was restricted to the SC lineage or not, Zhu et al. 2002 generated a conditional model in which a Cre recombinase ablated both floxed *Nf1* alleles in *Krox20* expressing cells ($Nf1^{flox/flox}$; *Krox20-Cre* mice). None of these mice generated any kind of neurofibroma. However, when Cre recombinase was expressed in *Krox20* positive cells in mice with a heterozygous *Nf1* background and a floxed *Nf1* allele ($Nf1^{flox/-}$; *Krox20-Cre* mice), all the progeny developed PNFs by one year of age. These findings confirmed that (i) only the *Nf1* loss in cells of the NC-SC lineage in heterozygous background resulted in neurofibroma formation, and (ii) highlighted the role of a heterozygous microenvironment in its formation.

Given these results, the key question was in which stage, or temporary developmental window, the *Nf1* inactivation had to occur for a neurofibroma to form? Which was the cell of origin of neurofibromas?

Different laboratories further developed conditional mice models using Cre-*LoxP* technology to answer this question. The strategy was again to delete the *Nf1* gene using the Cre recombinase expressed under the promoter of NC-SC stage-specific genes (Figure I11).

- Nancy M. Joseph et al. 2008 generated a mice strain that conditionally deleted *Nf1* from neural crest cells: *Wnt1-Cre* $Nf1^{fl/-}$. These mice did not develop tumors postnatally and could not form tumors upon transplantation into adult nerves.

- Wu et al. 2008 established conditional mice strain in which *Nf1* was deleted by a Cre recombinase in *Desert Hedgehog* (*Dhh*) expressing cells; $Nf1^{flox/flox}$; *Dhh-Cre* mice. These mice developed PNFs near the DRG, predominately at lower cervical or upper thoracic levels. Importantly, these mice did not require a heterozygous *Nf1*(+/-) background to develop PNFs.
- Zheng et al. 2008 generated conditional mice in which *Nf1* was deleted by a Cre recombinase in cells expressing *Myelin Protein 0* (*P0A*): $Nf1^{flox/-}$; *P0A-Cre* mice. These mice exhibited neurofibroma formation throughout the PNS.
- Le et al. 2011 generated conditional mice using a different Cre expression strategy. They established transgenic mice in which *Nf1* was deleted by a tamoxifen-inducible variant of the Cre recombinase (*Cre-ERT2*) under the control of the *proteolipid protein* (*PLP*) gene regulatory region: $Nf1^{flox/-}$; *PLP-Cre-ERT2* mice. Hence, to knock out the *Nf1* gene, tamoxifen was administrated orally to:

a) pregnant mice at day E12.5, in which developing SCP cells were already present (see section 3.2); b) lactating mothers at birth with iSC already present; c) old adult mice, favoring the presence of myelinating or non-myelinating mature SCs. When *Nf1* ablation occurred in adult mice, it hardly led to neurofibroma development. Mice only developed paraspinal neurofibromas near the DRG when *Nf1* was ablated before or during the neonatal period.

- Another work from Le and coworkers (Chen et al. 2014) sought to determine the specific cell population that causes neurofibroma formation. They generated another conditional mouse strain in which the *Nf1* gene was ablated by a tamoxifen-inducible variant of the Cre recombinase (*Cre-ERT*) in *PLP* expressing cells. At the same time, Cre-expressing cells would be marked by the expression of two reporters carrying *LacZ* and the *Yellow Fluorescent Protein* (*YFP*): *Nf1*$^{flox/flox}$; *PLP-Cre-ERT*; *R26R-LacZ-YFP* mice. They administrated tamoxifen orally to the pregnant mice of the above-mentioned strain at embryonic day 11.5 (E11.5), dissected the DRG/nerve roots from embryos at E13.5, established DRG/nerve root neurosphere cell cultures, performed a fluorescence-activated cell sorting (FACS) to obtain YFP$^+$ and YFP$^-$ cells that equal the PLP$^+$ and PLP$^-$ cells, respectively, and injected the PLP$^+$ and PLP$^-$ cells near the sciatic nerve of nude mice. Thirteen out of 20 mice injected with PLP$^+$ cells (65%), which also expressed *GAP43*, generated sciatic PNFs. Thus, these results suggested that a population at the SCP stage is the cell of origin of plexiform neurofibromas.

Although all these conditional mice models generated PNFs, none of them formed cNFs, favoring the possibility of distinct cell types originating PNFs and cNFs.

However, a previous work of the Lu Le group challenged this view. The group generated skin-derived precursors (SKPs) from conditional mice in which the *Nf1* gene was ablated by a *Cytomegalovirus* (*CMV*) promoter-driven tamoxifen-inducible variant of the Cre recombinase (*CMV-Cre-ER*^{T2}): *Nf1*$^{flox/-}$; *CMV-Cre-ER*^{T2} mice (Le et al. 2009). The *Nf1*(-/-) SKPs were injected into the sciatic nerve and formed a PNF. Besides, when investigators applied tamoxifen into the skin of neonatal *Nf1*$^{flox/-}$; *CMV-Cre-ER*^{T2} mice, *in vivo* cNFs developed and were visible after eight months post-application. These results supported the view of a common cell of origin in the development of cNFs and PNFs.

These experiments showed that cNFs and PNFs could be modeled independently; however, there were not any mice models that presented both.

In 2019, Le's laboratory found that ablating the *Nf1* gene in *Hoxb7*-positive cells during development leads to the formation of cNFs and PNFs (Chen et al. 2019).

Recently, an independent laboratory led by Piotr Topilko performed elegant experiments showing that NC-derived boundary cap cells expressing *Prss56* (see section 3.1.3) could produce cNFs and PNFs after *Nf1* gene ablation (Katarzyna J. Radomska et al. 2019). Prss56-expressing BC cells gave rise to glial and nonglial derivatives in nerve roots and skin nerve terminals. Although the *Nf1* biallelic inactivation occurred in BC cells around E11, the majority of mice, in addition to PNFs, also developed cNFs after ten months of

age. This model allowed the tracking of the *Nf1*(-/-) BC cells migrating from the nerve roots to the skin, and pointed to subepidermal glia as a likely candidate for the cellular origin of cNFs.

The investigators followed the full progression for a cNF to form and defined four stages in the development of the cNF. At birth, stage 1, the number of SC in the dermis almost doubled the control (mild hyperplasia). At three months of age, stage 2, the number of SC in the dermis increased even more (severe hyperplasia), and the SC presented a modified morphology (hypertrophy). In this stage, there was also an accumulation of fibroblasts and collagen fibers probably secreted by them. At six months, stage 3, many micro-cNFs were present that contained mutant SCs with altered morphologies that often have lost contact with axons. Fibroblasts, macrophages, and neutrophils infiltrated the micro-lesions. Investigators also found inflammation in these lesions. At twelve months of age, stage 4, there were visible diffuse cNFs.

Figure I11 summarized most of the reviewed neurofibroma mouse models, also showing whether the models generated PNFs, and/or cNFs. A great effort had been made to narrow the window in which PNFs, and cNFs originate.

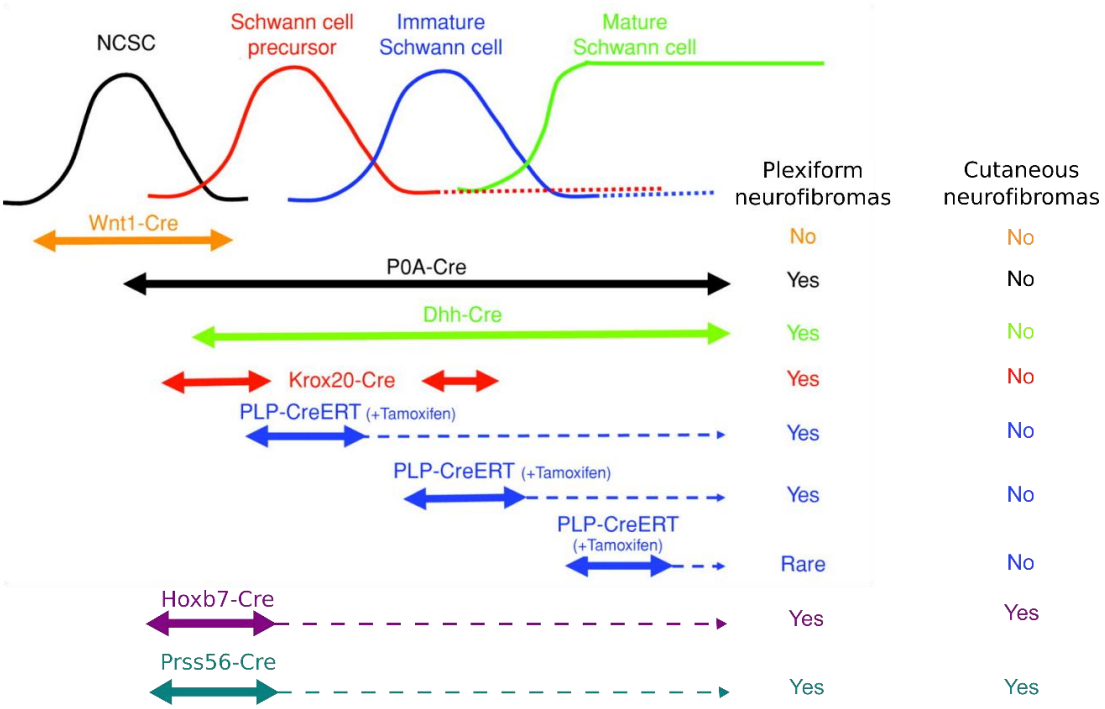

Figure I11. Schematic representation outlining the several stages of Schwann cell differentiation and the defined periods of the *Nf1* Cre-mediated recombination in several neurofibroma models. Adapted from Le et al. 2011.

4. Induced Pluripotent Stem Cells as a cellular model to study tumors

Stem cells are cells with a self-renew capacity capable of differentiating into different cell types depending on their potency (Lajtha 1979).

Thus, stem cells might be totipotent if they can generate all cell types in the body and the placenta; pluripotent, if they can produce all cell types in the body excepting the placenta; multipotent, if they can produce all cell types from a specific lineage; or unipotent, if cells only can produce one specific cell type.

The stem cell potency decreases from a totipotent stage in the zygote to a unipotent stage in a complete differentiated cell type. However, in adult tissues, there are some remaining multipotent stem cells called adult stem cells that maintain the proper homeostasis of organs. When damage is produced, or when cells naturally die, adult stem cells divide to produce the tissue-specific cell types needed while maintaining their multipotency capacity.

Embryonic stem cells (ESC) are pluripotent stem cells (PSC) that can be derived from the inner cell mass of the blastocyst and be cultured *in vitro* indefinitely, maintaining their pluripotency capacity. It was in 1998 that the first human ESC (hESC) line was derived (Thomson 1998).

4.1. Induced pluripotent stem cells

In the regenerative medicine field, the derivation of hESC lines has represented an unprecedented opportunity for new therapeutic strategies. However, the use of human pre-embryos for research purposes has also been the cause of a worldwide ethical discussion.

Nevertheless, in 2006 Kazutoshi Takashi and Shinya Yamanaka published the *in vitro* reprogramming of mouse adult fibroblast cultures into induced pluripotent stem cells (iPSCs) using the transient exogenous expression of 4 defined factors (Takahashi and Yamanaka 2006). The specific factors, called Yamanaka transcription factors, are OCT3/4, Sox2, c-Myc, and Klf4. These unprecedented results made Yamanaka won the Nobel prize in Medicine in 2012, only six years after the publication of the paper.

Classically, iPSCs are characterized by the expression of specific pluripotency markers as Nanog and their capacity to differentiate into the three different germ layers (ectoderm, mesoderm, and endoderm).

These iPSCs can be maintained *in vitro* in a pluripotent state or can be differentiated into any specific cell type. Well-defined media has to contain the particular molecules to activate the specific differentiation pathways to produce *in vitro* differentiated cells mimicking what occurs *in vivo* in the embryo or after birth.

Different tools exist to deliver Yamanaka transcription factors into somatic cells. These technologies can be classified into integrative if the delivered genetic material is integrated into the genome of the cells, and non-integrative if the delivered genetic material is not integrated (D. Zhu et al. 2018).

- Integrative: lentiviruses, and retroviruses.
- Non-integrative: adenoviruses, Sendai virus, mRNA transfection, miRNA infection/transfection, minicircle vectors, episomal vectors, and direct protein introduction.

The most common methodologies used nowadays are episomal plasmids and Sendai viruses, which are non-integrative, abolishing the insertional mutagenesis risk and facilitating their removal after iPSC establishment.

4.2. Induced pluripotent stem cells for disease modeling in cancer

Since the discovery of the generation of iPSCs in 2006, a lot of effort has been made to generate iPSCs from patients or healthy donors for disease modeling and drug discovery (Rowe and Daley 2019).

Patient-derived iPSCs from somatic cells such as fibroblasts can be differentiated into specific cell types to study the pathological mechanisms underlying human disease and seek new targeted treatment.

On the hereditary cancer predisposition syndrome field, a substantial endeavor has been made to generate patient-derived iPSCs from skin fibroblasts harboring constitutional specific mutations causative of different diseases: Fanconi anemia (13 different causative genes)(Raya et al. 2009), breast cancer predisposition (*BRCA1* and *BRCA2* mutations) (Soyombo et al. 2013), familial platelet disorder with a predisposition to acute myeloid leukemia (*RUNX1* mutations) (Antony-Debré et al. 2015), Li-Fraumeni syndrome (*TP53* mutation) (D. F. Lee et al. 2015), and familial adenomatous polyposis (*APC* and *MUTYH* mutations) (Crespo et al. 2017).

iPSC technology has also been used to reprogram cancer cells. However, the efficiency is very low, probably due to the chromosomal and genomic composition of cancer cells or the necessity of remodeling their epigenetic state (J. Kim and Zaret 2015). Despite the low efficiency, there are several examples of iPSC generated from cancer cells (Pan et al. 2017), mainly from established cell lines (Bernhardt et al. 2017) and much less from primary tumors (J. Kim et al. 2013; Kotini et al. 2017). It is worth noting that the majority of cancer reprogramming has been done on hematological malignancies, not in solid malignant tumors (Papapetrou 2019).

To reprogram tumor cells, the process begins with the isolation and establishment of cultures from human biopsies, on solid tumors, or from bone marrow aspirates or blood, on hematological malignancies (Papapetrou 2016). It is worth noticing that control iPSCs from the same patients might be generated to obtain isogenic iPSCs lacking the specific

mutations that the tumor cells harbor. In this case, non-tumoral tissue as skin, or non-tumoral cells as tumor-associated fibroblasts, may be reprogrammed parallelly. Hence, iPSC colonies obtained need to be genotyped, and then colonies carrying tumor mutations as well as control colonies, be selected.

4.2.1. 3D cellular models

Upon the establishment of differentiation protocols, iPSC-differentiated cells might be cultured in two dimensional (2D) attaching plates or three dimensional (3D) low attaching plates as spheroids or organoids. Spheroids are cell-derived *in vitro* culture models in 3D. Organoids have been defined as 3D structures derived from either PSCs, neonatal tissue stem cells, or adult stem cells, in which cells spontaneously self-organize into properly differentiated functional cell types and progenitors, and which resemble their primary counterparts and recapitulate at least some function of the organ of origin (Huch and Koo 2015; Clevers 2016).

Spheroids have also been used to study cancer with immortalized cell lines. Although conventional 2D immortalized cell lines are cheap and easy to culture, their experimental use generates outcomes of less predictive clinical value. The 3D structure of spheroids is more similar to some characteristics of solid tumors, making them a better model.

Within a spheroid, different zones with different proliferation rates and biodistribution of nutrients occur. In the most outer part, the concentration of nutrients and oxygen rate is much higher than in the inner. On the other hand, in the interior, the pH is lower as well as the cellular density. All these characteristics define three different zones within spheroids. In the interior, there might be a necrotic zone with a lower biodistribution of nutrients and pH. In the exterior, there is the proliferation zone, where the concentration of nutrients and oxygen is higher. In between the proliferation zone and the necrotic zone, there is the senescent zone (E. C. Costa et al. 2016).

Spheroids might be generated with some scaffold as hydrogel or without any scaffold. Furthermore, spheroids might be cultured as homotypic spheroids if only one specific cell type is used or as heterotypic spheroids if two or more cell types are cultured together. Heterotypic spheroids are a great model to mimic what happens *in vivo* in real tumors or organs (Weydert et al. 2020).

4.3. iPSC differentiation protocols towards the neural crest-Schwann cell lineage

4.3.1. Neural crest stem cell differentiation protocols

Since 2005 various differentiation protocols have been published regarding the generation of NC cells from PSC, either from ESC or iPSC (Pomp et al. 2005; G. Lee et al. 2007a; Chambers et al. 2009; G. Lee et al. 2010; Bajpai et al. 2010; Menendez et al. 2011; Mica et al. 2013; Denham et al. 2015; Leung et al. 2016; Tchieu et al. 2017; Hackland et

al. 2017; Frith et al. 2018; Hackland et al. 2019; Gomez et al. 2019). Some of these studies have helped in the understanding of critical signaling pathways to induce NC from PSC.

All these protocols vary on time required for the *in vitro* differentiation, the specific signaling pathways that they activate or inhibit, whether a purification step is needed either by Fluorescent Activated Cell Sorting (FACS) or manually, or not, and whether the media contains serum, Bovine Serum Albumin (BSA), or neither. From 2005 until now, every protocol has looked for better-defined conditions, moving from the use of co-culture, serum, and purification steps (even manually or by FACS) to develop conditions avoiding them. Moreover, all these improvements have increased the efficiency of generating NC, lowering the expansion of neuroectoderm lineages contaminating the cultures.

As explained before, one of them is the activation of the Wnt signaling pathway. Menendez et al. 2011 reported the first direct NC differentiation protocol without co-culture or purification steps. They used a chemically defined media activating the canonical Wnt signaling simultaneously with the suppression of transforming growth factor β (TGFβ) signaling. The activation of Wnt signaling can be achieved using a GSK3 inhibitor as CHIR 99021 (since GSK3 is an antagonist of Wnt) or using a recombinant Wnt. Moreover, the downregulation of TGFβ signaling through the use of TGFβ inhibitors such as SB432542 is another essential factor to induce NC.

The BMP signaling is also a distinct pathway to modulate to produce NC. In the earliest publications mentioned before, authors employed inhibitors of BMPs, although using serum-containing media (G. Lee et al. 2010; Mica et al. 2013b). However, currently, authors have observed that activation of the BMP signaling pathway also induces NC differentiation (Hackland et al. 2017; 2019). Thus, a certain degree of BMP signaling may also be required for NC induction.

After the application of a differentiation protocol, quality control of the differentiated populations is required (Tabar and Studer 2014). The analysis of specific lineage identity markers is essential through cytochemistry or expression analysis and functional validation.

A wide variety of NC markers can be used to monitor the differentiation process. These include transcription factors such as SOX9, SOX10, SNAIL, and TFAP2A, and also cytoplasmic and membrane markers such as p75, and HNK1 (see section 3.4).

Regarding the functional validation of NC, the assays used are based on their natural capacity to migrate and to produce different cell types (multipotency). Hence, classical migration scratch assays (or wound healing assay) might be used to evaluate the migration capacity of the ESCs or iPSCs-derived NCs, and distinct differentiation protocols might be applied to the ESCs or iPSCs-derived NCs to produce different cell types with a consequent evaluation of cell type-specific markers. In this case, differentiation protocols might be used towards pigmented cells (melanocytes), peripheral nervous system cells (peripheral neurons or SCs, etc.), or mesenchymal lineages (chondrocytes, osteoblasts, adipocytes, smooth muscle cells, etc.).

4.3.2. Schwann cell differentiation protocols

Several protocols have been published to generate *in vitro* SCs from ESCs or iPSC-derived NC cells (Rathjen et al. 2002; Motohashi et al. 2007; G. Lee et al. 2007b; Zhou and Snead 2008; Kawaguchi et al. 2010; Wang et al. 2011; Ziegler et al. 2011; Liu et al. 2012; and reviewed in M. Ma, Boddeke, and Copray 2015). In **Table 4,** there is a summary of the conditions used in different protocols.

The majority of them use the activation of the erbb2/erbb3 receptor complex by using exogenous type III neuregulin as neuregulin 1 (NRG1) or heregulin. As explained earlier, type III neuregulin is expressed on the axonal membrane of neurons and is essential for SCP survival and SC differentiation (Z. Ma 2011) and myelinization (Michailov et al. 2004; Taveggia et al. 2005).

The addition of ascorbic acid to the differentiating media also induces myelination (Eldridge, Bunge, and Wood 1987). Various differentiation protocols use ascorbic acid in the last steps of their protocols or when performing *in vitro* myelination assays (see below; H. S. Kim et al. 2017).

As stated before, it is crucial to perform quality control on the differentiated progeny. In this case, the analysis of the markers can be performed using stage-specific markers either dynamically through the differentiation process or at the end-point stage. There are plenty of different markers that can be used. The classical ones are S100β, p75, GFAP, GAP43, PLP1, MPZ, and PMP22 (section 3.4).

SC functional validation might be based on the biological capacity of SCs to myelinate axons, commonly performed through an *in vitro* myelination assay (Ziegler et al. 2011b; Liu et al. 2012). This assay consists of co-culturing rat or mouse DRG neurons with differentiating SCs and the evaluation of myelin production by SCs in contact with axons. Another possible functional assay is the sciatic nerve injury model (A. Wang et al. 2011) in which mice or rat sciatic nerve is damaged, differentiating SCs are injected in the damaged site, and their capacity to repopulate and myelinate the nerve is evaluated.

Author	Source	Culture condition	Progenitor stage	Purification	Intermediate stage markers	Differentiation potential	SC / glia induction medium	Markers	SC functionality	SC markers
(Rathjen et al. 2002)	Mouse ESCs	1) DMEM + 10%FCS + MEDII 2) DMEM + ITSS supplement and FGF2 + staurosporine	Neural crest		Sox10	Glial cells	1) 10 ng/ml FGF2, 20 ng/ml EGF, and 1 ug/ml laminin 2) 10 ng/ml FGF, and 10 ng/ml PDGF-AA	GFAP		
(Motohashi et al. 2007)	Mouse ESCs	ST2 stromal cells 10% FCS, dexamethasone, FGF2, cholera toxin, Et-3, RA	Neural crest	cKit+/ CD45- cells	Sox 10, Snail, Pax3, Miyf-M	Neurons, glia cells, and melanocytes	BMP2, NRG1	GFAP		
(Kawaguchi et al. 2010)	Mouse ESCs	EB formation N2, B27, RA, EGF, bFGF, noggin, Wnt3a, Lif, Et-3	Neural crest	Sox10+ cells	Sox10, Sox9, Id2, Id3, Slug, Snail	Neurons, glia cells	N2,B27, 20 ng/ml BMP4, 20 ng/ml GDNF	GFAP		
(G. Lee et al. 2007b)	Human ESCs	MS-5 stromal cells. 1) N2 medium sonic hedgehog, FGF8, BDNF, and AA 2) N2 medium FGF2, AA, and BDNF	Neural crest	p75+/ Hnk1+ cells	Sox10, Pou4F1, SCN3A, TFAP2B, ITGA4, …	Neurons, SCs, myofibroblast, adipocytes, chondrocytes, osteocytes	CNTF, neuregulin 1 β,10 ng/ml bFGF, and dbcAMP	S100B, GFAP, MBP		
(Zhou and Snead 2008)	Human ESCs	EB formation.	Neural crest	Frizzled3+/ Cadherin11 + cells	GFAP, type II collagen, peripherin, Runx2, SMA	Neurons, SCs, chondrocytes, osteoblasts, smooth muscle, and odontoblasts	20ng/ml IGF-1, and 1nM NRG1	GFAP		

(Ziegler et al. 2011b)	Human ESCs	PA6 stromal cells. Neurospheres	Neural crest		(Pomp 2008)	Neurons, and SCs	1% FCS, 1% N2, 10ng/ml bFGF, 4µM forskolin, 10ng/ml human neuregulin-1.	S100B+/ GFAP+ 60%, p75, Hnk1, MBP and PMP22.	Chick embryonic DRG neurons co-culture	S100B, MBP, GFAP
(A. Wang et al. 2011)	Human ESCs/ iPSCs	EB formation 20 ng/ml bFGF and 20 ng/ml EGF, neural rosettes	Neural crest	p75+	Sox10, Hnk1, TFAP2, nestin, Slug, Brn3a	Neurons, SCs, chondrocytes, osteoblasts, adipocytes, and smooth muscle precursors	CNTF, neuregulin 1 beta, and dbcAMP (G. Lee et al. 2007a)	S100B, GFAP	The sciatic nerve injury model	S100B
(Liu et al. 2012)**Liu 2012**	Human ESCs/ iPSCs	EB formation, B27, PA6-conditioned medium, 20ng/ml FGF2, 10 µM Rock inhibitor, and 200µM ascorbic acid	Neural crest	p75+	p75, Hnk1, Sox10, Sox9, Msx1, TFAP2, Slug	Neurons, SCs, chondrocytes, osteoblasts, and adipocytes	MesenPRO supplemented with 20ng/ml heregulin β1	S100B, GFAP, 75, S0X9, ErbB3, MBP, PLP1, PMP22	Rat embryonic DRG neurons coculture	MBP

Table I4. List of different publications using differentiation of neural crest cells and Schwann cells from pluripotent stem cells. ESC: embryonic stem cell; iPSC: induced pluripotent stem cell; MEDII: conditioned medium taken from the human hepatocellular carcinoma cell line, HepG2. FCS: fetal calf serum. Et-3: endothelin 3. SMA: smooth muscle actin, ITSS: insulin transferrin-sodium selenite. Adapted from Ma 2015.

5. Neurofibromatosis type 1 models

Different models for cNFs and PNFs have been developed, both *in vitro* cell-based, like primary cells, immortalized cells, and 3D culture models; and *in vivo*, like genetically modified mouse models (GEMMs; section 3.6). Moreover, iPSCs from skin-fibroblast of different NF1 patients have also been generated.

5.1. Primary and immortalization cell lines in 2D and 3D

Primary SCs and eFb cultures from neurofibromas have been established as primary models to study cNFs and PNFs (Rosenbaum et al. 2000; Serra et al. 2000; Muir et al. 2001). The engraftment of SC cultures into peripheral nerves of immunodeficient mice formed only incipient growths (Muir et al. 2001). However, these primary cultures are perishable models since, after several passages, SCs decrease their proliferation rate and finally stop dividing to either fully differentiate or undergo senescence. This reduces their use in mid-large-scale molecular and cellular experiments. Immortalized cell lines have been established to overcome this problem (H. Li et al. 2016). Nevertheless, immortalization changes the physiological state of the cells.

In 2018 R. Mattingly's laboratory developed a 3D culture model of PNF using immortalized SC lines (Kraniak et al. 2018). They compared the effects of three different drugs, Selumetinib (a MEK inhibitor), picropodophyllin (an IGF-1R inhibitor), and LDN-193189 (a BMP2 inhibitor), on SC proliferation in 2D and 3D cultures with dose-response experiments. Cell lines grown in 3D showed increased resistance to proliferation inhibition compared to 2D cell lines. This is a clear example that using 3D cultures can closer resemble what might occur in a real tumor.

Another example of a 3D model of neurofibroma has been developed recently in Stéphane Bolduc's lab (Roy et al. 2020). In this case, they produced a 3D cutaneous neurofibroma model using primary cell culture fibroblasts (Fbs), cNFs-derived SCs, and keratinocytes. The model has the drawback of a long period of culturing (52 days) and the use of perishable primary cell cultures. However, in specific contexts, this model could be used as a platform to seek new treatment possibilities for cNFs.

5.2. Genetically modified mouse models

GEMMS have been used in the NF1 field to study the cell of origin and, also, to use as a pre-clinical model in drug testing. Different GEMMS generating neurofibromas have been previously summarized in section 3.6.

5.3. Neurofibromatosis type 1 induced pluripotent stem cell models

As explained before, different patient-derived iPSCs from distinct hereditary predisposition cancer syndrome have been developed.

In the NF1 field, the first NF1 patient skin Fb-derived iPSCs were generated using the integration-free Sendai virus in D. H. Gutmann's laboratory (Anastasaki and Gutmann 2014; Anastasaki et al. 2015, and reviewed elsewhere (Wegscheid, Anastasaki, and Gutmann 2018). The group differentiated control iPSCs and NF1 patient-iPSCs into neural progenitor cells (NPCs) and evaluated the overall neurofibromin expression of iPSCs and NPCs (Anastasaki et al. 2015). Moreover, these investigators used Cas9 technology to obtain isogenic human iPSCs harboring different constitutional *NF1* mutations, differentiated them into NPC in 2D and 3D, and compared the potential effects caused by the distinct constitutional mutations (Anastasaki et al. 2020).

An independent laboratory also published the generation of NF1 patient skin fibroblast-derived iPSCs using a doxycycline-inducible lentiviral vector carrying the reprogramming factors OCT4, KLF4, SOX2, and c-Myc (Larribere et al. 2015). They showed that *NF1*(+/-) patient-derived iPSCs undergo abnormal melanocyte differentiation and that *NF1* loss induces senescence during melanocyte differentiation, like in patient-derived CALMs.

These works used patient-derived Fb bearing the constitutional *NF1* mutation as a source for *NF1*(+/-) iPSC generation but did not address the possibility of reprogramming *NF1*(-/-) cells, particularly those present in neurofibromas. So far, no group has used iPSCs to differentiate them into NC cells and further to SCs, to study neurofibroma initiation and development *in vitro*.

Objectives

The three main objectives of this thesis are:

1) To develop an unperishable model system to study plexiform neurofibromas (PNFs)
    - To develop an induced pluripotent stem cell (iPSC)-based differentiation model system for PNFs
    - To study the role of the *NF1* gene in Schwann cell (SC) differentiation
    - To get a deeper insight into the identity of the PNF cell of origin

2) To study the identity of the cells composing PNFs and their implication in PNF development
    - To study the heterogeneity of the PNFs SC component
    - To study the role of endoneurial fibroblast (eFb) in PNF formation

3) To study the signaling between SCs and eFbs in relation to cutaneous neurofibroma (cNF) growth
    - To identify a cell type-specific expression profile in cNFs produced by heterotypic interactions between SCs and eFbs
    - To translate gene expression profiles into signaling pathways and study their potential implication in cNF growth and potential druggability.

Materials & Methods

1. Human Samples: plexiform and cutaneous neurofibromas

Tumor samples as plexiform neurofibromas (PNFs) or cutaneous neurofibromas (cNFs) were kindly provided by Neurofibromatosis type 1 (NF1) patients after giving written informed consent for iPSC generation, genomic analysis studies, or neurofibroma-derived cultured cells. The patients were diagnosed according to standard diagnostic criteria (DeBella, Szudek, and Friedman 2000). Tumor samples were obtained by surgery, and, immediately after excision, placed in DMEM medium (Gibco) supplemented with 10% Fetal Bovine Serum (FBS; Gibco) + 1x GlutaMAX (Gibco) + 1x Normocin antibiotic cocktail (InvivoGene), and shipped at room temperature to our laboratory. Tumors were processed as follows under aseptic conditions: surrounding fat tissue and skin were removed, tumors were cut into 1-mm pieces and cryopreserved in 10% DMSO (Sigma) + 90% FBS(Gibco), and stored in liquid nitrogen until used.

2. Primary cell culture

2.1. Tumor digestion and primary cell culture establishment

2.1.1. Tumor digestion

Cryopreserved PNFs and cNFs were thawed, cut into smaller pieces using a scalpel, and digested with 160 U/mL Collagenase Type 1 and 0.8 U/mL Dispase (Worthington, Lakewood, NJ) for 16 hours at 37ºC. After that, cell suspension was passed through a glass pipette around 10 times to obtain a single-cell suspension that was collected and centrifuged at 1400 rpm 5 minutes. The pellet was collected and resuspended in a small volume of Schwann Cell Media (SCM, see recipe below). The supernatant was centrifuged again at 1400 rpm 5 minutes to increase the number of viable cells. This step was repeated a second time, and the pellets obtained were pulled together and counted using a hemocytometer (Neubauer chamber). Two types of cultures were established from digested tumors: Schwann cells (SCs) and endoneurial fibroblasts (eFbs).

2.1.2. Schwann cell culture

To establish SC cultures, dissociated tumor cells were seeded onto 0.1 mg/mL Poly-L-lysine (Sigma) and 4 mg/mL Laminin (Gibco)-coated dishes in SCM (Table M1) which is DMEM (Gibco) with 10% FBS (Gibco), 500 U/mL Penicillin/500 mg/mL Streptomycin (Gibco), 0.5 mM 3-iso-butyl-1-methilxantine (IBMX, Sigma), 2.5 mg/mL Insulin (Sigma), 10 nM Heregulin-b1 (PeproTech), and 0.5 mM Forskolin (Sigma). Cells were maintained at 37ºC under a 10% CO_2 atmosphere.

It is crucial to seed at least 5 x 10^4 cells per cm^2 to generate a viable SC culture. It is also essential not to touch the culture for 4 days to let cells attach to the plate. After 4-5 days the media was changed every other day.

Once the culture was established, cells were passaged when they reached confluency with 0.05% Trypsin-Ethylenediaminetetraacetic acid (EDTA) (Gibco) and plated in SCM. 24 hours later, the culture medium was replaced by SCM without Forskolin, and 24 hours later media was changed and replaced for SCM for an additional 2–3 days. This process was repeated in cycles. SC purity was assessed by performing S100B staining (see below). SCs were passaged approximately once a week, diluting the cells 1:2.

SCs were cryopreserved in 10% DMSO (Sigma) + 90% FBS(Gibco), and stored in liquid nitrogen until used.

SCM	
DMEM	
FBS	10%
Penicillin/Streptomycin	500 u/mL / 500 u/mL
3-iso-butyl-1-methilxantine	0.5mM
Heregulin-b1	10nM
Forskolin	0.5 mM

Table M1: Schwann cell media composition.

2.1.3. Endoneurial fibroblast culture

Tumor dissociated cells were plated in DMEM supplemented with 10% FBS media and 1x GlutaMAX (Gibco) and 500 U/mL Penicillin/500 mg/mL Streptomycin (Gibco) to isolate eFbs. Cells were maintained at 37ºC under a 5% CO_2 atmosphere. Cells were passaged when necessary using 0.25% Trypsin-EDTA, approximately once a week, diluting the cells 1:2-1:4.

EFbs were cryopreserved in 10% DMSO (Sigma) + 90% FBS(Gibco), and stored in liquid nitrogen until used.

2.1.4. Schwann cell and endoneurial fibroblast co-culture experiment

SC and eFb co-cultures were grown under SC culture conditions with some modifications, which are the following: cells were seeded onto 0.1 mg/mL Poly-L-lysine (Sigma) and 4 mg/mL Laminin (Gibco)-coated dishes in SCM without IBMX (Sigma) to favor eFb growth. A total of 5 x 10^4 cells per cm^2 were seeded, and 24 hours later, the media was changed to SCM without IBMX nor Forskolin. Co-cultures were maintained at 37ºC under a 10% CO_2 atmosphere for a total of 72 hours (24 hours with media containing Forskolin and 48 hours with media without Forskolin). At this point, supernatants were collected for further analysis, and cells were trypsinized using 0.25% Trypsin-EDTA. A fraction of cells was analyzed for p75 expression by flow cytometry, and another fraction was pelleted and frozen for RNA extraction.

3. Induced pluripotent stem cell generation, characterization, and differentiation

3.1. Induced pluripotent stem cell generation

The generation of PNF-derived iPSCs was performed in collaboration with the group of Dr. Ángel Raya at Centre de Medicina Regenerativa de Barcelona (CMRB).

Two different strategies were used to generate iPSC lines. The first one consisted of establishing SC and eFb cultures and reprogram them. The second one consisted of digesting the tumor and directly reprogram the dissociated cells after 48 hours of plating them. Primary cultures were prepared in our lab and transported to the CMRB for reprogramming.

Between 1 x 10^4 and 2 x 10^4 cells were reprogrammed through the delivery of human cDNA coding for OCT4, SOX2, KLF4, and cMYC transcription factors using the non-integrative reprogramming Cytotune-iPS 2.0 Sendai Reprogramming Kit (Thermo Fisher Scientific), according to the manufacturer's protocol. Approximately 3 or 4 weeks after transduction, colonies displaying embryonic stem cell-like morphology were selected for further characterization and genotyping. iPSC established lines were grown on dishes coated with growth factor-reduced Matrigel (BD Biosciences) in mTeSR medium (StemCell Technologies).

3.2. Standard induced pluripotent stem cell characterization

The standard characterization of the iPSC lines was performed in Dr. Ángel Raya laboratory at CMRB.

Alkaline phosphatase activity was demonstrated using the Alkaline Phosphatase Blue Membrane Substrate Solution (Sigma). Briefly, iPSCs were grown on top of mitotically inactivated human foreskin fibroblasts (HFF) for one week. Cells were fixed for 2 min in 3.7% paraformaldehyde (PFA) and exposed to the substrate solution. After 20 min incubation in the dark, blue staining was evident in iPSC colonies.

Detection of pluripotency-associated markers (nuclear: OCT4, SOX2, and NANOG; cytoplasmic: SSEA3, SSEA4, and Tra-1-81) was performed on iPSC cultured on HFF for 8 days and fixed with 4% PFA. Then, samples were processed for immunocytochemistry.

In vitro differentiation ability to the three germ layers was carried out through embryoid body (EB) formation. For endoderm, EBs were plated on 0.1% gelatin (Millipore) coated coverslips and cultured 3 weeks in KODMEM (Gibco) supplemented with 20% FBS (Hyclone), 1x penicillin/streptomycin (Gibco), 2mM Glutamax (Gibco), 0.05 mM 2-mercaptoethanol (Gibco), 1x non-essential amino acids (Lonza). For mesoderm induction, the same medium was used as before mentioned with the addition of 0.5 mM L-ascorbic acid (Sigma). Ectoderm differentiation was performed culturing the EBs in suspension in

N2B27 medium (Neurobasal: DMEM: F12 50:50 v/v, 1x N2 supplement, 1x B27 supplement, 1x Glutamax) supplemented with b-FGF. After 10 days in culture, EBs were plated on Matrigel (Corning) coated coverslips and cultured for an additional three weeks in N2B27 medium without b-FGF. Differentiated cells were fixed with 4% PFA. Immunocytochemistry was performed by standard methods. Primary antibodies used are listed in Table M5. Secondary antibodies were of the Alexa Fluor series from Jackson Immuno Research and used between 1:250 and 1:500 dilution. Cell nuclei were counterstained with 0.5 µg/mL DAPI (Invitrogen). Images were acquired with an SP5 Leica confocal microscope.

For karyotyping, iPSCs were cultured on Matrigel in the absence of HFF and treated with colcemid (Gibco) at a final concentration of 0.1 µg/mL and processed as described (Campos et al. 2009).

Sendai virus reprogrammed iPSC lines were subjected to qualitative PCR to check that they were vector-free at passage 10. The genetic expression of endogenous pluripotency-associated genes (*OCT4*, *NANOG*, *CRIPTO,* and *Rex1*) were confirmed by qPCR. Primers employed are listed in Table M4.

For DNA methylation analysis, genomic DNA was extracted from cell pellets using the QIAamp DNA Mini Kit (Qiagen 51304). DNA methylation analysis was performed with the Methylamp DNA Modification kit (Epigentek) according to the manufacturer's specifications. OCT4 and Nanog promoters were amplified by PCR using primers previously described in (Freberg et al. 2007), amplified in DH5a cells, purified, and sequenced.

Severe combined immunodeficient beige mice (Charles River Laboratories) were used to generate teratomas from two iPSC lines, 5PNFiPS(+/-)and 5PNFiPS(-/-). Animal assays were conducted following experimental procedures previously approved by the Institutional Ethics Committee on Experimental Animals, in full compliance with Spanish and European laws and regulations. Teratomas were stained with hematoxylin-eosin and also the detection of the three germ layers was done by immunocytochemistry. Antibodies used are included in Table M5.

3.3. Pluripotent stem cell culture

Embryonic stem cells and iPSCs were cultured in 1:20 diluted Matrigel-coated 6-well plates with mTeSR (StemCell Technologies) and maintained at 37ºC under a 5% CO_2 atmosphere. Cells were passaged when necessary with Accutase (Thermo Fischer Scientific).

3.4. Neurofibromin Western blot analysis

iPSCs were grown under their specific conditions. When cells reached 80% confluency, they were washed with chilled phosphate buffered saline (PBS) twice and lysed with RIPA

buffer (50 mM Tris-HCl (pH 7.4), 150mM NaCl, 1mM EDTA, 0.5% Igepal CA-630) supplemented with 3mM DTT (Roche), 1mM PMSF (Fluka), 1mM sodium orthovanadate (Sigma), 5mM NaF (Honeywell), 10 ug/mL leupeptin (Sigma), 5ug/mL aprotinin (Sigma) and 1xPhosSTOP (Roche). Protein was quantified with the Pierce BCA Protein Assay kit (ThermoFisher Scientific) following the manufacture's instructions.

Lysates were boiled with 1X Laemmli buffer, and 90 µg of protein was subjected to SDS-PAGE and transferred onto PVDF membranes (18 hours 90mA at 4ºC). Membranes were blocked with Odyssey Blocking Buffer (PBS)(LI-COR) and incubated with rabbit anti-neurofibromin Antibody (1:1000, Bethyl laboratories) at 4ºC overnight and with mouse anti-αtubulin (1:4000, Sigma-Aldrich) for 1 hour at room temperature. Membranes were then incubated with IRDye 680LT and IRDye 800CW secondary antibodies (1:25,000 and 1:15,000, respectively; LI-COR) for 1 hour at room temperature and scanned using the Odyssey Infrared Classic Imaging System (LI-COR).

3.5. Cell differentiation protocols

3.5.1. Neural crest differentiation

Neural crest (NC) differentiation was performed as described by (Menendez et al. 2013) with some modifications. In brief, iPSCs were plated at a density of 9 x 10^4 cells/cm^2 onto Matrigel-coated plates in mTeSR medium. The following day, the medium was replaced with hESC maintenance medium: DMEM:F12 (Gibco) 1:1; 5 mg/mL Bovine Serum Albumin (BSA, Sigma); 100 U/mL penicillin/100 µg/mL streptomycin (Gibco); 2 mM GlutaMAX (Gibco); 1 x MEM non-essential amino acids (Gibco); 1 x trace element A; 1 x trace element B; 1 x trace element C (Corning); 90 µM 2-β-mercaptoethanol (Gibco); 10 µg/mL apo-transferrin (Sigma); 50 µg/mL sodium L-ascorbate (Sigma); 10 ng/mL heregulin β1 (PeproTech); 10 ng/mL activin A (PeproTech); 200 mg/mL LONG R3 IGFR (PeproTech); 8 ng/mL basic fibroblast growth factor 2 (bFGF, PeproTech). Next day, the medium was replaced with neural crest media (NC media, Table M2): hESC medium without activin and supplemented with 2 µM CHIR99021 (StemCell Technologies) and 20 µM SB431542 (StemCell Technologies), and was replaced every day. NCs were maintained in this medium and split with Accutase when necessary.

The differentiated-NC cells could be frozen and thawed, maintaining their multipotency capacity.

NC media	
DMEM/F12	1:1
BSA	5 mg/mL
Penicillin /Streptomycin	100 U/mL / 100 µg/mL
GlutaMAX	2 mM
MEM non-essential amino acids	1x
Trace element A	1x
Trace element B	1x
Trace element C	1x
2-β-mercaptoethanol	90 µM
Apo-transferrin	10 µg/mL
Sodium L-ascorbate	50 µg/mL
Heregulin β1	10 ng/mL
LONG R3 IGFR	200 ng/mL
bFGF 2	8 ng/mL
CHIR99021	2 µM
SB431542	20 µM

Table M2: Neural crest media composition.

3.5.2. Schwann cell differentiation from neural crest cells

The SC differentiation protocol was based on the described protocol by (Ziegler et al. 2011c) with some modifications.

For SC differentiation in 2D, 4 x 10^4 NC cells/cm^2 were plated onto 0.1 mg/mL Poly-L-lysine (Sigma) and 4 mg/mL Laminin (Gibco)-coated plates and cultured in SC differentiation medium (Table M3): DMEM:F12 (3:1); 100 U/mL Penicillin/100 mg/mL Streptomycin antibiotics (Gibco); 1% FBS (Gibco); 5 µM Forskolin (Sigma); 50 ng/mL Heregulin β1; and 2% N2 supplement (Gibco). The medium was replaced twice a week and samples were collected at 7, 14, and 30 days for subsequent analysis.

SC differentiation media	
DMEM:F12	3:1
Penicillin/streptomycin	100 U/mL / 100 mg/mL
FBS	1%
Forskolin	5 µM
Heregulin β1	50 ng/mL
N2 supplement	2%

Table M3: Schwann cell differentiation media composition.

For SC differentiation in 3D, 4 x 10^4 NC cells/cm^2 were plated onto 0.1 mg/mL poly-L-lysine (Sigma) and 4 mg/mL laminin (Gibco)-coated plates and cultured in SC differentiation medium. At day 5, cells were detached from plates using Accutase, counted using a hemocytometer (Neubauer chamber), and transferred into AggreWell^{TM}800 24-well plates (Stem Cell Technologies) in SC differentiation media following manufacturer's instructions. AggreWell^{TM}800 plates allow the generation of a large number of highly uniform spheroids. Each well has approximately 300 microwells allowing for the generation of 300 spheroids, and each microwell is 800 µm in size.

Briefly, AggreWell plates were treated with an Anti-Adherence Rinsing Solution (Stem Cell Technologies) to avoid cells attaching to the plate surface. 1.2 x 10^6 SC differentiating cells were transferred into a well of the AggreWell™800 24-well plate in 2 mL of SC differentiation medium and centrifuged at 100 x *g* for 3 minutes to bring cells to the bottom of microwells.

We also generated heterotypic spheroids consisting of iPSC-differentiating SC mixed with primary eFb from PNFs. Briefly, 8.4 x 10^5 of 5-day differentiating SCs were transferred together with 3.6 x 10^5 of PNF-derived eFb into AggreWell ™800 plates.

The medium was changed twice a week, removing 1 mL and replacing it with 1 mL of fresh SC differentiation media. 9 days after (a total of 14 days of SC differentiation), spheroids were collected and processed for subsequent analysis.

3.5.3. Peripheral neuronal differentiation from neural crest cells

Peripheral neuronal differentiation from NC was based on the protocol published by Menéndez et al. (2013) with small modifications. In brief, 1 x 10^5 cells/cm^2 were seeded onto Matrigel-coated plates in NC differentiation medium. Next day, the media was changed to neural differentiation media: DMEM:F12 (Gibro) 1:1, 1% N2 supplement (Gibco); 1x penicillin-streptomycin, 10ng/ mL BDNF (Peprotech), 10 ng/mL NGF (Peprotech), 10 ng/mL GDNF (Peprotech), 10ng/mL NT3 (Peprotech), 200 µM ascorbic acid (Sigma), and 0.5mM 8-Bromo-cAMP. The media was replaced every 2 days for 14 days. At this point, cells were fixed in 4% PFA for immunocytochemistry analysis.

3.5.4. Melanocyte differentiation from neural crest cells

Melanocyte differentiation from NC was performed as described by (Fukuta et al. 2014). In brief, cells were plated onto fibronectin-coated dishes in NC media supplemented with 10 µM SB432542 (StemCell Technologies) and 1 µM CHIR99021 (StemCell Technologies). Next day, the media was changed into NC differentiation media supplemented with 1 µM CHIR9902 (StemCell Technologies), 25 ng/mL BMP4 (Peprotech), and 100 nM endothelin-3 (Sigma Aldrich). The media was replaced every 2 days for 7 days. At this point, cells were fixed with 4% PFA for immunocytochemistry analysis.

3.6. Functional assays

3.6.1. Proliferation assay

2 x 10^5 iPSCs (ES4, FiPS, and iPSC) were plated onto Matrigel-coated 6-well plates in mTeSR medium. After 72h, cells were treated with 20 µM EdU for 2 hours, fixed, permeabilized, and click labeled with Alexa Fluor 488 azide using Click-iT Plus EdU Flow Cytometry Assay Kits (Thermo Fisher) according to the manufacturer protocol. Cells were also stained with propidium iodide to detect DNA content. Data was collected and analyzed using a BD LSR Fortessa SORP and BD FACSDiva 6.2 software.

3.6.2. Migration assay

5 x 10^4 NC cells per cm^2 were plated onto Matrigel–coated 6-well plates in NC media. When cells reached confluence, a scratch area was created using a sterile tip. The medium was replaced, and migration was monitored after 6 and 24 hours by microscopy. To obtain cell migration data, 9 fields covering the scratch area were imaged with a 10x objective at 0, 6, and 24 hours after the scratch. 9 images were merged using a tile scan tool from the LAS X software (Leica), and the scratch area was indicated at 6 and 24 hours.

3.6.3. Myelination assays

In vitro myelination assay was performed as described in (H. S. Kim et al. 2017b) co-culturing rat dorsal root ganglia (DRG) neurons (Innoprot, Spain) with 7-day differentiating SCs for 30 days.

In brief, 1 x 10^4 neurons were seeded onto 0.1 mg/mL Poly-L-lysine (Sigma) and 4 mg/mL Laminin (Gibco)-coated 24-well plates with DRG growth media (B-27 Plus Neuronal Culture System (ThermoFisher Scientific)) for 2 days. The media was changed to DRG differentiation media (B-27 Plus Neuronal Culture System with 1% FBS, 4 g/L glucose, and 50 ng/mL NGF) for 2 days. Then, 2 x 10^4 7-day differentiating SCs were plated on top of the neurons with DRG differentiation media for 7 days. At this point, media was replaced with DRG myelination media (DRG differentiation media plus 50 mg/L L-ascorbic acid (Sigma-Aldrich)) during 3 weeks of changing media every day. Cells were then fixed in 4% PFA for immunocytochemistry analysis.

4. Molecular biology techniques

4.1. DNA extraction from tumors and cells

Genomic DNA from tumors was extracted using the Gentra Puregene Kit (Qiagen, Chatsworth, CA) following the manufacturer's instructions, after tissue homogenization using Tissue Lyser (Qiagen). DNA was quantified with Nanodrop 1000 spectrophotometer (ThermoScientific).

Genomic DNA from primary cells, iPSCs, NC cells, and differentiating SCs was extracted using Maxwell 16 Cell DNA Purification kit (Promega) following the manufacturer's instructions in the Maxwell 16 Instrument (Promega). DNA was quantified with Nanodrop 1000 spectrophotometer (ThermoScientific).

4.2. RNA extraction from tumors and cells

Tumors were thawed in DMEM supplemented with 10% FBS, homogenized using TissueRuptor II (Qiagen), and total RNA was extracted using TriPure Isolation Reagent (Roche) following the manufacturer's instructions. RNA was quantified with Nanodrop

1000 spectrophotometer (ThermoScientific). Quality was assessed with Bioanalitzador 2200 TapeStation (Agilent).

Total RNA from primary cells, iPSCs, NC cells, and differentiating SCs was extracted using the 16 LEV simplyRNA Purification Kit (Promega) following the manufacturer's instructions in the Maxwell 16 Instrument (Promega). RNA was quantified with Nanodrop 1000 spectrophotometer (ThermoScientific).

4.3. Germline and somatic *NF1* mutation analysis

NF1 germline and somatic small pathogenic variants were detected by NF1 cDNA Sanger sequencing or by gDNA sequencing using the I2HCP NGS custom panel (Castellanos et al. 2017). Changes in copy number (mid-size deletions, exons, or larger deletions) were detected by Multiplex Ligation-dependent Probe Amplification (MLPA) analysis from PNF-derived SCs treated with 250 µg/mL Puromycin (Sigma) or PNFs DNA following Genetic Diagnostics for Hereditary Cancer Unit protocols.

4.3.1. Sanger sequencing

NF1 constitutional and somatic mutations were confirmed by DNA Sanger sequencing (GATC Biotech). Sequences were analyzed using the CLC workbench 8 software.

4.3.2. Microsatellite Multiplex PCR Analysis

Loss of heterozygosity of the *NF1* locus was detected by Microsatellite Multiplex PCR Analysis (MMPA) of chromosome 17 (Garcia-Linares et al. 2011).

In brief, 50 ng of DNA was used in the QIAGEN Multiplex PCR Kit (QIAGEN). The 10x primer mix had been prepared before in the laboratory. The PCR conditions were 15 minutes a 95ºC, 23 cycles of 30 seconds at 94ºC, 3 minutes at 56ºC, and 1 minute and 30 seconds at 72ºC, and then an additional 30 minutes at 60ºC. For 1 µl of the PCR product, 9 µl of formamide was added as well as 0.5 µl of GeneScan™ 500 LIZ™ dye Size Standard (ThermoFisher Scientific). This mixture was sent to the Translational Genomic Unit at IGTP to analyze the microsatellite amplified fragments through the ABI Prism 3130 Genetic Analyzer (ABI). Raw data was analyzed using the Peak Scanner 2.0 software. LOH was assessed by comparing microsatellite peak-heights of constitutional and tumor samples as described elsewhere (Garcia-Linares et al. 2011).

4.4. Genomic analysis

4.4.1. SNP array

Single nucleotide polymorphism (SNP)-array analysis was performed at Centre de Regulació Genòmica (CRG)-Centre Nacional d'Anàlisis Genòmics (CNAG) on selected

samples using Illumina HumanOmniExpress v1 BeadChips (730,525 SNPs). B Allele Frequency (BAF) and log R ratio (LRR) were analyzed with the R package ASCAT (Van Loo et al. 2010) to obtain loss of heterozygosity (LOH) and allele-specific copy number (CN) profiles. All samples were analyzed independently and treated as unpaired samples, using the germline genotype prediction functionality from ASCAT.

4.4.2. Exome sequencing

Exome sequencing was performed at CNAG. Exome was captured using Agilent SureSelect Human All Exon V5 kit (Agilent, Santa Clara, CA, US) according to the manufacturer's instructions and sequenced in a HiSeq instrument (Illumina) producing 100-base long paired-end reads. Reads were aligned to the hs37d5 reference genome using BWA MEM (Li H 2013) (bwa-0.7.13). After that, duplicates were marked using Picard (v2.0.1), and the Genome Analysis Toolkit (GATK) (McKenna et al. 2010)(v.3.4.46) was used for local realignment around indels. GATK's Mutect2 (Cibulskis et al. 2013) was used to detect somatic variants specific to primary tumors, SCs, and iPSC with respect to their associated eFbs. Variants were annotated using annovar (K. Wang, Li, and Hakonarson 2010)(v20160201), filtered using custom R scripts, and further validated by manual inspection.

4.4.3. Analysis of coding variation

To analyze the cell type specific expression levels in SC-eFbs co-cultures, we first determined the specific Single Nucleotide Variant (SNV) call sets: for each individual we called SNVs using Strelka2 (S. Kim et al. 2018) on whole exome sequencing (WES) data from eFbs and SCs, joined them and filtered out non-exonic variants. For each co-culture, we selected the variants with different genotypes in the SC and eFbs samples, used bam-readcount software (https://github.com/genome/bam-readcount) to determine the bases observed in each variant position on single cell-type cultures and the co-culture RNA-seq data and normalized the counts using the ratio of total sequencing data between each sample and the co-cultures. Combining the normalized single cell-type counts with the ratio of SC to eFbs determined by flow cytometry on each co-culture (section 5.3.), we constructed a virtual co-culture and by comparing it against the real co-culture we determined the impact of the co-culture in the expression levels of each variant.

4.5. RT-qPCR

The reverse transcription quantitative PCR (RT-qPCR) technique was performed to analyze gene expression. 0.5 µg of RNA was reverse-transcribed using the Superscript III reverse transcriptase enzyme (Life Technologies) according to manufacturer's instructions in the Applied Biosystems™ 2720 Thermal Cycler (Thermo Fisher Scientific). Quantitative polymerase chain reaction (qPCR) was performed with the Roche Universal Probe Library (UPL) technology and analyzed using the Light-Cycler 480 Real-Time PCR System (Roche Diagnostics). Gene expression was normalized to two selected reference

genes (*EP300* and *TBP*) and expressed as Normalized Relative Expression (NRE). Primer sequences and the specific UPL (Roche Diagnostic) used are listed in Table M4. A Microsoft Excel spreadsheet was used to analyze qPCR data for relative expression calculations (Terribas et al. 2013).

Gene	Sequence(5´-3´)		UPL
POU5F1	*Forward*	cttcgcaagccctcatttc	60
	Reverse	gagaaggcgaaatccgaag	
NGFR	*Forward*	ccttccacgctgtctcca	60
	Reverse	cctaggcaagcatcccatc	
SOX10	*Forward*	gacacggttttccacttccta	25
	Reverse	gtcctcgcaaagagtccaac	
TFAP2A	*Forward*	ggtgaaccccaacgaagtc	73
	Reverse	accgtgaccttgtacttcgag	
S100B	*Forward*	ggaaggggtgagacaagga	73
	Reverse	ggtggaaaacgtcgatgag	
CDH19	*Forward*	tgtaccagaggaaatgaatacgac	78
	Reverse	catatatgtcacctgttctttcatca	
ITGA4	*Forward*	atgcaggatcggaaagaatc	78
	Reverse	ccacaaggttctccattaggg	
PLP1	*Forward*	cttcaacacctggaccacct	60
	Reverse	ccatgggagaacaccataca	
GAP43	*Forward*	gctccaagcctgatgagc	12
	Reverse	gctctgtggcagcatcac	
EGR2	*Forward*	gctgctacccagaaggcata	60
	Reverse	ggatgaggctgtggttgaa	
PMP22	*Forward*	ctgtcgatcatcttcagcattc	29
	Reverse	agcactcatcacgcacagac	
MPZ	*Forward*	ttcccatctcctgcatcc	55
	Reverse	ctgggccacctggtagag	
EP300	*Forward*	gcagcctgcaactccact	20
	Reverse	gaggatttgatacctgtccttca	
TBP	*Forward*	aggaattgaggaagttgctgag	67
	Reverse	cgctggaactcgtctcacta	
EndoKLF4	*Forward*	agcctaaatgatggtgcttggt	68
	Reverse	ttgaaaactttggcttccttgtt	
EndoMYC	*Forward*	cgggcgggcactttg	55
	Reverse	ggagagtcgcgtccttgct	
EndoOCT4	*Forward*	gggtttttgggattaagttcttca	63
	Reverse	gccccccacccttttgtgtt	
EndoSOX2	*Forward*	caaaaatggccatgcaggtt	63
	Reverse	agttgggatcgaacaaaagctatt	
TransKLF4	*Forward*	tggactacaaggacgacgatga	60
	Reverse	cgtcgctgacagccatga	
TransMYC	*Forward*	tggactacaaggacgacgatga	77
	Reverse	gttcctgttggtgaagctaacgt	
TransOCT4	*Forward*	tggactacaaggacgacgatga	58
	Reverse	caggtgtcccgccatga	
TransSOX2	*Forward*	gctcgaggttaacgaattcatgt	57
	Reverse	gcccggcggcttca	

CRIPTO	*Forward*	cggaactgtgagcacgatgt	66
	Reverse	gggcagccaggtgtcatg	
NANOG	*Forward*	acaactggccgaagaatagca	63
	Reverse	ggttcccagtcgggttcac	
REX	*Forward*	cctgcaggcggaaatagaac	61
	Reverse	gcacacatagccatcacataagg	

Table M4: Primers for RT-qPCR. The gene, the different primer sequences, and the UPL (Roche Diagnostics) are shown in the table.

4.6. RNA-Seq

RNA-seq libraries were prepared in the IGTP Genomics Core Facility using the TruSeq stranded mRNA Illumina, quantified with the KAPA library quantitation kit for Illumina GA and the Agilent Bioanalyzer, and sequenced at CNAG in a HiSeq platform pooling 3 samples per lane (paired-end, 2x100).

4.6.1. Differential gene expression analysis

RNA-seq data were aligned with Salmon v1.1.0 (Patro et al. 2017) for differential expression analysis, and with STARv2.7.1a (Dobin et al. 2013) for variant analysis against the reference genome and transcriptome (GRCh38 and gencode).

We used DESeq2 (Love, Huber, and Anders 2014) to perform differential expression analysis between samples. Quality control was performed using principal component analysis (PCA) representation of the samples. We used clusterProfiler (Yu et al. 2012) to perform Gene Ontology (GO) and KEGG pathways enrichment on differentially expressed genes with p-adjusted value below 0.05.

4.6.2. Selection of timepoint specific markers

We used DESeq2 with the standard Wald test to determine the differentially expressed genes (DEG) between all timepoints. Genes that were significantly up-regulated (log fold-change > 0) in a timepoint when compared to all others were deemed stage-specific markers.

4.6.3. Virtual co-cultures versus real co-cultures

To obtain the set of DEG between virtual and real co-cultures, we randomly sampled reads from BAM files after alignment with STAR v2.7.1a of the single cell-type cultures and mixed them following the exact proportions of SCs and eFbs calculated by flow cytometry for each combination. These virtual co-cultures represented the transcriptional profiles we would observe in the co-cultures if there was no transcriptional change due to the interaction between SC and eFb. We then performed differential gene expression analysis (as explained in 4.6.1.) between the virtual co-

culture and the real co-culture to obtain the genes that were differentially expressed due to the SC-eFb interaction.

4.7. Single-cell RNA-seq

4.7.1. Sample preparation

PNFs were thawed and digested, as explained in section 2.1.1.

After counting the cells, the Dead Cell Removal MicroBeads kit (Miltenyi Biotec) was used to get rid of dead cells, following the manufacturer's instructions.

Cells were resuspended in DMEM + 10% FBS + 1x GlutaMAX and transported in ice to the CNAG in less than two hours after cell suspension preparation. At CNAG, cell viability was calculated with the TC20™ Automated Cell Counter (Bio-Rad. Samples were filtered with a 40 µm filter before entering into the Chromium Single Cell Gene Expression (10X Genomics). This technology allowed the study of transcriptome 3' in thousands of single cells.

4.7.2. Analysis

We were able to analyze the expression of more than 2000 genes in 5087, 6155, and 9092 single cells in 19PNF, 20PNF1, and 23PNF, respectively. We used singleR (Aran et al. 2019) to identify clusters of cells representing different cell types composing PNFs. SingleR takes advantage of reference transcriptomic datasets of pure cell types (HumanPrimaryCellAtlas) to infer the cell type identity of every single cell independently.

5. Flow cytometry

5.1. Flow cytometry of p75 and Hnk1

For flow cytometry analysis of p75 and Hnk1, cells were dissociated with Accutase, washed with 1% BSA (Sigma) in PBS, incubated for 30 minutes on ice with unconjugated primary antibody p75 (see Table M5), washed with 1% BSA in PBS, incubated with Alexa Fluor 568-conjugated secondary antibodies 1:1000 (Thermo Fisher Scientific) for 30 minutes on ice and protected from light. After this step, every single step was performed, protecting cells from light. Then cells were incubated with unconjugated primary antibody Hnk1 (see table 2) for 30 minutes on ice, washed with 1% BSA in PBS, incubated with Alexa Fluor 488-conjugated secondary antibodies 1:1000 (Thermo Fisher Scientific) for 30 minutes on ice, washed with 1% BSA in PBS and resuspended in 1% BSA in PBS. Every centrifugation was performed at 300 g for 2 minutes at 4ºC in the 5415R Refrigerated Centrifuge (Eppendorf). Cells were resuspended in 100 µL of 1% BSA in PBS and analyzed by flow cytometry using BD LSR Fortessa SORP and BD FACSDiva 6.2 software.

5.2. Flow cytometry of p75 and S100B in neurofibromas

For flow cytometry analysis of p75 and S100B in neurofibroma-derived cells, neurofibroma pieces were digested with 160 U/mL collagenase type 1 and 0.8 U/mL dispase (Worthington, Lakewood, NJ) for 18 hours at 37ºC. After that, the cell suspension was passed through a glass pipette around 10 times to obtain a single-cell suspension. Once a single-cell suspension was obtained, the same protocol described in 5.2 was used. At least 125,000 cells were used as cell control, 500,000 cells for fixing, permeabilizing, and secondary antibodies control, and 1,000,000 cells for immunostaining. At least 100 cells were counted in each p75+/S100B-, p75+/S100B+, p75-/S100B+, and p75-/S100B- cell populations.

5.3. Flow cytometry of p75 in single cNF-derived cultures and co-cultures

For flow cytometry analysis of p75 in primary single SC and eFb cultures and SC-eFb co-cultures, cells were detached with 0.25% Trypsin-EDTA. Once a single-cell suspension was obtained, the protocol described in 5.2 was used without permeabilization, primary S100B antibody incubation, nor secondary antibody incubation steps.

6. Immunochemistry

6.1.1. Fluorescent immunocytochemistry of cells

Cells were grown in 8-well tissue culture chambers (Sarstedt) and fixed in 4% PFA (Chem Cruz) for 15 minutes at room temperature, permeabilized with 0.1%Triton-X 100 in PBS for 10 minutes at room temperature, blocked in 10% FBS in PBS for 15 minutes at room temperature, and incubated with the corresponding primary antibodies (see Table M5) overnight at 4ºC. Secondary antibodies were Alexa Fluor 488- and Alexa Fluor 568- 1:1000 (Thermo Fisher Scientific). Nuclei were stained with DAPI (1:1000, Stem Cell Technologies, 1:1000). Slides were mounted with Vectashield (Vector laboratories), and coverslips were secured with a polish nail. Images were captured using the DMI 6000B microscope (Leica) and the LAS X software (Leica).

6.1.2. Fluorescent immunocytochemistry of spheroids

Spheroids were fixed in 4% PFA for 30 minutes at room temperature. The staining protocol was the same as in 6.1.1. The only difference was that all incubations, spheroids were maintained in suspension, and when the slides were mounted with Vectashield (Vector laboratories), spheroids were squashed with the coverslips.

Confocal images from spheroids were captured using the Axio Observer Z1 Confocal LSM 710 microscope and the ZEN Black 2012 software (Zeiss).

6.1.3. Fluorescent immunohistochemistry of S100B for paraffin samples

Tissue samples were fixed in formalin, embedded in paraffin, and cut into 5 µm sections. Sections were rehydrated, immersing the slides in: xylene 2 times for 10 minutes, 100% ethanol 2 times for 10 minutes, 95% ethanol for 5 minutes, 70% ethanol for 5 minutes, 50% ethanol for 5 minutes, and rinsing with deionized H_2O, and rehydrating with PBS for 10 minutes. Antigen retrieval was performed with citric acid 10 mM pH=6 supplemented with 0.05% Tween-20 for 10 minutes at 100ºC. Slices were rinsed twice with PBS for 5 minutes and tissue sections were then surrounded with a hydrophobic barrier using a PAP pen, incubated with blocking buffer (1% BSA with 10% goat serum (Gibco) in PBS) for 1 hour at room temperature, and incubated with primary S100B antibodies diluted in incubation buffer (1% BSA with 10% goat serum in PBS and 0.3% TritonX100) overnight at 4ºC. Then, slides were washed 3 times for 15 minutes each in PBS1X, incubated with secondary antibodies (Alexa Fluor 568 anti-rabbit, 1:1000) diluted in incubation buffer for 45 minutes at room temperature protected from light, and washed 3 times for 15 minutes each in PBS protected from light. The tissue sections were incubated with DAPI (Stem Cell Technologies, 1:1000) diluted in PBS for 10 minutes at room temperature protected from light. Then, tissue sections were rinsed 1 time with PBS, and slides were mounted with Vectashield (Vector laboratories) and coverslips were secured with a polish nail. Images were captured using the DMI 6000B microscope (Leica) and the LAS X software (Leica).

6.1.4. Fluorescent immunohistochemistry of hNu for OCT samples

Tissue samples were fixed in 4% PFA overnight at 4ºC. Then samples were incubated in 15% sucrose solution until tissue shrinked and in 30% sucrose solution overnight at 4ºC. Samples were then embedded in optimal cutting temperature (OCT) compound (VWR) and frozen at −80 °C. 5 µm OCT slices were cut for subsequent staining. OCT was removed by PBS washing, and tissue sections were surrounded with a hydrophobic barrier using a PAP pen and permeabilized in 0.3% TritonX100 in PBS for 30 minutes. After, samples were incubated in blocking buffer (0.1% TritonX100, 1% BSA with 10% goat serum (Gibco) in PBS) for 1 hour at room temperature. Then, tissue sections were incubated with primary hNu antibodies diluted in incubation buffer (0.1% TritonX100, 1% BSA with 10% goat serum in PBS) overnight at 4ºC. Tissue sections were then washed 3 times for 15 minutes each in PBS1X and incubated with secondary antibodies (Alexa Fluor 488 anti-mouse, 1:1000) diluted in incubation buffer 2 hours at room temperature protected from light. Tissue sections were washed 3 times for 15 minutes each in PBS1X protected from light. The tissue sections were incubated with DAPI (Stem Cell Technologies, 1:1000) diluted in PBS1X for 10 minutes at room temperature protected from light. Tissue sections were rinsed 1 time with PBS, mounted with Vectashield (Vector laboratories), and coverslips were secured with a polish nail. Images were captured using the DMI 6000B microscope (Leica) and the LAS X software (Leica).

Antibody	Supplier	Reference	Dilution
Mouse IgG anti-OCT3/4	Santa Cruz Biotechnology	Sc-5279	1:60
Rabbit IgG anti-SOX2	Pierce Antibodies	PA1-16968	1:100
Goat IgG anti-NANOG	R&D Systems	AF1997	1:25
Rat IgM anti-SSEA3	Hybridoma Bank	MC-631	1:3
Mouse IgG anti-SSEA4	Hybridoma Bank	MC-813-70	1:3
Mouse IgM anti TRA-1-81	Millipore	MAB4381	1:200
Rabbit IgG anti-α-1-fetoprotein	Dako	A0008	1:400
Goat IgG anti-FOXA2	R&D Systems	AF2400	1:50
Rabbit IgG anti-GATA4	Santa Cruz Biotechnology	sc-9053	1:50
Mouse IgG anti-α-SMA	Sigma	A5228	1:400
Mouse IgM anti-ASA	Sigma	A2172	1:400
Mouse IgG anti-TUJ1	Bio Legend	MMS-435P	1:500
Rabbit IgG anti GFAP	Dako	Z0334	1:500
Rabbit IgG anti NF200	Sigma	N4142	1:100
Mouse IgG anti-Nerve growth factor (p75) receptor	Abcam	AB-N07	1:100 (ICC), 1:50 (IHC) 1:1000 (Flow cytometry)
Rabbit IgG anti-S100B	Dako	Z0311	1:1000 (ICC, IHC, and flow cytometry
Mouse IgG anti-AP2	Thermo Scientific	MA1-872	1:50
Rabbit IgG anti-Sox10	Abcam	ac108408	1:100
Mouse IgG anti-GFAP	Abcam	ab10062	1:500
Mouse IgG anti-MBP	Abcam	ab62631	1:500
Rabbit IgG anti-PLP	Abcam	ab28486	1:100
Rabbit IgG anti-GAP43	Novus Biologicals	NB300-143SS	1:500
Mouse IgG anti-Ki67	Santa Cruz Biotechnology	sc-23900	1:50
Mouse IgG anti-nuclear antigen (hNu)	Novus Biological	235-1	1:100

Table M5: Antibody list. The antibody, the supplier, the reference number and the specific dilution used. ICC: immunocytochemistry. IHC: immunohistochemistry

7. Luminex xMAP technology

Supernatants to be analyzed by Luminex Technology were collected 72 hours post-seeding the cells and transferred into clean polypropylene microcentrifuge tubes. Supernatants were centrifuged at 14,000 rpm for 10 minutes at 4ºC in the 5415R refrigerated centrifuge (Eppendorf) to remove any cellular debris. The clarified mediums were aliquoted into clean polypropylene microcentrifuge tubes. These samples were stored at -80ºC until used.

The day of the analysis, frozen samples were thawed on ice and centrifugated at 14,000 rpm for 10 minutes at 4ºC.

All supernatants from SCs, eFbs, and SC-eFb co-cultures were analyzed using the Luminex xMAP technology. The Luminex based Millipore's MILLIPLEX kits that were used were the following: the Human Neurodegenerative Disease Magnetic Bead Panel 3 (to analyze

BDNF, sICAM-1, and NCAM), the Human Neurodegenerative Disease Magnetic Bead Panel 4 (to analyze S100B and GDNF), and the Human Cytokine/Chemokine Magnetic Bead Panel (to analyze EGF, FGF2, Eotaxin, TGFα, G-CSF, fractalkine, MCP-3, PDGF-AA, IL-1α, IL-1β, IL-6, IL-8, CXCL10, MCP-1, MIP-1α, RANTES, and VEGF).

All procedures were performed following the manufacture's guidelines. All plates were run on Luminex 200 with xPONENT software (Luminex).

8. *In vivo* experiments

8.1. Mice

Both engraftment experiments were carried out in collaboration with Conxi Lázaro's group in the animal facilities of Institut Català d'Oncologia (ICO)-Institut d'Investigació Biomèdica de Bellvitge (IDIBELL). Juana Fernández-Rodrígued performed the manipulacion of the laboratory animals.

8.1.1. Engraftment 1

Six-week-old male nude Harlan mice were used. 2 x10^6 cells resuspended in 100 µL SC differentiation medium of control *NF1*(+/+) FiPS and the *NF1*(-/-) 5PNFiPS and the *NF1*(-/-) 3PNFiPS at NC stage, and 7 and 14 days of SC differentiation were injected into the exposed sciatic nerve of the mice using a 27G syringe. There were 2 mice per experimental condition; each mouse received two injections, one in the right sciatic nerve and the other in the left sciatic nerve making a total of 4 injections per group.

Tumor growth was monitored by manual palpation throughout the experiment.

After 4 months, mice were euthanized, and tumor samples were extracted and fixed for paraffin inclusion and immunohistochemical analysis.

8.1.2. Engraftment 2

Six-week-old male nude Harlan mice were used. Spheroids, containing approximately 2 million cells, were resuspended in 1:2 diluted Matrigel (in a total volume of 70 µL SC differentiation medium) and injected into the exposed sciatic nerve of the mice. Spheroids were injected using a 25 G syringe, which did not disrupt spheroid structure.

We engrafted a *NF1*(+/+) control cell line and 3 independent *NF1*(-/-) cell lines. For each cell line, we engrafted homotypic and heterotypic spheroids. As *NF1*(+/+) homotypic spheroids could not be generated; instead, we injected *NF1*(+/+) heterotypic spheroids as controls. PNF-derived eFbs used for the formation of spheroids were also injected, to control their capacity to engraft and generate cell growth as single cultures.

Tumor growth was monitored throughout the experiment by manual palpation.

After 4 months, mice were euthanized, and legs were dissected. Tumor samples were split into different parts: one for fixation and paraffin embedding, one for DNA extraction, and one piece to cryopreserve.

All tumors were embedded in paraffin, cut into 5 µm slices, and Hematoxylin & Eosin (H&E) staining in the IGTP-Hospital Universitari Germans Trias i Pujol (HUGTP) Biobank using standard protocols.

Immunohistochemistry of S100B and SOX10 was carried out in the Department of Anatomical Pathology of the HUGTP using standard protocols and antibodies from Table M5.

Results

1. Development of an iPSC-based cellular model for neurofibromas

1.1. Generation of *NF1*(-/-) iPSC lines by reprogramming PNFs

Plexiform neurofibromas (PNFs) originate during development through the inactivation of the *NF1* gene in a cell from the neural crest-Schwann cell (NC-SC) lineage. There is a need to establish a PNF model in which the different NC-SC stages are considered. The reprogramming of PNF-derived cells seemed a reasonable strategy to develop a PNF model in order to study the precise cell type that originates them.

We obtained five different PNFs from five independent NF1 patients diagnosed according to the standard diagnostic criteria (DeBella, Szudek, and Friedman 2000). The age at tumor resection were 8, 10, 33, 66, and 14 years old for code-named samples 3PNF, 5PNF, 6PNF, 7PNF, and 13PNF, respectively. 3PNF and 5PNF correspond to a girl and boy patients while 6PNF, 7PNF, and 13PNF correspond to two women and a teenage boy. Histological information of these tumors has already been published by our group (Carrió et al. 2018b).

PNFs are heterogeneous tumors composed mainly of Schwann cells (SCs) and endoneurial fibroblasts (eFbs). SCs harbor mutations inactivating the two *NF1* alleles, the constitutional and the somatic mutation, while eFbs, like all other cells in the patient, harbor only the constitutional mutation. To generate induced pluripotent stem cells (iPSCs) with different *NF1* genotypes, we first identified the *NF1* constitutional mutation of each patient and the *NF1* somatic mutation of each PNF, through a combination of cDNA Sanger sequencing, DNA copy-number Multiplex Ligation dependent probe amplification (MLPA) analysis (L. M. Messiaen and Wimmer 2008) and DNA Next Generation Sequencing (NGS) panel (Castellanos et al. 2017). In Table R1 there is a summary with the clinical and genetic information of the different PNFs.

After the identification of both mutations, tumors were dissociated enzymatically to obtain a cell suspension that was seeded for reprogramming either (i) after the establishment of specific SC and eFb cultures or (ii) directly from PNF digested cells (Figure R1). In both strategies, isogenic *NF1*(-/-) and *NF1*(+/-) iPSCs could be generated and identified by genetic analysis. There is a summary of the iPSC clones obtained using both strategies in Table R2. Although we tried both integrative and non-integrative reprogramming strategies, in this thesis, we only used iPSCs generated with non-integrative Sendai virus.

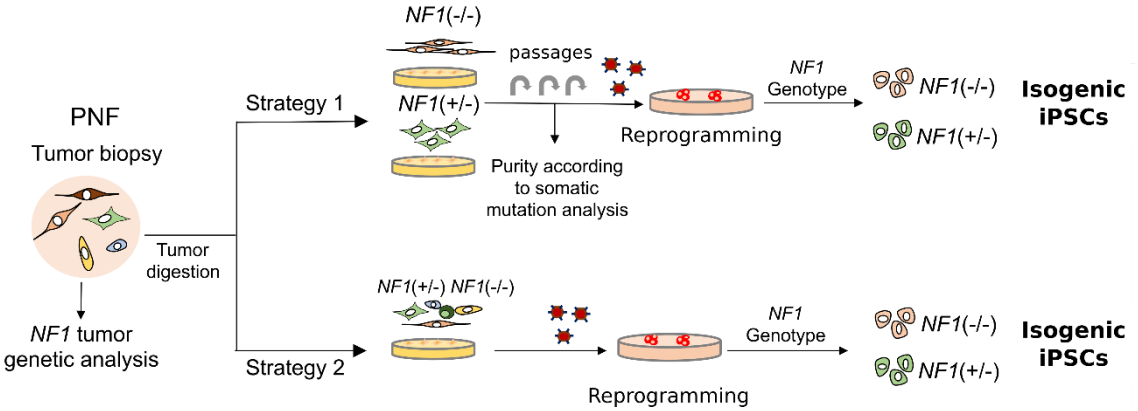

Figure R1. Schematic representation of the two different strategies used to generate isogenic iPSC from plexiform neurofibromas. In strategy 1, the generation of iPSCs was through the reprogramming of cultures of specific cell types. In strategy 2, PNF digested cells were directly reprogrammed.

Patient information				*Tumor information*			*iPSC lines generated*	
Patient ID	Sex	Age (at pNF resection)	*NF1* constitutional mutation	Tumor ID	Diagnostic	*NF1* somatic mutation	iPSC line (named in the thesis)	iPSC line (banking name)
3	XX	8	c.3943C>T; p.Gln1315*	3PNF	PNF with a diffuse extraneural invasion	LOH (HR) Whole ch.17q	*NF1*(+/-) 3PNFiPS	3PNF_FiPSsv_PM
							NF1(-/-) 3PNFiPS	3PNF_SiPSsv_MM
5	XY	10	Intragenic deletion (E16-35)	5PNF	PNF with a diffuse extraneural invasion	LOH (3,8Mb del)	*NF1*(+/-) 5PNFiPS	5PNF_TDiPSsv_PM
							NF1(-/-) 5PNFiPS	5PNF_TDiPSsv_MM
6	XX	33	c.2946delT; p.Leu983*	6PNF	PNF with a diffuse extraneural invasion	c.2033dupC; p.Ile679Aspfs*21	*NF1*(+/-) 6PNFiPS	6PNF_SiPSrv_PM
7	XX	66	c.2033dupC; p.Ile679Aspfs*21	7PNF	PNF with a diffuse extraneural invasion	LOH (1,4Mb del)	*NF1*(+/-) 7PNFiPS	7PNF_TDiPSrv_PM
13	XY	14	c.1318C>T; p.Arg440*	13PNF	PNF with a diffuse extraneural invasion	LOH (HR) Whole ch.17q	*NF1*(+/-) 13PNFiPS	Not banked

Table R1. Clinical data from Neurofibromatosis type 1 patients, plexiform neurofibromas, and iPSC lines generated. For patient information, patient ID, sex, age at PNF resection, and *NF1* constitutional mutations are provided. For tumor information, tumor ID, diagnostic data of the tumor, and *NF1* somatic mutations are provided. For the iPSC lines generated, iPSC line (named in the thesis) and iPSC line (banking name) are provided. LOH: loss of heterozygosity. HR: homologous recombination.

Reprogramming strategy		Tumor	Clones	*NF1* genotype	
				NF1(+/-)	*NF1*(-/-)
Digested		3PNF	-	-	-
		5PNF	12	1	11
		13PNF	27	27	0
		6PNF	10	10	0
		7PNF	-	-	-
Cultured	Schwann cells	3PNF	22	0	22
		5PNF	2	0	2
		13PNF	40	40	0
		6PNF	10	10	0
		7PNF	12	12	0
	Endoneurial fibroblasts	3PNF	-	-	-
		5PNF	0	0	0
		13PNF	11	11	0
		6PNF	1	1	0
		7PNF	1	1	0
	Skin fibroblasts*	3PNF	16	14	2

Table R2. Plexiform neurofibromas used in each reprogramming strategy, either through direct reprogramming or establishment of primary Schwann cell cultures, endoneurial fibroblast cultures, or skin fibroblast cultures. The number of iPSC clones analyzed is shown as well as the specific genotype of those: *NF1*(+/-) or *NF1*(-/-). The skin sample used to establish the skin fibroblast culture was covering the PNF. When the skin was separated, part of the tumor was still left. - Not reprogrammed.

1.1.1. iPSC characterization

1.1.1.1. Standard iPSC characterization

Reprogramming and standard characterization of the different iPSC clones were performed at the Centre de Medicina Regenerativa de Barcelona (CMRB) in collaboration with Dr. Angel Raya's laboratory.

From 3PNF and 5PNF, we were able to obtain isogenic *NF1*(+/-) and *NF1*(-/-) iPSC lines. The work presented in this thesis will be focused on these iPSC lines.

Selected iPSC clones were expanded and further characterized to confirm they were *bona fide* iPSCs: ensuring the expression of pluripotent markers and the capacity to differentiate into the three germ layers.

The characterization of the different 3PNF and 5PNF iPSC clones showed that they displayed a compact embryonic stem cell-like morphology, were positive for alkaline phosphatase, and expressed high levels of the pluripotency markers NANOG, OCT4, SOX2, TRA181, SSEA3, and SSEA4 (Figure R2A, B).

Further pluripotency characterization was performed differentiating the iPSC lines into the three germ layers ectoderm, endoderm, and mesoderm and that were stained respectively for the ectoderm markers TUJ1, and GFAP, for the endoderm markers AFP, and FOXA2; and for the mesoderm markers aSMA and GATA4 (Figure R2C).

Moreover, iPSC lines, when injected into mice, formed teratomas exhibiting differentiation towards ectoderm, endoderm, and mesoderm, also analyzed with the same markers (Figure R2D). The iPSC lines also showed demethylated CpG islands in *NANOG* and *POU5F1* promoters and karyotype stability after more than 15 passages (Figure R2E, F).

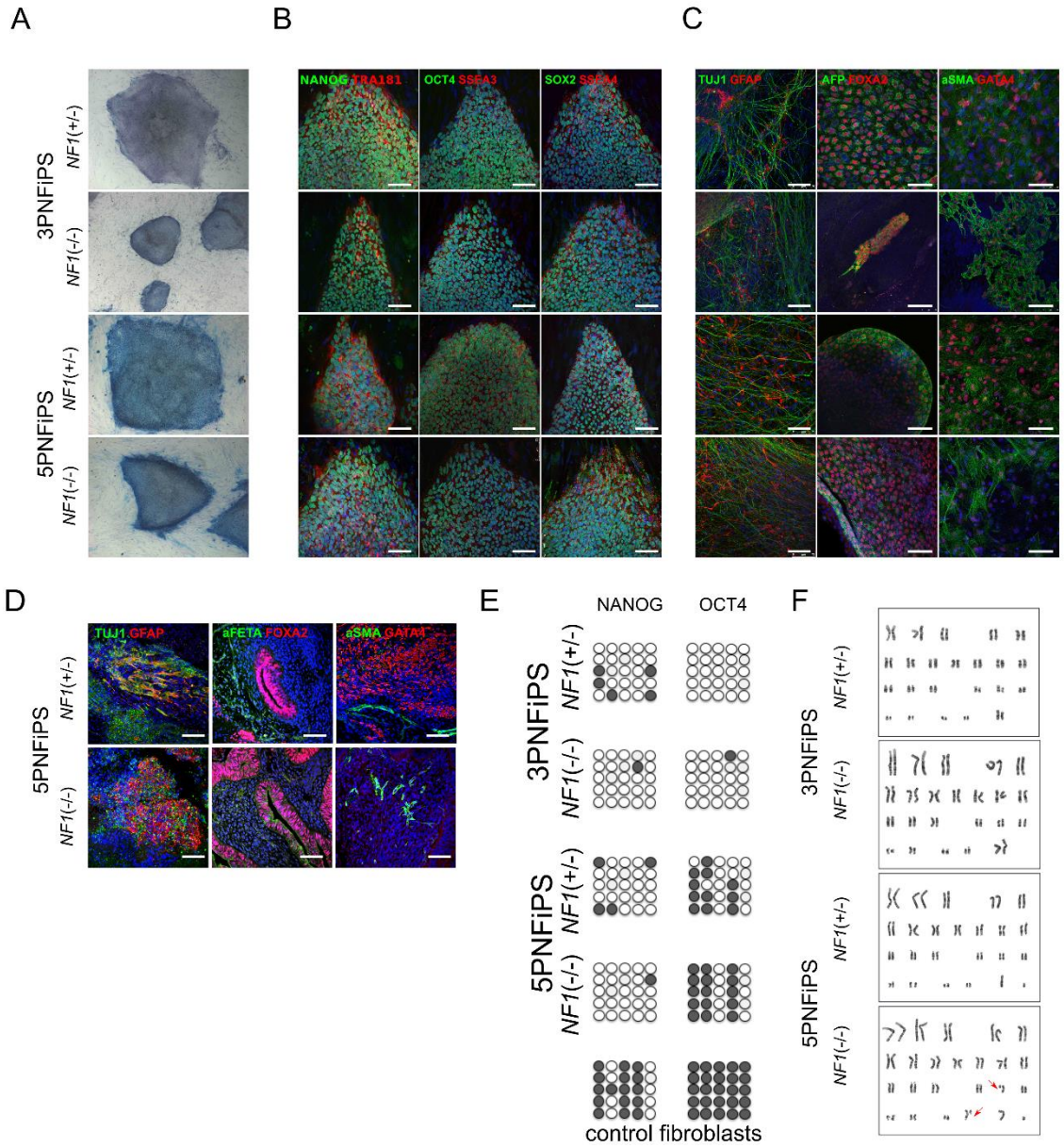

Figure R2. Standard characterization of plexiform neurofibromas-derived iPSC lines. A) Morphology and alkaline phosphatase staining of 3PNF and 5PNF iPSC colonies. Scale bars, 100 µm. **B)** Characterization of pluripotency markers. Representative images of 3PNF and 5PNF iPSC colonies stained positive for the pluripotency-associated markers NANOG, OCT4, and SOX2 (in green), and TRA-1-81, SSEA3, and SSEA4 (in red). Scale bars, 100 µm. **C)** *In vitro* differentiation potential of 3PNF and 5PNF iPSC lines. Generation of cell derivatives of the three primary germ layers, including ectoderm (TUJ1 in green and GFAP in red), endoderm (AFP in green and FOXA2 in red), and mesoderm (SMA in green and GATA4 in red). Scale bars, 100 µm. **D)** Teratoma formation from 5PNF iPSC, showing their differentiation toward ectoderm (TUJ1 in green and GFAP in red), endoderm (AFP in green and FOXA2 in red), and mesoderm (SMA in green and GATA4 in red). Scale bars, 100 µm. **E)** Bisulfite sequencing showing demethylation of the CpG islands in *NANOG* and *POU5F1* promoters in the 3PNF and 5PNF iPSC lines. **F)** Karyotype of 3PNF and 5PNF iPSC lines at passage 20.

1.1.1.2. Functional and genomic iPSC characterization

Further functional and genomic characterization of iPSC lines was performed in our lab at Institut de Recerca Germans Trias i Pujol (IGTP).

We analyzed neurofibromin expression through Western Blot. We confirmed that *NF1*(-/-)iPSCs did not express neurofibromin and that *NF1*(+/-)iPSCs expressed some levels, although less than control *NF1*(+/+) embryonic stem cell 4 (ES4) or fibroblast induced pluripotent stem cells (FiPS), used as control pluripotent cells (Figure R3A)

To study the effect of the *NF1* status on iPSC proliferation, we used flow cytometry-based Click-iT EdU assay. Interestingly, the *NF1*(-/-)iPSC lines exhibited a 10-15% significant increase in proliferation rate compared to *NF1*(+/+) cell lines. *NF1*(+/-)iPSC lines also showed a significantly increased proliferation rate, although it was not as pronounced as in *NF1*(-/-)iPSCs (Figure R3B). These results indicate that cell proliferation in pluripotent stem cells (PSC), as is the case for somatic cells, is influenced by neurofibromin activity.

To characterize the genomic structure of the iPSC lines generated, Single Nucleotide Polymorphism (SNP)-array analysis was performed in PNFs, PNF-derived SCs, PNF-derived eFbs, and iPSC lines. Figure R3C shows results from 3PNF (results from 5PNFs can be found in Annex 3: S3 from supplementary information). B allele frequency (BAF) and log2 ratio were calculated, and copy number estimation was performed. The genome of all samples was mostly 2n. SNP-array analysis showed the detection of somatic *NF1* mutations in 3PNF (copy neutral (CN) loss of heterozygosity (LOH) of 17q) and 5PNF (LOH due to a large deletion at 17q).

Indeed, in 3PNF there was a region in which the BAF was not around 0.5. This region (blue-shaded in Figure R3C) showed a somatic CN-LOH. Somatic *NF1* inactivation was produced by mitotic recombination generating CN-LOH in 17q and the reduction to homozygosity for the constitutional *NF1* mutation. LOH was observed in 3PNF and in 100% of cells in 3PNF-derived SCs and *NF1*(-/-) 3PNFiPS. 3PNF-derived eFb culture was an early passage and still exhibited a residual LOH due to the presence of ‘‘contaminating’’ neurofibroma SCs.

To identify the presence of small pathogenic variants in the generated iPSC lines, exome sequencing was performed for PNFs, PNF-derived SCs, and *NF1*(+/-) and *NF1*(-/-) 3PNFiPSC or 5PNFiPSC lines (Figure R3D). On average, we identified around ten additional point mutations in the iPSC lines generated not present in PNFs nor in PNF-derived SCs. Since iPSCs result from the clonal expansion of a single reprogrammed cell, these results agreed with the clonal expansion of a cell already harboring these mutations. None of the detected somatic mutations were recurrent among the PNFs analyzed (data not shown).

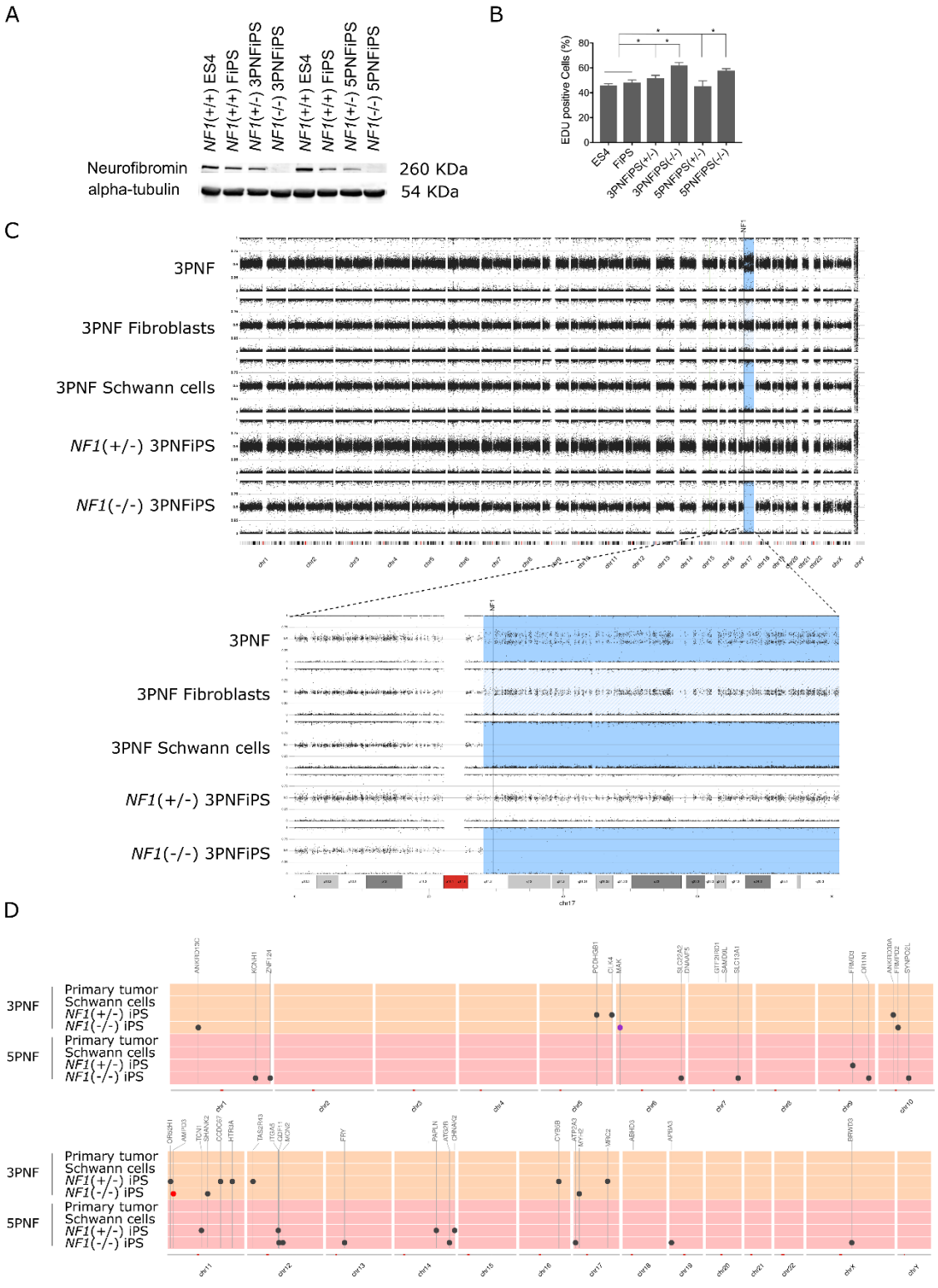

Figure R3. Functional and genomic characterization of iPSC lines. A) Western blot analysis of neurofibromin in the iPSC lines generated. This Western blot showed the absence of neurofibromin in *NF1*(-/-) 3PNFiPS and 5PNFiPS. The human embryonic stem cell (hESC) line ES4 and a control iPSC line generated from foreskin fibroblasts (FiPS), both *NF1*(+/+), were used as control cell lines. **B)** Proliferation capacity of 3PNF and 5PNF iPSC lines assessed by Click-iT EdU Flow Cytometry Assay. Double-positive cells (in S phase) are represented in the graph. Bars represent means from three independent experiments. *p < 0.05 (unpaired t-test). **C)** Genomic

structure of five samples associated with a 3PNF tumor characterized through an SNP array analysis. B allele frequency (BAF) data from SNP array analysis is shown for 3PNF, 3PNF-derived eFbs, 3PNF-derived SCs, and 3PNF-derived iPSC lines. The genome of all samples was mostly 2n. A blue-shaded region indicates somatic CN-LOH. A detailed view of BAF for chromosome 17 is shown below. Somatic *NF1* inactivation was produced by mitotic recombination generating CN-LOH in 17q and a reduction to homozygosity for the constitutional *NF1* mutation. LOH was observed in 3PNF and in 100% of cells in 3PNF-derived SC and *NF1*(-/-) 3PNFiPS. D) Summary of somatic exonic variants identified by exome sequencing. All samples associated with a PNF are represented by a wide horizontal line of the same color covering all chromosomes. Color dots indicate the type of genetic variant: missense (black), frameshift (orange), in-frame deletion (purple), and non-sense (red). The position of genes containing the variants is marked with vertical lines.

1.2. Establishment of *in vitro* neural crest-Schwann cell differentiation protocols from iPSCs

To establish a PNF model using PNF-derived iPSCs, adequate differentiation protocols towards the NC-SC lineage were needed since PNFs develop when *NF1* is lost in a precursor cell belonging to this lineage.

The generation of an *in vitro* NC-SC differentiation protocol required a two-step protocol: first, pluripotent stem cells (PSC) were differentiated into neural crest (NC) stem cells which can be maintained in a multipotent state. Second, NC stem cells were differentiated into SCs. These two differentiation protocols are shown one at a time.

1.2.1. Establishment of an *in vitro* neural crest differentiation protocol

1.2.1.1. Set up of a protocol for the generation of neural crest cells from *NF1*(+/+) iPSCs

We used a protocol developed in Stephen Dalton's lab (Menendez et al. 2011) to generate NC stem cells from iPSC lines, with some modifications (see Materials & Methods). This protocol uses chemically defined conditions to activate the canonical Wnt signaling simultaneously with the suppression of TGFβ-dependent signaling.

To generate NC cells, control *NF1*(+/+) PSC (ES4 and FiPS) were seeded on Matrigel and cultured with NC induction media for 20 days. Approximately 4 days after NC induction, cells started losing their colony morphology, and 12 days after, cells started adopting a stellate morphology typical of NC cells (Figure R4A). Cells were maintained in NC media and passaged using Accutase when reaching confluency.

These differentiated-NC cell population could be expanded in culture, frozen and thawed, maintaining their multipotency capacity.

We first established this protocol with control *NF1*(+/+) cells and then applied it to *NF1*(+/-) and *NF1*(-/-) iPSC lines (see below).

1.2.1.2. Characterization of neural crest lineage markers in differentiating *NF1*(+/+) pluripotent stem cells

To validate the NC differentiation protocol, we characterized the expression of different NC markers as p75 (*NGFR* gene), Hnk1 (*B3GAT1* gene), *SOX10*, and the *TFAP2α* through flow cytometry analysis, immunocytochemistry, and RT-qPCR.

Approximately 20% of control differentiated NC cells at passage 1 already acquired both p75 and Hnk1 markers, and at passage 4-5, approximately 90% of cells expressed both markers, constituting a highly homogenous population (Figure R4B).

We performed immunocytochemistry analysis, and a high proportion of differentiated NC cells expressed p75 (corroborating flow cytometry results), and the two transcription factors AP2α and SOX10 (Figure R4C). We also characterized the expression of these markers by RT-qPCR, confirming their expression (Figure R4D). Importantly, control differentiated NC cells did not express the pluripotent marker *POU5F1*, neither the SC lineage marker *S100B*, confirming NC identity.

Thus, *NF1*(+/+) differentiated NC cell lines (ES4 and FiPS) expressed lineage-specific NC markers homogeneously and robustly.

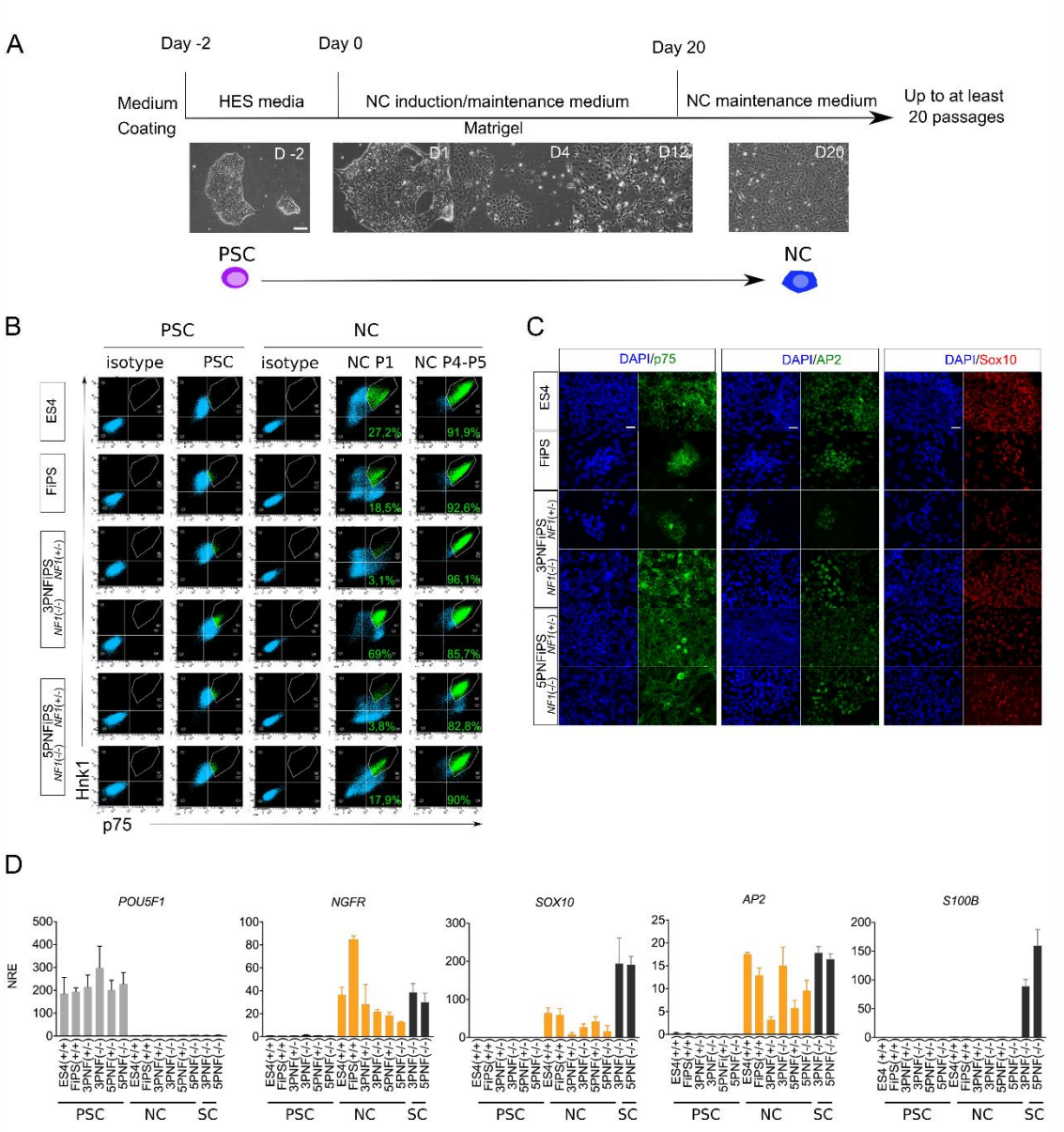

Figure R4. Neural crest differentiation from pluripotent stem cells. A) Schematic representation of the protocol used for differentiating pluripotent stem cells (PSCs) into neural crest (NC) cells. Control *NF1*(+/+) ES4 and FiPS and *NF1*(+/-) or *NF1*(-/-) PNF-derived iPSCs were seeded on Matrigel and cultured in NC induction medium for 20 days. Representative bright-field images of a control line are shown during the differentiation process. Scale bar, 50 µm. **B)** Flow cytometry analysis for p75 and Hnk1 markers before and after NC differentiation. The percentage of double p75 and Hnk1-positive cells is shown inside the graph in green. P1, passage 1; P4-5, passages 4–5. **C)** Immunocytochemistry analysis showing that both control *NF1*(+/+) ES4 and FiPS and PNF-derived iPSCs differentiated to NCs (passage 5) express p75 (green), AP2 (green), and SOX10 (red). DAPI was used to stain cell nuclei. Scale bar, 50 µm. **D)** RT-qPCR expression analysis of pluripotent (*POU5F1*), NC (*NGFR*, *SOX10*, *AP2*), and SCs (*S100B*) markers, in PSCs, PSCs differentiated to NCs and PNF-derived primary SCs. qRT-PCR values are expressed as the mean normalized relative expression (NRE) ± SEM from three independent differentiation experiments. SC: Schwann cells.

1.2.1.3. Functional assays for neural crest characterization

To test NC function, we assessed the differentiation potential of the generated NC and their migration capacity.

First, we differentiated the ES4-derived NC cells into known NC-derivatives like melanocytes and peripheral neurons and performed immunocytochemistry with specific markers for both cell types.

Differentiation of ES4-derived NC into peripheral neurons was highly efficient, showing a high amount of the neuronal marker Tuj1 (neuron-specific tubulin) and the classical neuron morphology (Figure R5A).

Differentiation of NC cells towards melanocytes was not as efficient as for peripheral neurons. However, we were able to detect cells co-expressing both markers S100B and MelanA, two specific markers of melanocytes (Figure R5B). These results corroborated the multipotency capacity of PSCs.

To assess for another functional characteristic of NC cells, we studied their migration capacity through a scratch assay. In this case, a scratch was performed with a pipette-tip when cultures were 100% confluent, and migration capacity was measured, taking pictures of the same gap region after 6h, and 24h (Figure R5C). Six hours after scratch, ES4 and FiPS-derived NC started to migrate, and after 24h they had occupied the entire gap proving their migration capacity.

Altogether, the NC functional characterization (differentiation potential and migration capacity) demonstrated that the generated *NF1*(+/+) NC cells were *bona fide* NC cells.

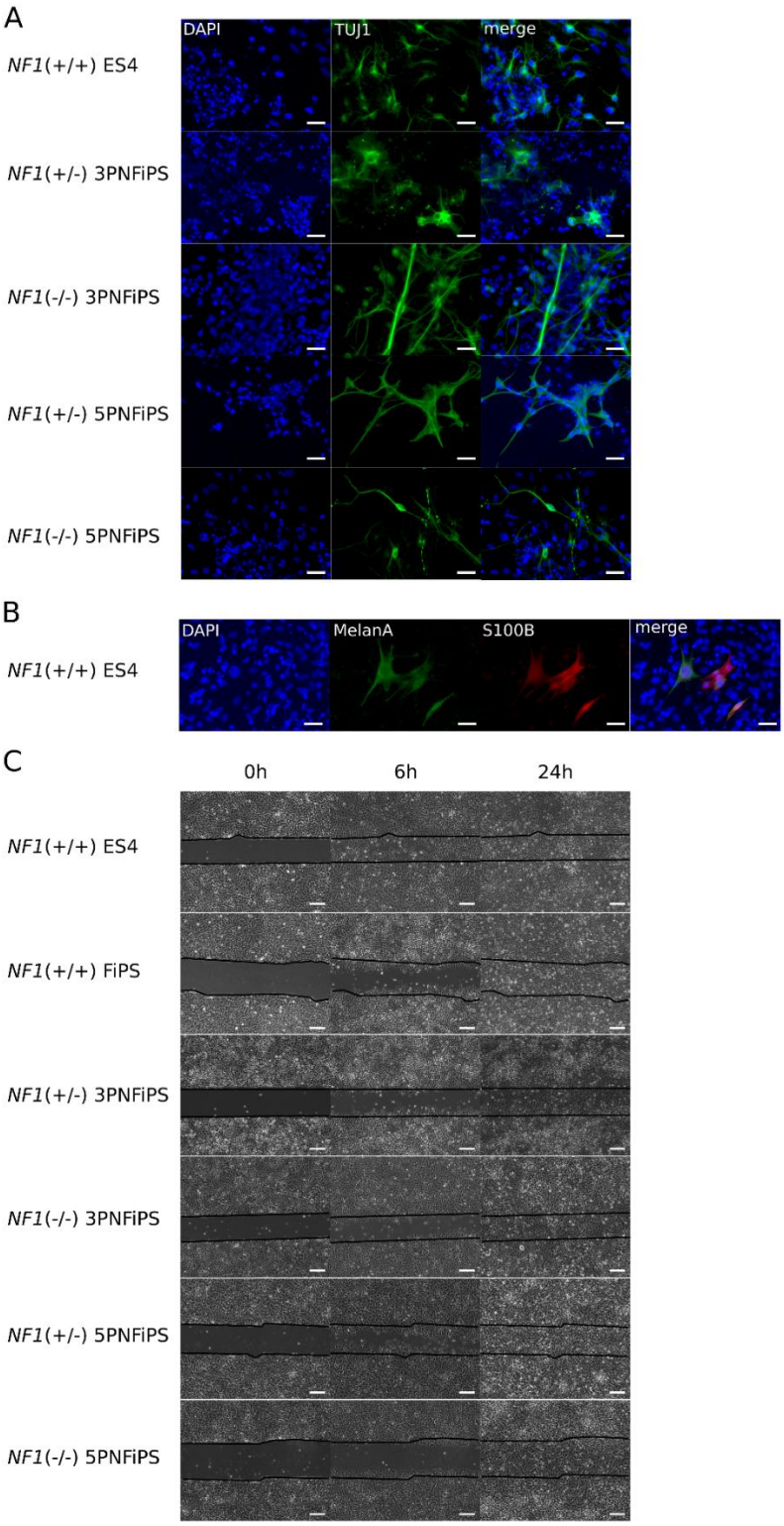

Figure R5. Functional characterization of neural crest cells differentiated from control and plexiform neurofibromas-derived iPSCs. A) Differentiation capacity of generated neural crest (NC) cells towards peripheral neurons. Immunocytochemistry for Tuj1 was performed. DAPI was used to stain cell nuclei. Scale bar= 50 µm **B)** Differentiation capacity of generated NC cells towards melanocytes. Immunocytochemistry for S100B and MelanA was performed. DAPI was used to stain cell nuclei. Scale bar= 50 µm **C)** Scratch assay. A cell free-gap was created using a pipette tip and migration capacity was measured by taking images of the same region at 6 and 24 hours after gap generation. Scale bar= 150 µm.

1.2.2. *NF1*(-/-) iPSC properly differentiate into neural crest

Once the NC differentiation protocol was established using control *NF1*(+/+) PSC lines, we studied the differential potential of PNF-derived *NF1*(+/-) and *NF1*(-/-) iPSC lines towards NC.

Like control *NF1*(+/+) iPSC lines, all PNF-derived *NF1*(+/-) and *NF1*(-/-) iPSC lines differentiated correctly to NC, showing a 90% homogenous population that co-expressed p75 and Hnk1 by passage 4 or 5 after NC induction (Figure R4B). These results were corroborated by immunocytochemistry in which p75 and the transcription factors SOX10 and AP2α were also detected (Figure R4C) and further confirmed by RT-qPCR analysis of the same markers (Figure R4D).

The PNF-derived *NF1*(+/-) and *NF1*(-/-) NC lines were also efficiently differentiated into peripheral neurons, as shown by the acquisition of TUJ1 expression (Figure R5A), showing their multipotency capacity. Moreover, the migration capacity of PNF-derived *NF1*(+/-) and *NF1*(-/-) iPSC lines was also confirmed by the scratch assay (Figure R5C).

Altogether, these results show that PNF *NF1*(+/-) and *NF1*(-/-) iPSC lines can generate homogeneous populations of genuine NC cells.

1.2.3. Establishment of an *in vitro* Schwann cell differentiation protocol

1.2.3.1. Set up a protocol for the generation of Schwann cells from *NF1*(+/+) neural crest cells

To generate SCs from control *NF1*(+/+) iPSC-derived NC cells, 400.000 cells were seeded onto Poly-L-lysine/Laminin-coated 6-well plates in SC differentiation media (containing N2, Forskolin, Heregulin, and bFGF) for 30 days. This differentiation protocol was based on the previously published by (Ziegler et al. 2011) with some modifications. Media was changed twice a week. To monitor the differentiation process, samples were analyzed at 7, 14, and 30 days along with SC differentiation.

1.2.3.2. Characterization of Schwann cell stage-specific markers

To monitor SC differentiation, we evaluated the expression profile of SC lineage markers. RNA was extracted at the differentiation timepoints of 7, 14, and 30 days throughout SC differentiation, and qualitative reverse transcription polymerase chain reaction (RT-qPCR) was performed. In parallel, differentiating cells at the stages of 7, 14, and 30 days of SC differentiation were fixed with 4% para formaldehyde (PFA) to perform immunocytochemistry.

As shown in Figure R6B, differentiating SCs started losing their rhomboid NC morphology by day 7 and changed morphology, becoming more elongated. They acquired the typical bipolar spindle cell morphology progressively. P75 was expressed homogenously in the culture along the whole SC differentiation process, while S100B, a specific SC marker, was first detected at 7 days of SC differentiation and increased gradually over time.

We then monitored the expression of stage-specific markers of the NC-SC lineage by RT-qPCR, comparing PSC, NC, and differentiating SCs (Figure R6D). *SOX10* and *NGFR*, two markers of the NC and NC-SC lineage, were expressed at the NC stage and maintained their expression throughout SC differentiation. Other markers as *ITGA4* and *CDH19* genes started their expression at 7 days and kept the same high levels until 30 days. Other myelin-related proteins like *PLP1* and *PMP22* genes or the specific SC marker *S100B* had an onset of expression at 7 days and raised progressively until 30 days of SC differentiation when they exhibited the highest expression levels. The *EGR2* gene was expressed at the NC stage, slightly decreasing until 14 days to exhibit its highest expression at 30 days.

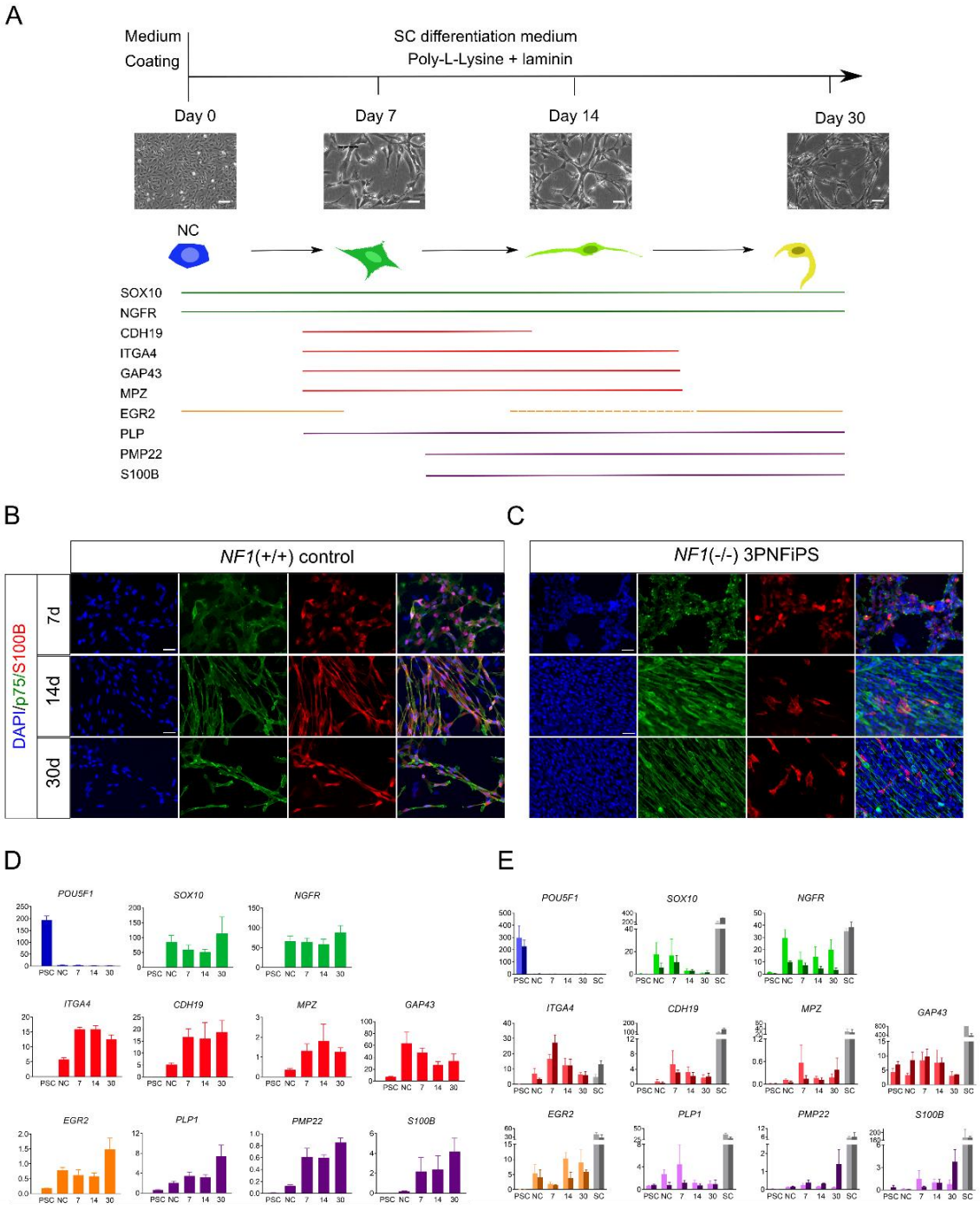

Figure R6. Schwann cell differentiation from neural crest cells. A) Top: Schematic representation of the protocol used for differentiating NC cells into SCs. After 7, 14, and 30 days, SC differentiation was monitored by RT-qPCR and immunocytochemistry analysis. Representative bright-field images during the differentiation process from a control cell line are shown. Scale bars, 50 µm. Bottom: Diagram showing the expression of markers associated with the NC-SC lineage. The colored horizontal bars represent the temporal window during differentiation when the corresponding marker is expressed *in vivo*, according to the literature (Jessen and Mirsky, 2005) **B, C)** Immunocytochemical analysis for S100B and p75 at different stages of SC differentiation (7, 14, and 30 days) in control *NF1*(+/+) FiPS (B) and 3PNFiPS(-/-) cells(C). DAPI was used to stain cell nuclei. Scale bars, 50 µm. **D, E)** RT-qPCR in control *NF1*(+/+) FiPS (D) and *NF1*(-/-) iPSCs (E) at five different timepoints during differentiation: pluripotent stage (PSC), neural crest

stage (NC) and at 7, 14, or 30 days of SC differentiation. For *NF1*(-/-) iPSC graphs (E): light bar represents SC differentiation for 3PNF-derived iPSC line and dark bar for 5PNF-derived iPSC line. Primary SC cultures (gray bars) from 3PNF (light gray) and 5PNF (dark gray) were used. Values are expressed as the mean of the Normalized Relative Expression (Y-axis) ± SEM from three independent differentiation experiments.

1.2.3.3. Functional assay for Schwann cell characterization

As for NCs, we analyzed SC identity not only by marker expression but also by functional characterization. For SCs, this validation was based on their biological capacity to myelinate axons. We performed a myelination assay consisting of co-culturing differentiating SCs and rat dorsal root ganglia (DRG) neurons and evaluating the resultant myelin production by SCs (Figure R7).

We differentiated FiPS-derived NC cells into SCs for 7 days. At this point, cells were detached and co-cultured with rat DRG neurons for 30 additional days. Next, we evaluated the presence of myelin through Myelin Protein Zero (MPZ) staining and its localization in neuronal axons by co-staining with the neuron-specific tubulin TUJ1 (Figure R7A). We observed that differentiating SCs (S100B+ cells) co-localized with TUJ1-expressing axons. At the same time, these axons were covered by the myelin sheath that colocalized with them. Moreover, we were able to detect myelin fragments longer than 400 µm.

This functional assay confirmed the myelinating capacity of control *NF1*(+/+) FiPS-derived SCs and validated the protocol used to differentiate NCs into SCs. Altogether, our results showed that we established robust differentiation protocols to obtain *bona fide* NCs and SCs.

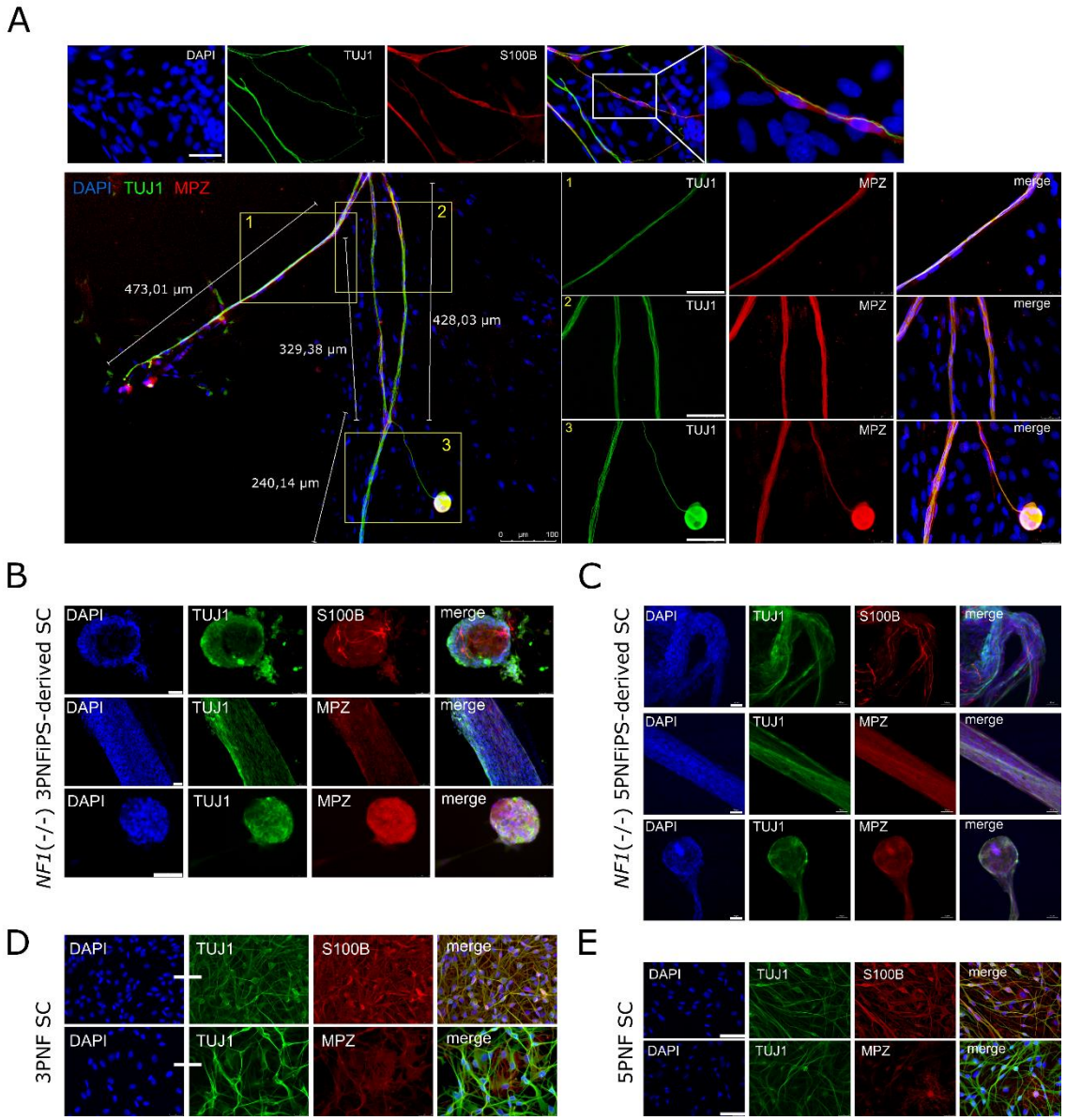

Figure R7. Functional Schwann cell characterization through a myelination assay. A, B, C) Myelination capacity of differentiating SC from *NF1*(+/+) FiPS (A), *NF1*(-/-) 3PNFiPSC (B), and *NF1*(-/-) 5PNFiPSC (C) was assessed by co-culturing cells at 7 days of differentiation with rat DRG neurons for 30 days. SC myelination capacity was measured by immunostaining for TUJ1 (green), S100B (red), and MPZ (red). The length of myelinated axons was measured using LEICA LAS X software and were marked by a white line. Scale bar: 50µm. **D, E)** 3PNF-derived SCs (D) and 5PNF-derived SCs (E) were immunostained with TUJ1 (in green), S100B (in red), and MPZ (in red). Scale bars, 50 µm. DAPI was used to stain cell nuclei.

1.2.4. iPSC-derived differentiating *NF1*(-/-) Schwann cells maintain a high proliferation rate

1.2.4.1. Characterization of Schwann cell-specific markers and functional assays

Once a SC differentiation protocol was established using a control *NF1*(+/+) iPSC line, we studied whether PNF-derived *NF1*(+/-) and *NF1*(-/-) iPSC lines were able to correctly differentiate into SCs.

Thus, we applied the SC differentiation protocol to PNF-derived *NF1*(+/-) and *NF1*(-/-) iPSC lines. After 7 days under SC differentiation conditions, *NF1*(-/-) cells resembled control *NF1*(+/+) cells, both morphologically and according to p75 and S100B expression (**Figure R6B, C**). However, at 14 days of differentiation, whereas control *NF1*(+/+) cultures progressively stopped proliferation and expressed homogeneous amounts of p75 and S100B, *NF1*(-/-) cells continued exhibiting a high proliferation capacity and heterogeneously expressed S100B.

Although differentiating *NF1*(-/-) SCs expressed specific NC-SC markers analyzed by RT-qPCR like *SOX10*, *NGFR*, and, *S100B*; the expression was lower than control differentiating *NF1*(+/+) SCs (**Figure R6D, E**).

To better characterize the proliferation capacity of *NF1*(-/-) differentiating SCs, we performed Ki67 immunostaining (**Figure R8A**). Control *NF1*(+/+) ES4 and FiPS-derived differentiating SCs reduced their proliferation rate during the period between 2 and 30 days of differentiation (**Figure R8B**). However, *NF1*(+/-) and *NF1*(-/-) differentiating SCs did not stop proliferating; instead, they maintained their already high proliferation rate. *NF1*(-/-) differentiating SCs coming from PNF-derived iPSC lines proliferated so much that naturally detached from plates and formed sphere-like structures visible to the naked eye (**Figure R8C**). Spheres grew attached to the plate surface or as free-floating cultures (**Figure R8D**).

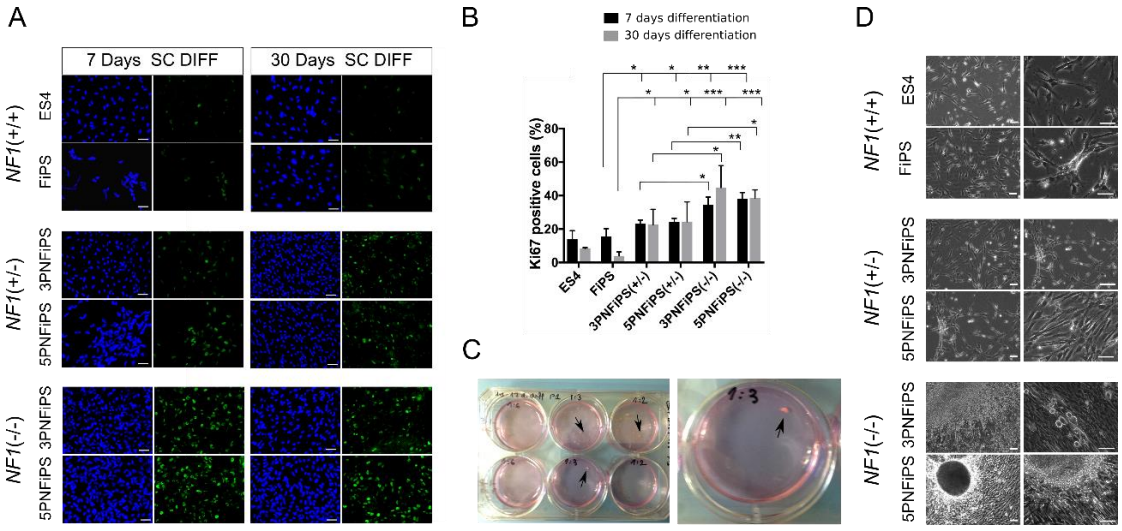

Figure R8. *NF1*(-/-) differentiating Schwann cells exhibited a continuous high proliferation rate. A) Proliferation capacity of differentiating SCs for the different *NF1* genotypes. Representative immunofluorescence images of Ki-67 (green) at 7 and 30 days of differentiation. DAPI was used

to stain cell nuclei. Scale bars, 50 µm. **B)** Quantification of Ki-67-positive cells (percentage over total DAPI-positive nuclei) expressed as the mean ± SE (n = 3 independent differentiation experiments). At least 300 nuclei were counted per timepoint and sample. *p < 0.05, **p < 0.01, ***p < 0.001 (unpaired t-test). **C)** Macroscopic detail of sphere formation in *NF1*(-/-) differentiating SCs. **D)** Representative bright-field images after 20 days of differentiation from NC cells to SCs for the different *NF1* genotypes. Differentiating *NF1*(-/-) SCs exhibited a high cell-culture density and the formation of 3D spheres. Scale bars, 50 µm.

We also evaluated the myelination capacity of the differentiating *NF1*(-/-) SCs by co-culturing them with rat DRG neurons. *NF1*(-/-) differentiating SCs kept proliferating and were not able to correctly associate with axons and form myelin around them as *NF1*(+/+) controls (**Figure R7B**, **C**).

1.2.4.2. iPSC-derived *NF1*(-/-) differentiating Schwann cells exhibit a natural tendency to form spheroids that recapitulate the expression pattern of PNF-derived primary Schwann cells

As explained before, iPSC-derived *NF1*(-/-)-differentiating SCs exhibited a natural tendency to detach from the plate surface and form spheroids. To better understand to which extent these *NF1*(-/-) spheroids recapitulated the expression of their primary PNF counterparts, we analyzed the expression of the SC markers p75, S100B, SOX10, PLP, and GAP43 in spheroids at 30 days of differentiation, and compared them with their parental PNF-derived primary SCs through immunocytochemistry (**Figure R9**). The expression pattern of PNF-derived primary SCs and iPSC-derived sphere-forming *NF1*(-/-) SCs were remarkably similar.

Sphere forming SCs bore the same genetic and genomic content as their primary SC counterparts and recapitulated both a high proliferation rate and the same expression pattern in a homogenous manner. Altogether our results showed that *NF1*(-/-) iPSC-derived SC spheres represented a valuable experimental model to study PNF formation.

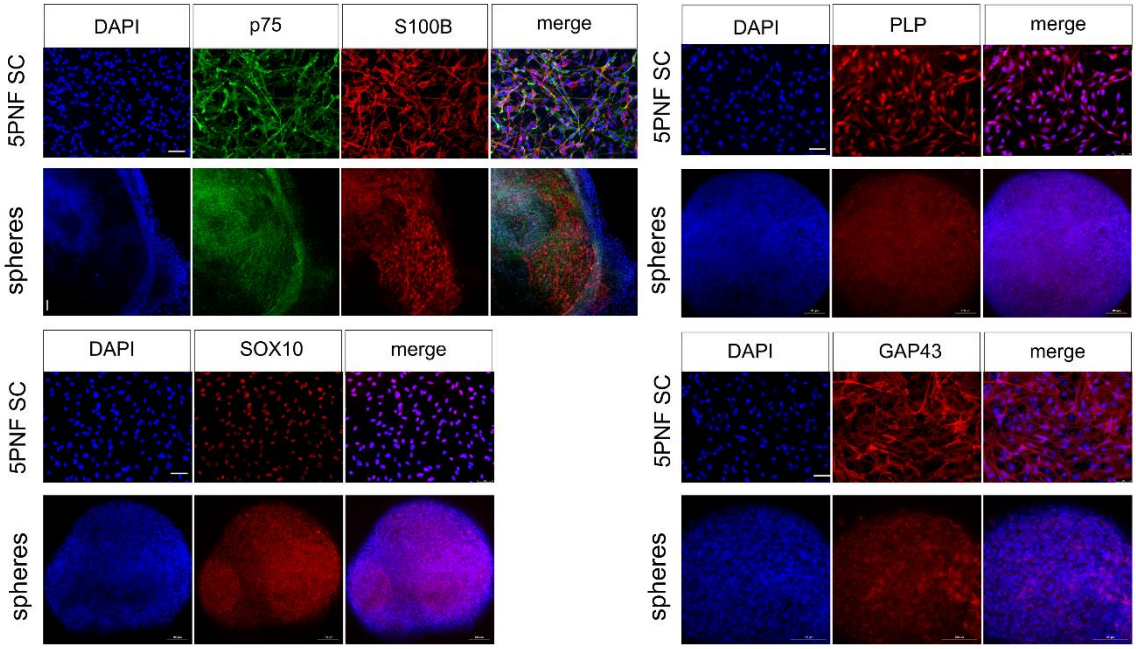

Figure R9. *NF1*(-/-) PNFiPS-derived sphere-forming Schwann cells recapitulate the expression pattern of their plexiform neurofibroma-derived Schwann cell counterparts. Representative immunofluorescence images showing expression of S100B, p75, SOX10, GAP43, and PLP, in 5PNF-derived primary SCs (5PNF SC) compared with *NF1*(-/-) 5PNFiPS sphere-forming differentiating SCs (spheres), at 30 days of differentiation. DAPI was used to stain nuclei. Scale bars, 100 µm.

1.3. Generation of an expression roadmap of the neural crest-Schwann cell differentiation axis with control *NF1*(+/+) cells

We were able to generate genuine *NF1*(+/+) NC cells and differentiate them into the NC-SC lineage, in which cells expressed the classic lineage-specific developmental markers. We considered that further characterization of the *in vitro* NC-SC differentiation process could help to (i) identify new lineage markers, (ii) better characterize the different stages of SC differentiation, (iii) unravel the role of *NF1* loss along the NC-SC axis, and, (iv) investigate the potential cell originating PNFs.

Thus, we performed a NC-SC differentiation experiment in which RNA was extracted at the pluripotent stage (PSC), NC, and 7, 14, and 30 days along with SC differentiation and performed RNA-sequencing. In parallel, we performed an *in vivo* experiment to evaluate at what differentiation state *NF1*(-/-) cells were able to engraft and generate tumors (see below).

For RNAseq analysis, control *NF1*(+/+) cells were analyzed from three independent differentiation experiments. For *NF1*(-/-) cells, a biological triplicate was analyzed: 3PNFiPS, 5PNFiPS, and a new CRISPR/Cas9 edited *NF1*(-/-) FiPS (see Appendix1 for details). This newly generated CRISPR/Cas9-edited *NF1*(-/-)iPSC, isogenic to our control *NF1*(+/+) FiPS, exhibited the same functional characteristics as the PNF-derived *NF1*(-/-)iPSCs: an increased proliferation capacity compared to controls; a genuine generation of NCs; a higher proliferation rate, altered differentiation and tendency to form spheres of differentiating SCs (Appendix1). These results demonstrated that, so far, all altered proliferation and differentiation properties of *NF1*(-/-) iPSC and iPSC-derived SCs could be attributed to the lack of neurofibromin function. To simplify naming iPSC lines, a new nomenclature was adopted (Table R3).

Old nomenclature	Simplified nomenclature
NF1(+/+) FiPS	WT
NF1(-/-) 5PNFiPS	NF1_A
NF1(-/-) 3PNFiPS	NF1_B
NF1(-/-) FiPS	NF1_C

Table R3. Simplified version of current iPSC lines nomenclature.

1.3.1. A gene expression road-map of the *in vitro NF1*(+/+) NC-SC differentiation process

We first analyzed RNA-seq data from control *NF1*(+/+) cells (wild type, WT). A Principal Component Analysis (PCA) of the *in vitro* NC-SC differentiation process was carried out (Figure R10A).

Principal component 1 (PC1) explained 64% of all the expression variance and correlated with the temporary PSC-NC-SC axis of differentiation. PC2 contained 26% of the variance and split the samples into three distinctive groups: pluripotent cells, NC cells, and differentiating SCs. Although differentiating SCs at 7, 14, and 30 days placed very close to each other, every timepoint clustered separately. These results indicated the existence of specific expression at each stage and differentiation timepoints, and importantly, demonstrated that the three independent NC-SC differentiation replicas behaved in the same way, supporting the robustness of the established NC-SC differentiation protocols and validating the quality of the data.

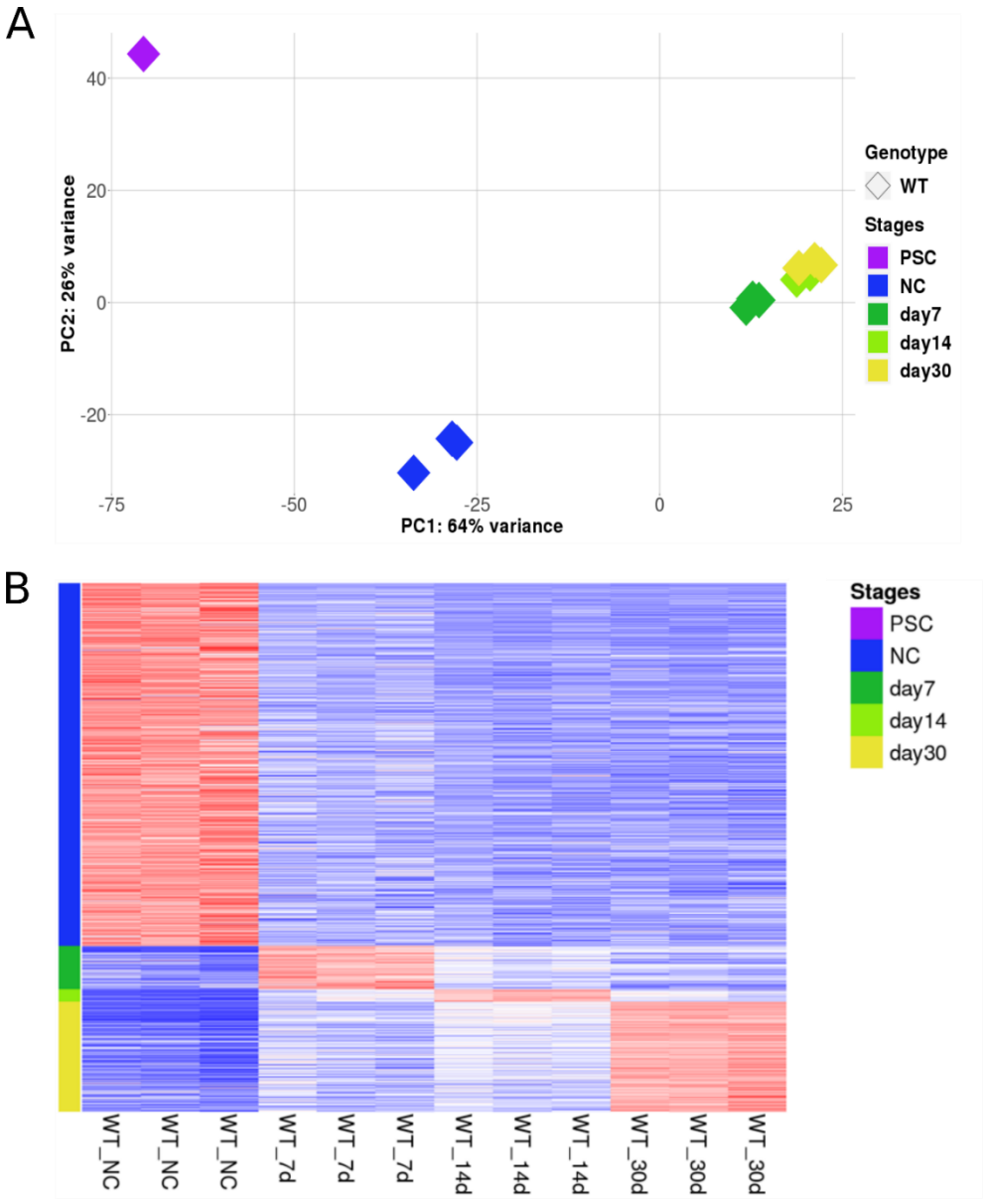

Figure R10. Generation of a robust expression roadmap of the neural crest Schwann cell differentiation axis using *NF1*(+/+) cells. A) Principal Component Analysis of the *in vitro* NC-SC differentiation process using *NF1*(+/+) FiPS cells (WT). Pluripotent stem cell (PSC)-stage (purple), neural crest (NC)- stage (dark blue), 7-day (dark green), 14-day (light green), and 30-day (yellow) SC-differentiation timepoints are depicted. Notably, samples clustered by stage. Principal component 1 (PC1) correlates with the temporary PSC-NC-SC axis. **B)** Heatmap representing a

supervised expression analysis of all differentially expressed genes composing the NC-SC expression roadmap. In red, up-regulated genes are shown, and in blue down-regulated ones. Thousands of upregulated stage-specific markers were identified in the NC-stage, some hundreds at the 7-day stage and 30-days stage, and a few tens at the 14-day stage. Three independent differentiation experiments are shown.

We then performed a differential expression analysis, considering the distinct differentiation stages and timepoints. We grouped all differentially upregulated genes in each stage/timepoint and constructed an expression roadmap of the NC-SC *in vitro* differentiation process. Thousands of upregulated specific genes were identified at the NC-stage, some hundreds at 7-day and 30-day SC timepoints, and a few tens at 14-day. The expression roadmap signature was visualized on a heatmap (Figure R10B), clearly highlighting the specific expression along the NC-SC axis of differentiation. A gene enrichment analysis of the expression signature constituting the roadmap highlighted some biological processes related to glial and peripheral nervous system differentiation such as "glial cell differentiation", "SC differentiation", or "peripheral nervous system development", further validating the NC-SC differentiation conditions established and uncovering potential new markers of the NC-SC differentiation axis.

1.3.2. *NF1*(-/-) differentiating Schwann cells in 2D cultures switch from a neural crest- Schwann cell axis to a neural crest-mesenchymal cell axis

The generation of an expression roadmap of the NC-SC *in vitro* differentiation process using *NF1*(+/+) control cells provided a framework for the analysis of the role of the *NF1* gene in this differentiation by comparing the expression of *NF1*(-/-) cells. We already observed an altered SC differentiation capacity of iPSC-derived *NF1*(-/-) cells in 2D cultures (Figures R6C). Although able to differentiate into SCs, most parts of the *NF1*(-/-) differentiating cell population did not acquire markers of SC commitment (like S100B) and exhibited a deficient capacity of myelinating neurons (Figures R7C).

We then analyzed RNA-seq data from the three *NF1*(-/-) iPSC lines, using the same stages and differentiation timepoints as for control *NF1*(+/+) cells. We performed a new PCA analyzing together the *NF1*(+/+) and *NF1*(-/-) cell lines (Figure R11A). *NF1*(-/-) cells clustered together at the pluripotent and NC stages, locating very close to *NF1*(+/+) controls. However, during SC differentiation, *NF1*(-/-) cells started to disperse and localize away from controls in the PCA plot, indicating different expression signatures between them and controls, and suggesting an altered differentiation. In addition, a high degree of variability among the three *NF1*(-/-) cell lines was observed. To further evaluate this presumably altered differentiation, the expression of genes configuring the NC-SC expression roadmap were compared for *NF1*(-/-) cells and *NF1*(+/+) controls and visualized in a heatmap (Figure R11B).

At the NC stage, all *NF1*(-/-) cell lines exhibited the same expression pattern as *NF1*(+/+) cell line, despite their genotype. Although *NF1*(-/-) 5PNFiPS cell line (NF1_A) presented the same expression pattern at the 7-day timepoint as the *NF1*(+/+) cell line, the rest of

NF1(-/-) cell lines did not. In fact, at the 14-day timepoint, all *NF1*(-/-) cell lines already lost the *NF1*(+/+) NC-SC roadmap signature. Thus, heatmap representation clearly showed the "loss of track" of the *NF1*(-/-) cells along the NC-SC differentiation process defined by controls (**Figure R11B**).

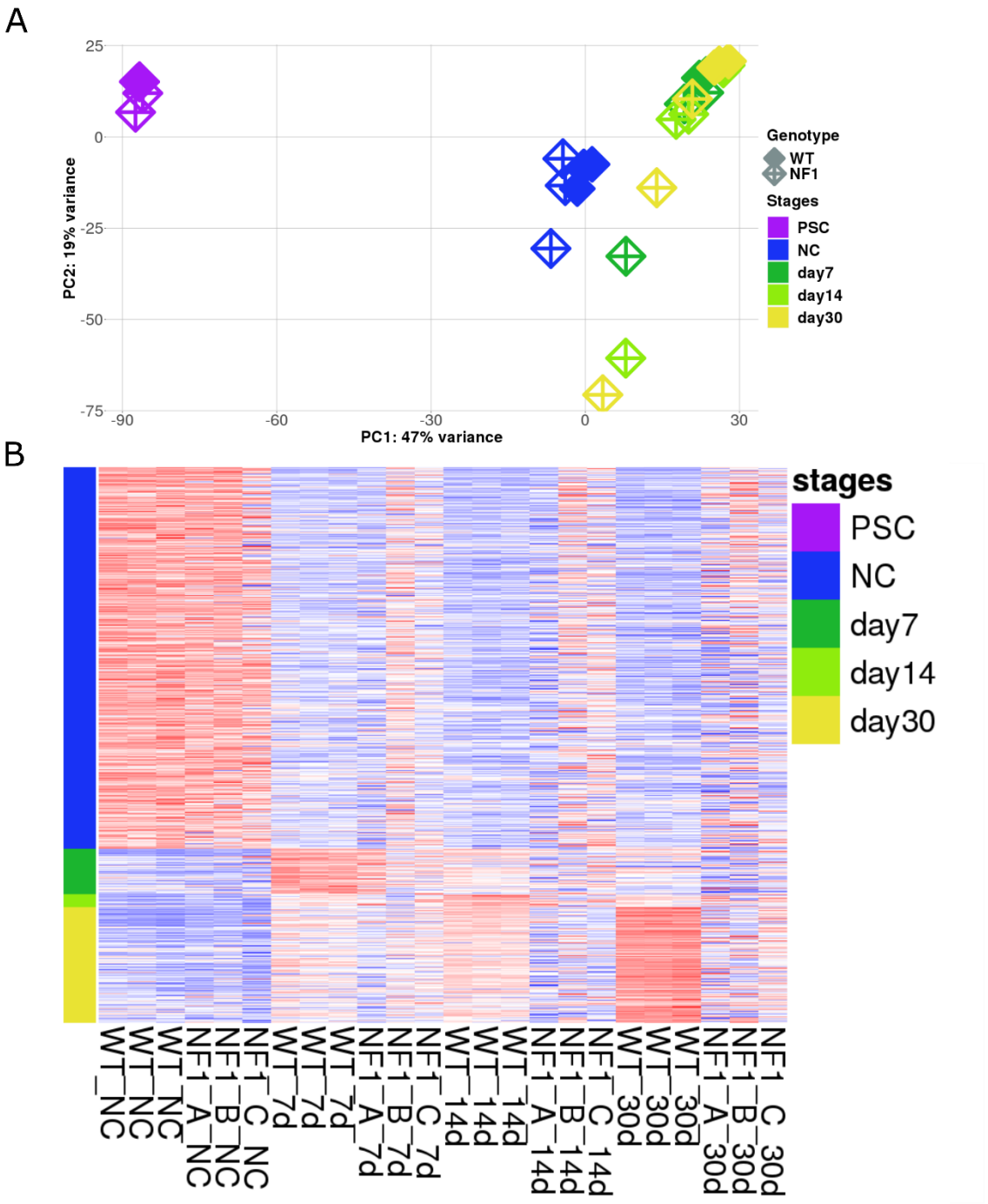

Figure R11. *NF1*(-/-) differentiating Schwann cells did not follow the neural crest-Schwann cell expression roadmap defined by *NF1*(+/+) cells. A) A PCA of the *NF1*(+/+) FiPS cell line (WT, full rhomboids) and the *NF1*(-/-) PNF-derived and edited iPSCs (NF1, crossed rhomboids). Pluripotent stem cells (PSC, purple), NC (dark blue), 7-day (dark green), 14-day (light green), and 30-day

(yellow) of SC differentiation are depicted. WT and NF1 cell lines clustered together mainly at pluripotent and neural crest stages. However, NF1 cell lines did no longer cluster at 7-day, 14-day, or 30-day timepoints. **B)** Heatmap representing a supervised cluster analysis showing the stage-specific markers of NC stage, 7-day, 14-day, and 30-day of SC differentiation in WT and NF1 cell lines. NC stage-specific genes (dark blue) and 7-day (dark green), 14-day (light green), and 30-day (yellow) timepoint-specific genes are depicted. The expression color ranges from dark blue, showing down-regulated genes, to red, showing up-regulated genes.

Since the *NF1*(-/-) differentiating cells were escaping from NC-SC expression roadmap defined by *NF1*(+/+) cells, we wondered the identity that they were adopting. To analyze their expression, a differential gene expression analysis was performed comparing *NF1*(-/-) cells at 30 days under SC differentiation conditions with WT cells. Differentially expressed genes at 30 days were used in a gene enrichment analysis to underscore the most representative biological processes (Figure R12). Cell line NF1_A was enriched in biological processes like “bone development”, “chondrocyte differentiation”, “ossification”, “cartilage development”. NF1_B was enriched in biological processes like “muscle contraction”, “muscle organ development”, “muscle cell differentiation”, and “muscle system process”. The edited NF1_C cell line was enriched in processes such as “collagen metabolic process”, “chondrocyte differentiation”, and “cartilage development” similar to NF1_A. We validated this *in silico* analysis by studying the expression of specific muscle and chondrocyte genes (Appendix 2 Figure 1).

These results suggested that most *NF1*(-/-) differentiating cells in 2D cultures were switching from a NC-SC axis of differentiation to a NC-mesenchymal cell axis.

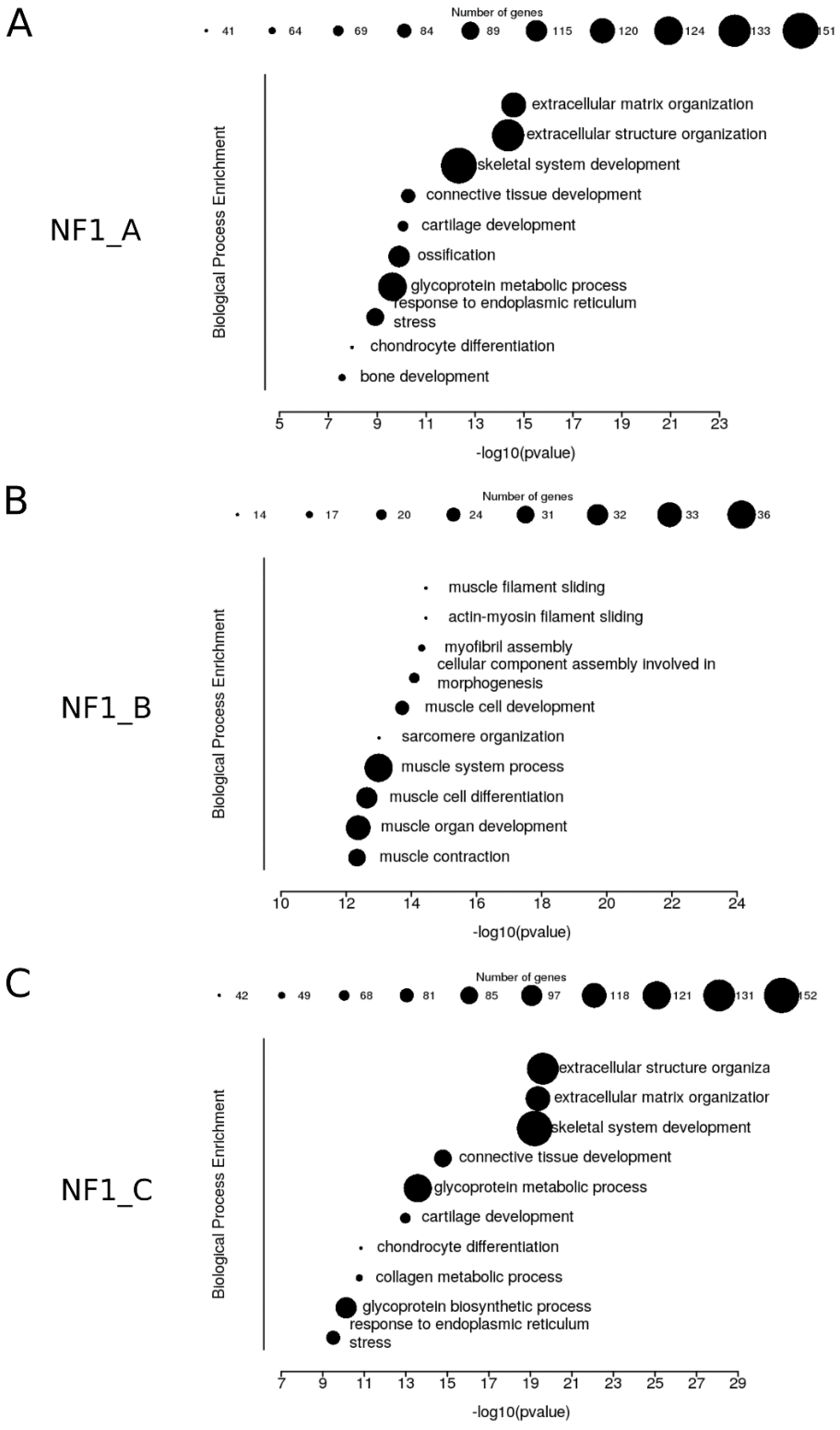

Figure R12. *NF1*(-/-) differentiating Schwann cells in 2D cultures switched from a neural crest-Schwann cell axis to a neural crest-mesenchymal axis. Top differentially expressed genes in *NF1*(-/-) cell lines compared to control *NF1*(+/+) at 30 days were used to perform an enrichment analysis of biological processes. The X-axis indicates the p-value associated with each biological process. The Y-axis concentrated the ten most significant biological processes after enrichment analysis. The size of the black circle represents the number of genes that each biological process contained. NF1_A (A); NF1_B (B); NF1_C (C).

In parallel to RNA-seq analysis, we performed an engraftment assay into the sciatic nerve of nude mice using the same *NF1*(+/+) and *NF1*(-/-) cells to study their capacity to engraft and generate tumors *in vivo*. We used cells at NC stage and at 7 and 14 days of SC differentiation, since GEM models (see introduction section) pointed to a SCP stage as the most probable PNF cell of origin.

These experiments were performed in collaboration with Dr. Conxi Lázaro's laboratory at Institut Català d'Oncologia (ICO)- Institut d'Investivació Biomèdica de Bellvitge (IDIBELL). Cells were grown and differentiated in our laboratory at IGTP and then engrafted at the animal facility of ICO-IDIBELL.

Two million cells of control *NF1*(+/+) and *NF1*(-/-) cell lines at each stage/timepoint (NC, 7, and 14 days of SC differentiation) were injected into the sciatic nerve of immunodeficient male mice (Figure R13A). Each mouse received two injections, one in each leg, and 2 mice were used per condition. Tumor growth was monitored by manual palpation.

After 2 months, thickening of the thighs of some mice were observed, and at 4 months post-injection, all mice were euthanized and dissected.

None of the *NF1*(+/+) cell cultures at any differentiation stage (NC, 7 or 14 days of SC differentiation) generated tumors (Table R4). On the contrary, we observed a tumor-like grown cell mass in mice engrafted with *NF1*(-/-) cells at 14 days of SC differentiation (not at NC stage, neither at 7 days of SC differentiation) (Figure R13B).

iPSC line	Neural crest stage	7d SC differentiation	14d SC differentiation
NF1(+/+) FiPS	0/4	0/4	0/4
NF1_A	0/4	0/2*	4/4
NF1_B	0/4	0/4	1/2*

Table R4. Summary of tumor masses formed *in vivo* after engraftment of *NF1*(+/+) and *NF1*(-/-) cells at neural crest stage, and at 7 and 14 days of Schwann cell differentiation. The number of tumors grown/the number of injections is shown per condition and cell line. *Some mice died due to an infection before the end of the experiment.

Tumors were analyzed histologically by hematoxylin and eosin (H&E) staining. Those formed by the engraftment of NF1_A cell line (14 days of SC differentiation) contained areas of immature mesenchymal proliferative cells and areas of chondrocyte differentiation (Figure R13C), which stained positive for S100B (Figure R13C). No areas resembling a PNF were observed. On the other hand, in the case of NF1_B cell engraftment (14 days) H&E staining revealed tumors containing mostly muscle and undifferentiated cells. Remarkably, these *in vivo* results were completely in agreement with the differentially expressed genes and enriched biological processes detected by RNA-seq analysis in NF1_A and NF1_B cell lines.

Altogether, these results demonstrated that *NF1*(-/-) differentiating SCs in 2D cultures, switched from a NC-SC axis to a NC-mesenchymal cell axis of differentiation (towards chondrocytes and muscle cells), both *in vitro* and *in vivo*. They also support the lack of capacity of *NF1*(-/-) NC to form neurofibromas (Joseph N et al. 2008). Results also highlight a high correlation between the expression identity acquired *in vitro* by differentiating cells and the cell type developed *in vivo* after engraftment (either muscle cells or chondrocytes).

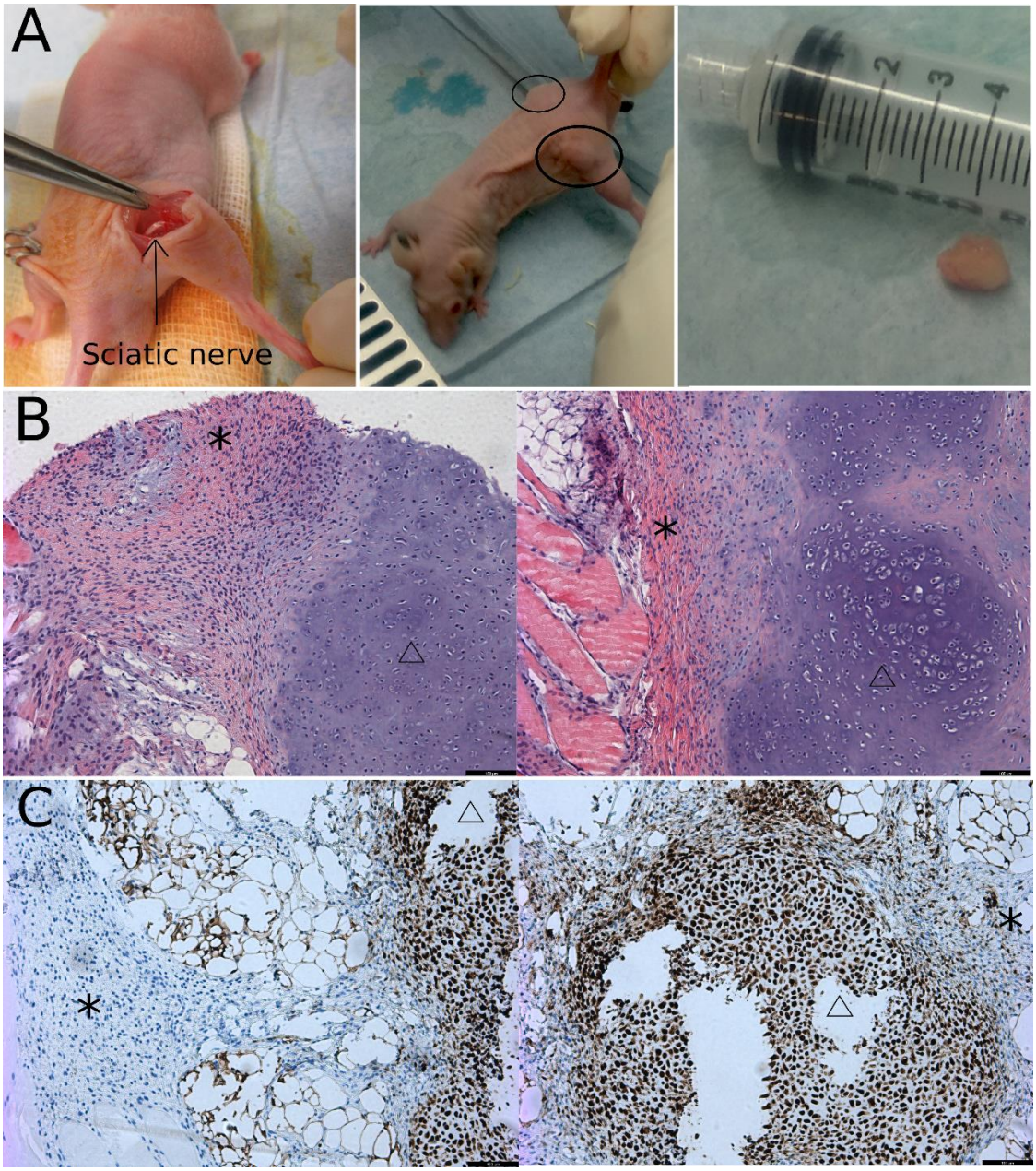

Figure R13. Engraftment of *NF1*(-/-) differentiating Schwann cells at 14 days formed mesenchymal tumors. A) Two million cells of control *NF1*(+/+) and *NF1*(-/-) cell lines (NF1_A and NF1_B) at NC stage and 7 and 14 days of SC differentiation were injected into the sciatic nerve of immunodeficient male mice. Four months later, all mice were euthanized. Tumors appeared only in mice that had been injected with *NF1*(-/-) cell lines (NF1_A and NF1_B) at 14 days of SC differentiation. **B)** H&E staining of developed tumors after injecting NF1_A cells showing an

immature proliferative population (asterisk) and an immature chondrocyte population (triangle). C) S100B staining of the same tumors. The immature proliferative population (asterisk) is S100B negative. The immature chondrocyte population (triangle) is S100B positive. Black scale bar; 100 µm.

1.4. Generation of a 3D Schwann cell differentiation model using a multiplex system: homotypic and heterotypic spheroids

1.4.1. Set up of differentiating Schwann cell 3D cultures

Our *in vitro* and *in vivo* results indicated that 2D cultures of *NF1*(-/-) differentiating SCs were too heterogeneous to model PNFs. Most cells ended up switching from a NC-SC axis towards a NC-mesenchymal axis. On the other hand, differentiating *NF1*(-/-) cells preserved a high proliferation rate and an increased tendency to form spheres that homogenously expressed SC markers. Spheres recapitulated the expression of their PNF-derived SC counterparts. Thus, we decided to develop a 3D culture methodology to efficiently generate spheres using iPSC-derived differentiating SCs in a multiplex and proficient way to improve our PNF model system.

To set up the 3D SC differentiation protocol, we seeded cells onto Poly-L-lysine and Laminin-coated plates with SC differentiation media, and after five days, cells were detached and transferred into AggreWell™800 24-well plates in SC differentiation media (see details in Materials & Methods). Each well of the 24-well plate had approximately 300 microwells allowing for the generation of 300 spheroids per well. We grew spheroids until day 14 of SC differentiation, 9 days after spheroid induction.

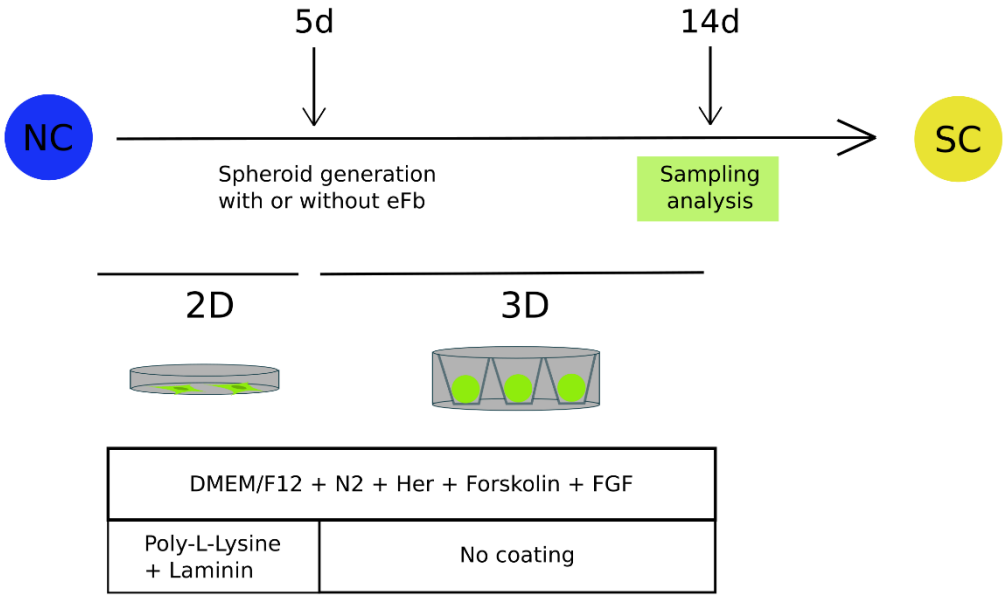

Figure R14. Schematic representation of spheroid generation. At day 0, cells were plated in Poly-L-lysine and Laminin-coated plates in SC differentiation media containing DMEM/F12, N2, heregulin (Her), forskolin, and 1%FGF. After 5 days, cells were detached, counted, and transferred into AggreWell™800 24-well plates in SC differentiation media until day 14 of differentiation.

In addition to *NF1* loss in the SC lineage cells, the tumor microenvironment has been described as a critical factor for neurofibroma development (Liao, 2016; Liao, 2018). The second main cell type within neurofibromas, after SCs, are eFbs.

So, we decided to generate, in addition to homotypic spheroids containing differentiating SCs, heterotypic spheroids that contained a mixture of differentiating SCs and eFbs from already established PNF-derived cultures. In this case, we seeded 70% differentiating SCs and 30% eFbs to simulate the proportions that are frequently found in neurofibromas.

We generated homotypic spheroids from all *NF1*(-/-) iPSC lines (PNF-derived and CRISPR/Cas9). Unfortunately, due to the incapacity of differentiating SCs from control *NF1*(+/+) FiPS cells to compact when transferred into AggreWell^{TM}800 plates, we could not obtain control *NF1*(+/+) homotypic spheroids. On the contrary, we were able to establish heterotypic spheroids from control *NF1*(+/+) as well as from all *NF1*(-/-) iPSC lines.

We mixed each PNF-derived eFb culture with the respectively *NF1*(-/-) differentiating SCs to reproduce better the original PNFs (summarized in Table R5).

Homotypic spheroids	Heterotypic spheroids	
Cell line	Cell line 1	Cell line 2
-	*NF1*(+/+) FiPS (WT)	5PNF-derived eFbs (FB_A)
NF1(-/-) 5PNFiPSCs (NF1_A)	*NF1*(-/-) 5PNFiPSCs (NF1_A	5PNF-derived eFbs (FB_A)
NF1(-/-) 3PNFiPSCs (NF1_B)	*NF1*(-/-) 3PNFiPSCs (NF1_B)	3PNF-derived eFbs (FB_B)
Edited *NF1*(-/-) FiPS (NF1_C)	Edited *NF1*(-/-) FiPS (NF1_C)	3PNF-derived eFbs (FB_B)

Table R5. Table summarizing the specific cell lines that composed homotypic and heterotypic spheroids. In brackets, a simplified nomenclature is shown.

1.4.2. 3D model characterization

To obtain morphological data from generated spheroids, phase-contrast images with the microscope were obtained (Figure R15A). The diameter of spheroids widely varied between iPSC lines and between homotypic and heterotypic spheroids, being heterotypic spheroids slightly bigger. The diameter of homotypic spheroids ranged from 150 µm in NF1_C cell line to almost 250 µm in NF1_A and NF1_C. On the other hand, heterotypic spheroid diameter ranged from approximately 200 µm up to 400 µm.

Spheroids had to be handled very carefully, especially when eFbs were not present. eFbs brought structural support to the spheroids as well as compaction (see DAPI staining in Figure R15B, C). Immunostaining showed that both types of spheroids expressed, in a generalized way, NC-SC markers such as p75 and S100B (Figure R15B, C).

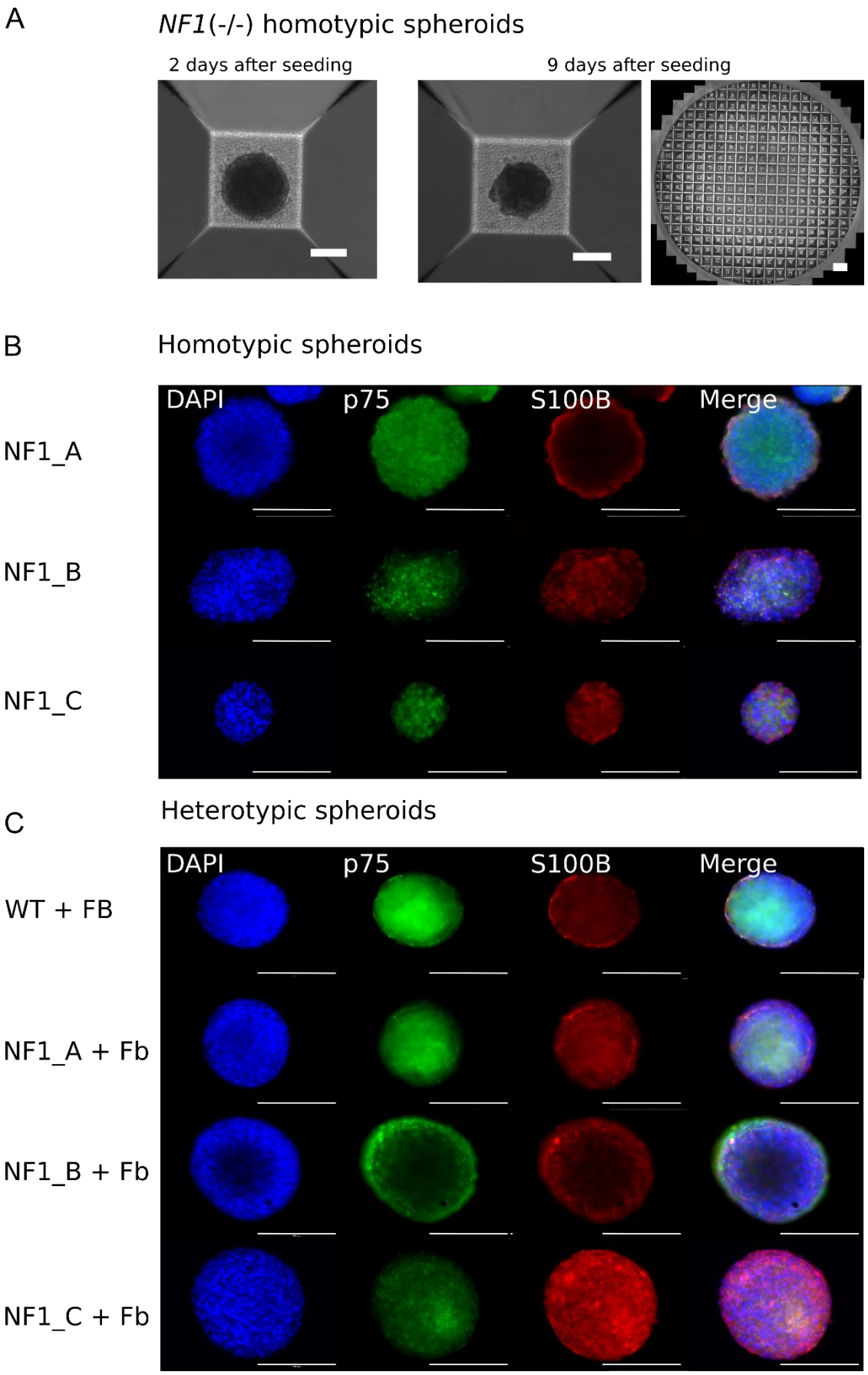

Figure R15. p75 and S100B characterization in homotypic and heterotypic spheroids at 14 days of Schwann cell differentiation in 3D. A) Representative phase-contrast image of a microwell of a

NF1(-/-) homotypic spheroid 2 days (left) and 9 days (right) after seeding. Scale bar, 100 µm. A tile scan of an entire 6-well plate is shown with the approximately 300 *NF1*(-/-) homotypic spheroids. Scale bar, 1000 µm. **B, C)** Representative images from immunocytochemical analysis of homotypic (A) and heterotypic (B) spheroids, evaluating the expression of p75 and S100B. All spheroids expressed p75 and S100B. DAPI was used to stain the nuclei. Scale bar, 200 µm.

In addition to a morphological characterization, we extracted RNA from *NF1*(+/+) and *NF1*(-/-) spheroids and confirmed the expression of NC-SC lineage markers by RT-qPCR (**Figure R15B,C and R16**). Results showed that in general, SC lineage markers were increased when differentiating SCs grew in multiplexed 3D spheroids as compared to 2D standard differentiation conditions.

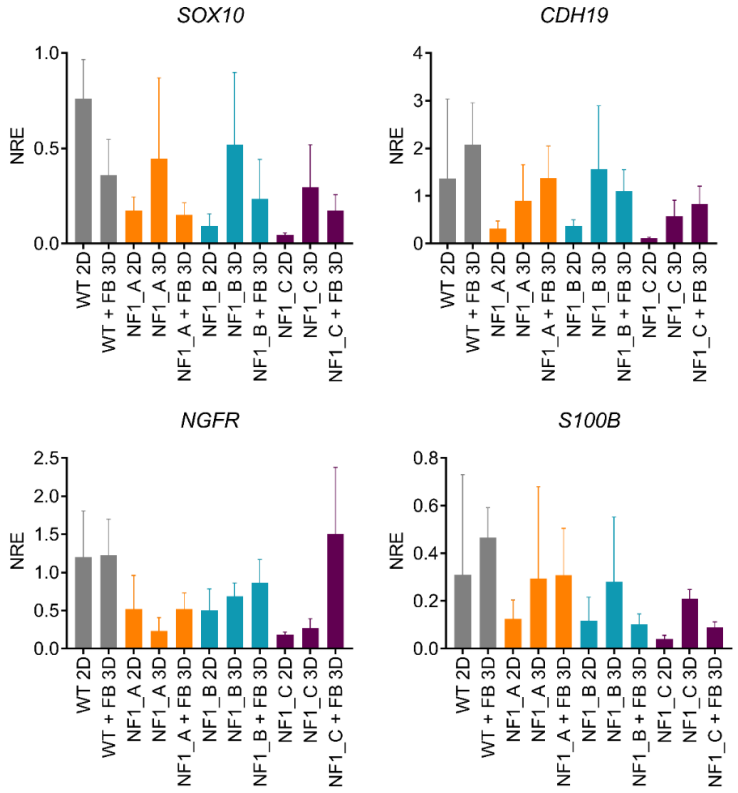

Figure R16. Characterization of some markers in spheroids through RT-qPCR at 14 days of Schwann cell differentiation. The normalized relative expression (NRE) of four different markers, *SOX10*, *CDH19*, *NGFR*, and *S100B* was calculated at 14 days of SC differentiation in 2D and 3D. *NF1*(+/+) FiPS (WT, in grey); *NF1*(-/-) 5PNF-derived iPSCs (NF1_A, in orange); *NF1*(-/-) 3PNF-derived iPSCs (NF1_B, in blue); and edited *NF1*(-/-)FiPS (NF1_C, in purple). *NF1*(-/-) spheroids, either homotypic or heterotypic, expressed higher amounts of these four markers compared to 2D cultures. Values are expressed as the mean NRE ± SEM from three independent differentiation experiments.

1.4.3. *NF1*(-/-) heterotypic spheroids recapitulate the neural crest-Schwann cell roadmap expression signature at 30 days of Schwann cell differentiation

To get a global insight of spheroid expression profiles, we digested spheroids to obtain a single-cell suspension and performed RNA-sequencing analysis of homotypic and heterotypic spheroids. The identified *in vitro* NC-SC roadmap expression signature was used to compare control *NF1*(+/+) cell line, both in 2D and 3D (heterotypic spheroids), with homotypic and heterotypic spheroids from the three independent *NF1*(-/-) cell lines (**Figure R17**). *NF1*(+/+) heterotypic spheroids exhibited an expression roadmap profile closer to the one displayed by *NF1*(+/+) differentiating SCs in 2D cultures at 30 days of SC differentiation. Remarkably, two of the *NF1*(-/-) heterotypic spheroid lines (NF1_B and NF1_C) also expressed a quite similar expression roadmap profile. However, this was not the case for the third *NF1*(-/-) heterotypic spheroid line (NF1_A) and for none of the three independent homotypic spheroid cultures. These spheroids were not following a clear NC-SC path according to the expression roadmap profile, despite the detection of classic markers by RT-qPCR (**Figure R15**) and by immunostaining (p75, S100B) (**Figure R16**).

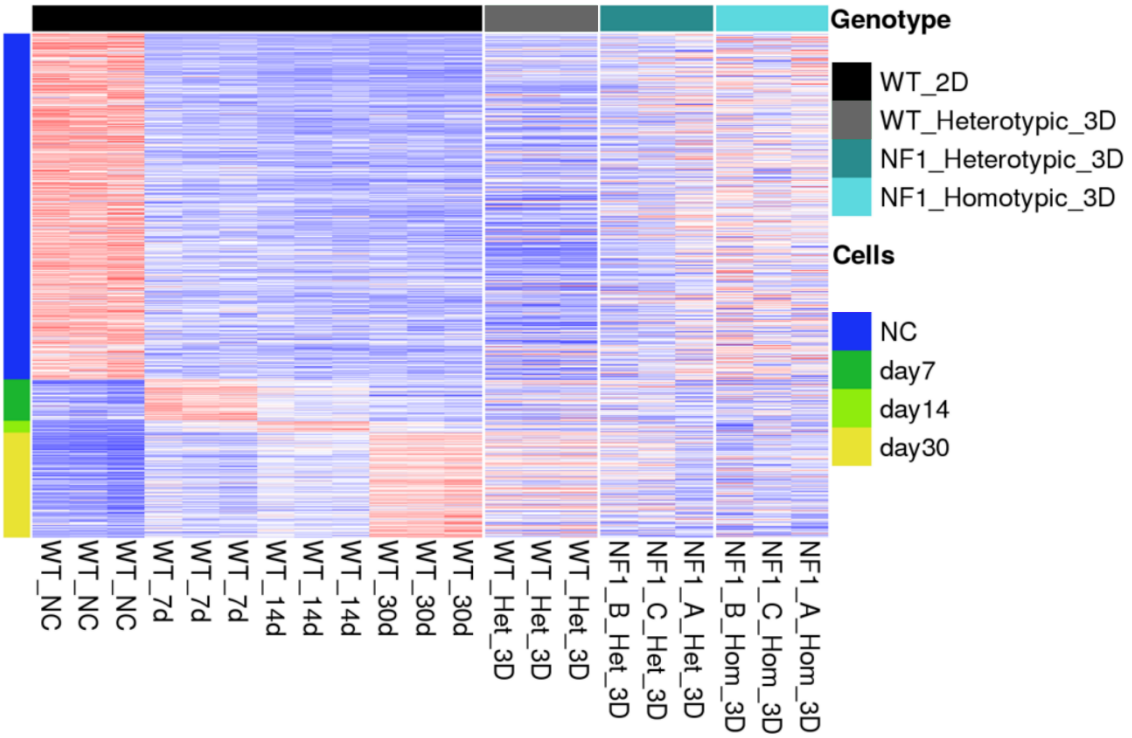

Figure R17. *NF1*(-/-) heterotypic spheroids recapitulate the neural crest-Schwann cell roadmap expression signature at 30 days of Schwann cell differentiation. Heatmap showing the NC-SC roadmap signature at NC stage, 7-day, 14-day, and 30-day timepoints in control *NF1*(+/+) differentiating SCs in 2D and also in 3D (heterotypic spheroids), as well as for *NF1*(-/-) heterotypic and homotypic spheroids. Neural crest (NC) specific roadmap markers are shown in dark blue, and 7, 14, and 30 day roadmap markers in dark green, light green, and yellow, respectively. The expression color ranges from dark blue, showing down-regulated genes, to red, showing up-regulated genes.

To further evaluate gene expression in 2D and 3D models, we used the *in vitro* NC-SC expression roadmap signature defined by control *NF1*(+/+) 2D cultures as a reference. We constructed a framework of a spider plot with 4 tips, each representing a differentiation stage/timepoint (NC, and 7, 14, and 30 days of SC differentiation). We then calculated the Manhattan distances of each heterotypic or homotypic spheroid sample to the expression roadmap of each stage/timepoint and plotted results as overlaying spider plots (**Figure R18**). In this way, we obtained a global representation of the expression roadmap signatures of all 2D and 3D models compared to the one of the control *NF1*(+/+) 2D cultures as a baseline. The Manhattan distance of a given sample to each specific stage/timepoint would specify the distance between the vertex (total similarity) and the center (total difference) of each ax of the plot (**Figure R18**).

Spider plots clearly showed that the expression roadmap profile exhibited by WT *NF1*(+/+) heterotypic spheroids (**Figure R18A**) highly correlated with those expressed by NF1_B and NF1_C heterotypic spheroids (**Figure R18C** and, **D**). On the other hand, the roadmap expression by *NF1*(-/-) 2D differentiating SCs and the *NF1*(-/-) homotypic spheroids did not resemble the one of the *NF1*(+/+) heterotypic spheroids. These results highlight the influence of primary PNF-derived eFbs on differentiating *NF1*(-/-) SCs for a correct establishment of a NC-SC axis of differentiation.

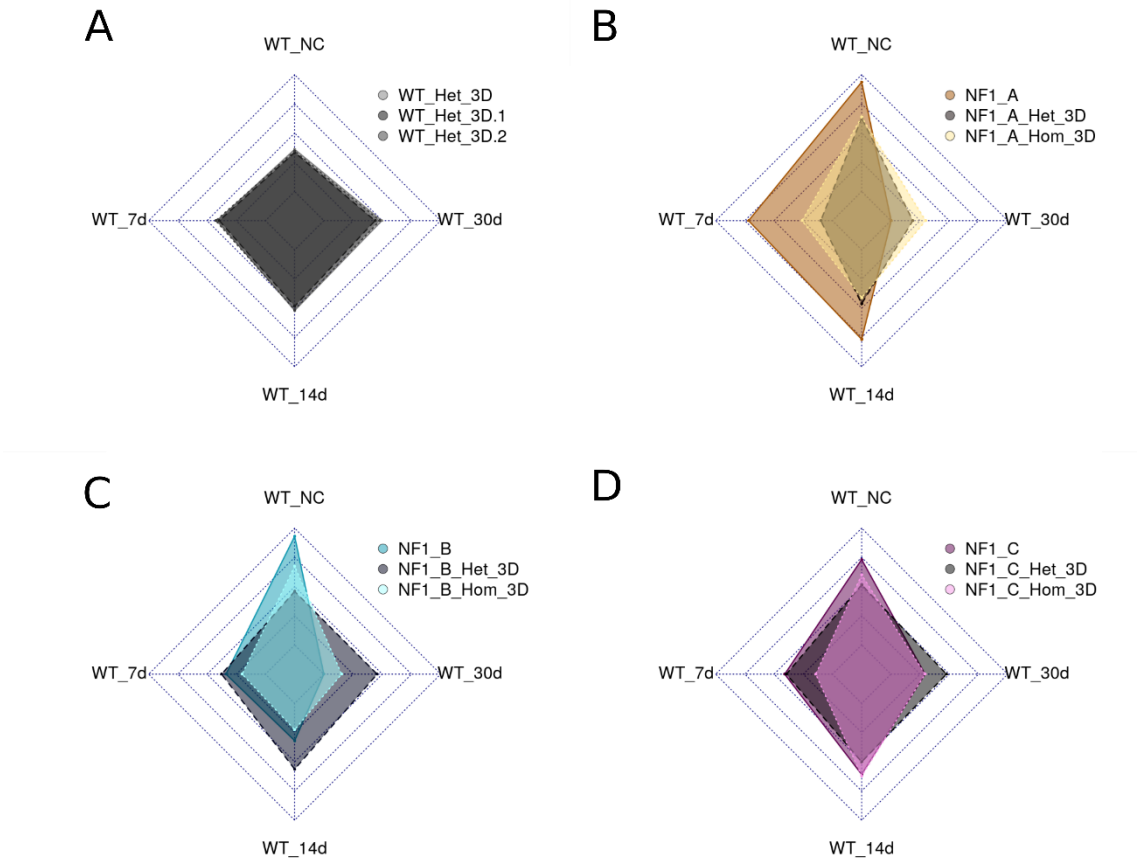

Figure R18. The expression roadmap of *NF1*(-/-) heterotypic spheroids of NF1_B and NF1_C closely resembles the one of *NF1*(+/+) heterotypic spheroids. Taking into account the stage-specific markers of the neural crest-Schwann cell (NC-SC) roadmap, the Manhattan distance of

each heterotypic or homotypic spheroid was calculated. Each Manhattan distance was plotted into radar plots: the upper tip represents the *NF1*(+/+) NC stage, left the *NF1*(+/+) 2D differentiating SC at the 7-day stage, bottom the *NF1*(+/+) 2D differentiating SC at the 14-day stage, and right tip the *NF1*(+/+) 2D differentiating SC at the 30-day stage. **A)** *NF1*(+/+) heterotypic spheroid triplicates are represented. Each replicate is very similar to the others. **B)** 5PNFiPSC (NF1_A) at 14-days of SC differentiation (orange), 5PNF-derived heterotypic spheroid (NF1_A_Het_3D, light brown), and homotypic spheroid (NF1_A_Hom_3D,yellow). **C)** 3PNFiPSC (NF1_B) at 14-days of SC differentiation (blue), 3PNF-derived heterotypic spheroid (NF1_B_Het_3D, grey), and homotypic spheroid (NF1_B_Hom_3D, light blue). **D)** Edited *NF1*(-/-) FiPS (NF1_C) at 14-days of SC differentiation (purple), heterotypic spheroid of the edited *NF1*(-/-) FiPS (NF1_C_Het_3D, grey), and homotypic spheroids (NF1_C_Hom_3D, pink).

1.5. Engraftment of heterotypic spheroids generate human neurofibroma-like tumors in nude mice

The same homotypic and heterotypic spheroid cultures from which RNA was extracted were used to test in parallel their capacity to engraft and form tumors *in vivo*. As explained above, engraftments were performed in collaboration with Dr. Conxi Lázaro's lab (ICO-IDIBELL).

Spheroids containing approximately a total of 2 million cells were resuspended in Matrigel and injected into the sciatic nerve of nude mice. We injected homotypic and heterotypic spheroids from the 3 *NF1*(-/-) cell lines. Each condition was injected into six different sciatic nerves. Homotypic and heterotypic spheroids from the same *NF1*(-/-) cell lines were injected in the left and right sciatic nerve of the same mouse, respectively. PNF-derived eFbs used to form heterotypic spheroids were also injected to control their capacity to engraft and generate cell growth as single cultures. **Figure R19** shows a schematic representation of the experiment.

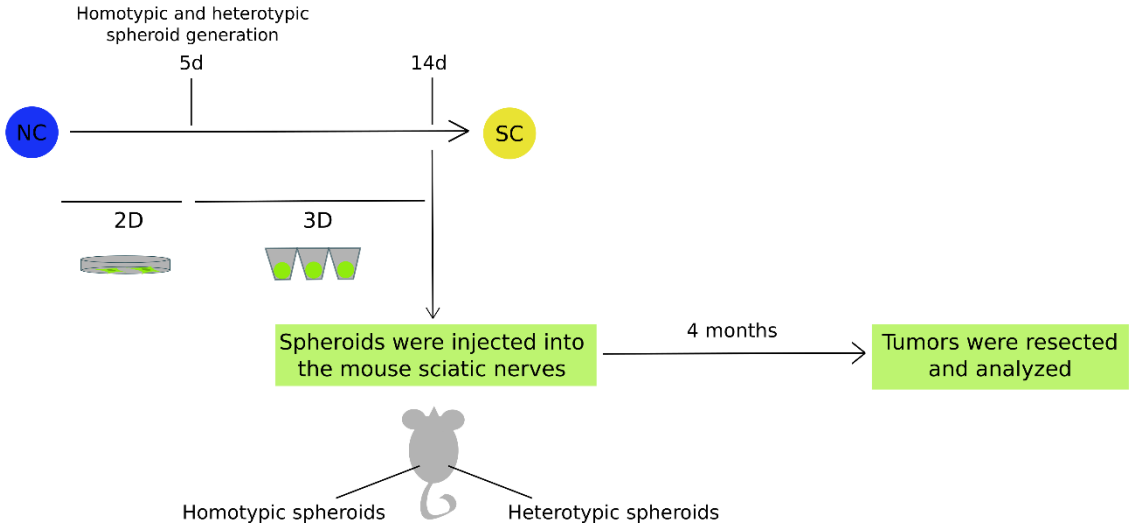

Figure R19. Schematic representation of the spheroid engraftment experimental design. NC cells were differentiated into SCs following the 2D differentiation protocol. At 5 days, cells were detached from plates and transferred into AggreWell™800 24-well plates with SC differentiation media with or without eFbs to generate heterotypic or homotypic spheroids, respectively. At 14 days, homotypic spheroids were injected in the left sciatic nerve and heterotypic spheroids in the right sciatic nerve. Each condition was injected into 6 different sciatic nerves. After 4 months, all mice were euthanized, and tumors were resected and analyzed.

Tumor growth was monitored throughout time by manual palpation. After 4 months, all mice were euthanized, and the sciatic nerve region was dissected. One mouse had to be euthanized 2 weeks earlier since it showed a prominent growth in its right leg that impaired its movement.

None of the *NF1*(+/+) heterotypic spheroid cultures were able to generate tumors or cell mass outgrowths in the engrafted mice. Neither did the PNF-derived single eFb cultures. In clear contrast, *NF1*(-/-) homotypic and heterotypic spheroids were able to engraft and

generate tumor masses. Interestingly, heterotypic spheroids generated more tumors and in a more consistent way. *NF1*(-/-) homotypic and heterotypic spheroids engrafted and generated 5 and 8 tumors, respectively. Table R6 summarizes the *in vivo* engraftment results.

	Injections	Grown tumors	Grown tumors S100B+	Grown tumors with Meissner-like corpuscles
NF1(+/+) Heterotypic spheroids				
- FiPS	6	0		
Total	6	0 (0%)		
eFb cultures				
- 5PNF-derived	2	0		
- 3PNF-derived	2	0		
Total	4	0 (0%)		
NF1(-/-) Homotypic spheroids				
- NF1_A	6	2	1	0
- NF1_B	5	2	1	1
- NF1_C	6	1	1	0
Total	17	5 (29.4%)	3 (17.6%)	1 (5.88%)
NF1(-/-) Heterotypic spheroids				
- NF1_A	6	0	0	0
- NF1_B	5	4	3	2
- NF1_C	6	4	4	0
Total	17	8 (47.1%)	7 (41.2%)	2 (11.8%)

Table R6. Summary table showing the results of the second engraftment experiment. The number of injections, grown tumors, tumors expressing S100B, and tumors with Meissner-like corpuscles for each cell line are shown. The percentage of tumors, tumors expressing S100B, and Meissner-like corpuscles per number of injections are shown.

Tumor samples were excised and, when possible, divided into three parts for: (i) fixation and paraffin/optimal cutting temperature (OCT) compound embedding for histological analysis; (ii) DNA extraction for genetic analysis; (iii) cryopreservation.

In general, tumors grew as independent tumor masses attached to the gastrocnemius (GC) muscle (Figure R20A, B), but sometimes, they also infiltrated into this muscle generating tumors inside it (Figure R20B, C).

Histological and Immunohistochemical analysis of tumors was evaluated by Dr. Cleofé Romagosa, a pathologist from Vall d'Hebron Hospital, an expert in NF1 tumors. In general, most of the tumors showed neurofibroma-like features, presenting immature cellularity and expression of the SC marker S100B (Figure R20C, E). We confirmed these tumors arose from transplanted spheroids by performing fluorescence IHC with hNu, an antibody that labels explicitly human nuclei (Figure R20D).

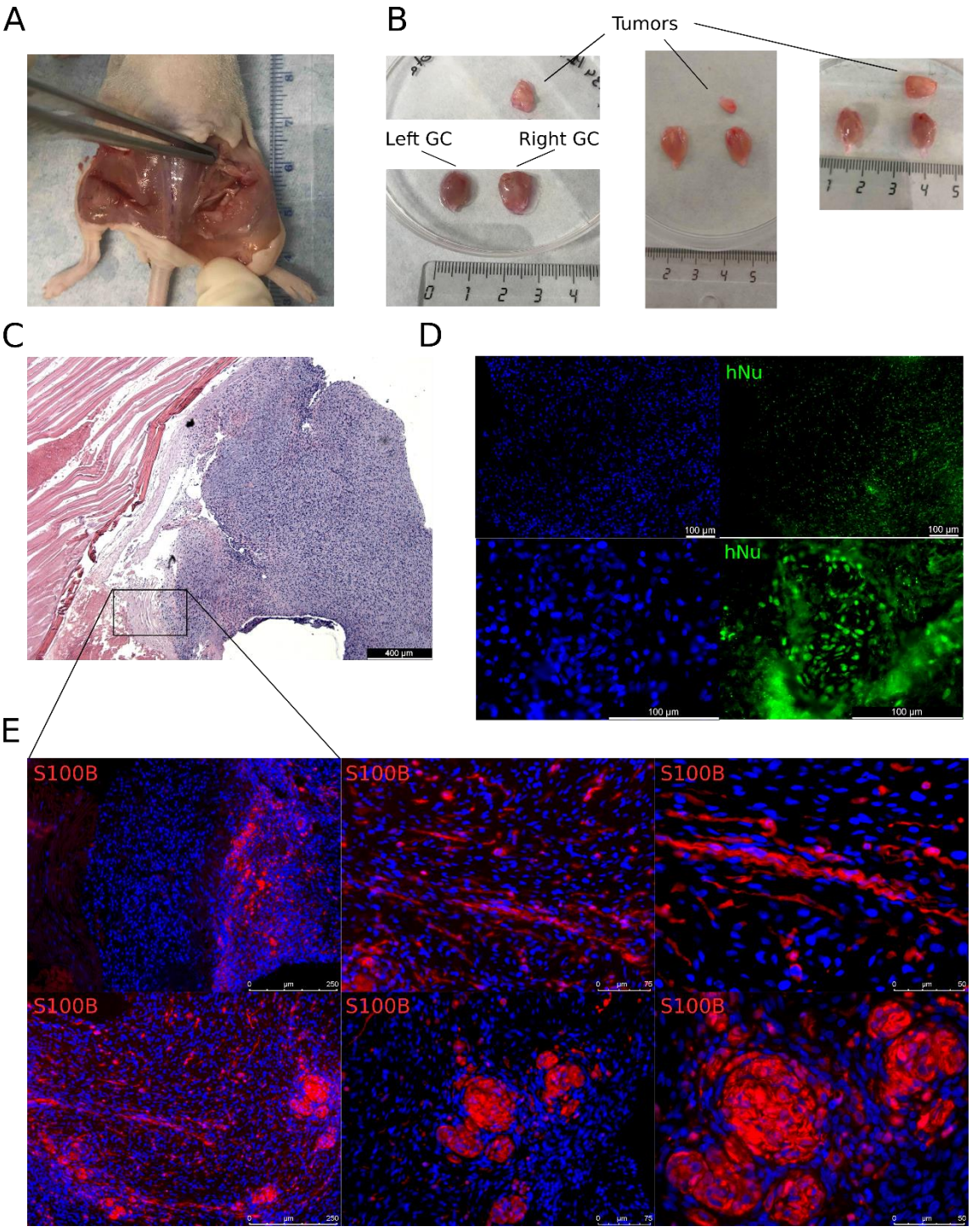

Figure R20. Engrafted spheroids generated human tumors that grew independently or inside the gastrocnemius muscle. A) Picture of a euthanized mouse in which sciatic nerves were exposed before dissecting the leg. **B)** The dissected parts of the mice and some tumors are shown. Left pictures: the left and right gastrocnemius muscles (GC) and a tumor from the right leg that grew attached to the GC muscle. The right GC muscle was slightly more prominent than the left GC muscle due to another tumor inside this muscle. Middle and right pictures: other dissected GCs and tumors are shown. **C)** H&E staining of tumor in B (left) that grew inside the right GC. Scale bar, 400 µm **D)** hNu fluorescence IHC of OCT embedded tumor shown in C. hNu stains human nuclear cells. DAPI was used to stain nuclei. Scale bar, 100µm **E)** S100B fluorescence IHC of

paraffin-embedded tumor shown in C. DAPI was used to stain nuclei. Left scale bar, 250µm; Middle scale bar, 75 µm; Right scale bar, 50 µm.

NF1(-/-) homotypic tumors were small, and the H&E staining showed immature (Figure R21A) and infiltrative (Figure R21B) neurofibroma-like features. In contrast, *NF1*(-/-) heterotypic spheroids generated bigger tumors, presenting various neurofibroma features such as Meissner-like corpuscles (Figure R20E, R21C), abundant collagen matrix (Figure R21D and F), infiltrating mast cells (Figure R21F), and disorganized spindle neurofibroma-like SCs (Figure R20E, R21G, and H). Besides, heterotypic spheroid from the NF1_C iPSC line also generated areas of chondrocyte and adipose tissue (Figure R21E, G, and H). It is known that the presence of Meissner-like corpuscles (also known as Wagner-Meissner corpuscles or pseudo-Meissner corpuscles) points to a neural origin of the tumor, especially in the context of neurofibromas, neurinomas, and neuromas (Kaiserling and Geerts 1986), indicating a SC maturation.

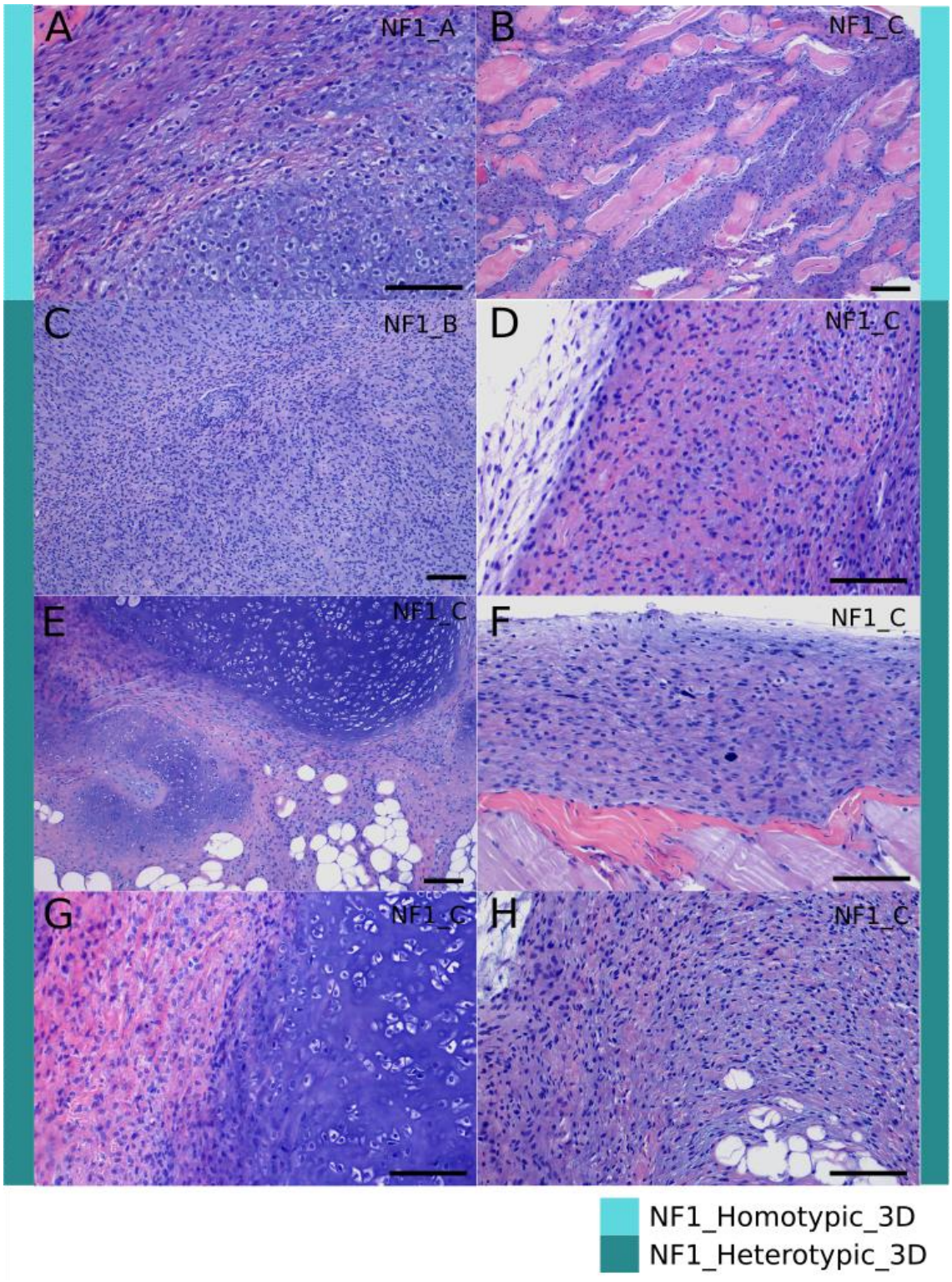

Figure R21. Hematoxylin and eosin staining of different homotypic and heterotypic neurofibroma-like tumors. A, B) Homotypic spheroid from NF1_A (A) and NF1_C (B) iPSC generated an immature neurofibroma-like (A) and infiltrative (B) tumors. **C, D, E, F, G, H)** Heterotypic spheroids from NF1_B (C) and NF1_C (D, E, F, G, H) generated tumors presenting various neurofibroma features like Meissner-like corpuscles (C), collagen (D and F), infiltrating mast cells (F), and neurofibroma-like SCs (G and H). Scale bars, 100 µm.

We further characterized tumors performing S100B and SOX10 IHC analysis.

As it is observed in PNFs, we identified two different patterns of S100B staining in tumors generated from homotypic and heterotypic spheroids engraftment: diffuse (**Figure R22A, B**) and focal (**Figure R22C, D**). Focal immunostaining was observed in individual cells (**Figure R22C**) as well as in Meissner-like corpuscles (**Figure R22D**).

Three of the tumors formed from *NF1*(-/-) homotypic spheroids (one of each cell line) were positive for S100B (**Table R6**), and one of them also showed Meissner-like corpuscles. Seven of the tumors formed from *NF1*(-/-) heterotypic spheroids were positive for S100B. Two presented Meissner-like corpuscles. Only two *NF1*(-/-) heterotypic cell lines generated tumors (NF1_B and NF1_C), and from those, all except for one resembled neurofibroma-like tumors.

The SOX10 staining also showed positivity in tumors cells, either scattered (**Figure R22E**) or forming part of Meissner-like corpuscles (**Figure R22F**).

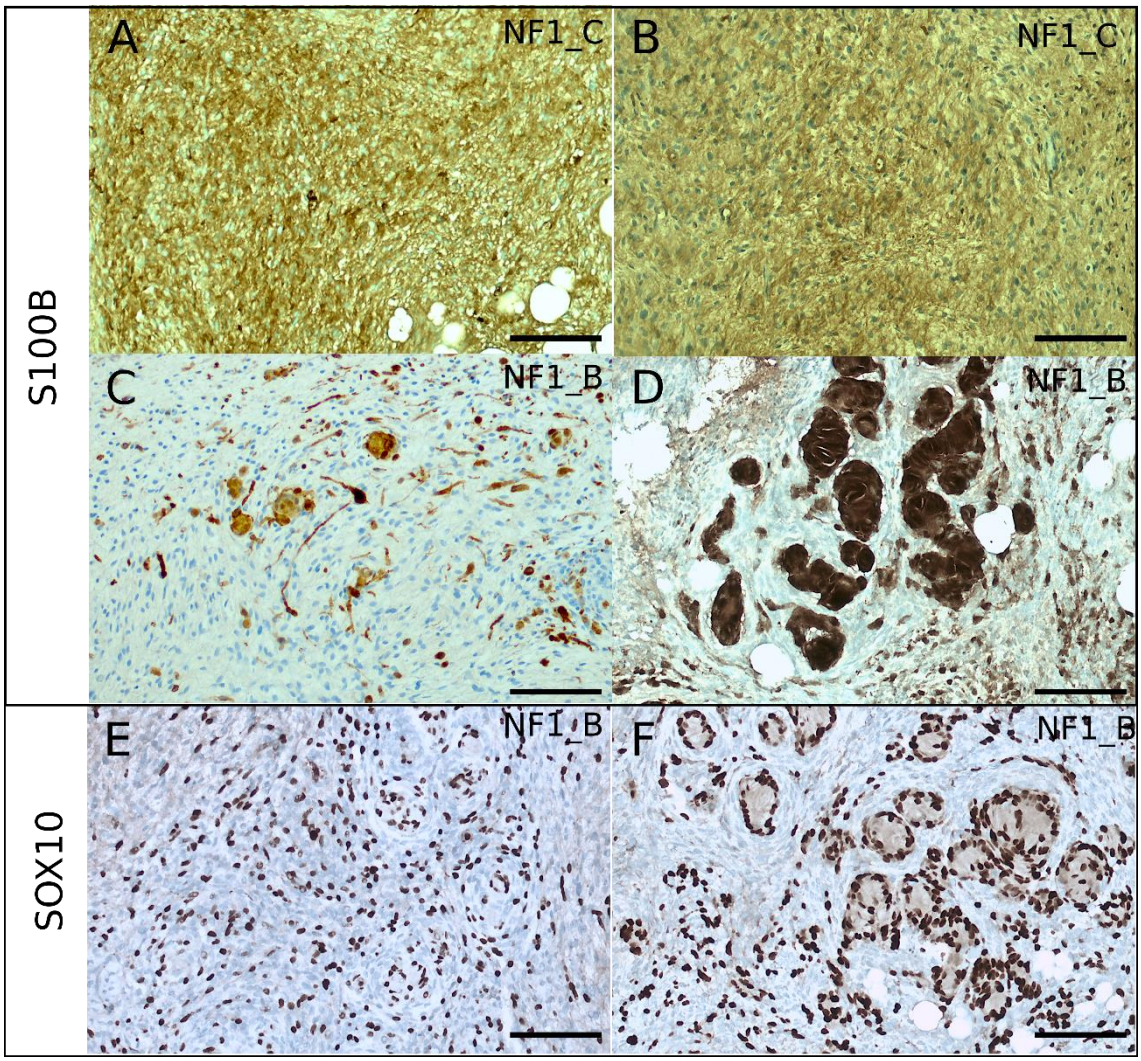

Figure R22. Neurofibroma-like tumors from heterotypic spheroids showed diffuse and focal S100B staining patterns. A, B, C, D) Representative images from immunohistochemical analysis of S100B showing a diffuse (A, B) and a local pattern (C, D). Notably, the focal immunostaining pattern was observed in Meissner-like corpuscles (D) as well as in individual cells (C). **E, F)**

Representative images from immunohistochemical analysis of SOX10 showing SOX10+ cells scattered in the tumor or forming part of cells in Meissner-like corpuscles. Scale bars, 100 μm.

To sum up, heterotypic spheroids generated a higher number of tumors (8 out of 17, 47.1%) than homotypic spheroids (5 out of 17, 29.4%). Besides, heterotypic spheroid tumors exhibited neurofibroma-like features (S100B positive immunostaining and Meissner-like corpuscles) more consistently than homotypic spheroids. These results showed that our 3D model has the full potential to generate human neurofibroma-like tumors in mice in a robust way.

Remarkably, the *NF1*(-/-) heterotypic spheroids that were able to form neurofibroma-like tumors upon sciatic nerve engraftment (NF1_B and NF1_C) were the ones that also exhibited a NC-SC expression roadmap profile similar to *NF1*(+/+) differentiating SCs at 30 days and similar to PNF-derived primary SC cultures (Figure R10 and R17). Again, the cell identity provided by the expression signatures obtained *in vitro* in heterotypic spheroids cultures remarkably coincided with the identity of the cell types that engrafted and expanded *in vivo.* These results highlight the utility of the NC-SC expression roadmap to monitor the successful generation of neurofibroma-like tumors upon *NF1*(-/-) heterotypic spheroid engraftment.

2. Neurofibroma cell composition: heterogeneity of the Schwann cell component

2.1. PNF-derived Schwann cells express markers from different stages along the NC-SC *in vitro* differentiation

Neurofibromas are mainly composed of SCs and eFbs, but also contain other cell types like perineurial cells, infiltrating immune cells, and endothelial cells. Despite the multiple cell type content, only cells of the SC lineage bear the double inactivation of the *NF1* gene. Since PNFs are originated during development, a still open question was whether all cells of the SC lineage have the same identity, or on the contrary, within PNFs co-exist SCs at different differentiation or maturation states.

As we showed earlier, we performed RNA-seq analysis of three independent PNF-derived SC cultures. We were able to analyze the NC-SC expression roadmap signature in these cells (Figure R23A, also in Figure R10B). PNF-derived SCs expressed a NC-SC roadmap signature resembling the signature of control *NF1*(+/+) cells at 30 days of SC differentiation. In addition, PNF SCs also expressed some genes from NC stage, 7 and 14 days of SC differentiation, suggesting they were expressing genes representing different differentiation or maturation states. However, we wondered whether all SCs were homogeneously expressing all genes, or there was heterogeneity regarding the expression of genes representing different SC states.

To better characterize this expression profile, we first performed an enrichment analysis of the genes expressed in the three independent PNF-derived SC cultures (Figure R23B). Some of the most significant biological processes (BP) identified by this analysis were “Schwann cell differentiation”, “gliogenesis”, and “glial cell differentiation”, emphasizing the expression of genes implicated in SC differentiation and the value of the NC-SC expression roadmap.

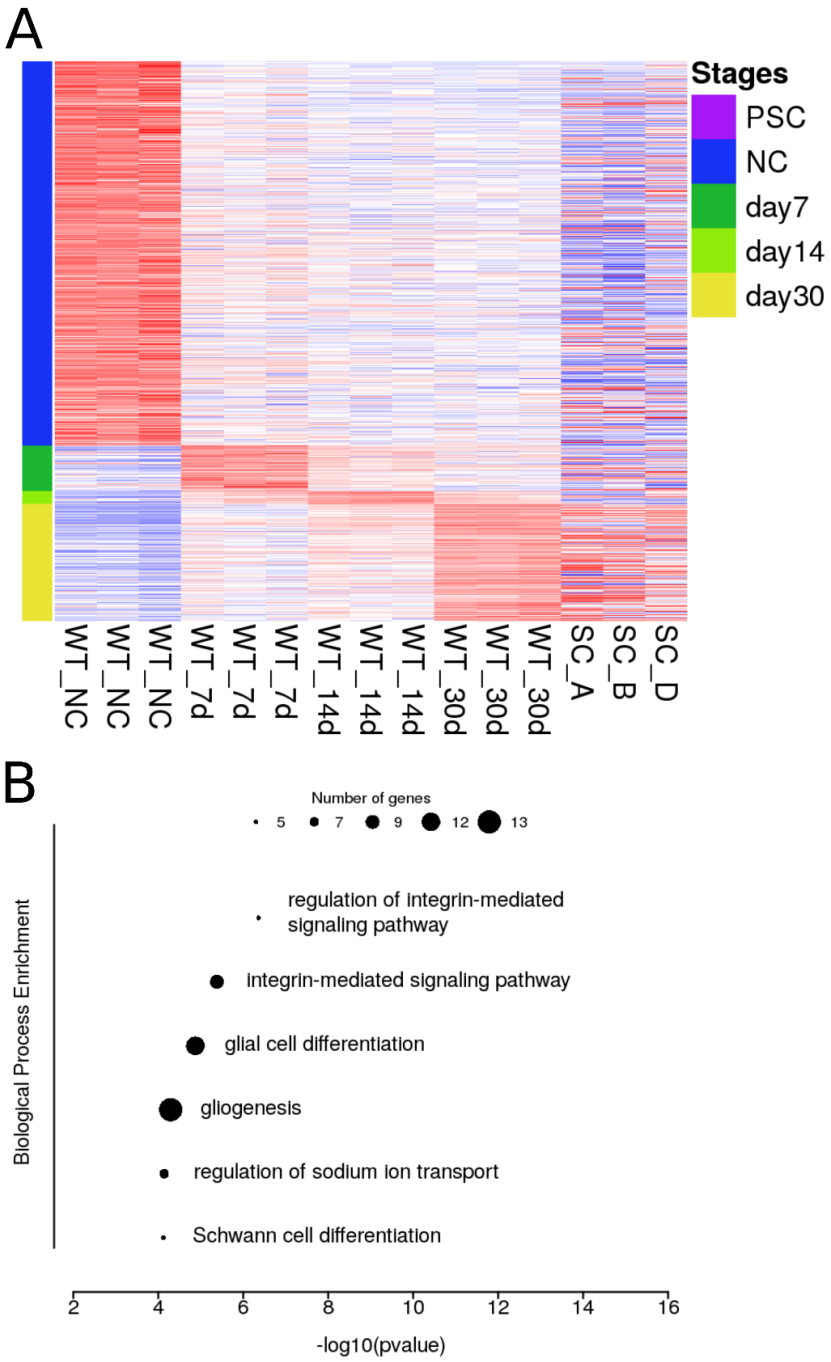

Figure R23. Plexiform neurofibroma-derived Schwann cells expressed markers from different stages of the neural crest-Schwann cell *in vitro* model. A) Heatmap with the stage-specific markers in the 2D *NF1*(+/+) differentiating SCs and in three independent PNF-derived SC cultures: SC_A (5PNF-derived SCs), SC_B (3PNF-derived SCs), and SC_D (6PNF-derived SCs). NC-stage specific markers (dark blue), and 7-day (dark green), 14-day (light green), and 30-day (yellow) stage-specific markers are shown in the left. The expression color range goes from dark blue, showing down-regulated genes to red showing up-regulated genes. Three independent differentiation experiments are shown. **B)** Enrichment analysis of the expressed genes in the three independent PNF-derived SC cultures showing the six most significant biological processes (BP) represented by genes of the NC-SC *in vitro* model. In the X-axis the p-value associated with each enriched BP is represented. In the Y-axis the six most significant BP are presented. The size of the full black circle represents the number of genes contained in each BP.

2.2. P75 and S100B are differentially expressed along the neural crest-Schwann cell lineage

To further investigate the degree of homogeneity in the expression of NC-SC lineage genes within the PNF SC component, we selected two lineage markers with a different pattern of expression: *NGFR* and *S100B*. *NGFR* gene (p75) is expressed from the NC stage throughout the entire SC differentiation axis. The gene *S100B* is expressed in SC committed cells (Jessen and Mirsky, 2005). We first used RNA-seq data from the *in vitro* NC-SC differentiation process of control *NF1*(+/+) iPSC and analyzed the expression levels of both markers (**Figure R24**). As already shown (**Figure R6D**), the *NGFR* gene was not expressed at the pluripotent stage abut was highly expressed in the NC stage, and maintained in the 7, 14 and 30 days of SC differentiation. *S100B* gene, instead, showed a different expression pattern, in which no expression was observed at the pluripotent or NC stages, was expressed at low levels at 7 and 14 days differentiating SC timepoints and at high levels at the 30 day.

These results were representing the expression at a population level, not at an individual cell level. However, our results indicated that the expression levels of these two markers were able to distinguish different populations along the NC-SC lineage. A cell at an earlier stage, precursor-like cell, would express significant levels of p75 but not of S100B. A cell of a later stage, already committed to a SC identity, would express both p75 and S100B.

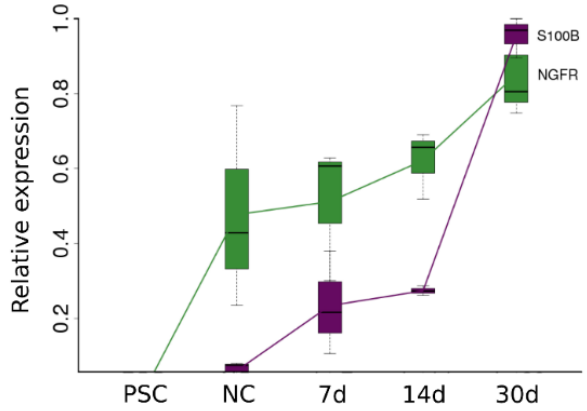

Figure R24. Differential expression patterns of *NGFR* and *S100B* along with the neural crest-Schwann cell *in vitro* differentiation process. Boxplot representing *NGFR* and *S100B* relative expression (RNA-seq analysis) in control *NF1*(+/+) FiPS at different stages/timepoints along the NC-SC *in vitro* differentiation. Three independent differentiation experiments are shown.

2.3. Plexiform neurofibroma-derived Schwann cells heterogeneously express p75 and S100B

We then focused our p75/S100B co-expression analysis directly in PNF-derived SC cultures. We performed co-immunostaining of p75 and S100B in SC cultures from different PNFs (Figure R22). We observed that most cells in PNF SC cultures co-expressed both markers, but also that some cells expressed only one of the markers, either p75 or S100B. The results supported the existence of cell heterogeneity in the SC component of PNFs.

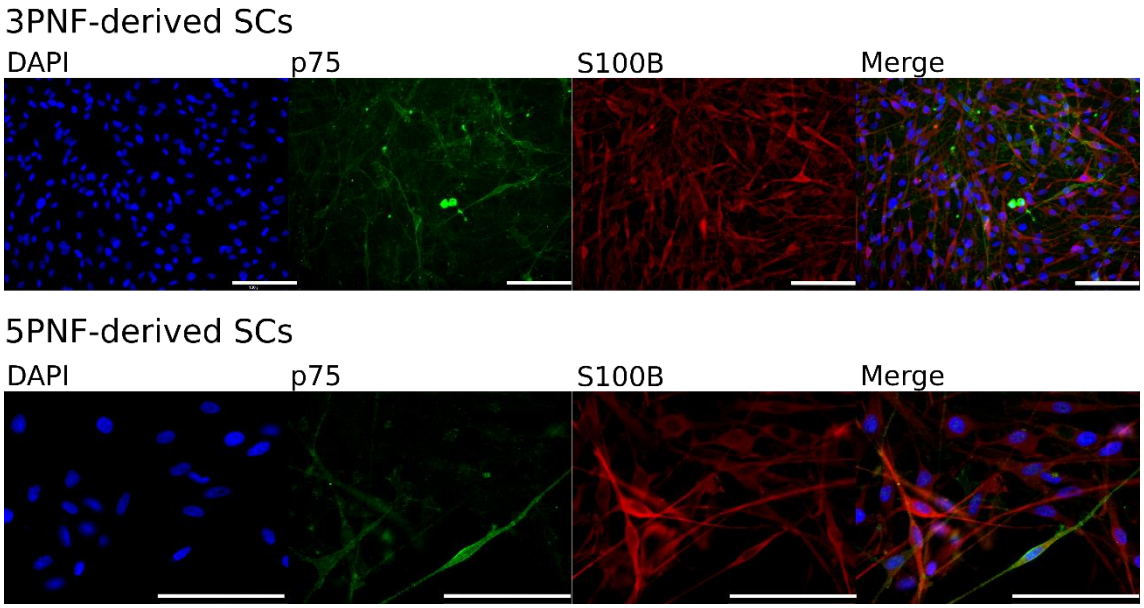

Figure R25. p75 and S100B double staining evidenced cell heterogeneity in plexiform neurofibroma-derived Schwann cell cultures. Immunocytochemistry analysis of p75 and S100B markers in 3PNF- and 5PNF-derived SC cultures. DAPI was used to stain the nuclei. Scale bars, 100 µm.

To control for the effect of culturing SCs on the expression of p75 and S100B and asses a real PNF SC heterogeneity, we decided to analyze these two markers directly in PNF dissociated single cells. To have quantitative analysis, we used flow cytometry to analyze thousands of individual cells of each PNF. We selected 5 PNFs from 5 independent NF1 patients (Table R7), digested them into single-cell suspensions, and immunolabeled them to analyze p75 and S100B expression by flow cytometry (Figure R26).

Tumor	3PNF	19PNF	20PNF1	23PNF	30PNF
Age at resection	8	45	11	8	19
Gender	Female	Female	Male	Female	Male

Table R7. Clinical data of the 5 plexiform neurofibromas from independent NF1 patients used in flow cytometry analysis.

Flow cytometry analysis revealed the existence of four populations of cells within all 5 PNFs, according to the co-expression of p75 and S100B: a large population of cells negative for both markers and three populations being p75+/S100B-, p75+/S100B+, and p75-/S100B+. The direct analysis of p75 and S100B on PNF dissociated cells also evidenced the presence of cells with different identities conforming the SC component (Figure R26A). To provide reliable percentages of these populations, at least 100 cells had to be counted. Moreover, each dissociated-PNF exhibited different percentages of these 4 populations (Figure R26B). Some PNFs as 20PNF1 or 30PNF displayed a high proportion of double-positive p75+/S100B+ cells while others as 23PNF presented a high proportion of the p75+/S100B- cells. There was not found any correlation between the different proportions of cells and the age at tumor resection nor the gender of the patient.

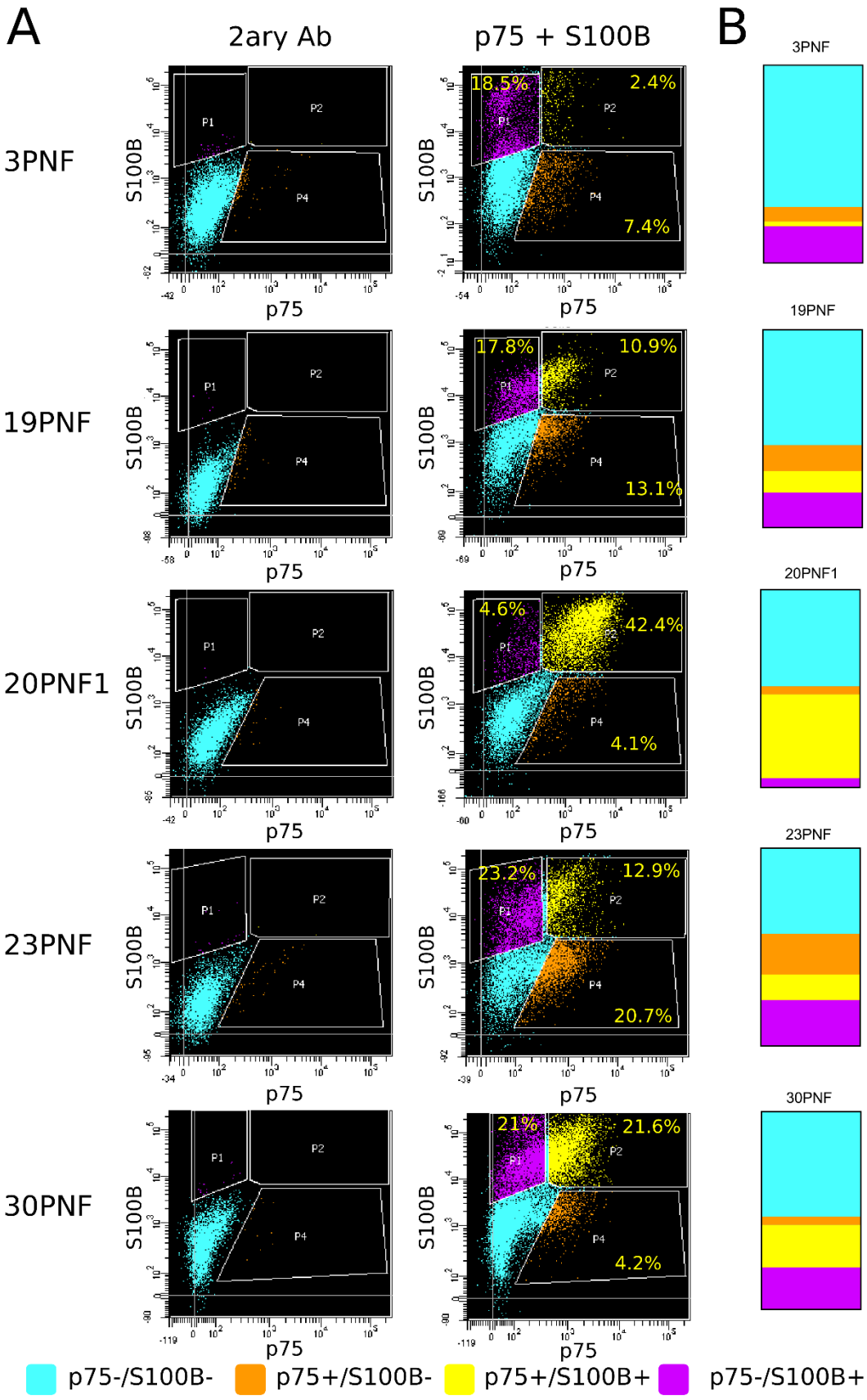

Figure R26. P75 and S100B double staining uncovered cell heterogeneity of the Schwann cell component within plexiform neurofibromas. A) Flow cytometry analysis of p75 and S100B of 5 independent PNFs. Left panel of PNF reflects the signal of the secondary antibodies (2ary Ab) as

controls. In the X-axis, the p75 expression is represented, while in the Y-axis, the S100B expression. Each dot represents a cell. Each dissociated-PNF exhibited a homogenous negative population for both antibodies. Right panels, each dissociated-PNF was incubated with primary and secondary antibodies. Double-negative p75-/S100B- cells (light blue), p75+/S100B- cells (orange), double-positive p75+/S100B+ cells (yellow), and p75-/S100B+ cells (purple) are shown. **B)** Companion graphs showing the proportions of each different cell population within PNFs. The entire square represents 100% of the population, and the area of each color represents the proportion of each cell population. Some PNFs as 20PNF1 or 30PNF displayed a high proportion of double-positive p75+/S100B+ cells while others as 23PNF presented a high proportion of the p75+/S100B- cells.

2.4. Heterogeneity of the Schwann cell component of PNFs revealed by scRNAseq

The heterogeneity of p75/S100B co-expression observed within the SC component of PNFs, both by analyzing SC cultures and directly dissociating PNF cells, reinforced the idea that the SC component of PNFs was heterogeneous, containing cells with a precursor-like (or less differentiated) identity of the NC-SC axis (p75+/S100B- cells) and cells already committed to SCs (p75+/S100B+ cells). To get a better insight in this regard, we performed single-cell RNA-seq (scRNAseq) analysis in three different PNFs (19PNF, 20PNF1, and 23PNF) using 10x genomics technology. We were able to analyze the expression of more than 2000 genes in 5087, 6155, and 9092 single cells, respectively.

ScRNAseq analysis identified clusters of cells representing different cell types composing PNFs: SCs, eFbs, endothelial cells, T cells, macrophages, etc. (**Figure R27**). We used singleR, which takes advantage of reference transcriptomic datasets of pure cell types (HumanPrimaryCellAtlas) to infer the cell type identity of each single cell independently (**Annex2 Figure A2-R**).

Different clusters were identified as part of the SC component, eFb component, or endothelial cell components, indicating the complexity of inferring cell identities from variable gene expression and from the limited data on cell types that we still have as a reference. Interestingly, within the SC component, we identified different SC clusters, probably representing SC subpopulations (**Figure R28**). The majority of the cells of the SC component expressed markers like *SOX10,* a NC marker expressed throughout SC differentiation. Even more cells expressed *CDH19,* a SCP marker. Opposed to a SC component level of expression, other markers had a restricted expression to subpopulations of SC component cells, like *S100B* and *PLP1*, genes commonly expressed in committed SCs (**Figure R28**). Thus, PNFs seemed to be composed of distinct SC subpopulations. At least, one expressing marker that appear early in the NC-SC axis, suggesting a precursor-like identity, and another subpopulation expressing these markers and also SC committed markers, suggesting a singular committed SC expressing most of the classical markers of the NC-SC axis. These results were in accordance with flow cytometry data analyzing co-expression of p75 and S100B markers (**Figure R26**).

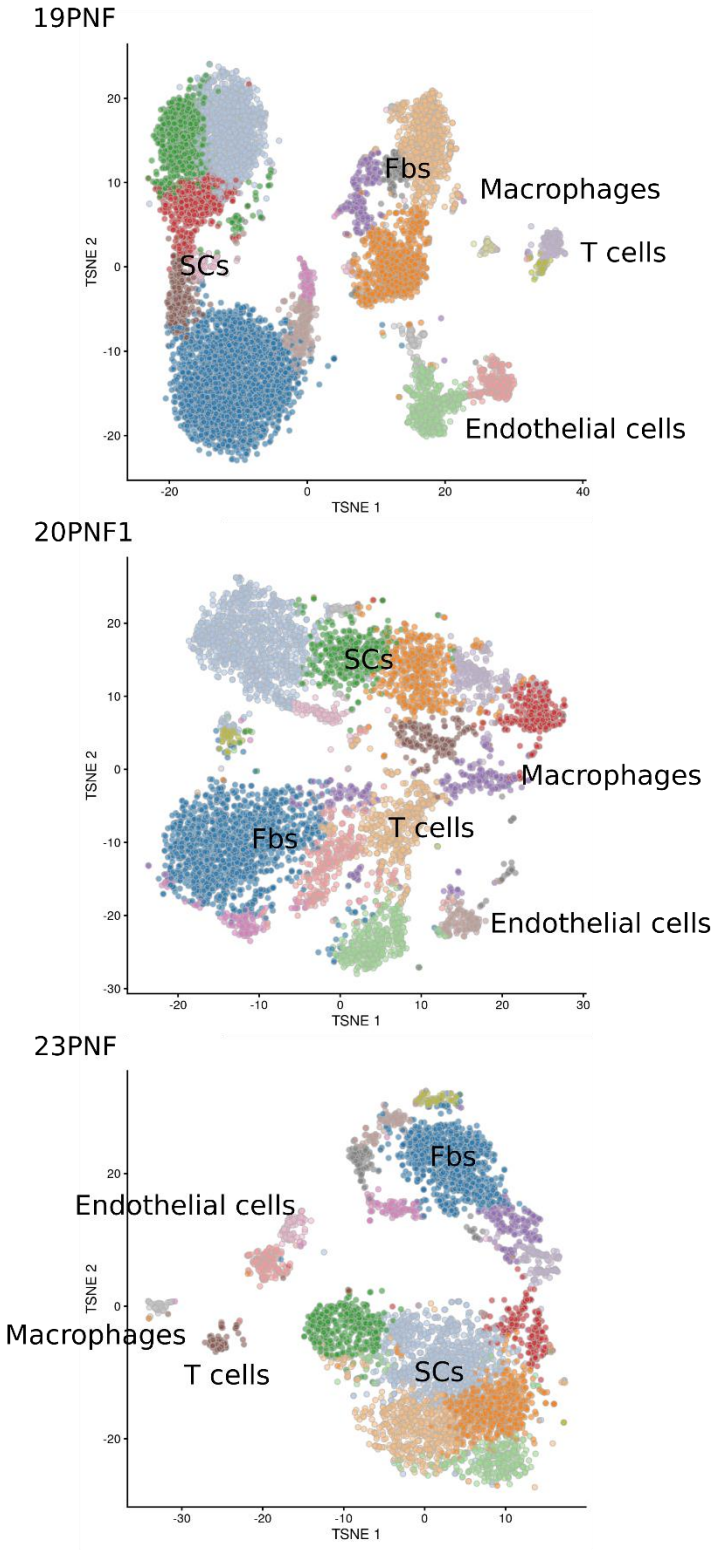

Figure R27. Decomposing cell types within plexiform neurofibromas using scRNAseq analysis. Schwann cell component (SCs), fibroblast components (eFbs)m endothelial cells, macrophages, and T cells were identified as cell types composing PNFs. A t-distributed stochastic neighbor embedding (tSNE) plots displaying the different cell clusters identified for each PNF (19PNF, 20PNF, and 23PNF) are shown.

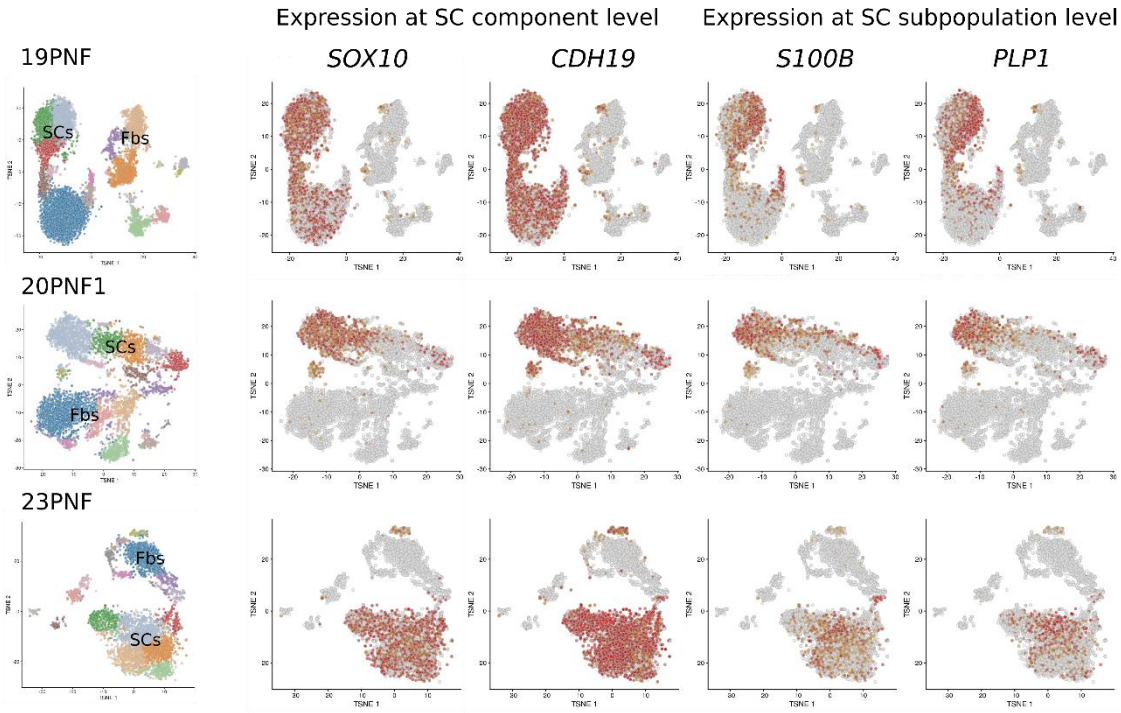

Figure R28. Schwann cell component of plexiform neurofibromas is composed of two different Schwann cell subpopulations. TSNE plots displaying single cell expression data of *SOX10*¸ *CDH19*, *S100B*, and *PLP1* markers in three different PNFs. Most cells forming the SC component expressed *SOX10*, and *CDH19* while just a subpopulation of cells expressed *S100B*, and *PLP1.* These results suggest the existence of at least two SC subpopulations, one expressing markers of a precursor-like cell, and another expressing these markers together with markers of a committed SC.

2.5. Heterogeneity of the endoneurial fibroblast component of PNFs

In addition, we also identified distinct subpopulations of eFbs (**Figure R27**), all of them defined by markers such as *MEDAG1* and the key mesenchymal transcription factors *PRRX1*, and *TWIST1* (**Figure R29**). The majority of cells expressed *MEDAG*, and *PRXX1*, and a portion of them expressed *TWIST*. The eFb component displayed less heterogeneity than the SC component.

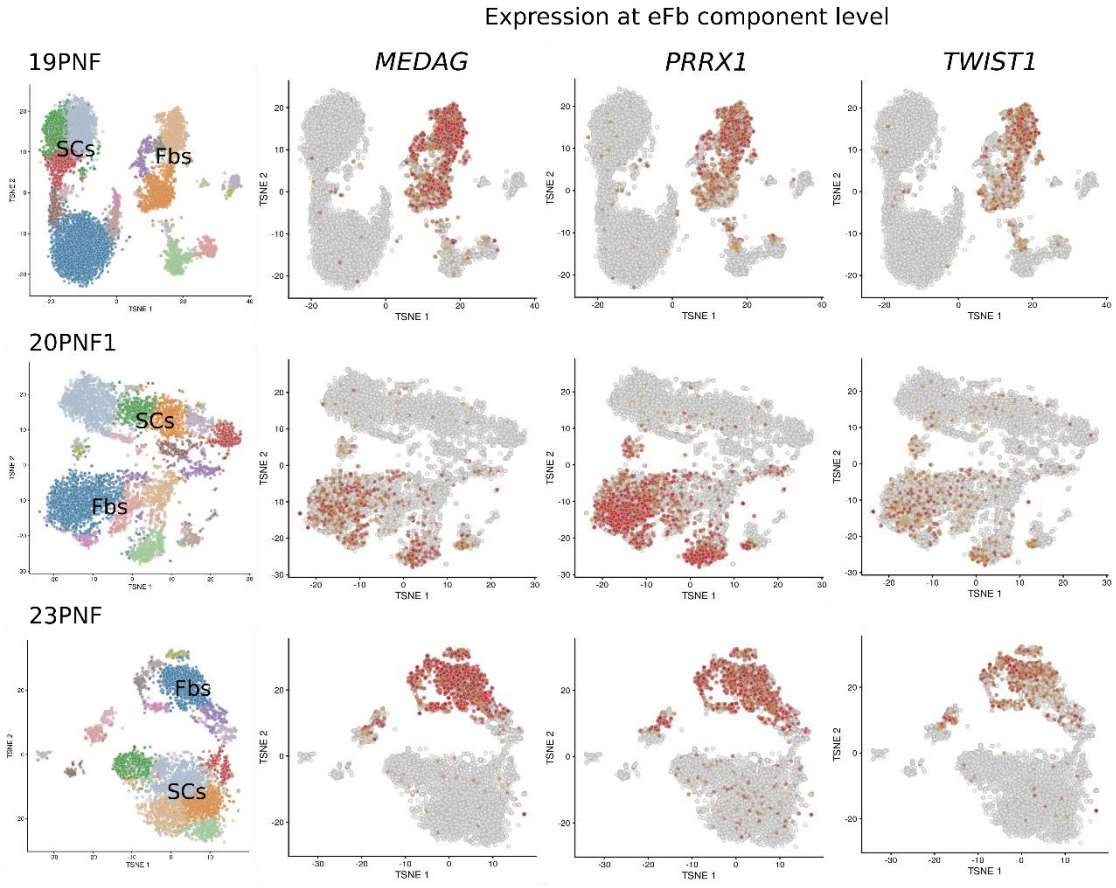

Figure R29. Different fibroblast subpopulations were identified. TSNE displaying single cell expression data of *MEDAG*¸ *PRRX1*, and *TWIST* markers in three different PNFs.

3. Study of intracellular signaling in cutaneous neurofibroma

3.1. Experimental design to study intercellular signaling between Schwann cells and fibroblasts in cNFs

Cutaneous neurofibromas (cNF) are present in nearly all NF1 individuals, representing for many of them, the most important clinical manifestation affecting their quality of life. We need to better understand cNF formation and growth to identify ways for an effective treatment. It is thought that the inactivation of the *NF1* gene in SC precursors triggers cNF formation. Recent sequencing projects seem to indicate that from a genetic perspective, there is no other additional recurrent genetic alteration in SCs besides the *NF1* inactivation involved in cNFs. But cNFs are composed of multiple different cell types in addition to *NF1*(-/-) SCs, like eFbs and others. It is well established the importance of tumor microenvironment and the role of other cell types in the formation of cNFs. However, the specific signaling among different cell types and their functional implication on neurofibroma formation need to be further analyzed and dissected. We aimed to identify a cell type-specific expression profile in cNFs produced by heterotypic interactions between SCs and eFbs, and translate these changes in expression into signaling pathways.

We designed a co-culture experiment in which cNF-derived SC cultures and cNF-derived eFb cultures were grown together to analyze the specific expression profile of each cell type due to heterotypic cell interaction (Figure R30). By comparing the expression of single cell cultures (SC; eFb) with SC-eFb co-cultures, we planned to identify those genes that changed their expression due to the interaction between both cell types (physical interaction or through secretion). To ascertain the cell type within co-cultures responsible of specific differential gene expression, we planned to analyze the genetic variation of expressed genes. We first aimed to identify the individual genetic variation of each of the 4 cNFs used (each from a different individual) and planned to perform co-cultures mixing SCs and eFbs from different cNFs (up to 16 different co-cultures). Specific coding variants in differentially expressed genes could allow the identification of the cell type expressing them. So that, we performed sequencing on cNF and identified genetic variation, we established cultures of specific cell types for each cNF and co-cultures, and finally collected RNA and supernatant from all cultures to perform RNA-seq analysis as well as secretory profile analysis.

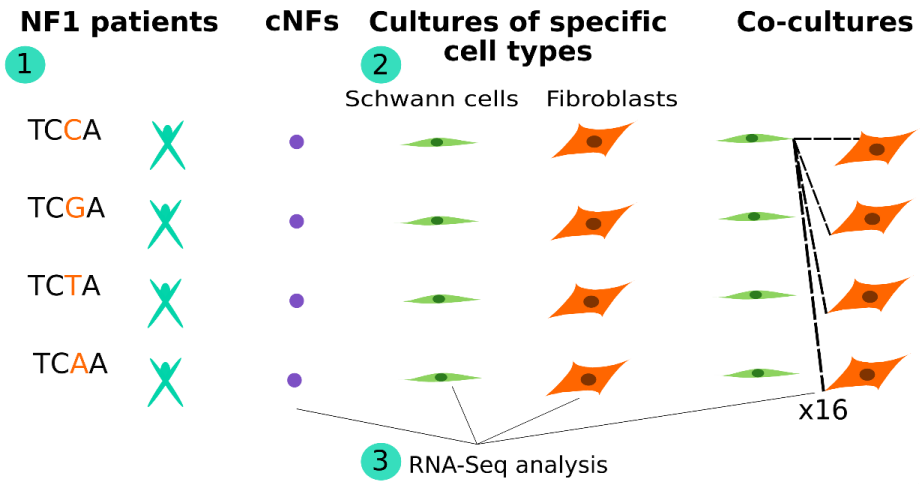

Figure R30. Schematic representation of the experimental design to study heterotypic signaling between Schwann cells, and endoneurial fibroblasts from cutaneous neurofibromas. First (1), individual coding genetic variation of each NF1 patient was identified. Then (2), specific cell type cultures, SCs (green), and eFbs (orange) of each cNF (purple) were established, facilitating the generation of 16 different co-cultures. Finally (3), RNA from cNFs, SC, and eFb single cultures, and SC-eFb co-cultures was obtained and sequenced.

3.2. *NF1* germline and somatic mutation characterization of cNFs and selection of cNFs

To end up selecting 4 suitable cNF for co-culture experiments, we first had to analyze several more. We dissociated 9 different cNFs from 7 independent NF1 patients: 1 from patient 1 (1cNF), 1 from patient 17 (17cNF1), 2 from patient 21 (21cNF1 and 21cNF2), 2 from patient 18 (18cNF1 and 18cNF2), 1 from patient 27 (27cNF12), 1 from patient 28 (28cNF1) and 1 from patient VGL (VGL1). From these 9 different cNFs, we established SC and eFb cultures and extracted DNA from each culture (Table R8).

The somatic inactivation of the *NF1* gene in approximately 25% of cNFs is evidenced by a LOH (Serra et al. 1997). LOH might be due to homologous recombination reducing to homozygosity most part of the 17q arm or to deletions involving *NF1* gene that may range in size from 80kb to 8 Mb of 17q (Garcia-Linares, 2011). To maximize the detection of heterozygous variants on chromosome 17 in the selected cNFs, we looked for neurofibromas not harboring LOH as a somatic mutation.

Hence, we performed a Multiplex Microsatellite PCR Analysis (MMPA) analyzing 16 different microsatellites, mostly located in chromosome 17 (Figure R31) (Garcia-Linares et al. 2011). DNA from *NF1*(+/-) cNF-derived eFbs, containing only the constitutional *NF1* mutation, was compared to DNA from *NF1*(-/-) cNF-derived SCs, bearing the constitutional and the somatic *NF1* mutations. We compared all alleles from the eFb and SC cultures. LOH was detected as the loss of one of the alleles in a specific microsatellite in SCs. Although the specific breakpoint could not be detected, we were able to estimate the size of the LOH approximately.

From 9 different cNFs analyzed, only three cNFs (18cNF, 18cNF2, and 21cNF2) harbored a LOH as a somatic mutation (Figure R31).

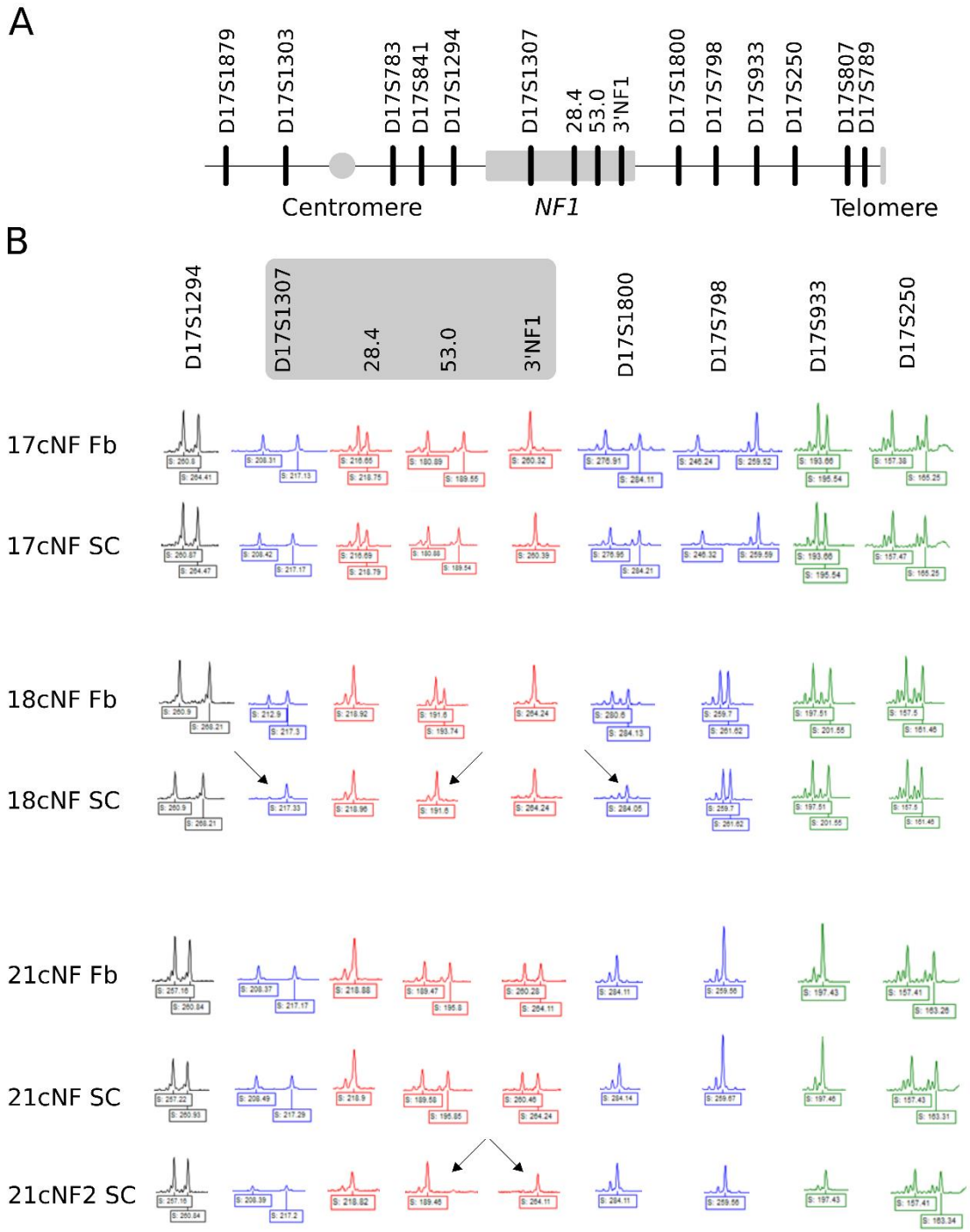

Figure R31. Loss of heterozygosity in the *NF1* gene can be seen as the loss of one of the alleles in specific microsatellites in chromosome 17. A) Schematic representation of the 15 microsatellites located in chromosome 17 analyzed by the MMPA technique. Two microsatellites were located in the p arm of chromosome 17, and thirteen in the q arm, four of which were located inside the *NF1* gene (grey rectangle). Another analyzed microsatellite was located in chromosome 2 (not shown). The centromere (grey circle) and the telomere (the grey vertical line at the end of the chromosome) are depicted. Each vertical black line represents the location of each microsatellite. **B)** Top: 9 microsatellites in q arm were represented: 1 is located 5' of the *NF1* gene (grey rectangle), 4 are located inside the gene, and 4 are located 3' downstream. Bottom: specific microsatellite profiles of four different cNFs from three independent NF1 patients. For each patient, a microsatellite profile of cNF-derived eFbs is shown as well as microsatellite profiles

from related cNF derived-SCs. Below each peak, the size of the amplified allele of each microsatellite is indicated inside a square. LOH in SCs is indicated with arrows.

A summary of the LOH analysis of 6 independent cNFs is shown in Figure R32. All patients had between 2 and 5 homozygous microsatellites.

Thus, with all these data, we discarded 18cNF, 18cNF2, and 21cNF2 as candidates for the co-culture experiment since they harbored LOH as a somatic mutation.

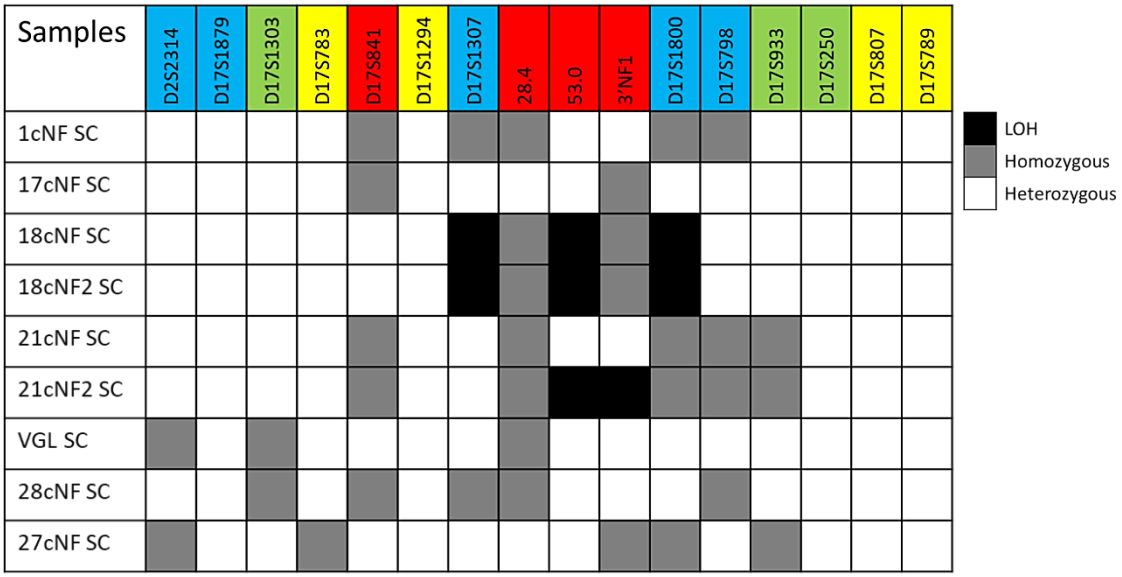

Figure R32. Summary of the results from the Multiplex Microsatellite PCR Amplification technique in 9 independents cutaneous neurofibromas. Microsatellites are labelled in different colors. Heterozygous microsatellites (white), homozygous microsatellites (grey), and LOH (black) are shown.

After discarding 3 tumors exhibiting LOH at 17q, 6 cNFs were still available, and we had to select only 4 of them.

We selected those that, after digestion, showed a high cellular content and the best SC viability. Taking this into account, we excluded VGL1N as a candidate due to low cellular density after tumor digestion and 21cNF1 due to low SC viability.

1cNF, 17cNF1 (17cNF from now on), 27cNF12 (27cNF from now on), and 28cNF1 (28cNF from now on) were the selected cNFs (Table R8). SC cultures from selected cNFs were analyzed to identify, using a custom Next Generation Sequencing panel (Castellanos et al. 2017), the specific constitutional and somatic *NF1* point mutations that were validated by Sanger sequencing.

cNF	LOH	SC culture	Cand.	Constitutional mutation	Somatic mutation
1cNF	No	Optimal	Yes	c.5898_5899delGA	c.4120C>T
17cNF1	No	Optimal	Yes	c.3826C>T	c.4537C>T
21cNF1	No	Not good	No		
21cNF2	Yes	Optimal	No		
18cNF1	Yes	Bad	No		
18cNF2	Yes	Bad	No		
27cNF	No	Optimal	Yes	c.4309G>T	c.810_833delAATCATTCTCCTTATCTTGTGTCC
28cNF	No	Optimal	Yes	c.3233C>G	c.3158C>G
VGL1N	No	Bad	No		

Table R8. Summary table showing all cutaneous neurofibromas analyzed. cNFs: cutaneous neurofibromas. Loss of heterozygosity analysis (LOH); SC culture wield (SC culture), selected candidates (Cand.), and constitutional and somatic mutations are shown.

Clinical data of patients and selected neurofibromas is shown in **Table R9**. Two were from men (1 and 17), 46 and 34 years old, respectively, and two from women (27 and 28) 34 and 76 years old, respectively.

Patient information				*Tumor information*			
Patient ID	Sex	Decade of birth	Age (at tumor resection)	Tumor ID	Location	Growth status at the time of sampling	Type of tumor
1	M	1970s	46	1CNF1	shoulder	10cm	CNF Diffuse
17	M	1980s	34	17CNF1	Left arm	2-3cm	CNF
27	F	1970s	34	27cNF12	-	-	CNF
28	F	1930s	76	28cNF1	-	-	CNF

Table R9. Patient and neurofibroma data from the 4 selected cutaneous neurofibromas.

3.3. Co-culture experiment

cNFs are benign tumors containing many cells types with different proportions depending on the cNF. However, the main cell types are SCs and eFbs and on average, they are approximately composed by 60-70% of SCs and 30-40% of other cell types, mainly eFbs (Carrió et al. 2018b). To reproduce in SC-eFb co-cultures the same proportion of cells present in cNFs, we tested different number of SCs and eFb that needed to be seeded at the beginning of the co-culture experiment to end up with approximately 70% SCs and 30% eFb.

We used a SC culture from 21cNF2 and an eFb culture from 1cNF. In addition to single cell cultures, we seeded different proportions of cells, 70% SCs– 30% eFb, 80% SCs – 20% eFb, and 90% SCs – 10% eFb in Poly-L-lysine and Laminin-coated dishes and Schwann cell media (SCM) conditions without IBMX at 37ºC and 10% CO_2 (see Materials & Methods for more details) (Figure R33). Twenty-four hours later, the media was changed to SCM without forskolin nor IBMX, and cells were left in these conditions until 72 hours after seeding them.

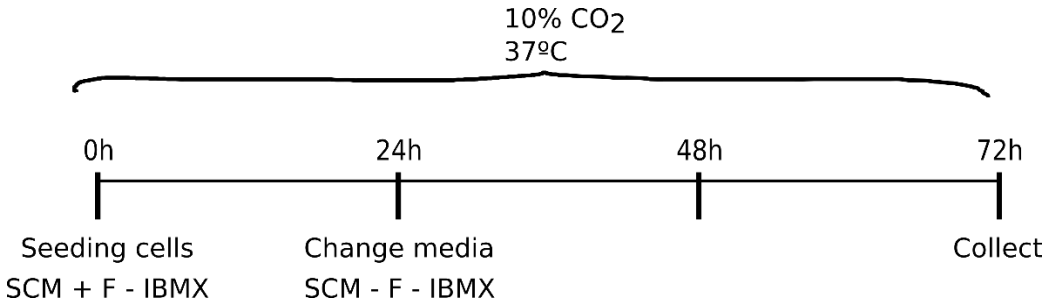

Figure R33. Schematic representation of the co-culture experimental conditions.

After 72 hours, single cultures and co-cultures were analyzed by flow cytometry using p75 labeling (Figure R34). 98.1% of SC cultures were p75+, indicating an almost pure SC culture. Contrarily, 2.6% of cells in eFb culture were positive for p75, indicating a low proportion of SC "contaminating" EFb cultures. These results indicated that single cultures were highly pure, although the presence of a small percentage of contaminating cells. We then examined results from co-cultures bearing different initial proportions of cells (Figure R34C). Flow cytometry analysis of p75 positive cells indicated that an initial 70% SCs– 30% eFb provided a proportion of 65.2% of 75+ at 72 hours. Initial conditions of 80% SCs– 20% eFb provided a final 74.2% of p75+ cells. And the 90% SCs– 10% eFb of initial cells ended up constituting a 84.7% of p75+ cells.

This analysis evidenced that seeding an initial proportion of 70% SCs– 30% eFb was enough to obtain a percentage of cells at 72 hours closely resembling cNF composition.

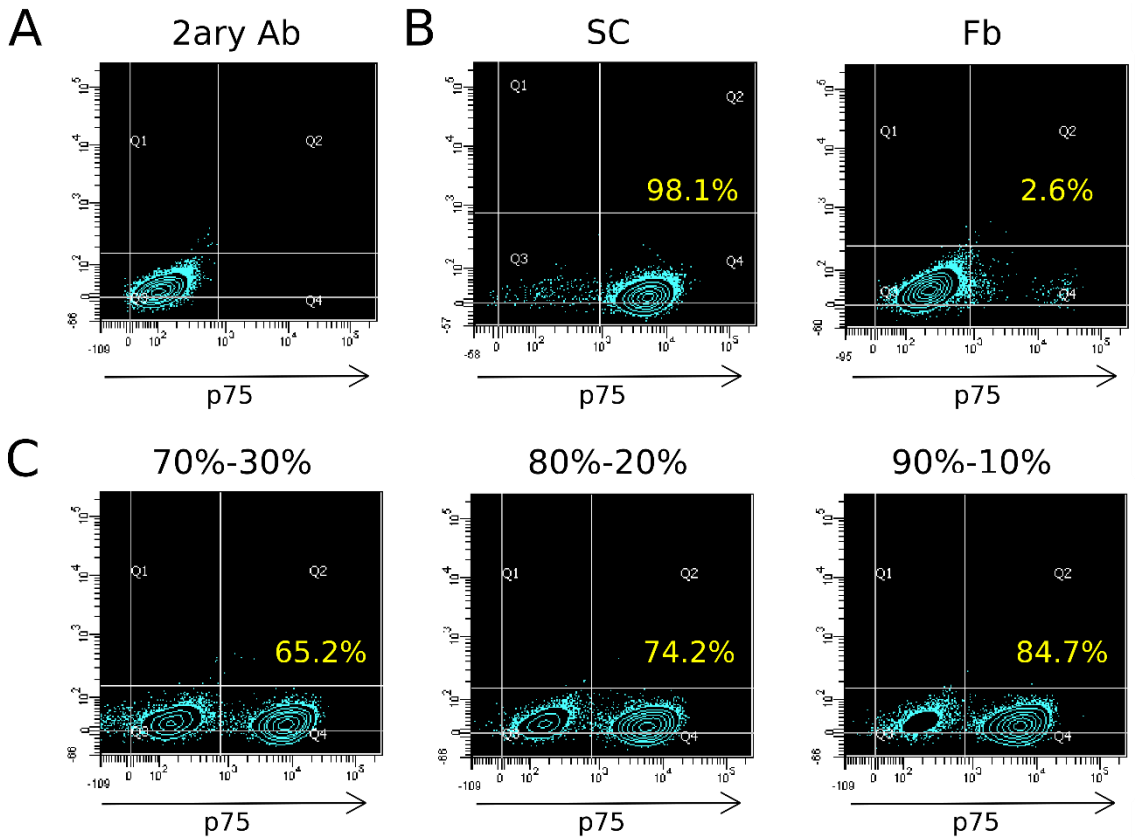

Figure R34. Seeding 70% Schwann cell– 30% endoneurial fibroblast co-culture is enough to obtain a percentage of cells at 72 hours, closely resembling cutaneous neurofibroma composition. **A)** Fortessa flow cytometry results for a SC-eFb co-culture at 72h incubated with the secondary antibody Alexa Fluor 488. **B)** SC and eFb single cell cultures incubated with primary and the secondary antibody Alexa Fluor 488. **C)** Co-cultures incubated with primary and the secondary antibody Alexa Fluor 488. Percentages of p75 positive cells in SC-eFb co-cultures after 72h, at different initial seeding conditions (70% SCs– 30% eFb; the 80% SCs– 20% eFb and the 90% SCs – 10% eFb; respectively). Percentages of p75 positive cells are indicated in yellow.

Moreover, we also characterized the expression of p75, S100B, and vimentin by fluorescent immunocytochemistry in 70% SCs– 30% eFb co-cultures (**Figure R35**). So far, there is no suitable antibody to label eFbs in culture selectively, not even CD34, widely used in immunohistochemistry. Thus, we used vimentin, a type III intermediate filament, to label both cell types. S100B and p75 specifically labeled SCs. SCs displayed their typical spindle morphology, were substantially smaller, and contained smaller nuclei than eFbs. SCs in co-cultured liked to grow on top of eFbs.

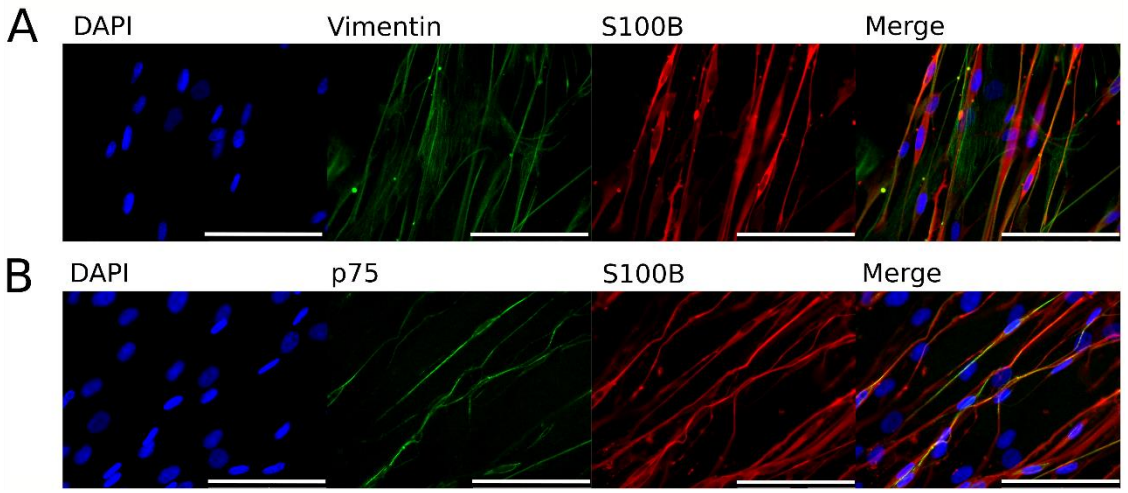

Figure R35. Schwann cells preferentially located on top of endoneurial fibroblasts in Schwann cell-endoneurial fibroblast co-cultures. A) A representative field from the immunostaining analysis of vimentin and S100B of the 70% SC- 30% eFb co-culture conditions. Vimentin labels the intermediate cytoskeleton of both cell types, while S100B specifically labels SCs. DAPI was used to stain nuclei. Scale bars, 100 µm. **B)** Same analysis for the co-staining of p75 and S100B markers. DAPI was used to stain nuclei. Scale bars, 100 µm.

After selecting 4 independent cNFs, determining the constitutional and somatic *NF1* mutations of each tumor, identifying their individual coding genetic variation by exome sequencing, and setting up adequate cell culture conditions for single cultures and SC-eFb co-cultures, we initiated a final experiment.

Using a large pool of freshly grown SCs and eFbs from each neurofibroma, we cultured in parallel, 4 independent single SC cultures, 4 independent single eFb cultures, and up to 16 combinations of SC-eFb co-cultures. We left cultures grow for up to 72h. At this point, we processed cells of each culture and co-culture for flow cytometry analysis to determine the proportions of SC and eFb, RNA analysis to analyze gene expression, DNA analysis to authenticate samples, and we also collected all supernatants to analyze the secretory profile (**Figure R36**).

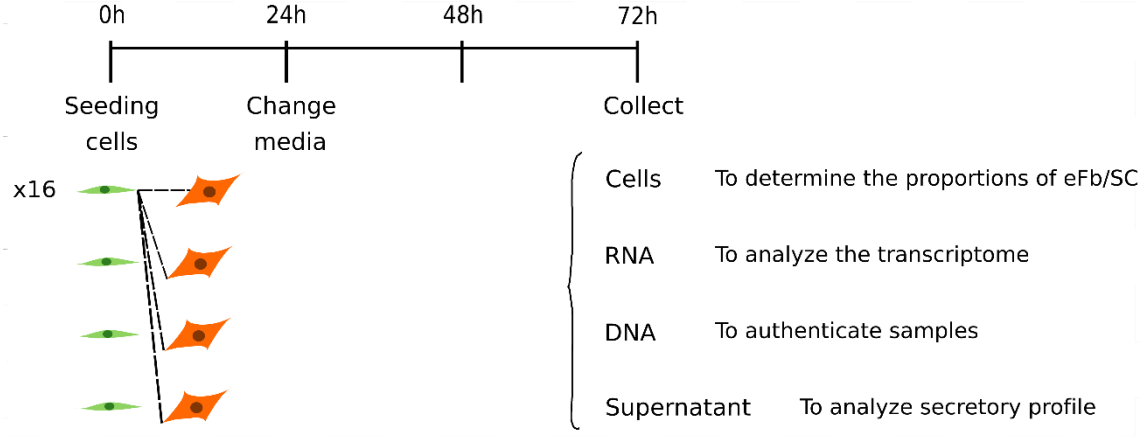

Figure R36. Schematic representation of the co-culture experimental design. Single SC and eFb cultures and co-cultures (16 different combinations) were seeded. 24 hours later, media was changed. Cultures were left for up to 72 hours. Cells of each single culture and co-culture were

used for flow cytometry analysis, RNA extraction, and DNA extraction. We also collected all supernatants.

To simplify the names of the samples in the co-culture experiment, we adopted a new nomenclature (**Table R10**).

cNFs	Simplified cNFs	Simplified SC cultures	Simplified eFb cultures
1cNF	cNF1	SC1	Fb1
17cNF	cNF2	SC2	Fb2
28cNF	cNF3	SC3	Fb3
27cNF	cNF4	SC4	Fb4

Table R10. Simplified nomenclature for cutaneous neurofibroma-derived Schwann cell and endoneurial fibroblast cultures.

The exact proportions of SCs and eFbs in all co-cultures at the end of the experiment were analyzed by flow cytometry, the precise proportions of each cell type (**Figure R37**, **Table R11**). This information was used later on, and when required, in all bioinformatics analyses performed.

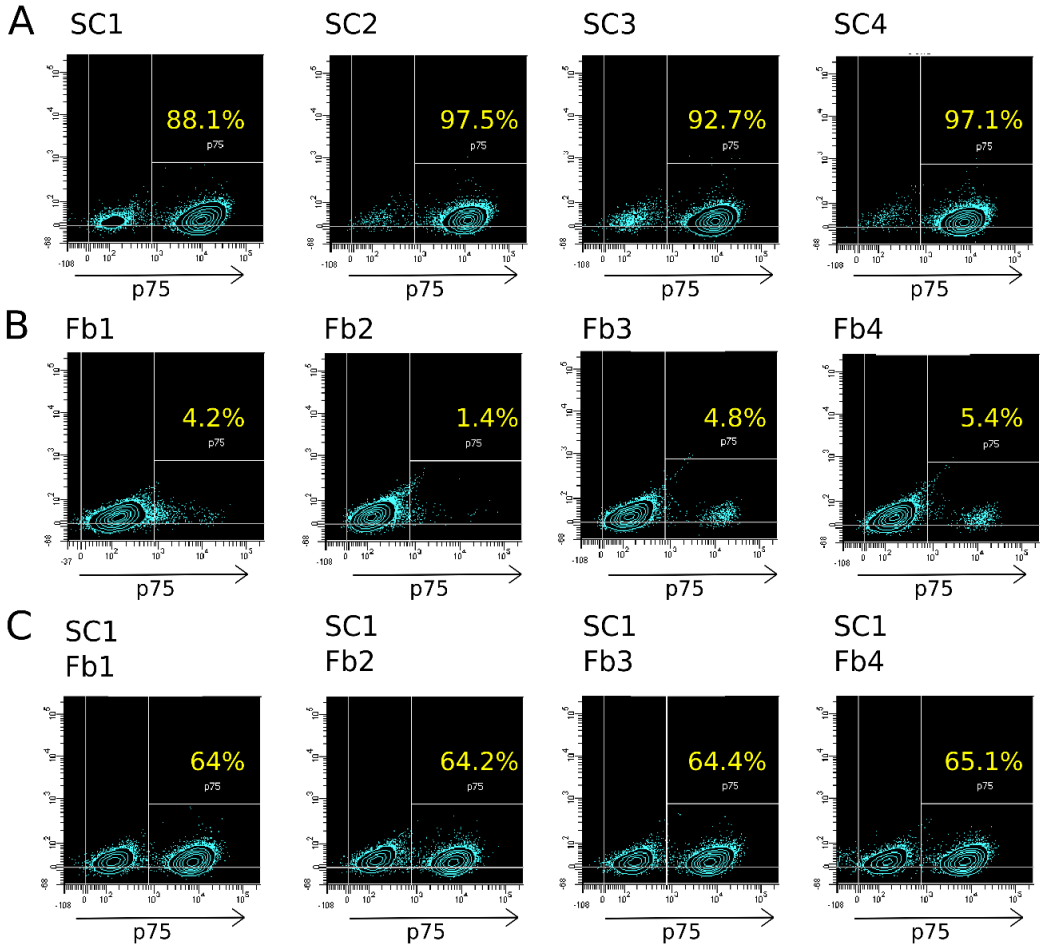

Figure R37 Flow cytometry analysis of single Schwann cell and endoneurial fibroblast cultures and Schwann cell-endoneurial fibroblast co-cultures. Four single cNF-derived SC cultures, four single

cNF-derived eFb cultures, and four different co-culture combinations at 72 hours are shown. The exact percentage of cells expressing p75 is shown in yellow, analyzed using Fortessa flow cytometer. A) 4 independent single SC cultures. B) 4 independent single eFb cultures. C) 4 independent co-cultures combinations using SC1 Schwann cells and eFbs from the 4 independent cNFS (Fb1, Fb2, Fb3, and Fb4).

	SC1	SC2	SC3	SC4
Fb1	64	57.3	71.4	69.3
Fb2	64.2	53.8	68.2	66
Fb3	64.4	60.6	69	76.2
Fb4	65.1	59.9	69.6	69.6

Table R11. Summary of the different percentages of p75-expressing cells in the sixteen different co-culture combinations at 72 hours.

3.4. Analysis of cell type-specific changes in gene expression due to heterotypic interactions between Schwann cell and endoneurial fibroblasts

RNA-seq was used to analyze the expression of primary SC and eFb single cultures, co-cultures, and cNF counterparts. To determine the impact of the heterotypic interactions within co-cultures on the transcriptional profiles of SCs and eFbs we used an *in silico* co-culture approach, which we refer to as virtual co-cultures. For this, once we mapped the NGS reads against the reference genome and transcriptome (GRCh38 and GENCODE), we randomly sampled a number of reads from the BAM files of the single cell type cultures and mixed them following the exact proportions of SC and eFb calculated by flow cytometry for each specific co-culture combination (**Table R11**). In **Figure R38** a schematic representation of the bioinformatic analysis used for the generation of a virtual co-culture is shown. These virtual co-cultures represented the expected transcriptional profiles in co-cultures if there were no transcriptional changes due to the interaction between SCs and eFbs.

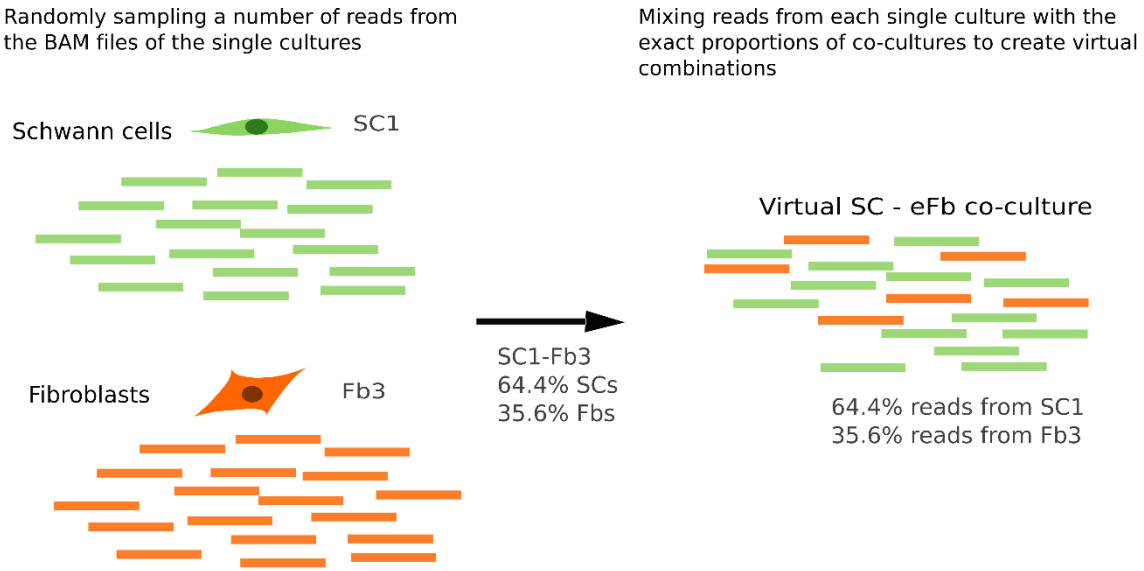

Figure R38. Schematic representation of the *in silico* co-culture approach to generate virtual co-cultures.

We performed a PCA comparing the expression data of all samples (**Figure R39A**). PC1 explained 39% of all expression variance and split the samples into two main groups: cNFs on one side and cell cultures (either real or virtual) on the other. PC2 explained 21% of the variance among samples and split them into three main groups: SC cultures, eFb cultures, and a group consisting of cNFs and all co-cultures (either real or virtual), indicating a higher expression similarity between co-cultures and cNFs considering the represented genes. Notably, virtual co-cultures were located next to real co-cultures, although not in the same spot, probably reflecting a transcriptional change due to the

heterotypic interaction between SCs and eFbs. Real co-cultures were located closer to cNFs than virtual co-cultures.

We then used DESeq2 (Love, Huber, and Anders 2014) to perform a differential expression analysis between virtual and real co-cultures, thus capturing the impact of SCs-eFbs (see Annex 2 Table 3). Differentially expressed genes were used in unsupervised cluster analysis and plotted in a heatmap (Figure R39B).

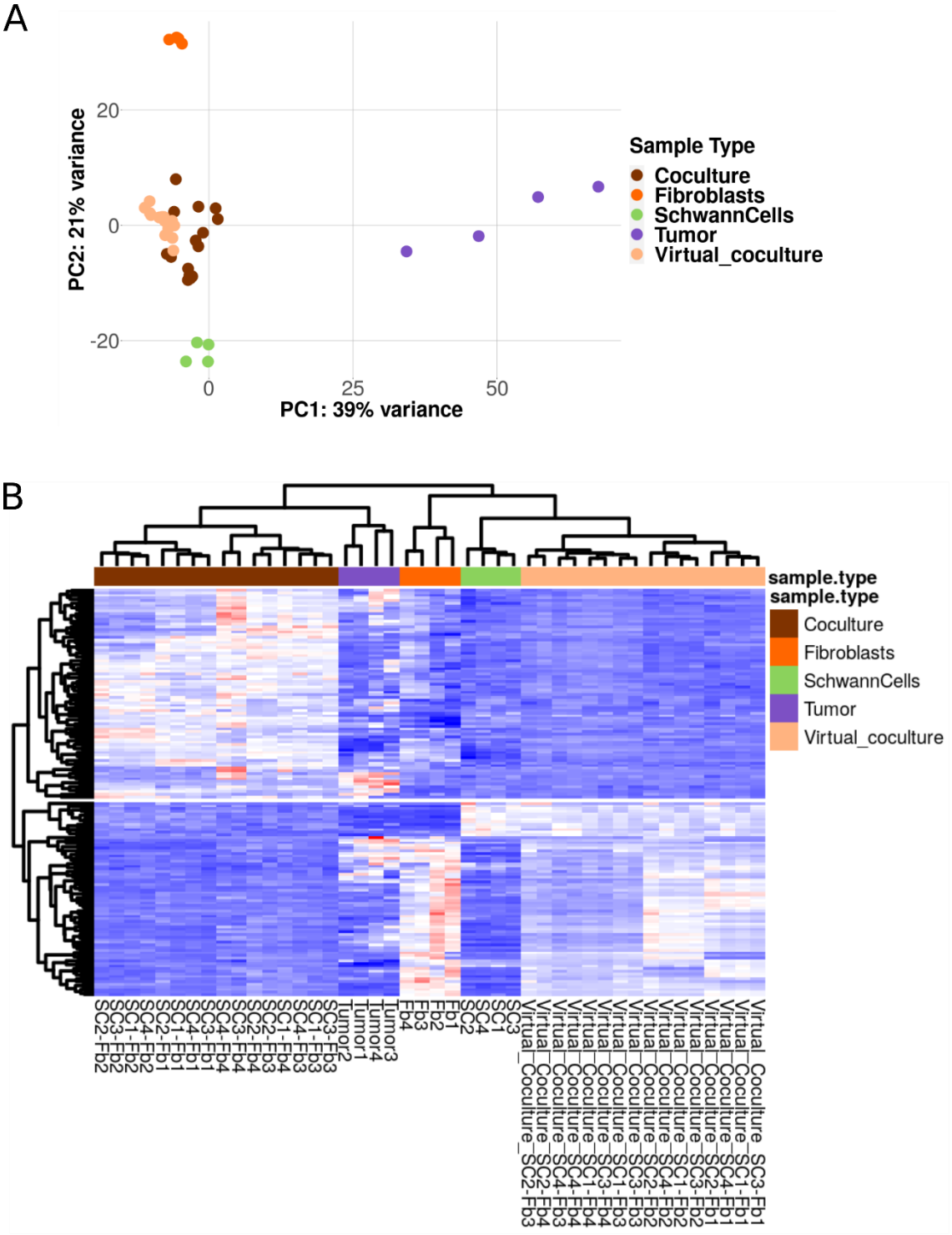

Figure R39. Gene expression analysis comparison of Schwann cell and endoneurial fibroblast single cultures, real and virtual Schwann cell-endoneurial fibroblast co-cultures, and cutaneous neurofibromas. A) PCA of the gene expression of SC cultures (green), eFb cultures (orange), real SC-eFb co-cultures (brown), virtual co-cultures (salmon), and primary original cNFs (purple). **B)** Heatmap representing an unsupervised cluster analysis of differentially expressed genes between real and virtual SC-eFb co-cultures. The expression color range goes from dark blue, showing down-regulated genes, to red, representing up-regulated genes. On the top part of the heatmap, genes differentially up-regulated in real vs. virtual co-cultures are depicted. This group of genes were used to generate **Figure R40**. On the bottom part, there are represented those genes

differentially down-regulated in real vs virtual co-cultures SC (SC culture); Fb (eFb culture); SC-eFb (real co-cultures); Tumor (primary cNF); Virtual_Co-culture_SC-eFb (*in silico* co-cultures generated from SC and eFb single cultures).

3.4.1. Identification of signaling pathways

After identifying genes presumably differentially expressed by the interaction between SCs and eFbs in co-cultures, we aimed to identify potential pathways represented by these genes. These pathways could indicate the intercellular signaling or crosstalk between these two cell types, resulting from physical interactions or secretion. The final aim was to identify those influencing cNF development and growth. As a first step, we performed an enrichment analysis of those differentially expressed genes (p-adjusted value < 0.05) up-regulated in real co-cultures compared to virtual co-cultures using clusterProfiler R package (Yu et al. 2012). We obtained Gene Ontology (GO), and KEGG pathways enriched terms of those genes. We followed the same procedure to obtain enriched terms of differentially expressed genes between eFbs and SCs to complement this analysis.

Several of the biological processes captured by differentially up-regulated genes in real versus virtual co-cultures are represented in Figure R40. Many of them represent interesting pathways worth to be further analyzed at a functional level, both by studying their secretion and by performing a functional evaluation of their role on SC and eFb proliferation. To name a few, these biological processes were related to: the positive regulation of GTPase activity; the regulation of cytokine (like interleukins) and chemokine production involved in immune response; regulation of calcium homeostasis; mesenchymal cell proliferation and development; and female pregnancy.

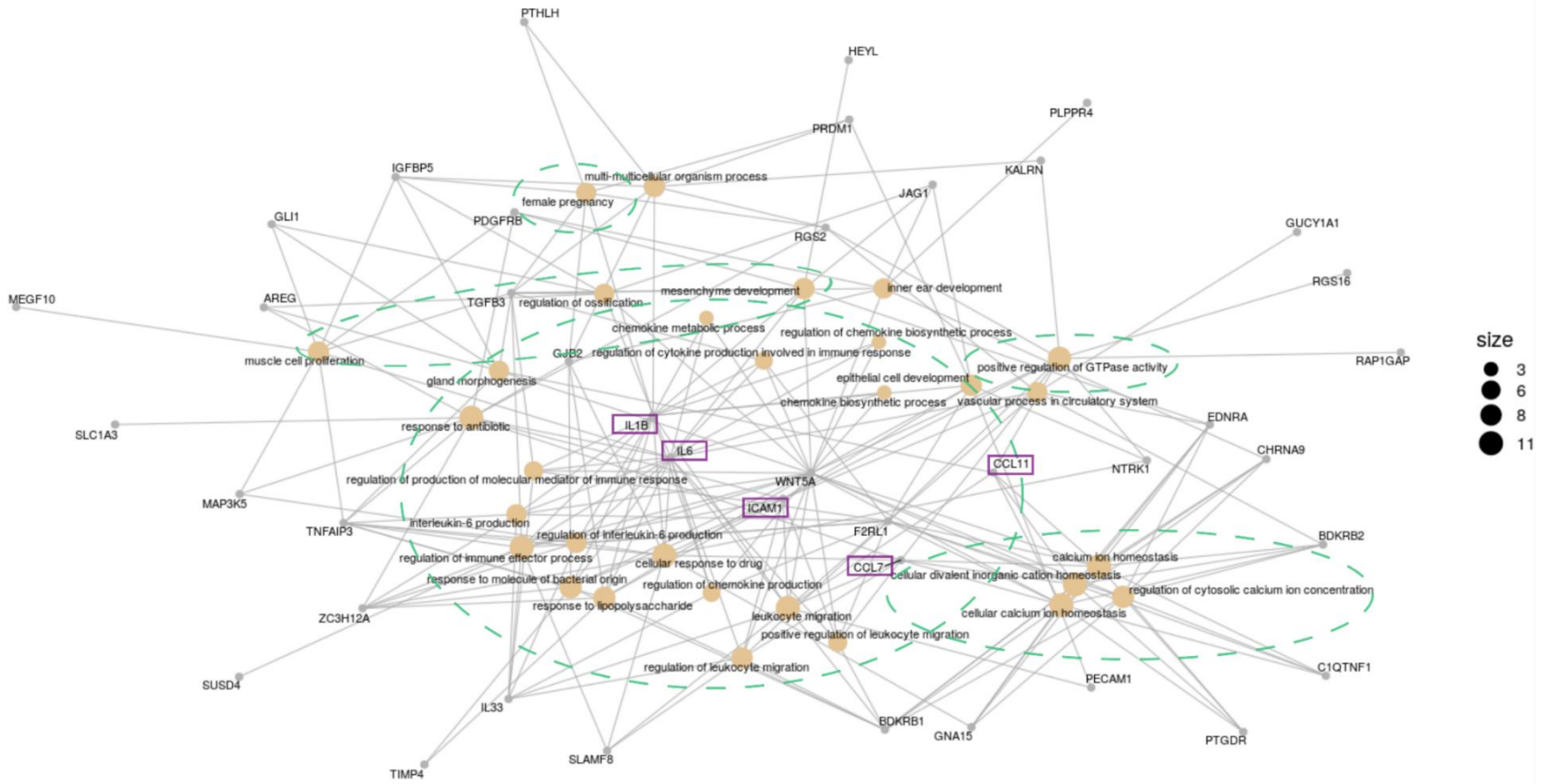

Figure R40. Graphical representation of the biological processes captured by the differential upregulated genes in real vs. virtual co-cultures. Differentially upregulated genes participating in these BPs are also represented. Lines define shared genes among the distinct BPs. The size of the sphere representing the BP is proportional to the number of genes contained. We grouped some BPs together under five selected groups (green dashed circles): the positive regulation of GTPase activity; the regulation of cytokine (like interleukins), and chemokine production involved in immune response; the regulation of calcium homeostasis; mesenchymal cell proliferation and development; and female pregnancy. The products encoded by five genes highlighted in purple were also analyzed by Luminex (see next section).

3.5. Analysis of co-culture supernatants: cytokines, chemokines, and other analytes

In parallel to RNA extraction and flow cytometry analysis, supernatants from single cultures and SC-eFb co-cultures were collected (**Figure R36**). Several of the differentially upregulated genes in real versus virtual co-cultures represented genes coding for products secreted out of the cells. The analysis of culture and co-culture supernatants gave us the opportunity to validate several of these secreted protein products potentially induced by SC-eFb interactions.

Thus, we selected some of these gene products and analyzed them in the same supernatants of cultures and co-cultures used for RNA-seq analysis.

All supernatants from SCs, eFbs, and SCs-eFbs co-cultures were analyzed using the Luminex xMAP technology. The analytes assayed were chosen according to RNAseq data and pathway analysis. A total of 22 analytes were assayed that were grouped in 3 different commercial panels listed in **Table R12**:

Human Cytokine/Chemokin Panel
EGF, FGF2, Eotaxin*, TGFα, G-CSF, fractalkine, MCP-3*, PDGF-AA, IL-1α, IL-1β*, IL-6*, IL-8, CXCL10, MCP-1, MIP-1α, RANTES, VEGF
Human Neurodegenerative Panel 3
BDNF, sICAM-1*, NCAM
Human Neurodegenerative Panel 4
S100B and GDNF

Table R12. Summary of the different commercial panels used to analyze 22 analytes. *These five analytes (Eotaxin (CCL11), MCP-3 (CCL7) IL-1β, IL-6, and sICAM-1) constituted hubs of the biological processes represented in **Figure R40**.

Analyte analysis was performed using the manufacturer's guidelines, and plates were run on Luminex 200 and analyzed using xPONENT software (Luminex). The supernatant concentrations of a few analytes were out of a linear range and could not be quantified. We generated graphics representing the secretion profiles obtained for all analytes measured in single cultures (SC or eFb), and co-cultures (virtual and real) (**Figure R41**, **42**). The levels of secreted products of virtual co-cultures were calculated in a similar way as the virtual co-culture expression (**Figure R38**). Co-culture virtual secretions were generated using secretion data from single cultures and considering the exact proportions of SCs and eFbs calculated by flow cytometry in each co-culture.

Notably, six analytes showed promising patterns: eotaxin (*CCL11*), rantes (*CCL5*), VEGF, MCP-3 (*CCL7*), NCAM, and siCAM (**Figures R41, 42**).

- Eotaxin (*CCL11*) was not secreted in either of the single SC or eFb cultures. However, there was a significant increase in real co-cultures compared to virtual co-cultures (**Figure R41B** and **C**).

- Rantes (*CCL5*) was moderately secreted in single eFb cultures and almost not secreted in single SC cultures. Significantly, secretion in real co-cultures was remarkably increased compared to virtual co-culture (Figure R41B and C).
- VEGF was secreted in single SC cultures at higher levels than in single eFb cultures. A significant secretion increase was observed in real compared to virtual co-cultures (Figure R41B and C).
- MCP-3 (*CCL7*) and sICAM (*ICAM1*) were secreted in single SC and eFb cultures. However, in real co-cultures their secretion was significantly higher than in the virtual ones (Figure R42B and C). These genes were highlighted in purple in the enrichment analysis (Figure R39).
- NCAM was highly secreted in single SC cultures, not in eFb cultures, and secretion was significantly higher in real compared to virtual co-cultures (Figure R42B and C).

Notably, there was a high correlation between differential expression and secretion analysis (Figure R41, Figure R42).

In the future, we will evaluate the functional impact of these 6 promising signaling pathways on SC proliferation ether in single SC or SC-eFb co-cultures using agonists or antagonists.

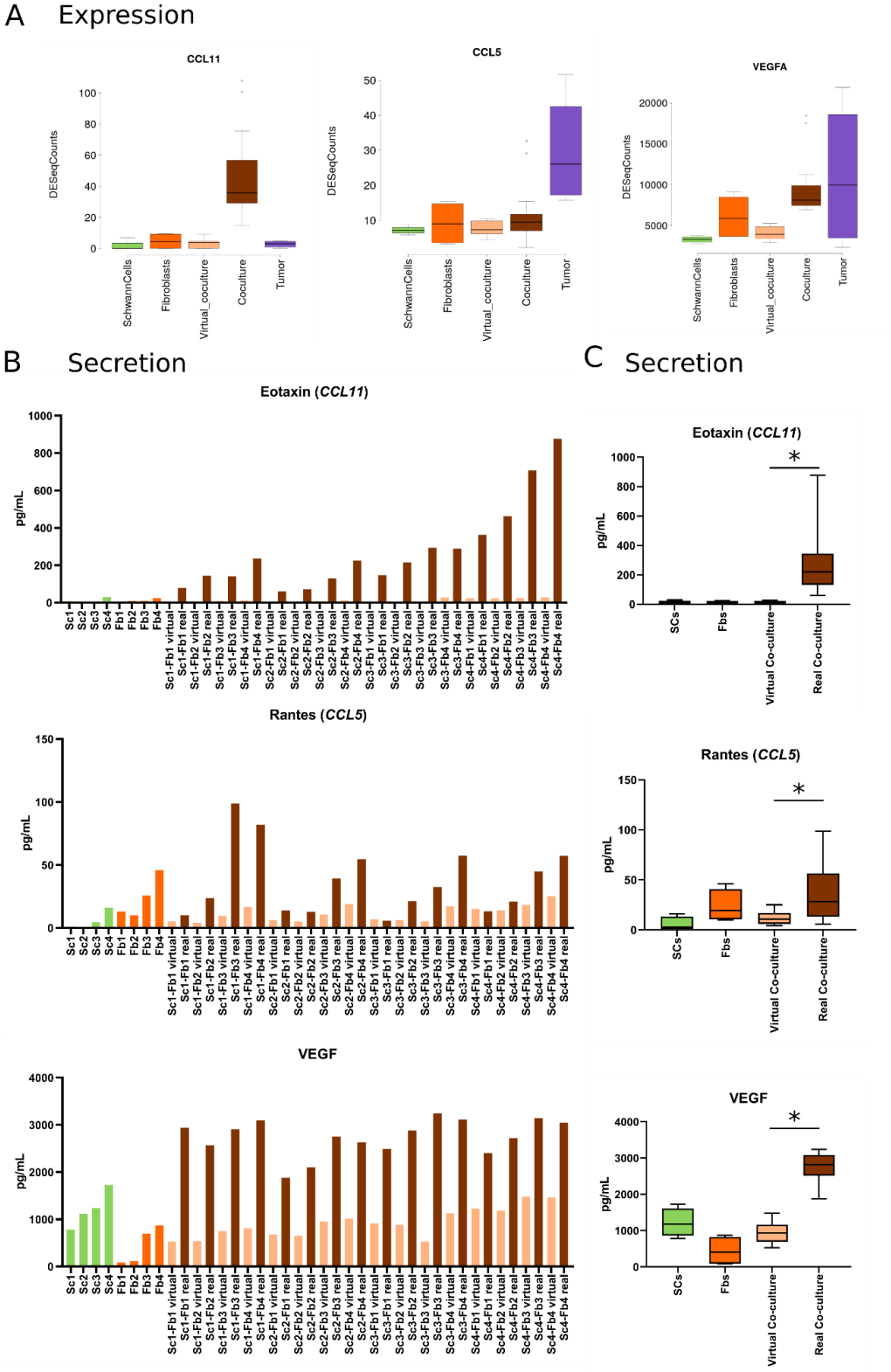

Figure R41. Correlation between differential expression and secretion analysis of three upregulated genes (*CCL11*, *CCL5,* and *VEGFA*) in real vs. virtual co-cultures. A) Expression analysis from RNA-seq data of *CCL11*, *CCL5*, and *VEGFA*. **B)** Secretion analysis of CCL11, CCL5, and VEGF in SC (green) or eFb (orange) single cultures, and virtual (salmon) and real (brown) co-culture supernatants. **C)** Boxplots of CCL11, CCL5, and VEGF in single SC (green) or eFb (orange) cultures, and co-culture (virtual and real) supernatants. A non-parametric test was performed in real vs co-culture supernatants ($\alpha = 0.05$).

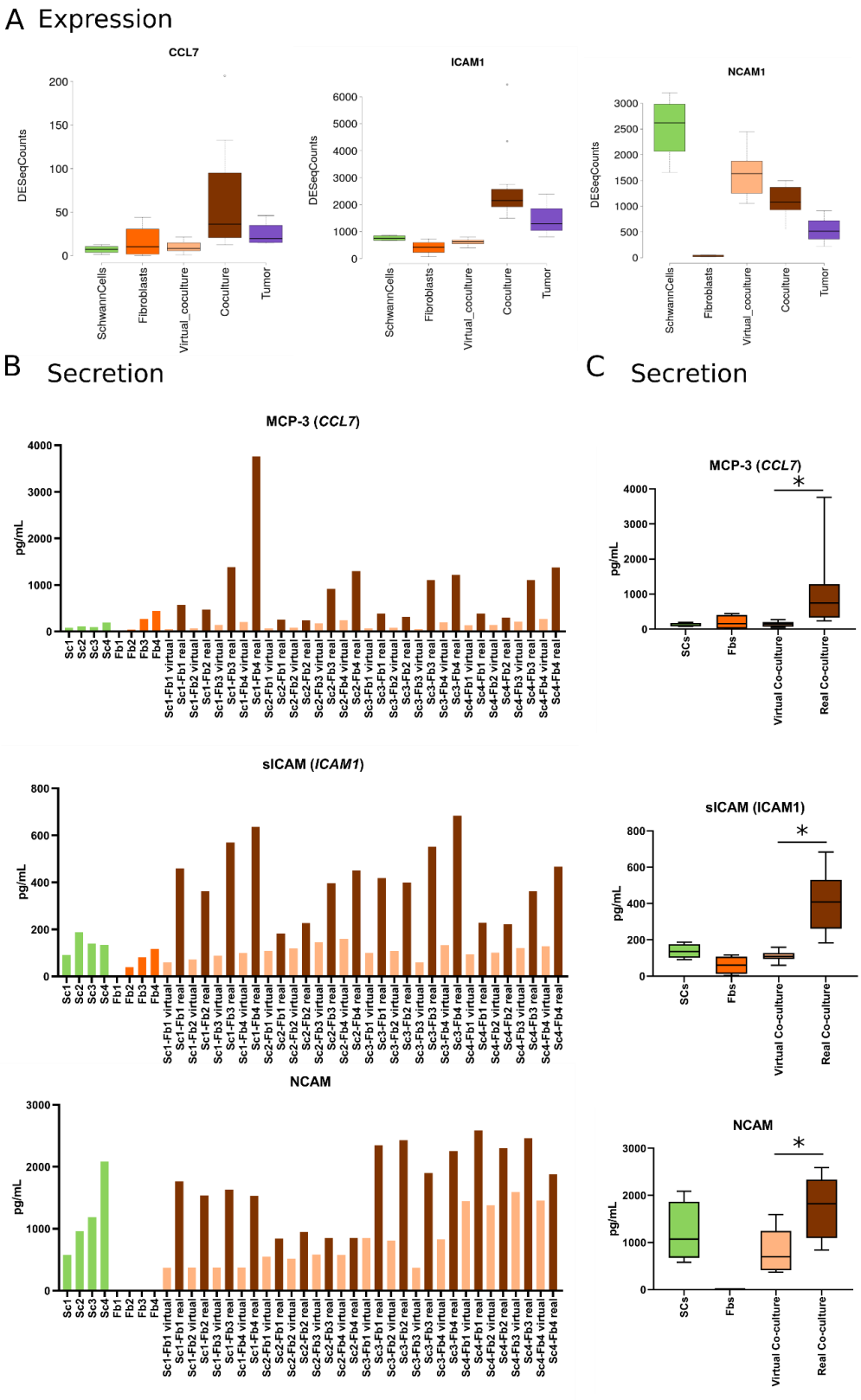

Figure R42. Correlation between differential expression and secretion analysis of three more genes (MPC-3, sICAM, and NCAM). A) Expression analysis from RNA-seq data of *CCL7*, *ICAM1*, and *NCAM1*. **B)** Secretion analysis of CCL7, sICAM, and NCAM in SC (green) or eFb (orange) single cultures and virtual (salmon) and real (brown) co-culture supernatants. **C)** Boxplots of CCL7, sICAM, and NCAM in single SC (green) or eFb (orange) cultures and co-culture (virtual and real) supernatants. Non-parametric test was performed in real vs co-culture supernatants ($\alpha = 0.05$).

3.6. Differentially upregulated genes in real co-cultures were mostly expressed in iPSC derived heterotypic spheroid 3D model

3.6.1. Endoneurial fibroblast cultures derived from cNFs and PNFs exhibit a high expression similarity

The characterization of cNF-derived SC and eFb cultures gave us the opportunity of comparing the transcriptome of these cell cultures from both types of neurofibromas, cNFs, and pNFs. To analyze the similarities and differences between cells of both tumor types, we first used RNA-seq data to perform a PCA of all samples (Figure R43A). Most of the expression variance (68%) was captured by PC1 that split the samples according to cell types regardless of neurofibroma type. However, the combination of PC1 and PC2, split SCs in the ones derived from cNFs, from those derived from PNFs. Instead, eFbs derived from both neurofibroma types remained mixed. This observation suggested that eFbs from both neurofibromas were more similar than their SCs counterparts.

To gain more in-depth insight, we performed a differential gene expression analysis between different sample types and globally identified 3373 differentially expressed genes, summing up differentially expressed genes between SCs and eFbs, and between cNF and PNF derived SC cultures. We only identified 195 differential expressed genes between PNF-derived and cNF-derived eFbs (not shown). We performed an unsupervised cluster analysis using this gene signature and plotted it in a heatmap (Figure R43B). These results highlighted that eFb cultures were closely similar despite their different neurofibroma origin, while SC cultures from distinct neurofibromas, despite many similarities, exhibited a clear differentially expressed gene signature.

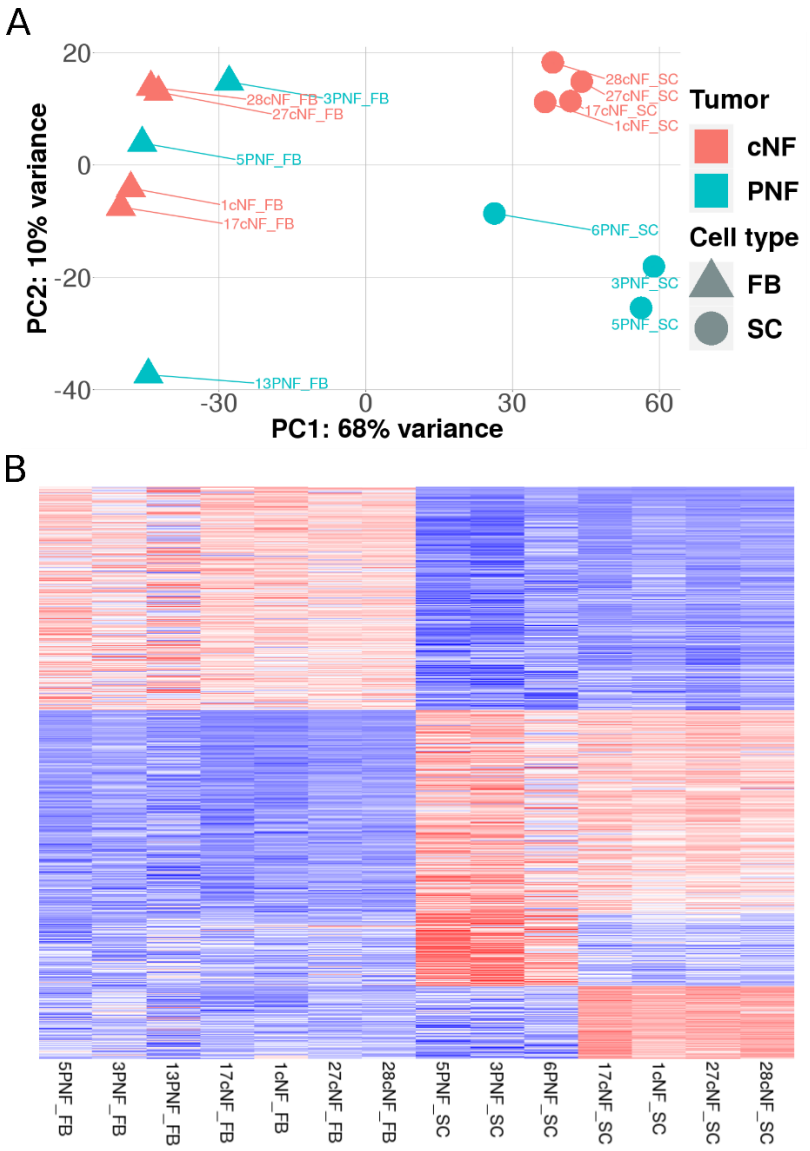

Figure R43. Endoneurial fibroblasts derived from plexiform and cutaneous neurofibromas displayed similar expression profiles. A) PCA of cNF-derived (salmon) and PNF-derived (blue) eFbs (triangle) and SCs (circles) samples. **B)** Heatmap displaying the differentially expressed genes in SCs and eFbs derived from PNFs and cNFs. The expression color ranges from dark blue, showing down-regulated genes, to red, showing up-regulated genes.

3.6.2. Expression analysis of differentially upregulated genes in cNF Schwann cell- endoneurial fibroblast co-cultures in the heterotypic PNF model

After observing the high expression similarity between PNF and cNF eFb cultures, we wondered whether cNF SC-eFb co-cultures could inform us also about SC-eFb interaction in PNFs, and specifically in the developed heterotypic spheroid model. This model was composed by iPSC-derived *NF1*(-/-) differentiating SCs and primary PNF-derived eFbs, grown as spheres. Again, RNA-seq analysis facilitated us to analyze the status of

differentially expressed genes in real versus virtual cNF SC-eFb co-cultures in the PNF heterotypic spheroid model.

We performed an unsupervised cluster analysis of the gene signature constituted by the differentially upregulated genes in real co-cultures from the following samples: cNF, real SC-eFb co-cultures, virtual SC-eFb co-cultures; homotypic and heterotypic spheroids from different WT and *NF1*(-/-) cell lines. Results were plotted in a heatmap (**Figure R44**). Remarkably, cNF real-coculture samples and PNF heterotypic spheroids clustered together, indicating a higher degree of expression similarity compared to the other samples. In fact, heterotypic spheroids expressed a significant part of the upregulated genes in cNF SC-eFb co-cultures. Homotypic spheroids composed only by differentiating SCs just expressed approximately 1/6 of these genes. These results suggest that the same heterotypic interactions that we detected in cNF SC-eFb co-cultures might also be occurring in PNF heterotypic spheroids, opening the possibility of identifying shared signaling pathways influencing both cNF and PNF growth.

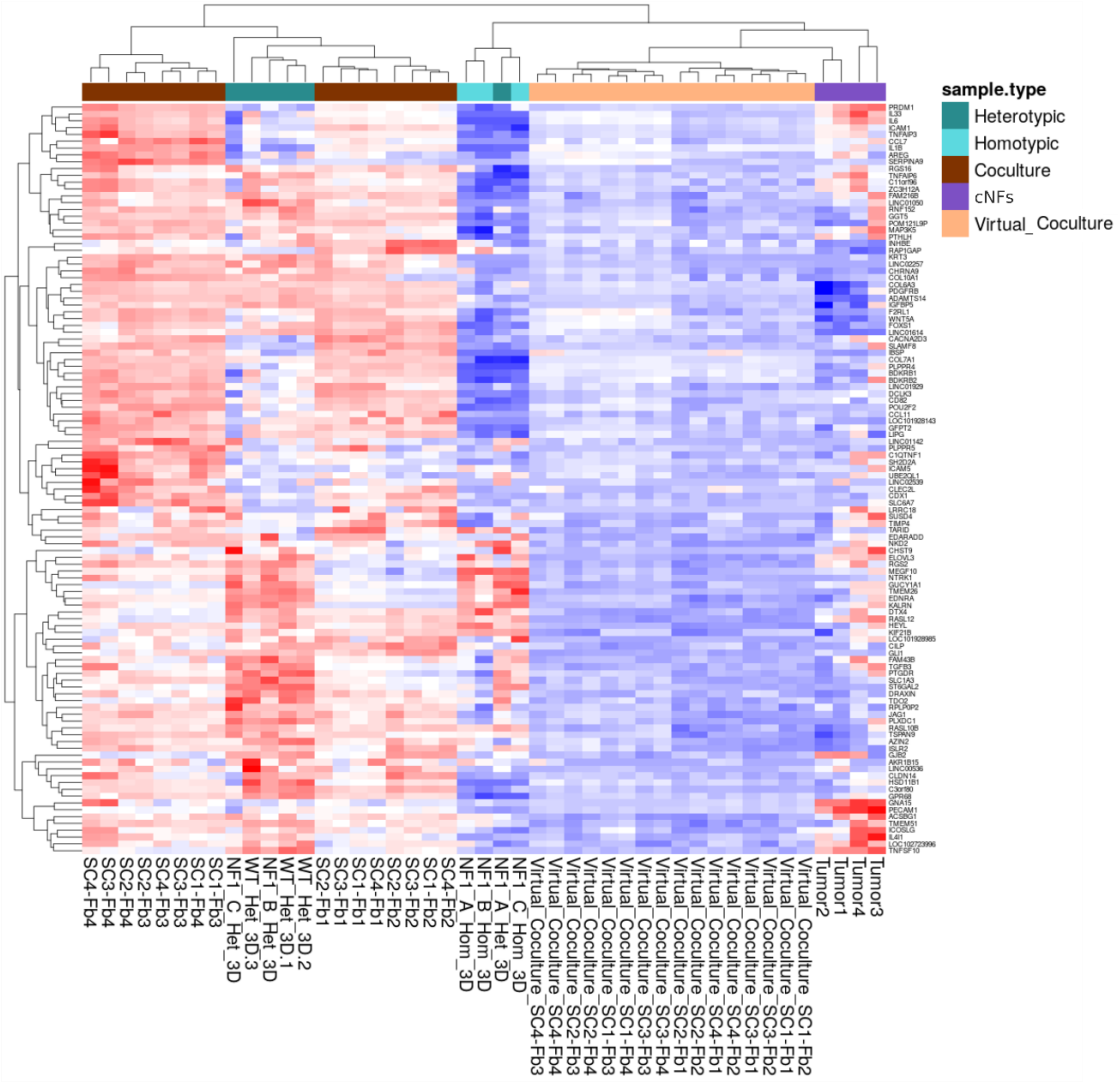

Figure R44. iPSC-derived heterotypic spheroids express most genes upregulated in cutaneous neurofibroma Schwann cell – endoneurial fibroblast co-cultures. Heatmap showing the unsupervised cluster analysis of differentially upregulated genes in SC-eFb co-cultures for

different samples: homotypic (light turquoise) and heterotypic (dark turquoise) spheroids generated from *NF1*(+/+) (WT) and *NF1*(-/-) (NF1) iPSCs; real (brown) and virtual (salmon) SC-eFb cocultures; and in cNFs (purple). The expression color ranges from dark blue, showing down-regulated genes, to red, showing up-regulated genes.

Discussion

1. Generation of an iPSC-based model

1.1. Why using iPSC as a model?

Plexiform neurofibromas (PNFs) are complex benign tumors composed of an admixture of *NF1*(-/-) and *NF1*(+/-) cells. These tumors arise during development when a progenitor cell completely inactivates the *NF1* gene. In this context, the use of induced pluripotent stem cell (iPSC) is a reasonable strategy to obtain the precise cell type to recreate PNF initiation and formation, combining iPSC differentiation potential with the correct *NF1* genotype.

There are at least two ways of generating these iPSC lines: reprogramming PNF cells with distinct *NF1* genotypes or editing the *NF1* gene in already established iPSC lines. The reprogramming approach allows the preservation of the entire genetic background, both the *NF1* status and also any potential patient or PNF-specific genetic variants. The persistence of gene expression and differentiation propensity of the starting cell has been described in iPSCs (Marchetto et al. 2009; Ghosh et al. 2010; Hu et al. 2010; Feng, Jacobsen, and Reik 2010). These observations led to speculation that iPSCs possess epigenetic and transcriptomic remnants of the donor tissue, which was termed "epigenetic memory" (Bar-Nur et al. 2011; Vaskova et al. 2013). This idea is controversial, as subsequent studies did not find evidence of any epigenetic memory. Furthermore, the reprogramming of PNF cells, as opposed to genome editing, overcomes any potential off-target effect related to genome editing.

On the other hand, the editing approach allows the generation of isogenic *NF1*(+/-) and *NF1*(-/-) iPSCs, with the advantage of also having the isogenic *NF1*(+/+) cell line. Although not required for PNF modeling, *NF1*(+/+) cells can provide additional control to study the effects of specific *NF1* mutations. Moreover, any reprogramming bottleneck related to culture conditions of PNF-derived cells, to cell type specificities, or to the lack of *NF1* could be overcome with this approach.

In the present thesis, we characterize *NF1*(-/-) iPSCs generated using both strategies, mainly by reprogramming PNF cells, but also by *NF1* editing of control *NF1*(+/+) iPSCs. We characterized these *NF1*(-/-) iPSCs for their proliferation capacity and their differentiation ability towards neural crest (NC) and up to Schwann cells (SCs). So far, we identified exactly the same behavior and biological properties in iPSCs generated with both strategies, with no distinction.

1.2. The efficiency of reprogramming plexiform neurofibroma cells

Reprogramming to pluripotency is a complex process involving different stages, in which multiple players synergistically converge to remodel transcriptional and epigenetic programs. Various factors have been identified to affect the efficiency of reprogramming, like cell cycle regulators, chromatin remodelers, and facilitators of the mesenchymal-to-

epithelial transition (Buganim, Faddah, and Jaenisch 2013). Most somatic cell types reprogram to pluripotency with a very low efficiency, and Yamanaka (Yamanaka 2009) proposed two alternative explanations for this. In the elite-cell model, reprogramming occurs only in a few predisposed cells within a population (Shakiba et al. 2019). On the contrary, in the stochastic model, most or all cells are competent for reprogramming at low probabilities (Hanna et al. 2009). Are all cells equally capable of reprogramming? Recent technical developments that allow identifying and following single cells in heterogeneous populations do not seem to indicate so. By combining cellular barcoding, mathematical modeling, and lineage tracing approaches, Shakiba et al. (Shakiba et al. 2019) demonstrated that reprogramming dynamics in heterogeneous populations of mouse embryonic fibroblasts (Fbs) were driven by dominant elite clones expressing Wnt1.

To model PNFs, both *NF1*(+/-) and *NF1*(-/-) iPSCs are required, but especially the latter, since PNFs are initiated upon *NF1* inactivation in specific cells during development. Our group has attempted to reprogram 5 PNFs from 5 independent NF1 patients. We obtained *NF1*(+/-) iPSCs from all of them but *NF1*(-/-) iPSCs only from 2, suggesting a lower reprogramming efficiency of *NF1*(-/-) cells. Despite the low number of reprogrammed tumors, which does not allow us to draw any definitive conclusions, we identified several factors potentially influencing the reprogramming efficiency of PNF-derived *NF1*(+/-) and *NF1*(-/-) cells worth mentioning. In addition to the possibility that the complete loss of *NF1* reduces reprogramming efficiency, other identified factors were: the age of the PNF donor, the cell type, and culture conditions. Independently of the reprogramming strategy used, we obtained *NF1*(-/-) iPSC clones from two PNFs belonging to children of 10 years or younger. Young children present the most rapidly growing PNFs (Akshintala et al. 2020). These tumors could exhibit a higher number of elite or progenitor cells with a higher replicative capacity, two factors known to influence reprogramming efficiency (Eminli et al. 2009; Utikal et al. 2009). These factors could have facilitated the reprogramming of *NF1*(-/-) cells.

Another interesting observation is the lower reprogramming efficiency obtained in *NF1*(+/-) endoneurial fibroblast (eFb) primary cultures (Table R2). In contrast, using the same culture conditions, Fb-enriched cultures derived from skin produced many *NF1*(+/-) clones, indicating that Fbs of different origins may have other reprogramming efficiencies. The only apparent exception to this observation was the eFb culture from 13PNF that produced a high number of *NF1*(+/-) clones. However, it has to be taken into account that 13PNF was the only analyzed PNF developing in the face of an NF1 individual. Pathology analysis of this tumor showed that it was highly vascularized. In addition, RNA-seq analysis of 13PNF Fbs, revealed a clear, distinct expression pattern compared to other PNF-derived eFb cultures, with some of the most differentially expressed genes being markers of endothelial cells (like CD34). All these pieces of evidence suggest the possibility that 13PNF eFb cultures were highly enriched also in other cell types (like endothelial cells) with a higher reprogramming efficiency than eFbs, explaining the different reprogramming efficiency observed in these eFb cultures.

To our experience, *NF1*(-/-) reprogramming efficiency was increased when selective culturing was avoided, and digested tumor cells were directly reprogrammed, as more *NF1*(-/-) clones were obtained from the same PNF (Table R2). This strategy may reduce selection pressure imposed by culture conditions and minimize loss of cell heterogeneity during *in vitro* passaging. Nonetheless, when we used the selective culturing approach to reprogram primary *NF1*(-/-) SCs, in one case, we established SC primary cultures that were >95% enriched in *NF1*(-/-) SCs and still only obtained *NF1*(+/-) iPSC clones, suggesting that those *NF1*(-/-) cultures had low (if any) reprogramming capacity.

2. Establishment of a neural crest-Schwann cell *in vitro* differentiation system and generation of an expression roadmap signature

Our results showed that control *NF1*(+/+) iPSC could be differentiated with high efficiency towards NCs, which homogenously expressed NC lineage markers and were able to undergo further differentiation into NC-derived cell types (peripheral neurons and melanocytes), as well as migrate, indicating a clear NC identity. Moreover, NC cells could be maintained as a stable, self-renewing population and could be expanded, frozen, and thawed without loss of self-renewing potential. NC batches could be produced and cryopreserved for multiple subsequent differentiation assays.

We established a reproducible differentiation protocol towards SCs from *NF1*(+/+) NCs. Differentiating SCs expressed the classical stage-specific markers along the NC-SC differentiation axis and properly myelinated axons from peripheral neurons when they were in close contact. However, despite the genuine nature of generated SCs, at 30 days of the *in vitro* NC-SC differentiation system, we cannot assure the specific stage (immature SCs, mature SCs, etc.) that these cells have acquired, according to the current multistep model of SC differentiation (Kristjan R. Jessen and Mirsky 2005). On the one hand, SCs at 30 days express S100B marker, a marker of SC commitment, and other late-stage markers (PLP, PMP22, ERG2). However, at the same time, these cells also express markers of an earlier stage, like the specific SCP marker CDH19 (Kristjan R. Jessen and Mirsky 2005). PNF-derived primary *NF1*(-/-) SC cultures also express all these classical markers simultaneously, although, as we discuss later, this expression pattern characterizes only one SC subpopulation within PNFs. Besides, primary PNF-derived SCs express a roadmap expression signature closely resembling that of SCs at 30 days of differentiation. It seems that *in vitro* differentiated SCs at 30 days, as well as a subpopulation of PNF SCs, adopted a singular committed SC identity. Altogether, we were able to generate an imperishable model system to generate NCs and SCs.

After setting up a consistent NC-SC *in vitro* differentiation protocol, we performed RNA-seq to characterize better the NC stage and several SC differentiation timepoints (7, 14, and 30 days along with SC differentiation). Expression analysis of control *NF1*(+/+) cells supported the robustness of the *in vitro* NC-SC differentiation process and allowed the generation of a NC-SC *in vitro* expression roadmap, consisting of the sum of all

differentially upregulated genes at the NC stage or SC differentiation timepoints. Enrichment analysis of the roadmap signature revealed many biological processes related to the development of the peripheral nervous system and Schwann cell biology, strengthening the genuine NC-SC differentiation process. Classical markers of the NC-SC axis (Kristjan R. Jessen and Mirsky 2005) had been obtained using developing mouse embryos. The NC-SC *in vitro* system and the identified expression roadmap signature may facilitate the discovery of new markers in a more amenable and straight forward approach.

One of the limitations of using iPSCs to generate specific cell types is the need to use highly efficient conditions to generate homogeneous cell cultures. When differentiating *NF1*(-/-) cells in 2D, some cells committed to SCs, but most of the population ended up scaping from the NC-SC axis. By RT-qPCR we were able to detect certain expression of classic NC-SC markers. However, the roadmap signature was clearly different, and certain cells of the NC-mesenchymal axis developed after engraftment. Contrarily, *NF1*(-/-) heterotypic spheroids from NF1_B and NF1_C samples generated a NC-SC expression roadmap closely resembling the one of *NF1*(+/+) cells at 30 days (either in 2D or in heterotypic spheroids). The engraftment of these spheroids resulted in the most consistent generation of neurofibroma-like tumors *in vivo*. These results suggest that the roadmap signature may have a predictive value for proper PNF-model formation (both *in vitro* and *in vivo*), also reflecting the generation of highly homogeneous spheroid cultures. If so, then a NanoString panel analysis (or similar multiplex gene expression analysis tool) of a selection of NC-SC roadmap genes may constitute a useful tool for monitoring the correct development of heterotypic spheroids.

3. Role of *NF1* in induced pluripotent stem cells, neural crest cells, and differentiating Schwann cells

The work presented in this Ph.D. thesis clarified the role of the *NF1* gene in the proliferation and differentiation capacity of different types of cells, like iPSCs, NCs, or differentiating SCs. It has been shown that *NF1*-deficient cells exhibit a higher proliferation rate than their cellular counterparts carrying one or two wild-type copies of the *NF1* gene (H. A. Kim et al. 1995; H. A. Kim, DeClue, and Ratner 1997; Bollag et al. 1996). We quantify the effect of the *NF1* status on the iPSC proliferation rate.

At the pluripotent stage *NF1*(-/-) and *NF1*(+/-) iPSCs exhibited a higher proliferation rate compared to control *NF1*(+/+) iPSCs, specially neurofibromin deficient cells that on average exhibited a 10%–15% increase in cell proliferation rate compared with controls. This is quite a significant result since iPSCs are characterized by their already quick cell cycle (Ruiz et al. 2011). These results indicate that cell proliferation rate in pluripotent stem cells (PSC), as is the case for somatic cells, is influenced by neurofibromin activity. This higher proliferation rate was not as pronounced at the NC stage. However, differentiating *NF1*(-/-) SCs again exhibited a significantly higher proliferation rate compared to control *NF1*(+/+) cells. These highly proliferating cells had a natural

tendency to form spheres, big enough to be visible to the naked eye. Under differentiation conditions defined with *NF1*(+/+) NCs to generate genuine SCs (change in morphology, marker expression, myelination capacity), *NF1* deficient differentiating SCs exhibited a poor ability to commit towards SCs. The majority of *NF1* (-/-) cells in 2D conditions adopted a NC-mesenchymal axis of differentiation, corroborated by *in vivo* sciatic nerve engraftments. In addition, in 2D culture conditions, *NF1* deficient differentiating SCs showed poor ability to *in vitro* myelinate DRG axons. All these results highlight the importance of the *NF1* function to maintain a proper NC-SC differentiation axis.

Interestingly, *NF1*(-/-) CRISPR/Cas9 edited iPSCs exhibited the same proliferation properties as PNF-derived *NF1*(-/-) iPSCs. Differentiating SCs reproduced the same altered proliferation and differentiation properties as those SCs generated from PNF-derived *NF1*(-/-) iPSCs. These results indicated that all these altered properties were mainly conferred by the loss of *NF1* function and not by the reprogramming strategy used or reprogrammed cell type.

4. Comparing 2D and 3D models

Two-dimension (2D) cell cultures have been used since the early 1900s and are still used for the majority of cell research for several reasons: they are inexpensive and well established, there is a lot of comparative literature, and they are typically easier to analyze than more complex cell culture systems. However, they have some inherent disadvantages: they aren't representative of real cell environments, and 2D cell testing isn't always predictive, which increases the cost and failure rate of new drug discovery and clinical trials. For all this, in recent years, three-dimension (3D) cell culture techniques have received much attention as they might provide more accurate and relevant cellular and tissue models. In our case, we have established an *in vitro* and i*n vivo* PNF model only when applying a 3D culture system.

However, some aspects regarding the 3D PNF model should be addressed: *NF1*(-/-) homotypic spheroids, as well as one of the three NF1(-/-) heterotypic spheroid lines (NF1_A), were not following a clear NC-SC path upon SC differentiation protocol, according to the expression roadmap profile, despite the detection of classical NC-SC markers by immunostaining and RT-qPCR. *NF1*(-/-) homotypic spheroids generated neurofibroma-like tumors upon engraftment into the sciatic nerve of mice, although less consistently than *NF1*(-/-) heterotypic spheroids (fewer tumors and smaller).

Two of the *NF1*(-/-) heterotypic spheroid samples, NF1_B and NF1_C, expressed a quite similar expression roadmap profile closer to the one displayed by *NF1*(+/+) differentiating SCs in 2D cultures and by PNF-derived primary SC cultures. Furthermore, the engraftment of these spheroids into the sciatic nerve generated neurofibroma-like tumors consistently.

There are three factors that we think are key for the successful generation of PNFs upon engraftment: a) the generation of *NF1*(-/-) cells from iPSCs facilitates the obtention of large amounts of *NF1*(-/-) differentiating SCs for the spheroid formation and enough to form a tumor; b) the higher proliferation rate of *NF1*(-/-) cells, much higher than *NF1*(+/+) cells, not able to form tumors upon engraftment; c) eFbs present in heterotypic spheroids aided maintaining the capacity of *NF1*(-/-) cells to highly proliferate and at the same time preserving the SC commitment ability of descendant cells, suggesting a potential niche effect.

To sum up, we have developed a human *in vitro*/*in vivo* 3D heterotypic to model PNFs. This is the first time human PNFs can develop on the sciatic nerve of mice since engrafted PNF cell lines, either immortalized or not, were not able to go further beyond a thickness of a nerve or a little outgrowth (Ling et al. 2005; Perrin et al. 2007; H. Li et al. 2016b). Furthermore, neither PNFs nor atypical neurofibromas (aNFs) have been able to grow upon xenotransplant into mice sciatic nerve (Conxi Lázaro, Juana Fernández-Rodríguez, Alberto Villanueva, personal communication) using the same methodology as for the successful generation of MPNST xenografts (Castellsagué et al. 2015).

5. PNF cell of origin

PNFs are congenital. Most of what we know about the cell type originating PNFs come from the generation of GEMMs in which the selective ablation of *NF1* had been performed in cells at different developmental stages along the NC-SC axis (Nancy M. Joseph et al. 2008; Wu et al. 2008; Zheng et al. 2008; Y. Zhu et al. 2002). Altogether these models point to a Schwann cell precursor (SCP) as the most probable PNF cell of origin (Le et al. 2011). In this context, the development of an *in vitro/in vivo* NC-SC differentiation system starting from *NF1*(-/-) iPSCs could add very valuable information. For instance, we know now that the engraftment of *NF1*(-/-) NCs in the sciatic nerve of mice did not form neurofibroma-like tumors, in accordance with previous GEMM results (Nancy M. Joseph et al. 2008). *NF1*(-/-) differentiating SCs at 7 days after SC induction from NCs, did not form tumors either. Only *NF1*(-/-) cells that had differentiated for 14 days towards SCs were able to generate tumors. In addition, neurofibroma-like tumors were robustly obtained when these *NF1*(-/-) differentiating SCs at 14 days of differentiation were mixed with eFb primary cultures in 3D spheroids. These results seem to indicate the existence of a specific window at which cells can form neurofibromas and that a certain degree of commitment capacity towards a SC is required for a neurofibroma to form.

There are different aspects of the *in vitro* NC-SC differentiation procedure that difficulties a clear identification of a specific cell type: a) we have not identified SC stages but generated a continuum in SC differentiation in which we sample at different timepoints; b) in contrast to the obtention of NCs, SC differentiation cultures are not homogeneous, and cells at specific differentiation points may be actually a mixture of different identities; c) in the generation of heterotypic spheroids, we differentiate SCs in 2D up to day 5, and then we led cells to differentiate for 9 more days in 3D, up to 14 days. We do not know how differently these SCs differentiate compared to 2D cultures, but we know that the expression roadmap signature of those neurofibroma-generating heterotypic spheroids is similar to *NF1*(+/+) cells at 30 days of differentiation and to primary PNF-derived SC cultures. Another piece of information obtained is that eFbs help maintaining an apparent balance of *NF1*(-/-) cells between a precursor identity with self-renewal capacity and a SC commitment ability. The NC-SC expression characterization at different timepoints may help identify potential markers of cells originating neurofibromas. However, also, we will have to dissociate, sort, and characterize specific single cells or SC subpopulations from heterotypic spheroids to characterize better the cell that potentially originates neurofibroma-like tumors after engraftment.

6. Improvements and uses of the iPSC-based *in vitro*/*in vivo* human 3D plexiform neurofibroma model

We have generated an iPSC-based 3D *in vitro/in vivo* human PNF model. However, some improvements could be made. Only two out of three *NF1*(-/-) heterotypic spheroids were able to generate neurofibroma-like tumors, while the third *NF1*(-/-) heterotypic spheroid line (NF1_A) did not follow a clear NC-SC path.

One possibility could be that the eFbs that were part of the NF1_A heterotypic spheroids, 5PNF-derived eFbs, were not correctly supporting *NF1*(-/-) cells as eFbs that were part of the other two *NF1*(-/-) heterotypic spheroids, 3PNF-derived eFbs. To rule out this possibility, we could generate different heterotypic spheroids combining the three *NF1*(-/-) differentiating SCs with different PNF-derived eFbs (from 3PNF, 5PNF, and other PNFs) and characterize these spheroids by expression and some by engraftment. Another factor could be related to the purity of the PNF-derived Fb cultures, which are generated letting the PNF-digested cells grow in DMEM media supplemented with 10% FBS. Using this strategy, we obtained cultures highly enriched in eFbs. Nevertheless, other cell types like endothelial cells, perineurial cells, immune cells and remaining SCs, might be present in these eFb cultures. Thus, we should better characterize the cell type content of these eFb cultures and understand each cell type's potential functional contribution. We could purify the current PNF-derived eFb cultures either by Fluorescent Activated Cell Sorting (FACS) or manually using some specific Fb markers.

Besides the potential role of eFb cultures, we need to generate homogeneous differentiating *NF1*(-/-) SC populations. We know that the differentiation process is effective and that it can be improved in terms of culture homogeneity. This could also be a possibility why NF1_A culture did not follow a correct NC-SC path. In addition, we observed that despite the generation of neurofibroma-like tumors, other types of mesenchymal-derived tissues were also developing after homotypic spheroid engraftment, particularly, and also, to a lesser extent, in some engrafted heterotypic spheroids. We think that a correct and more homogeneous cell population of *NF1*(-/-) cells initiating spheroid formation is critical for successfully correct heterotypic spheroid formation. We will have to improve culture conditions, maybe using markers to sort specific cell populations (FACS, magnetic bead sorting), to improve homogeneity.

6.1. Potential uses of the iPSC-based 3D plexiform neurofibroma model

The 3D *in vitro* /*in vivo* human PNF model is a robust model that can be used to (i) study neurofibromagenesis and tumor microenvironment, (ii) study tumor progression towards malignancy, and (iii) constitute a platform for drug screening (**Figure D1**).

6.1.1. Neurofibromagenesis and tumor microenvironment

The generation of spheroids from differentiating SCs combined with their capacity to engraft into the sciatic nerve of nude mice and form neurofibroma-like tumors is a powerful strategy to capture the exact identity of PNF-originating cells. Furthermore, PNFs are complex cellular tumors, and microenvironment components can be easily incorporated into 3D models (Weydert et al. 2020). In this regard, we incorporated niche elements from the tumor microenvironment like the PNF-derived eFbs in the heterotypic spheroid 3D PNF model. Nevertheless, other cell types involved in neurofibroma development, like patient-derived immune cells, could also be added (Saraiva et al. 2020). Spheroids with progressive cellular complexity to mimic PNFs can be envisioned.

6.1.2. Modeling neurofibroma progression towards malignancy

The molecular pathogenesis of PNF-aNF-MPNST progression is well established. While PNFs bear the complete inactivation of *NF1*, aNFs in addition inactivate the *CDKN2A* locus (Beert et al. 2011; Carrió et al. 2018a). The most frequent genetic alteration found in MPNSTs added to the two-preceding tumor suppressors inactivation is the functional loss of the PRC2 by mutations in the *SUZ12* or *EED* genes (W. Lee et al. 2014). Alterations in these three tumor suppressors constitute a core signature of MPNSTgenesis (Serra et al. 2020). iPSCs are especially amenable to CRISPR/Cas9 genome editing (Hockemeyer and Jaenisch 2016). In this regard, *NF1*(-/-) iPSCs constitute a base in which to introduce in a step-wise manner specific mutations to the core signature of genes involved in progression towards MPNST. Due to their amenability, an alternative way of modeling progression would be editing at the NC stage. In both scenarios, tumor formation capacity and tumor type generation could be tested and analyzed by engrafting spheroids formed with the newly edited cells into the sciatic nerve of nude mice.

6.1.3. Plexiform neurofibroma drug development platform

Spheroid and 3D technology have greatly improved. One example is the growing number of available microplate systems for producing large quantities of individualized spheroids. These multiplex systems allow collecting fluorescence and luminescence-based signals without the need for transferring to other platforms, allowing the collection of different physiological readouts, like viability, apoptosis, etc. 3D assay systems are being explored to create more clinically relevant models of tumors for drug development (Weydert et al. 2020). Our developed multiplexed heterotypic spheroid 3D culture system is amenable to mid and high throughput drug testing and could be used to speed up the testing of new compounds on 3D PNF models.

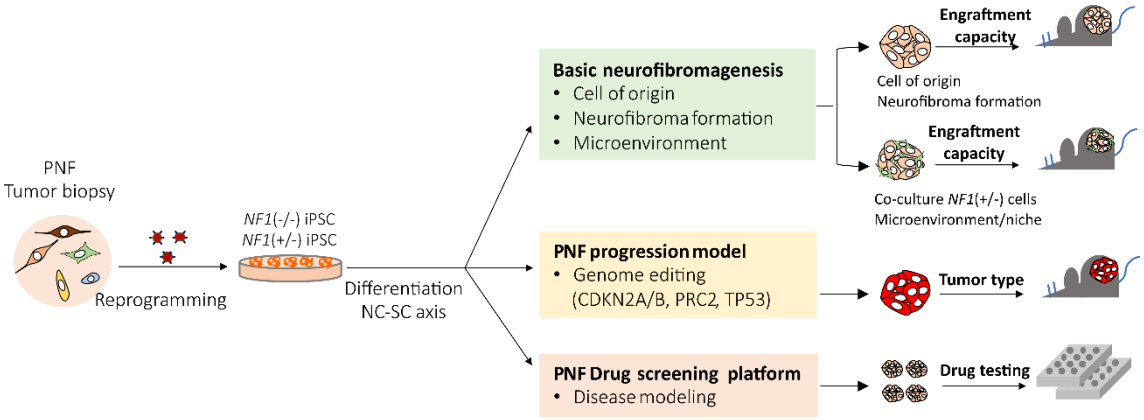

Figure D1. Schematic representation of the potential uses of the iPSC-based 3D plexiform neurofibroma model. Plexiform neurofibroma (PNF) cells are reprogrammed and *NF1*(+/-) and *NF1*(-/-) iPSC clones are established and characterized. *NF1*(-/-) PNF-derived iPSC lines are then differentiated towards the neural crest (NC)- Schwann cell (SC) lineage. These differentiated cells can be used to generate tumor spheroids to study basic neurofibromagenesis either alone or after adding microenvironment components, or to study PNF progression to malignancy by incorporating specific mutations using genome editing. Either of these can then be transplanted into xenograft models. PNF-derived differentiated spheroids can also serve as a drug screening platform to identify and validate therapeutic targets.

7. Role and importance of endoneurial fibroblasts in neurofibromas

eFbs were described more than 70 years ago (Brown 1946), but understanding its physiological role in the PNS is still incomplete (Richard, Topilko, Magy, Decouvelaere, et al. 2012). Similarly, the importance of eFb in neurofibroma formation was early acknowledged (Krone, Zörlein, and Mao 1981; Peltonen et al. 1986), but precise knowledge of the molecular and cellular basis of their implication in neurofibroma formation is still lacking.

Our results, as previously highlighted, evidenced that eFbs present in heterotypic spheroids allowed *NF1*(-/-) differentiating SCs to maintain a specific NC-SC lineage commitment and generate more consistently neurofibroma-like tumors.

Previous work in Lu Le's laboratory (Liao et al. 2016) generated neurofibroma-like tumors in mice upon the transplantation of *in vitro* 3D constructions containing mouse *Nf1*(-/-) skin-derived precursors, *Nf1*(+/-) nerve tissues (DRGs or sciatic nerves), collagen Type I, and human-derived Fbs as skin structure. They attributed to peripheral neurons being the critical factor that drove *Nf1*(-/-) skin-derived precursors to generate neurofibroma-like tumors. Our results highlight the impact of eFb cultures in the generation of neurofibroma-like tumors. In eFb cultures, despite being composed mainly of eFbs, a minority of other cell types is also present (endothelial cells, immune cells, SCs, etc.). However, the presence of neurons is presumed to be scarce. In their 3D model, skin-

derived Fbs as well as eFbs (being part of nerve tissues), were added into 3D constructions. To study the role of eFb in helping maintain *NF1*(-/-) differentiating SCs in the NC-SC path, we could generate new 3D heterotypic spheroids using NF1 patient-derived skin Fbs and *NF1*(-/-) differentiating SCs and engraft them into the sciatic nerve of nude mice. Considering the high heterogeneity of Fbs regarding their tissue of origin (Lynch, 2018), it is more likely that eFbs forming part of nerve possess such niche capacity than any other Fbs in the human body.

Moreover, the interaction between SCs and eFbs derived from cNFs changed the expression profile of each cell type and generated an expression and secretion profile favoring a pro-inflammatory reaction with the secretion of, for instance, IL1β, IL6, sICAM1, CCL7 or CCL11. Interestingly, PNF heterotypic spheroids expressed a significant part of this expression profile in cNF SC-eFb co-cultures. In contrast, PNF homotypic spheroids composed of only differentiating SCs just expressed approximately 1/6 of these genes. These results, together with the fact that eFbs from PNF and cNFs are very similar to each other, according to their expression signatures, suggest that these interactions could take place *in vivo* in cNFs, as well as in PNFs.

The importance of the immune system in neurofibroma development has already been shown in the *Nf1*$^{flox/flox}$; *Dhh*-Cre; *Cxcr3*-null mouse model (Fletcher et al. 2019). In the *Nf1*$^{flox/flox}$; *Dhh*-Cre PNF mouse model, the chemokine CXCL10 is expressed in *Nf1*(-/-) SCs recruiting CXCR3 expressing T-cells and dendritic cells. However, in the *Nf1*$^{flox/flox}$; *Dhh*-Cre; *Cxcr3*-null mouse model, although *Nf1*(-/-) SCs were present in the mice, no PNF was formed. The authors argued the lack of PNF being related to the absence of the CXCL10 receptor CXCR3, impeding the recruitment of T cells and dendritic cells. These results highlight the importance of infiltrating immune cells in neurofibroma initiation and development. Our results showed, that although we could detect the secretion of CXCL10 in cNF-derived single cultures, either SC or eFb cultures, we could not detect a prominent increased in the secretion of CXCL10 in co-cultures.

In the *Prss56*-Cre mouse model, the *Nf1* gene is ablated in *Prss56* expressing boundary cap (BC) cells and their derivatives (Katarzyna J. Radomska et al. 2019). The authors described the development of cNF in different stages. In stage 2, the authors described an eFb accumulation and SC hyperplasia, followed by a stage in which micro-cNFs are already observed with abundant eFbs present, and macrophages and neutrophils infiltrating them, as signs of inflammation. Our results are in accordance with this model and suggest that the modification of these pro-inflammatory signals might have an impact on neurofibroma development. Thus, after validating *in vitro* some of the promising signaling pathways identified due to the SC-eFb interaction, it would be wise to validate them in *Prss56*-Cre mouse model and to study whether these therapies could have a potential therapeutic (i.e., reducing the size of PNFs) or a preventive (i.e., avoiding the appearance of cNFs) effect in neurofibroma development and progression, or hopefully both.

Some markers are used in a clinical pathology setting to detect eFb in neurofibromas, like CD34 (Hirose et al. 2003). However, most PNF- and cNF-derived eFb cultures did not

express this marker. There is a need to identify new eFb markers to characterize neurofibromas and derived cell cultures. We will use the data generated in this thesis to identify new potential markers and to study their expression in PNFs and cNFs and their derivative eFb cultures.

eFbs derived from PNFs and cNFs were remarkably similar according to their expression pattern. However, eFb cultures might be complex cultures since, in addition to the potential "contamination" by other cell types (endothelial cells, immune cells, etc.), scRNA-seq analysis of PNFs identified distinct subpopulations of eFb.

Moreover, eFbs have been postulated to arise from NC cells (Morrison et al. 1999; N. M. Joseph 2004; Richard, Topilko, Magy, Decouvelaere, et al. 2012), and our data seem to agree with these results. Single-cell data from the Fb compartment show that these cells express two essential transcription factors that define the NC-mesenchymal differentiation axis: *PRRX1* and *TWIST1* (Soldatov et al. 2019). Further characterization of eFb subpopulations are needed to uncover the real nature of these cells.

8. Heterogeneity of the Schwann cell component of plexiform neurofibromas

RT-qPCR and RNA-seq analysis from primary PNF-derived SC cultures evidenced the expression of markers expressed along the NC-SC lineage (Kristjan R. Jessen and Mirsky 2005a). To rule out whether this marker expression covering the whole NC-SC axis was happening homogeneously in all SCs or heterogeneously in cultured cells, we used two markers of the NC-SC axis: p75, expressed from NC up to mature SC, and S100B expressed from committed SC up to mature SC. Thus, detecting both markers at the same time, we were able to identify cells at an early stage (p75+, S100B -) or a later stage (p75+, S100B+). Co-immunostaining and flow cytometry analysis evidenced distinct subpopulations of SCs within PNFs, some cells only expressing p75, others expressing both markers, and some only S100B. These results suggested that PNFs were composed by SCs at different mature states, some committed to SCs and others not.

This heterogeneity of the SC component was also identified by single-cell RNA-seq analysis. Results evidenced the existence of at least two SC subpopulations, one expressing only early NC-SC lineage markers, suggesting a precursor-like cell, and another expressing the same markers together with later NC-SC lineage markers present in committed SCs, denoting a singular committed SC type, expressing at the same time most of the classical markers of the NC-SC axis. These unexpected results evidence the complex biology of the SC compartment and suggest that the precursor-like SC population being the source of all PNF SCs, some remaining at an early stage and others undergoing SC commitment, possibly by the presence of niche effects of surrounding eFbs. These results may change the current view of PNF development and growth.

Flow cytometry analysis of cNFs using p75 and S100B co-staining also uncovered a similar SC heterogeneity, as in PNFs (Figure A2-2). These findings suggest that cNFs might probably be composed of similar SC subpopulations as in PNFs.

The different SC subpopulations composing neurofibromas need to be further characterized, and their role in neurofibroma growth established. Functional characterization of them might help designing better treatments for neurofibromas since different subpopulations might exhibit different responses to specific therapies (Rybinsky, 2016).

Conclusions

The main conclusions of this thesis are:

- Two *NF1*(-/-) induced pluripotent stem cell (iPSC) lines were generated directly from plexiform neurofibromas (PNFs), sharing the same constitutional and somatic *NF1* mutations; as well as the entire genetic background, as the cell originating them. In addition, five independent *NF1*(+/-) iPSCs were generated from 5 PNFs, two being isogenic to the *NF1*(-/-) iPSC lines established. These iPSCs represent an imperishable source of cells to generate cell-based PNF models.

- A robust differentiation protocol to generate *bona fide* neural crest (NC) cells from iPSCs was established. NC cells were able to migrate and differentiate into different NC-derived cell types indicating their multipotency capacity.

- A reproducible differentiation protocol to generate Schwann cells (SCs) from NCs was established. *NF1*(+/+)-derived SCs were capable of myelinating axons, indicating they were able to reach a functional mature state.

- Neurofibromin function influences iPSC cell proliferation since *NF1*(-/-) iPSCs exhibited a significantly higher proliferation rate compared to control *NF1*(+/+) iPSCs. Neurofibromin is also involved in the proliferation and differentiation of cells of the NC-SC lineage. *NF1*(-/-) differentiating SCs exhibited a higher proliferation rate than controls, showed a natural tendency to form spheres and a poor ability to myelinate axons. These same properties were observed in *NF1*(-/-) CRISPR/Cas9 edited iPSCs, demonstrating a direct involvement of *NF1* function.

- A gene expression roadmap signature was obtained from the NC-SC *in vitro* differentiation system, consisting of thousands of differentially expressed genes at NC-SC stages and differentiation timepoints. NC-SC expression roadmap may facilitate the identification of new lineage markers and may constitute a useful tool for monitoring the correct development of heterotypic spheroids as PNF models.

- *NF1*(-/-) differentiating SCs in 2D cultures did not constitute an adequate system to model PNFs, since they did not adopt a correct expression of NC-SC markers, did not generate homogeneous populations of functional SCs and were not able to generate neurofibroma-like tumors upon engraftment in mice.

- A reproducible multiplexed 3D homotypic and heterotypic SC differentiation model was established using *NF1*(+/+) and *NF1*(-/-) iPSCs. Only *NF1*(-/-) spheroids were able to form neurofibroma-like tumors after their engraftment in the sciatic nerve of nude mice. However, the engraftment of heterotypic spheroids, composed of *NF1*(-/-) differentiating SC and primary endoneurial fibroblasts (eFbs), represented the most efficient and consistent way of producing them. This is the first time that human neurofibroma-like tumors are generated in mice.

- We identified the existence of different SC subpopulations within PNFs according to their marker expression. We identified at least two distinct SC subpopulations, one expressing markers appearing early in the NC-SC axis, suggesting a precursor-like identity, and another subpopulation expressing both early and late markers along the NC-SC lineage, suggesting a singular committed SC.

- We identified differentially upregulated genes due to the interplay between SCs and eFbs derived from cNFs. Most of these genes were also expressed in iPSC-derived heterotypic spheroids modeling PNFs. Among the enriched signaling pathways represented by these genes, those involved in the infiltration of immune cells were significantly represented, and were confirmed by the secretion profile analysis of SC-eFb co-cultures.

- A human *in vitro*/*in vivo* multiplexed 3D heterotypic model system was established to model PNFs. This model system: (i) will facilitate the study of PNF formation and the role of tumor microenvironment; (ii) constitute the basis to model PNF progression to malignancy; (iii) could be used as a multiplexed drug testing platform.

Bibliography

Abeshouse, Adam, Clement Adebamowo, Sally N. Adebamowo, Rehan Akbani, Teniola Akeredolu, Adrian Ally, Matthew L. Anderson, et al. 2017. “Comprehensive and Integrated Genomic Characterization of Adult Soft Tissue Sarcomas.” *Cell* 171 (4): 950-965.e28. https://doi.org/10.1016/j.cell.2017.10.014.

Ackerman, Sarah D., Rong Luo, Yannick Poitelon, Amit Mogha, Breanne L. Harty, Mitchell D’Rozario, Nicholas E. Sanchez, et al. 2018. “GPR56/ADG RG1 Regulates Development and Maintenance of Peripheral Myelin.” *Journal of Experimental Medicine* 215 (3): 941–61. https://doi.org/10.1084/jem.20161714.

Akshintala, Srivandana, Andrea Baldwin, David J Liewehr, Anne Goodwin, Jaishri O Blakeley, Andrea M Gross, Seth M Steinberg, Eva Dombi, and Brigitte C Widemann. 2020. “Longitudinal Evaluation of Peripheral Nerve Sheath Tumors in Neurofibromatosis Type 1: Growth Analysis of Plexiform Neurofibromas and Distinct Nodular Lesions.” *Neuro-Oncology* d (March): 1–11. https://doi.org/10.1093/neuonc/noaa053.

Anastasaki, Corina, and David H. Gutmann. 2014. “Neuronal NF1/RAS Regulation of Cyclic AMP Requires Atypical PKC Activation.” *Human Molecular Genetics* 23 (25): 6712–21. https://doi.org/10.1093/hmg/ddu389.

Anastasaki, Corina, Michelle L. Wegscheid, Kelly Hartigan, Jason B. Papke, Nathan D. Kopp, Jiayang Chen, Olivia Cobb, Joseph D. Dougherty, and David H. Gutmann. 2020. “Human IPSC-Derived Neurons and Cerebral Organoids Establish Differential Effects of Germline NF1 Gene Mutations.” *Stem Cell Reports* 14 (4): 541–50. https://doi.org/10.1016/j.stemcr.2020.03.007.

Anastasaki, Corina, Albert S. Woo, Ludwine M. Messiaen, and David H. Gutmann. 2015. “Elucidating the Impact of Neurofibromatosis-1 Germline Mutations on Neurofibromin Function and Dopamine-Based Learning.” *Human Molecular Genetics* 24 (12): 3518–28. https://doi.org/10.1093/hmg/ddv103.

Antony-Debré, Iléana, Vladimir T. Manchev, Nathalie Balayn, Dominique Bluteau, Cécile Tomowiak, Céline Legrand, Thierry Langlois, et al. 2015. “Level of RUNX1 Activity Is Critical for Leukemic Predisposition but Not for Thrombocytopenia.” *Blood* 125 (6): 930–40. https://doi.org/10.1182/blood-2014-06-585513.

Aquino, Jorge B., Jens Hjerling-Leffler, Martin Koltzenburg, Thomas Edlund, Marcelo J. Villar, and Patrik Ernfors. 2006. “In Vitro and in Vivo Differentiation of Boundary Cap Neural Crest Stem Cells into Mature Schwann Cells.” *Experimental Neurology* 198 (2): 438–49. https://doi.org/10.1016/j.expneurol.2005.12.015.

Aran, Dvir, Agnieszka P. Looney, Leqian Liu, Esther Wu, Valerie Fong, Austin Hsu, Suzanna Chak, et al. 2019. “Reference-Based Analysis of Lung Single-Cell Sequencing Reveals a Transitional Profibrotic Macrophage.” *Nature Immunology* 20 (2): 163–72. https://doi.org/10.1038/s41590-018-0276-y.

Bajpai, Ruchi, Denise A. Chen, Alvaro Rada-Iglesias, Junmei Zhang, Yiqin Xiong, Jill Helms, Ching Pin Chang, Yingming Zhao, Tomek Swigut, and Joanna Wysocka. 2010. “CHD7 Cooperates with PBAF to Control Multipotent Neural Crest Formation.” *Nature* 463 (7283): 958–62. https://doi.org/10.1038/nature08733.

Ballester, Roymarie, Douglas Marchuk, Mark Boguski, Ann Saulino, Roxanne Letcher, Michael Wigler, and Francis Collins. 1990. "The NF1 Locus Encodes a Protein Functionally Related to Mammalian GAP and Yeast IRA Proteins." *Cell* 63 (4): 851–59. https://doi.org/10.1016/0092-8674(90)90151-4.

Bar-Nur, Ori, Holger A. Russ, Shimon Efrat, and Nissim Benvenisty. 2011. "Epigenetic Memory and Preferential Lineage-Specific Differentiation in Induced Pluripotent Stem Cells Derived from Human Pancreatic Islet Beta Cells." *Cell Stem Cell* 9 (1): 17–23. https://doi.org/10.1016/j.stem.2011.06.007.

Barron, Victoria A., and Hua Lou. 2012. "Alternative Splicing of the Neurofibromatosis Type I Pre-MRNA." *Bioscience Reports* 32 (2): 131–38. https://doi.org/10.1042/BSR20110060.

Beert, E., H. Brems, B. Daniëls, I. De Wever, F. Van Calenbergh, J. Schoenaers, M. Debiec-Rychter, et al. 2011. "Atypical Neurofibromas in Neurofibromatosis Type 1 Are Premalignant Tumors." *Genes, Chromosomes and Cancer* 50: 1021–32.

Bentley, C. A., and K. F. Lee. 2000. "P75 Is Important for Axon Growth and Schwann Cell Migration during Development." *Journal of Neuroscience* 20 (20): 7706–15. https://doi.org/10.1523/jneurosci.20-20-07706.2000.

Bergqvist, Christina, Amandine Servy, Laurence Valeyrie-Allanore, Salah Ferkal, Patrick Combemale, Pierre Wolkenstein, Henri Adamski, et al. 2020. "Neurofibromatosis 1 French National Guidelines Based on an Extensive Literature Review since 1966." *Orphanet Journal of Rare Diseases* 15 (1): 1–23. https://doi.org/10.1186/s13023-020-1310-3.

Bernhardt, Mathias, Daniel Novak, Yassen Assenov, Elias Orouji, Nathalie Knappe, Kasia Weina, Maike Reith, et al. 2017. "Melanoma-Derived IPCCs Show Differential Tumorigenicity and Therapy Response." *Stem Cell Reports* 8 (5): 1379–91. https://doi.org/10.1016/j.stemcr.2017.03.007.

Betters, Erin, Ying Liu, Anders Kjaeldgaard, Erik Sundström, and Martín I. García-Castro. 2010. "Analysis of Early Human Neural Crest Development." *Developmental Biology* 344 (2): 578–92. https://doi.org/10.1016/j.ydbio.2010.05.012.

Bollag, G., D. Wade Clapp, S. Shih, F. Adler, Y.Y. Zhang, P. Thompson, B.J. Lange, et al. 1996. "Loss of NF1 Results in Activation of the Ras Signaling Pathway and Leads to Aberrant Growth in Haematopoietic Cells." *Nature Medicine* 2 (4): 534–39.

Brannan, Camilynn I., Archibald S. Perkins, Kristine S. Vogel, Nancy Ratner, Michael L. Nordlund, Susan W. Reid, Arthur M. Buchberg, Nancy A. Jenkins, Luis F. Parada, and Neal G. Copeland. 1994. "Targeted Disruption of the Neurofibromatosis Type-1 Gene Leads to Developmental Abnormalities in Heart and Various Neural Crest-Derived Tissues." *Genes and Development* 8 (9): 1019–29. https://doi.org/10.1101/gad.8.9.1019.

Brossier, Nicole M., and Steven L. Carroll. 2012. "Genetically Engineered Mouse Models Shed New Light on the Pathogenesis of Neurofibromatosis Type I-Related Neoplasms of the Peripheral Nervous System." *Brain Research Bulletin* 88 (1): 58–71. https://doi.org/10.1016/j.brainresbull.2011.08.005.

Brown, D. 1946. “Importance of Neural Fibroblasts in the Regeneration of Nerve.” *Archives of Neurology and Psychiatry* 55 (3): 171–215.

Buganim, Yosef, Dina A. Faddah, and Rudolf Jaenisch. 2013. “Mechanisms and Models of Somatic Cell Reprogramming.” *Nature Reviews Genetics* 14 (6): 427–39. https://doi.org/10.1038/nrg3473.

Campos, Priscila B., Rafaela C. Sartore, Stacie N. Abdalla, and Stevens K. Rehen. 2009. “Chromosomal Spread Preparation of Human Embryonic Stem Cells for Karyotyping.” *Journal of Visualized Experiments*, no. 31: 4–7. https://doi.org/10.3791/1512.

Carey, D. J., C. F. Eldridge, C. J. Cornbrooks, R. Timpl, and R. P. Bunge. 1983. “Biosynthesis of Type IV Collagen by Cultured Rat Schwann Cells.” *The Journal of Cell Biology* 97 (2): 473–79. https://doi.org/10.1083/jcb.97.2.473.

Carrió, Meritxell, Bernat Gel, Ernest Terribas, Adriana Carolina Zucchiatti, Teresa Moliné, Inma Rosas, Álex Teulé, et al. 2018a. “Analysis of Intratumor Heterogeneity in Neurofibromatosis Type 1 Plexiform Neurofibromas and Neurofibromas with Atypical Features: Correlating Histological and Genomic Findings.” *Human Mutation*, no. February: 1112–25. https://doi.org/10.1002/humu.23552.

Castellanos, Elisabeth, Bernat Gel, Inma Rosas, Eva Tornero, Sheila Santín, Raquel Pluvinet, Juan Velasco, et al. 2017. “A Comprehensive Custom Panel Design for Routine Hereditary Cancer Testing: Preserving Control, Improving Diagnostics and Revealing a Complex Variation Landscape.” *Scientific Reports* 7 (November 2016): 1–12. https://doi.org/10.1038/srep39348.

Castellsagué, Joan, Bernat Gel, Juana Fernández-Rodríguez, Roger Llatjós, Ignacio Blanco, Yolanda Benavente, Diana Pérez-Sidelnikova, et al. 2015. “Comprehensive Establishment and Characterization of Orthoxenograft Mouse Models of Malignant Peripheral Nerve Sheath Tumors for Personalized Medicine.” *EMBO Molecular Medicine* 7 (5): 608–27. https://doi.org/10.15252/emmm.201404430.

Chambers, Stuart M., Christopher A. Fasano, Eirini P. Papapetrou, Mark Tomishima, Michel Sadelain, and Lorenz Studer. 2009. “Highly Efficient Neural Conversion of Human ES and IPS Cells by Dual Inhibition of SMAD Signaling.” *Nature Biotechnology* 27 (3): 275–80. https://doi.org/10.1038/nbt.1529.

Chen, Zhiguo, Chiachi Liu, Amish J. Patel, Chung Ping Liao, Yong Wang, and Lu Q. Le. 2014. “Cells of Origin in the Embryonic Nerve Roots for NF1-Associated Plexiform Neurofibroma.” *Cancer Cell* 26 (5): 695–706. https://doi.org/10.1016/j.ccell.2014.09.009.

Chen, Zhiguo, Juan Mo, Jean Philippe Brosseau, Tracey Shipman, Yong Wang, Chung Ping Liao, Jonathan M. Cooper, et al. 2019. “Spatiotemporal Loss of NF1 in Schwann Cell Lineage Leads to Different Types of Cutaneous Neurofibroma Susceptible to Modification by the Hippo Pathway.” *Cancer Discovery* 9 (1): 114–29. https://doi.org/10.1158/2159-8290.CD-18-0151.

Cibulskis, K., M. S. Lawrence, S. Carter, A. Sivachenko, D. Jaffe, C. Sougnez, S. Gabriel, M. Meyerson, E. S. Lander, and G. Getz. 2013. “MuTect.” *Nature Biotechnology* 31 (3):

213–19. https://doi.org/10.1038/nbt.2514.Sensitive.

Cichowski, Karen, and Tyler Jacks. 2001. “NF1 Tumor Suppressor Gene Function: Narrowing the GAP.” *Cell* 104 (4): 593–604. https://doi.org/10.1016/S0092-8674(01)00245-8.

Cichowski, Karen, T. Shane Shih, Earlene Schmitt, Sabrina Santiago, Karlyne Reilly, Margaret E. McLaughlin, Roderick T. Bronson, and Tyler Jacks. 1999. “Mouse Models of Tumor Development in Neurofibromatosis Type 1.” *Science* 286 (5447): 2172–76. https://doi.org/10.1126/science.286.5447.2172.

Clevers, Hans. 2016. “Modeling Development and Disease with Organoids.” *Cell* 165 (7): 1586–97. https://doi.org/10.1016/j.cell.2016.05.082.

Colman, Steven D, Charles A Williams, and Margaret R Wallace. 1995. “Deletions of the NF1 Gene” II (september): 90–92.

Costa, Elisabete C, André F Moreira, Duarte De Melo-diogo, Vítor M Gaspar, Marco P Carvalho, and Ilídio J Correia. 2016. “3D Tumor Spheroids : An Overview on the Tools and Techniques Used for Their Analysis.” *Biotechnology Advances* 34 (8): 1427–41. https://doi.org/10.1016/j.biotechadv.2016.11.002.

Costa, Sónia, Raquel Tojal, and Ana Valverde. 2012. “Neurofibromatosis – Diagnostic Assessment.” In *Neurodegeneration*, 257–78.

Coulpier, Fanny, Stéphane Le Crom, Géraldine S. Maro, Jan Manent, Marco Giovannini, Zofia Maciorowski, Andreas Fischer, Manfred Gessler, Patrick Charnay, and Piotr Topilko. 2009. “Novel Features of Boundary Cap Cells Revealed by the Analysis of Newly Identified Molecular Markers.” *Glia* 57 (13): 1450–57. https://doi.org/10.1002/glia.20862.

Crespo, Miguel, Eduardo Vilar, Su Yi Tsai, Kyle Chang, Sadaf Amin, Tara Srinivasan, Tuo Zhang, et al. 2017. “Colonic Organoids Derived from Human Induced Pluripotent Stem Cells for Modeling Colorectal Cancer and Drug Testing.” *Nature Medicine* 23 (7): 878–84. https://doi.org/10.1038/nm.4355.

Dasgupta, B, L L Dugan, and D H Gutmann. 2003. “The Neurofibromatosis 1 Gene Product Neurofibromin Regulates Pituitary Adenylate Cyclase-Activating Polypeptide-Mediated Signaling in Astrocytes.” *Journal of Neuroscience* 23 (26): 8949–54. https://doi.org/23/26/8949 [pii].

Daston, Maryellen Maneri, and Nancy Ratner. 1992. “Neurofibromin, a Predominantly Neuronal GTPase Activating Protein in the Adult, Is Ubiquitously Expressed during Development.” *Developmental Dynamics* 195 (3): 216–26. https://doi.org/10.1002/aja.1001950307.

DeBella, Kimberly, Jacek Szudek, and Jan Marshall Friedman. 2000. “Use of the National Institutes of Health Criteria for Diagnosis of Neurofibromatosis 1 in Children.” *Pediatrics* 105 (3): 608–14. https://doi.org/10.1542/peds.105.3.608.

Declue, Jeffrey E, Bruce D Cohen, and Douglas R Lowy. 1991. “Identification and Characterization of the Neurofibromatosis Type 1 Protein Product” 88 (November): 9914–18.

Denham, Mark, Kouichi Hasegawa, Trevelyan Menheniott, Ben Rollo, Dongcheng Zhang, Shelley Hough, Abdullah Alshawaf, et al. 2015. “Multipotent Caudal Neural Progenitors Derived from Human Pluripotent Stem Cells That Give Rise to Lineages of the Central and Peripheral Nervous System.” *Stem Cells* 33 (6): 1759–70. https://doi.org/10.1002/stem.1991.

Dobin, Alexander, Carrie A. Davis, Felix Schlesinger, Jorg Drenkow, Chris Zaleski, Sonali Jha, Philippe Batut, Mark Chaisson, and Thomas R. Gingeras. 2013. “STAR: Ultrafast Universal RNA-Seq Aligner.” *Bioinformatics* 29 (1): 15–21. https://doi.org/10.1093/bioinformatics/bts635.

Dombi, Eva, Andrea Baldwin, Leigh J. Marcus, Michael J. Fisher, Brian Weiss, Aerang Kim, Patricia Whitcomb, et al. 2016. “Activity of Selumetinib in Neurofibromatosis Type 1-Related Plexiform Neurofibromas.” *New England Journal of Medicine* 375 (26): 2550–60. https://doi.org/10.1056/NEJMoa1605943.

Donato, R, B R Cannon, G Sorci, F Riuzzi, K Hsu, D J Weber, and C L Geczy. 2013. “Functions of S100 Proteins.” *Current Molecular Medicine* 13 (1): 24–57. https://doi.org/10.2174/1566524011307010024.

Donato, Rosario, Guglielmo Sorci, Francesca Riuzzi, Cataldo Arcuri, Roberta Bianchi, Flora Brozzi, Claudia Tubaro, and Ileana Giambanco. 2009. “S100B’s Double Life: Intracellular Regulator and Extracellular Signal.” *Biochimica et Biophysica Acta - Molecular Cell Research* 1793 (6): 1008–22. https://doi.org/10.1016/j.bbamcr.2008.11.009.

Dugoff, Lorraine, and Eva Sujansky. 1996. “Neurof Ibromatosis Type 1 and Pregnancy” 10: 7–10.

Dunzendorfer-matt, Theresia, Ellen L Mercado, Karl Maly, Frank Mccormick, and Klaus Scheffzek. 2016. “The Neurofibromin Recruitment Factor Spred1 Binds to the GAP Related Domain without Affecting Ras Inactivation” 113 (27): 7497–7502. https://doi.org/10.1073/pnas.1607298113.

Duong, T. A., S. Bastuji-Garin, L. Valeyrie-Allanore, E. Sbidian, S. Ferkal, and P. Wolkenstein. 2011. “Evolving Pattern with Age of Cutaneous Signs in Neurofibromatosis Type 1: A Cross-Sectional Study of 728 Patients.” *Dermatology* 222 (3): 269–73. https://doi.org/10.1159/000327379.

Dupin, Elisabeth, and Lukas Sommer. 2012. “Neural Crest Progenitors and Stem Cells: From Early Development to Adulthood.” *Developmental Biology* 366 (1): 83–95. https://doi.org/10.1016/j.ydbio.2012.02.035.

Eldridge, Charles E, Richard P Bunge, and M Wood. 1987. “Differentiation of Axon-Related Schwann Cells In Vitro. I. Ascorbic Acid Regulates Basal Lamina Assembly and Myelin Formation” 105 (August).

Eminli, Sarah, Adlen Foudi, Matthias Stadtfeld, Nimet Maherali, Tim Ahfeldt, Gustavo Mostoslavsky, Hanno Hock, and Konrad Hochedlinger. 2009. “Differentiation Stage Determines Potential of Hematopoietic Cells for Reprogramming into Induced Pluripotent Stem Cells.” *Nature Genetics* 41 (9): 968–76. https://doi.org/10.1038/ng.428.

Evans, D. G., E. Howard, C. Giblin, T. Clancy, H. Spencer, S. M. Huson, and F. Lalloo. 2010. "Birth Incidence and Prevalence of Tumor-Prone Syndromes: Estimates from a UK Family Genetic Register Service." *American Journal of Medical Genetics, Part A* 152 (2): 327–32. https://doi.org/10.1002/ajmg.a.33139.

Feng, Suhua, Steven E. Jacobsen, and Wolf Reik. 2010. "Epigenetic Reprogramming in Plant and Animal Development." *Science* 330 (6004): 622–27. https://doi.org/10.1126/science.1190614.

Ferner, Rosalie E. 2007. "Neurofibromatosis 1." *European Journal of Human Genetics* 15 (2): 131–38. https://doi.org/10.1038/sj.ejhg.5201676.

Ferner, Rosalie E., Susan M. Huson, Nick Thomas, Celia Moss, Harry Willshaw, D. Gareth Evans, Meena Upadhyaya, et al. 2007. "Guidelines for the Diagnosis and Management of Individuals with Neurofibromatosis." *Journal of Medical Genetics* 44 (2): 81–88. https://doi.org/10.1136/jmg.2006.045906.

Fletcher, Jonathan S, Jay Pundavela, and Nancy Ratner. 2019. "After Nf1 Loss in Schwann Cells, Inflammation Drives Neurofibroma Formation." *Neuro-Oncology Advances*, no. November 2019: 1–10. https://doi.org/10.1093/noajnl/vdz045.

Fletcher, Jonathan S, Jianqiang Wu, Walter J Jessen, Jay Pundavela, Jacob A Miller, Eva Dombi, Mi-ok Kim, et al. 2019. "Cxcr3-Expressing Leukocytes Are Necessary for Neurofibroma Formation in Mice." *JCI Insight* 4 (3). https://doi.org/https://doi.org/10.1172/jci.insight.98601.

Freberg, C., J. Arne Dahl, S. Timoskainen, and P. Collas. 2007. "Epigenetic Reprogramming of OCT4 and NANOG Regulatory Regions by Embryonal Carcinoma Cell Extract." *Molecular Biology of the Cell* 18 (May): 1543–53. https://doi.org/10.1091/mbc.E07.

Frith, Thomas J.R., Ilaria Granata, Matthew Wind, Erin Stout, Oliver Thompson, Katrin Neumann, Dylan Stavish, et al. 2018. "Human Axial Progenitors Generate Trunk Neural Crest Cells in Vitro." *ELife* 7: 1–27. https://doi.org/10.7554/eLife.35786.

Fujiwara, Sayaka, Shinya Hoshikawa, Takaaki Ueno, Makoto Hirata, Taku Saito, Toshiyuki Ikeda, Hiroshi Kawaguchi, et al. 2014. "SOX10 Transactivates S100B to Suppress Schwann Cell Proliferation and to Promote Myelination." *PLoS ONE* 9 (12): 1–17. https://doi.org/10.1371/journal.pone.0115400.

Fukuta, Makoto, Yoshinori Nakai, Kosuke Kirino, Masato Nakagawa, Kazuya Sekiguchi, Sanae Nagata, Yoshihisa Matsumoto, et al. 2014. "Derivation of Mesenchymal Stromal Cells from Pluripotent Stem Cells through a Neural Crest Lineage Using Small Molecule Compounds with Defined Media." *PLoS ONE* 9 (12): 1–25. https://doi.org/10.1371/journal.pone.0112291.

García-Castro, Martín I, Christophe Marcelle, and Marianne Bronner-Fraser. 2002. "Ectodermal Wnt Function as a Neural Crest Inducer." *Science (New York, N.Y.)* 297 (5582): 848–51. https://doi.org/10.1126/science.1070824.

Garcia-Linares, Carles, Juana Fernández-Rodríguez, Ernest Terribas, Jaume Mercadé, Eva Pros, Llúcia Benito, Yolanda Benavente, et al. 2011. "Dissecting Loss of Heterozygosity (LOH) in Neurofibromatosis Type 1-Associated Neurofibromas:

Importance of Copy Neutral LOH." *Human Mutation* 32 (1): 78–90. https://doi.org/10.1002/humu.21387.

Ghosh, Srimoyee, Allan J. Yates, Michael C. Frühwald, Jeffrey C. Miecznikowski, Christoph Plass, and Dominic J. Smiraglia. 2010. "Tissue Specific DNA Methylation of CpG Islands in Normal Human Adult Somatic Tissues Distinguishes Neural from Non-Neural Tissues." *Epigenetics* 5 (6): 527–38. https://doi.org/10.4161/epi.5.6.12228.

Gomez, Gustavo A., Maneeshi S. Prasad, Nabjot Sandhu, Patrick B. Shelar, Alan W. Leung, and Martín I. García-Castro. 2019. "Human Neural Crest Induction by Temporal Modulation of WNT Activation." *Developmental Biology* 449 (2): 99–106. https://doi.org/10.1016/j.ydbio.2019.02.015.

Granstörm, Sofia, Anna Langenbruch, Matthias Augustin, and Victor Felix Mautner. 2012. "Psychological Burden in Adult Neurofibromatosis Type 1 Patients: Impact of Disease Visibility on Body Image." *Dermatology* 224 (2): 160–67. https://doi.org/10.1159/000337548.

Green, Stephen A., Marcos Simoes-Costa, and Marianne E. Bronner. 2015. "Evolution of Vertebrates as Viewed from the Crest." *Nature* 520 (7548): 474–82. https://doi.org/10.1038/nature14436.

Gresset, Aurélie, Fanny Coulpier, Gaspard Gerschenfeld, Alexandre Jourdon, Graziella Matesic, Laurence Richard, Jean Michel Vallat, Patrick Charnay, and Piotr Topilko. 2015. "Boundary Caps Give Rise to Neurogenic Stem Cells and Terminal Glia in the Skin." *Stem Cell Reports* 5 (2): 278–90. https://doi.org/10.1016/j.stemcr.2015.06.005.

Gross, Andrea M., Pamela L. Wolters, Eva Dombi, Andrea Baldwin, Patricia Whitcomb, Michael J. Fisher, Brian Weiss, et al. 2020. "Selumetinib in Children with Inoperable Plexiform Neurofibromas." *New England Journal of Medicine* 382 (15): 1430–42. https://doi.org/10.1056/NEJMoa1912735.

Guo, H F, I The, F Hannan, a Bernards, and Y Zhong. 1997. "Requirement of Drosophila NF1 for Activation of Adenylyl Cyclase by PACAP38-like Neuropeptides." *Science (New York, N.Y.)* 276 (5313): 795–98. https://doi.org/10.1126/science.276.5313.795.

Gutmann, David H., Rosalie E. Ferner, Robert H. Listernick, Bruce R. Korf, Pamela L. Wolters, and Kimberly J. Johnson. 2017. "Neurofibromatosis Type 1." *Nature Reviews Disease Primers* 3: 17004. https://doi.org/10.1038/nrdp.2017.4.

Hackland, James O.S., Tom J.R. Frith, Oliver Thompson, Ana Marin Navarro, Martin I. Garcia-Castro, Christian Unger, and Peter W. Andrews. 2017. "Top-Down Inhibition of BMP Signaling Enables Robust Induction of HPSCs Into Neural Crest in Fully Defined, Xeno-Free Conditions." *Stem Cell Reports* 9 (4): 1043–52. https://doi.org/10.1016/j.stemcr.2017.08.008.

Hackland, James O.S., Patrick B. Shelar, Nabjot Sandhu, Maneeshi S. Prasad, Rebekah M. Charney, Gustavo A. Gomez, Thomas J.R. Frith, and Martín I. García-Castro. 2019. "FGF Modulates the Axial Identity of Trunk HPSC-Derived Neural Crest but Not the Cranial-Trunk Decision." *Stem Cell Reports* 12 (5): 920–33.

https://doi.org/10.1016/j.stemcr.2019.04.015.

Hanna, Jacob, Krishanu Saha, Bernardo Pando, Jeroen Van Zon, Christopher J. Lengner, Menno P. Creyghton, Alexander Van Oudenaarden, and Rudolf Jaenisch. 2009. "Direct Cell Reprogramming Is a Stochastic Process Amenable to Acceleration." *Nature* 462 (7273): 595–601. https://doi.org/10.1038/nature08592.

Hernández-Martín, A., and A. Duat-Rodríguez. 2016. "Neurofibromatosis Tipo 1: Más Que Manchas Café Conleche, Efélides y Neurofibromas. Parte I. Actualización Sobre Los Criterios Dermatológicos Diagnósticos de La Enfermedad (15) (PDF) An Update on Neurofibromatosis Type 1: Not Just Café-Au-Lait Spots, Freck." *Actas Dermosifiliogr.* 107 (6): 454–64.

Higham, Christine S., Eva Dombi, Aljosja Rogiers, Sucharita Bhaumik, Steven Pans, Steve E.J. Connor, Markku Miettinen, et al. 2018. "The Characteristics of 76 Atypical Neurofibromas as Precursors to Neurofibromatosis 1 Associated Malignant Peripheral Nerve Sheath Tumors." *Neuro-Oncology* 20 (6): 818–25. https://doi.org/10.1093/neuonc/noy013.

Hirata, Yasuko, Hilde Brems, Mayu Suzuki, Mitsuhiro Kanamori, Masahiro Okada, Rimpei Morita, Isabel Llano-Rivas, et al. 2016. "Interaction between a Domain of the Negative Regulator of the Ras-ERK Pathway, SPRED1 Protein, and the GTPase-Activating Protein-Related Domain of Neurofibromin Is Implicated in Legius Syndrome and Neurofibromatosis Type 1." *Journal of Biological Chemistry* 291 (7): 3124–34. https://doi.org/10.1074/jbc.M115.703710.

Hirose, Takanori, Takayuki Tani, Tetsuya Shimada, Keisuke Ishizawa, Shio Shimada, and Toshiaki Sano. 2003. "Immunohistochemical Demonstration of EMA/Glut1-Positive Perineurial Cells and CD34-Positive Fibroblastic Cells in Peripheral Nerve Sheath Tumors." *Modern Pathology* 16 (4): 293–98. https://doi.org/10.1097/01.MP.0000062654.83617.B7.

Hjerling-Leffler, Jens, Frédéric Marmigère, Mikael Heglind, Anna Cederberg, Martin Koltzenburg, Sven Enerbäck, and Patrik Ernfors. 2005. "The Boundary Cap: A Source of Neural Crest Stem Cells That Generate Multipe Sensory Neuron Subtypes." *Development* 132 (11): 2623–32. https://doi.org/10.1242/dev.01852.

Hockemeyer, Dirk, and Rudolf Jaenisch. 2016. "Induced Pluripotent Stem Cells Meet Genome Editing." *Cell Stem Cell* 18 (5): 573–86. https://doi.org/10.1016/j.stem.2016.04.013.

Hu, Bao Yang, Jason P. Weick, Junying Yu, Li Xiang Ma, Xiao Qing Zhang, James A. Thomson, and Su Chun Zhang. 2010. "Neural Differentiation of Human Induced Pluripotent Stem Cells Follows Developmental Principles but with Variable Potency." *Proceedings of the National Academy of Sciences of the United States of America* 107 (9): 4335–40. https://doi.org/10.1073/pnas.0910012107.

Huch, Meritxell, and Bon Kyoung Koo. 2015. "Modeling Mouse and Human Development Using Organoid Cultures." *Development (Cambridge)* 142 (18): 3113–25. https://doi.org/10.1242/dev.118570.

Huson, S. M., D. A. Compston, P Clark, and Peter S Harper. 1989. "A Genetic Study of von

Recklinghausen Neurofibromatosis in South East Wales. I. Prevalence, Fitness, Mutation Rate, and Effect of Parental Transmission on Severity." *J Med Genet* 26 (11): 704–11. https://doi.org/10.1136/jmg.26.11.704.

Jaakkola, S, M L Chu, and J Uitto. 1989. "Type 1 Neurofibromatosis : Selective Expression of Extracellular Matrix Genes by Schwann Cells , Perineurial Cells , and Fibroblasts in Mixed Cultures . Find the Latest Version :"

Jacks, Tyler, T Shane Shih, Earlene M Schmitt, Roderick T Bronson, Andre Bernards, and Robert A Weinberg. 1994. "Mutation in Nf1" 7 (july): 353–61.

Jacob, Claire. 2015. "Transcriptional Control of Neural Crest Specification into Peripheral Glia." *Glia* 63 (11): 1883–96. https://doi.org/10.1002/glia.22816.

Jacob, Claire, Pirmin Lötscher, Stefanie Engler, Arianna Baggiolini, Sandra Varum Tavares, Valérie Brügger, Nessy John, et al. 2014. "HDAC1 and HDAC2 Control the Specification of Neural Crest Cells into Peripheral Glia." *Journal of Neuroscience* 34 (17): 6112–22. https://doi.org/10.1523/JNEUROSCI.5212-13.2014.

Jessen, K R, R Mirsky, and A C Lloyd. 2015. "Schwann Cells: Development and Role in Nerve Repair." *Cold Spring Harb Perspect Biol* 7 (7): a020487. https://doi.org/10.1101/cshperspect.a020487.

Jessen, Kristjan R., and Rhona Mirsky. 2005. "The Origin and Development of Glial Cells in Peripheral Nerves." *Nature Reviews Neuroscience* 6 (9): 671–82. https://doi.org/10.1038/nrn1746.

Jessen, Kristjan R., and Rhona Mirsky. 2019. "Schwann Cell Precursors; Multipotent Glial Cells in Embryonic Nerves." *Frontiers in Molecular Neuroscience* 12 (March): 1–16. https://doi.org/10.3389/fnmol.2019.00069.

Joseph, N. M. 2004. "Neural Crest Stem Cells Undergo Multilineage Differentiation in Developing Peripheral Nerves to Generate Endoneurial Fibroblasts in Addition to Schwann Cells." *Development* 131 (22): 5599–5612. https://doi.org/10.1242/dev.01429.

Joseph, Nancy M., Jack T. Mosher, Johanna Buchstaller, Paige Snider, Paul E. McKeever, Megan Lim, Simon J. Conway, Luis F. Parada, Yuan Zhu, and Sean J. Morrison. 2008. "The Loss of Nf1 Transiently Promotes Self-Renewal but Not Tumorigenesis by Neural Crest Stem Cells." *Cancer Cell* 13 (2): 129–40. https://doi.org/10.1016/j.ccr.2008.01.003.

Kaiserling, E., and M.L. Geerts. 1986. "Tumour of Wagner-Meissner Touch Corpuscles Wagner-Meissner Neurilemmoma." *Pathol Anat* 409: 241–50.

Kallionpää, Roope A., Elina Uusitalo, Jussi Leppävirta, Minna Pöyhönen, Sirkku Peltonen, and Juha Peltonen. 2018. "Prevalence of Neurofibromatosis Type 1 in the Finnish Population." *Genetics in Medicine* 20 (9): 1082–86. https://doi.org/10.1038/gim.2017.215.

Kawaguchi, Jitsutaro, Jennifer Nichols, Mathias S Gierl, Tiago Faial, and Austin Smith. 2010. "Isolation and Propagation of Enteric Neural Crest Progenitor Cells from Mouse Embryonic Stem Cells and Embryos" 704: 693–704.

https://doi.org/10.1242/dev.046896.

Kim, H. A., T. Rosenbaum, M. A Marchionni, N. Ratner, and J E DeClue. 1995. “Schwann Cells from Neurofibromin Deficient Mice Exhibit Activation of P21ras, Inhibition of Cell Proliferation and Morphological Changes.” *Oncogene* 11 (2): 325–35.

Kim, H A, J E DeClue, and N Ratner. 1997. “CAMP-Dependent Protein Kinase A Is Required for Schwann Cell Growth: Interactions between the CAMP and Neuregulin/Tyrosine Kinase Pathways.” *J Neurosci Res* 49 (2): 236–47. https://doi.org/10.1002/(SICI)1097-4547(19970715)49:2<236::AID-JNR12>3.0.CO;2-Z [pii].

Kim, Han Seop, Jungwoon Lee, Da Yong Lee, Young Dae Kim, Jae Yun Kim, Hyung Jin Lim, Sungmin Lim, and Yee Sook Cho. 2017a. “Schwann Cell Precursors from Human Pluripotent Stem Cells as a Potential Therapeutic Target for Myelin Repair.” *Stem Cell Reports* 8 (6): 1714–26. https://doi.org/10.1016/j.stemcr.2017.04.011.

Kim, Jungsun, John P. Hoffman, R. Katherine Alpaugh, Andrew D. Rhimm, Maximilian Reichert, Ben Z. Stanger, Emma E. Furth, et al. 2013. “An IPSC Line from Human Pancreatic Ductal Adenocarcinoma Undergoes Early to Invasive Stages of Pancreatic Cancer Progression.” *Cell Reports* 3 (6): 2088–99. https://doi.org/10.1016/j.celrep.2013.05.036.

Kim, Jungsun, and Kenneth S Zaret. 2015. “Reprogramming of Human Cancer Cells to Pluripotency for Models of Cancer Progression.” *The EMBO Journal* 34 (6): 739–47. https://doi.org/10.15252/embj.201490736.

Kim, Sangtae, Konrad Scheffler, Aaron L. Halpern, Mitchell A. Bekritsky, Eunho Noh, Morten Källberg, Xiaoyu Chen, et al. 2018. “Strelka2: Fast and Accurate Calling of Germline and Somatic Variants.” *Nature Methods* 15 (8): 591–94. https://doi.org/10.1038/s41592-018-0051-x.

Kluwe, Lan, Reinhard Friedrich, and Victor F. Mautner. 1999. “Loss of NF1 Allele in Schwann Cells but Not in Fibroblasts Derived from an NF1-Associated Neurofibroma.” *Genes Chromosomes and Cancer* 24 (3): 283–85. https://doi.org/10.1002/(SICI)1098-2264(199903)24:3<283::AID-GCC15>3.0.CO;2-K.

Knudson, A. G. 1971. “Mutation and Cancer: Statistical Study of Retinoblastoma.” *Proceedings of the National Academy of Sciences* 68 (4): 820–23. https://doi.org/10.1073/pnas.68.4.820.

Koczkowska, Magdalena, Tom Callens, Yunjia Chen, Alicia Gomes, Alesha D. Hicks, Angela Sharp, Eric Johns, et al. 2020. “Clinical Spectrum of Individuals with Pathogenic NF1 Missense Variants Affecting p.Met1149, p.Arg1276, and p.Lys1423: Genotype–Phenotype Study in Neurofibromatosis Type 1.” *Human Mutation* 41 (1): 299–315. https://doi.org/10.1002/humu.23929.

Kotini, Andriana G., Chan Jung Chang, Arthur Chow, Han Yuan, Tzu Chieh Ho, Tiansu Wang, Shailee Vora, et al. 2017. “Stage-Specific Human Induced Pluripotent Stem Cells Map the Progression of Myeloid Transformation to Transplantable Leukemia.” *Cell Stem Cell* 20 (3): 315-328.e7. https://doi.org/10.1016/j.stem.2017.01.009.

Kraniak, Janice M., Anita Chalasani, Margaret R. Wallace, and Raymond R. Mattingly. 2018. “Development of 3D Culture Models of Plexiform Neurofibroma and Initial Application for Phenotypic Characterization and Drug Screening.” *Experimental Neurology* 299 (October 2017): 289–98. https://doi.org/10.1016/j.expneurol.2017.10.012.

Krone, W., S. Zörlein, and R. Mao. 1981. “Cell Culture Studies on Neurofibromatosis (von Recklinghausen). I. Comparative Growth Experiments with Fibroblasts at High and Low Concentrations of Fetal Calf Serum.” *Human Genetics* 58 (2): 188–93.

Lajtha, L.G. 1979. “Stem Cell Concepts.” *Differentiation1* 14 (1–2): 23–24. https://doi.org/10.1111/j.1432-0436.1979.tb01007.x.

Lammert, Marga, Jan M. Friedman, Lan Kluwe, and Victor F. Mautner. 2005. “Prevalence of Neurofibromatosis 1 in German Children at Elementary School Enrollment.” *Archives of Dermatology* 141 (1): 71–74.

Larribere, Lionel, Huizi Wu, Daniel Novak, Marta Galach, Mathias Bernhardt, Elias Orouji, Kasia Weina, et al. 2015. “NF1 Loss Induces Senescence during Human Melanocyte Differentiation in an IPSC-Based Model.” *Pigment Cell and Melanoma Research* 28 (4): 407–16. https://doi.org/10.1111/pcmr.12369.

Laura, Feltri M, Poitelon Yannick, and Previtali Stefano Carlo. 2016. “How Schwann Cells Sort Axons: New Concepts” 22 (3): 252–65. https://doi.org/10.1177/1073858415572361.How.

Le, Lu Q., Chiachi Liu, Tracey Shipman, Zhiguo Chen, Ueli Suter, and Luis F. Parada. 2011. “Susceptible Stages in Schwann Cells for NF1-Associated Plexiform Neurofibroma Development.” *Cancer Research* 71 (13): 4686–95. https://doi.org/10.1158/0008-5472.CAN-10-4577.

Le, Lu Q, Tracey Shipman, Dennis K Burns, and Luis F Parada. 2009. “Cell of Origin and Microenvironment Contribution for NF1- Associated Dermal Neurofibromas.” *Cell Stem Cell* 4 (5): 453–63. https://doi.org/10.1016/j.stem.2009.03.017.Cell.

Lee, Dung Fang, Jie Su, Huen Suk Kim, Betty Chang, Dmitri Papatsenko, Ruiying Zhao, Ye Yuan, et al. 2015. “Modeling Familial Cancer with Induced Pluripotent Stem Cells.” *Cell* 161 (2): 240–54. https://doi.org/10.1016/j.cell.2015.02.045.

Lee, Gabsang, Stuart M. Chambers, Mark J. Tomishima, and Lorenz Studer. 2010. “Derivation of Neural Crest Cells from Human Pluripotent Stem Cells.” *Nature Protocols* 5 (4): 688–701. https://doi.org/10.1038/nprot.2010.35.

Lee, Gabsang, Hyesoo Kim, Yechiel Elkabetz, George Al Shamy, Georgia Panagiotakos, Tiziano Barberi, Viviane Tabar, and Lorenz Studer. 2007. “Isolation and Directed Differentiation of Neural Crest Stem Cells Derived from Human Embryonic Stem Cells.” *Nature Biotechnology* 25 (12). https://doi.org/10.1038/nbt1365.

Lee, William, Sewit Teckie, Thomas Wiesner, Leili Ran, Carlos N. Prieto Granada, Mingyan Lin, Sinan Zhu, et al. 2014. “PRC2 Is Recurrently Inactivated through EED or SUZ12 Loss in Malignant Peripheral Nerve Sheath Tumors.” *Nature Genetics* 46 (11): 1227–32. https://doi.org/10.1038/ng.3095.

Leppig, Kathleen A., Paige Kaplan, David Viskochil, Molly Weaver, June Ortenberg, and Karen Stephens. 1997. “Familial Neurofibromatosis 1 Microdeletions: Cosegregation with Distinct Facial Phenotype and Early Onset of Cutaneous Neurofibromata.” *American Journal of Medical Genetics* 73 (2): 197–204. https://doi.org/10.1002/(SICI)1096-8628(1997)73:2<197::AID-AJMG17>3.0.CO;2-P.

Leung, Alan W., Alan W. Leung, Barbara Murdoch, Ahmed F. Salem, Maneeshi S. Prasad, Gustavo A. Gomez, and Martín I. García-Castro. 2016. “WNT/β-Catenin Signaling Mediates Human Neural Crest Induction via a Pre-Neural Border Intermediate.” *Development (Cambridge)* 143 (3): 398–410. https://doi.org/10.1242/dev.130849.

Li, Hua, Lung-Ji Chang, Debbie R Neubauer, David F Muir, and Margaret R Wallace. 2016a. “Immortalization of Human Normal and NF1 Neurofibroma Schwann Cells.” *Laboratory Investigation; a Journal of Technical Methods and Pathology* 96 (10): 1105–15. https://doi.org/10.1038/labinvest.2016.88.

Li, Ying, Peter O’connell, Heidi Huntsman Breidenbach, Richard Cawthon, Jeff Stevens, Gangfeng Xu, Shannon Neil, Margaret Robertson, Ray White, and David Viskochil. 1995. “Genomic Organization of the Neurofibromatosis 1 Gene (NF1).” *Genomics* 25 (1): 9–18. https://doi.org/10.1016/0888-7543(95)80104-T.

Liao, Chung-Ping, Sanjay Pradhan, Zhiguo Chen, Amish J. Patel, Reid C. Booker, and Lu Q. Le. 2016. “The Role of Nerve Microenvironment for Neurofibroma Development.” *Oncotarget* 7 (38): 61500–508. https://doi.org/10.18632/oncotarget.11133.

Ling, Benjamin C., Jianqiang Wu, Shyra J. Miller, Kelly R. Monk, Rania Shamekh, Tilat A. Rizvi, Gabrielle Decourten-Myers, Kristine S. Vogel, Jeffrey E. Declue, and Nancy Ratner. 2005. “Role for the Epidermal Growth Factor Receptor in Neurofibromatosis-Related Peripheral Nerve Tumorigenesis.” *Cancer Cell* 7 (1): 65–75. https://doi.org/10.1016/j.ccr.2004.10.016.

Liu, Qiuyue, Steven C. Spusta, Ruifa Mi, Rhonda N.T. Lassiter, Michael R. Stark, Ahmet Höke, Mahendra S. Rao, and Xianmin Zeng. 2012. “Human Neural Crest Stem Cells Derived from Human ESCs and Induced Pluripotent Stem Cells: Induction, Maintenance, and Differentiation into Functional Schwann Cells.” *STEM CELLS Translational Medicine* 1 (4): 266–78. https://doi.org/10.5966/sctm.2011-0042.

Loo, Peter Van, Silje H. Nordgard, Ole Christian Lingjærde, Hege G. Russnes, Inga H. Rye, Wei Sun, Victor J. Weigman, et al. 2010. “Allele-Specific Copy Number Analysis of Tumors.” *Proceedings of the National Academy of Sciences of the United States of America* 107 (39): 16910–15. https://doi.org/10.1073/pnas.1009843107.

Love, Michael I., Wolfgang Huber, and Simon Anders. 2014. “Moderated Estimation of Fold Change and Dispersion for RNA-Seq Data with DESeq2.” *Genome Biology* 15 (12): 1–21. https://doi.org/10.1186/s13059-014-0550-8.

Ma, Ming-san, Erik Boddeke, and Sjef Copray. 2015. “Pluripotent Stem Cells for Schwann Cell Engineering,” no. November 2014: 205–18. https://doi.org/10.1007/s12015-014-9577-1.

Ma, Zhenzhong. 2011. “Axogial Communication Mediated by Soluble Neuregulin-1 and Bdnf.”

Maertens, O., H. Brems, J. Vandesompele, T. De Raedt, I. Heyns, T. Rosenbaum, S. De Schepper, et al. 2006. “Comprehensive NF1 Screening on Cultured Schwann Cells from Neurofibromas.” *Human Mutation* 27 (10): 1030–40. https://doi.org/10.1002/humu.20389.

Malhotra, Ritu, and Nancy Ratner. 1994. “Localization of Neurofibromin to Keratinocytes and Melanocytes in Developing Rat and Human Skin.” *Journal of Investigative Dermatology* 102 (5): 812–18. https://doi.org/10.1111/1523-1747.ep12379925.

Marchetto, Maria C.N., Gene W. Yeo, Osamu Kainohana, Martin Marsala, Fred H. Gage, and Alysson R. Muotri. 2009. “Transcriptional Signature and Memory Retention of Human-Induced Pluripotent Stem Cells.” *PLoS ONE* 4 (9). https://doi.org/10.1371/journal.pone.0007076.

Marol, Géraldine S., Matthieu Vermeren, Octavian Voiculescu, Lisa Melton, James Cohen, Patrick Charnay, and Piotr Topilko. 2004. “Neural Crest Boundary Cap Cells Constitute a Source of Neuronal and Glial Cells of the PNS.” *Nature Neuroscience* 7 (9): 930–38. https://doi.org/10.1038/nn1299.

Martin, George A., David Viskoohil, Gideon Bollag, Peter C. McCabe, Walter J. Crosier, Heinz Haubruck, Leah Conroy, et al. 1990. “The GAP-Related Domain of the Neurofibromatosis Type 1 Gene Product Interacts with Ras P21.” *Cell* 63 (4): 843–49. https://doi.org/10.1016/0092-8674(90)90150-D.

Mayor, R., and E. Theveneau. 2013. “The Neural Crest.” *Development* 140 (11): 2247–51. https://doi.org/10.1242/dev.091751.

McKenna, A., M. Hanna, E. Banks, A. Sivachenko, K. Cibulskis, A. Kernytsky, K. Garimella, et al. 2010. “The Genome Analysis Toolkit: A MapReduce Framework for Analyzing next-Generation DNA Sequencing Data.” *Genome Research* 20: 1297–1303. https://doi.org/10.1101/gr.107524.110.20.

Menendez, Laura, Michael J Kulik, Austin T Page, Sarah S Park, James D Lauderdale, Michael L Cunningham, and Stephen Dalton. 2013. “Directed Differentiation of Human Pluripotent Cells to Neural Crest Stem Cells.” *Nature Protocols* 8 (1): 203–12. https://doi.org/10.1038/nprot.2012.156.

Menendez, Laura, Tatiana A. Yatskievych, Parker B. Antin, and Stephen Dalton. 2011. “Wnt Signaling and a Smad Pathway Blockade Direct the Differentiation of Human Pluripotent Stem Cells to Multipotent Neural Crest Cells (Proceedings of the National Academy of Sciences (2011) 108, 48 (19240-19245) DOI: 10.1073/Pnas.1113746108).” *Proceedings of the National Academy of Sciences of the United States of America* 109 (23): 9220. https://doi.org/10.1073/pnas.1207810109.

Messiaen, L. M. 2020. “Molecular Diagnosis for NF1.” In *Multidisciplinary Approach to Neurofibromatosis Type 1*, edited by G. Tadini, E. Legius, and H. Brems, 15–34. Springe Nature Switzerland. https://doi.org/https://doi.org/10.1007/978-3-319-92450-2_3.

Messiaen, L. M., and K. Wimmer. 2008. “NF1 Mutational Spectrum.” *Monographs in Human Genetics* 16 (i): 63–77. https://doi.org/10.1159/000126545.

Messiaen, Ludwine M., Tom Callens, Geert Mortier, Diane Beysen, Ina Vandenbroucke, Nadine Van Roy, Frank Speleman, and Anne De Paepe. 2000. “Exhaustive Mutation Analysis of the NF1 Gene Allows Identification of 95% of Mutations and Reveals a High Frequency of Unusual Splicing Defects.” *Human Mutation* 15 (6): 541–55. https://doi.org/10.1002/1098-1004(200006)15:6<541::AID-HUMU6>3.0.CO;2-N.

Mica, Yvonne, Gabsang Lee, Stuart M. Chambers, Mark J. Tomishima, and Lorenz Studer. 2013a. “Modeling Neural Crest Induction, Melanocyte Specification, and Disease-Related Pigmentation Defects in HESCs and Patient-Specific IPSCs.” *Cell Reports* 3 (4): 1140–52. https://doi.org/10.1016/j.celrep.2013.03.025.

Michailov, Galin V, Michael W Sereda, Bastian G Brinkmann, Tobias M Fischer, Bernhard Haug, Carmen Birchmeier, Lorna Role, Cary Lai, and Markus H Schwab. 2004. “Axonal Neuregulin-1 Regulates Myelin Sheath Thickness” 304 (April): 700–704.

Miettinen, Markku M., Cristina R. Antonescu, Christopher D.M. Fletcher, Aerang Kim, Alexander J. Lazar, Martha M. Quezado, Karlyne M. Reilly, et al. 2017. “Histopathologic Evaluation of Atypical Neurofibromatous Tumors and Their Transformation into Malignant Peripheral Nerve Sheath Tumor in Patients with Neurofibromatosis 1—a Consensus Overview.” *Human Pathology* 67 (October 2016): 1–10. https://doi.org/10.1016/j.humpath.2017.05.010.

Miller, Shyra J., Walter J. Jessen, Japan Mehta, Atira Hardiman, Emily Sites, Sergio Kaiser, Anil G. Jegga, et al. 2009. “Integrative Genomic Analyses of Neurofibromatosis Tumours Identify SOX9 as a Biomarker and Survival Gene.” *EMBO Molecular Medicine* 1 (4): 236–48. https://doi.org/10.1002/emmm.200900027.

Mogha, Amit, Andrew E. Benesh, Chinmoy Patra, Felix B. Engel, Torsten Schöneberg, Ines Liebscher, and Kelly R. Monk. 2013. “Gpr126 Functions in Schwann Cells to Control Differentiation and Myelination via G-Protein Activation.” *Journal of Neuroscience* 33 (46): 17976–85. https://doi.org/10.1523/JNEUROSCI.1809-13.2013.

Monk, K. R., M. L. Feltri, and C. Taveggia. 2015. “New Insights on Schwann Cell Development.” *Glia* 63 (8): 1376–93. https://doi.org/10.1002/glia.22852.

Monk, Kelly R, Stephen G Naylor, Thomas D Glenn, Sara Mercurio, Julie R Perlin, Claudia Dominguez, Cecilia B Moens, and William S Talbot. 2009. “A G Protein-Coupled Receptor Is Essential for Schwann Cells to Initiate Myelination” 325 (5946): 1402–5. https://doi.org/10.1126/science.1173474.A.

Moreno-Cabrera, José Marcos, Jesús del Valle, Elisabeth Castellanos, Lidia Feliubadaló, Marta Pineda, Joan Brunet, Eduard Serra, Gabriel Capellà, Conxi Lázaro, and Bernat Gel. 2020. “Evaluation of CNV Detection Tools for NGS Panel Data in Genetic Diagnostics.” *European Journal of Human Genetics*. https://doi.org/10.1038/s41431-020-0675-z.

Morrison, Sean J., Patricia M. White, Christiane Zock, and David J. Anderson. 1999. “Prospective Identification, Isolation by Flow Cytometry, and in Vivo Self-Renewal of Multipotent Mammalian Neural Crest Stem Cells.” *Cell* 96 (5): 737–49. https://doi.org/10.1016/S0092-8674(00)80583-8.

Motohashi, T., H. Aoki, K. Chiba, N. Yoshimura, and T. Kunisada. 2007. “Multipotent Cell

Fate of Neural Crest-Like Cells Derived From." *Stem Cells* 25: 402–10. https://doi.org/10.1634/stemcells.2006-0323.

Muir, David, Debbie Neubauer, Ingrid T. Lim, Anthony T. Yachnis, and Margaret R. Wallace. 2001. "Tumorigenic Properties of Neurofibromin-Deficient Neurofibroma Schwann Cells." *American Journal of Pathology* 158 (2): 501–13. https://doi.org/10.1016/S0002-9440(10)63992-2.

Niederländer, Christiane, and Andrew Lumsden. 1996. "Late Emigrating Neural Crest Cells Migrate Specifically to the Exit Points of Cranial Branchiomotor Nerves." *Development* 122 (8): 2367–74.

Nishi, T., PSY. Lee, K. Oka, VA. Levin, S. Tanase, Y. Morino, and H. Saya. 1991. "Differential Expression of Two Types of the Neurofibromatosis Type 1 (NF1) Gene Transcripts Related to Neuronal Differentiation." *Oncogene* 6 (9): 1555–59.

Ortonne, Nicolas, Pierre Wolkenstein, Jaishri O. Blakeley, Bruce Korf, Scott R. Plotkin, Vincent M. Riccardi, Douglas C. Miller, et al. 2018a. "Cutaneous Neurofibromas: Current Clinical and Pathologic Issues." *Neurology* 91 (2): S5–13. https://doi.org/10.1212/WNL.0000000000005792.

Paavola, Kevin J., Harwin Sidik, J. Bradley Zuchero, Michael Eckart, and William S. Talbot. 2014. "Type IV Collagen Is an Activating Ligand for the Adhesion G Protein-Coupled Receptor GPR126." *Science Signaling* 7 (338): 1–10. https://doi.org/10.1126/scisignal.2005347.

Pan, Xiu Yang, Ming Ho Tsai, Kenly Wuputra, Chia Chen Ku, Wen Hsin Lin, Ying Chu Lin, Shotaro Kishikawa, et al. 2017. "Application of Cancer Cell Reprogramming Technology to Human Cancer Research." *Anticancer Research* 37 (7): 3367–77. https://doi.org/10.21873/anticanreS.11703.

Papapetrou, Eirini P. 2016. "Patient-Derived Induced Pluripotent Stem Cells in Cancer Research and Precision Oncology." *Nature Medicine* 22 (12): 1392–1401. https://doi.org/10.1038/nm.4238.

Papapetrou, Eirini P. 2019. "Modeling Leukemia with Human Induced Pluripotent Stem Cells." *Cold Spring Harbor Perspectives in Medicine* 9 (12): 1–20. https://doi.org/10.1101/cshperspect.a034868.

Patro, Rob, Geet Duggal, Michael I. Love, Rafael A. Irizarry, and Carl Kingsford. 2017. "Salmon Provides Fast and Bias-Aware Quantification of Transcript Expression." *Nature Methods* 14 (4): 417–19. https://doi.org/10.1038/nmeth.4197.

Patthey, Cédric, Thomas Edlund, and Lena Gunhaga. 2009. "Wnt-Regulated Temporal Control of BMP Exposure Directs the Choice between Neural Plate Border and Epidermal Fate." *Development* 136 (1): 73–83. https://doi.org/10.1242/dev.025890.

Peltonen, J., T. Marttala, T. Vihersaari, S. Renvall, and R. Penttinen. 1981. "Collagen Synthesis in Cells Cultured from v. Recklinghausen's Neurofibromatosis." *Acta Neuropathologica* 55 (3): 183–87. https://doi.org/10.1007/BF00691316.

Peltonen, J., R Penttinen, H. Larjava, and H. Aho. 1986. "Collagens in Neurofibromas and Neurofibroma Cell Cultures." *Annals of the New York Academy of Sciences* 486 (1):

260–70. https://doi.org/10.1111/j.1749-6632.1986.tb48079.x.

Pemov, A., N. F. Hansen, S. Sindiri, R. Patidar, C. S. Higham, E. Dombi, M. M. Miettinen, et al. 2019. "Low Mutation Burden and Frequent Loss of CDKN2A/B and SMARCA2, but Not PRC2, Define Pre-Malignant Neurofibromatosis Type 1-Associated Atypical Neurofibromas." *Neuro-Oncology* 21 (8): 981–92.

Pennanen, Paula, Sirkku Peltonen, Roope A. Kallionpää, and Juha Peltonen. 2018. "The Effect of Estradiol, Testosterone, and Human Chorionic Gonadotropin on the Proliferation of Schwann Cells with NF1+/−or NF1−/−genotype Derived from Human Cutaneous Neurofibromas." *Molecular and Cellular Biochemistry* 444 (1–2): 27–33. https://doi.org/10.1007/s11010-017-3227-2.

Perrin, G., L. Fishbein, S.A. Thomson, S. T. Thomas, K. Stephens, J. Y. Garbern, G. H. DeVries, A. T. Yachnis, M. R. Wallace, and D. Muir. 2007. "Plexiform-Like Neurofibromas Develop in the Mouse by Intraneural Xenograft of an NF1 Tumor-Derived Schwann Cell Line." *Journal of Neuroscience Research* 85 (April): 1347–57. https://doi.org/10.1002/jnr.

Petersen, Sarah C., Rong Luo, Ines Liebscher, Stefanie Giera, Sung Jin Jeong, Amit Mogha, Monica Ghidinelli, et al. 2015. "The Adhesion GPCR GPR126 Has Distinct, Domain-Dependent Functions in Schwann Cell Development Mediated by Interaction with Laminin-211." *Neuron* 85 (4): 755–69. https://doi.org/10.1016/j.neuron.2014.12.057.

Pomp, Oz, Irina Brokhman, Israel Ben-Dor, Benjamin Reubinoff, and Ronald S. Goldstein. 2005. "Generation of Peripheral Sensory and Sympathetic Neurons and Neural Crest Cells from Human Embryonic Stem Cells." *Stem Cells* 23 (7): 923–30. https://doi.org/10.1634/stemcells.2005-0038.

Poyhonent, M., S. Kytola, and J. Leisti. 2000. "Epidemiology of Neurofibromatosis Type 1 (NF1) in Northern Finland." *Journal of Medical Genetics* 37 (8): 632–36. https://doi.org/10.1136/jmg.37.8.632.

Prada, Carlos E., Edwin Jousma, Tilat A. Rizvi, Jianqiang Wu, R. Scott Dunn, Debra A. Mayes, Jose A. Cancelas, et al. 2013. "Neurofibroma-Associated Macrophages Play Roles in Tumor Growth and Response to Pharmacological Inhibition." *Acta Neuropathologica* 125 (1): 159–68. https://doi.org/10.1007/s00401-012-1056-7.

Pummi, Kati P., Heikki J. Aho, Matti K. Laato, Juha T K Peltonen, and Sirkku A. Peltonen. 2006. "Tight Junction Proteins and Perineurial Cells in Neurofibromas." *Journal of Histochemistry and Cytochemistry* 54 (1): 53–61. https://doi.org/10.1369/jhc.5A6671.2005.

Radomska, K. J., and P. Topilko. 2017. "Boundary Cap Cells in Development and Disease." *Current Opinion in Neurology* 47: 209–15.

Radomska, Katarzyna J., Fanny Coulpier, Aurelie Gresset, Alain Schmitt, Amal Debbiche, Sophie Lemoine, Pierre Wolkenstein, Jean Michel Vallat, Patrick Charnay, and Piotr Topilko. 2019. "Cellular Origin, Tumor Progression, and Pathogenic Mechanisms of Cutaneous Neurofibromas Revealed by Mice with Nf1 Knockout in Boundary Cap Cells." *Cancer Discovery* 9 (1): 130–47. https://doi.org/10.1158/2159-8290.CD-18-

0156.

Raedt, T. De, H. Brems, P. Wolkenstein, D. Vidaud, S. Pilotti, F. Perrone, V. Mautner, S. Frahm, R. Sciot, and Eric Legius. 2003. “Elevated Risk for MPNST in NF1 Microdeletion Patients.” *American Journal of Human Genetics* 72 (5): 1288–92. https://doi.org/10.1086/374821.

Raedt, T. De, O. Maertens, E. Serra, and E. Legius. 2008. “Somatic NF1 Mutations in Tumors and Other Tissues.” In *Neurofibromatoses*, 146–53. https://doi.org/https://doi.org/10.1159/000126580.

Rasi, Karolina, Merja Hurskainen, Mika Kallio, Saara Stavén, Raija Sormunen, Anthony M. Heape, Robin L. Avila, et al. 2010. “Lack of Collagen XV Impairs Peripheral Nerve Maturation and, When Combined with Laminin-411 Deficiency, Leads to Basement Membrane Abnormalities and Sensorimotor Dysfunction.” *Journal of Neuroscience* 30 (43): 14490–501. https://doi.org/10.1523/JNEUROSCI.2644-10.2010.

Rathjen, Joy, Bryan P Haines, Kathryn M Hudson, Antonietta Nesci, Stephanie Dunn, and Peter D Rathjen. 2002. “Directed Differentiation of Pluripotent Cells to Neural Lineages : Homogeneous Formation and Differentiation of a Neurectoderm Population” 2661: 2649–61.

Raya, Ángel, Ignasi Rodríguez-Piz, Guillermo Guenechea, Rita Vassena, Susana Navarro, María José Barrero, Antonella Consiglio, et al. 2009. “Disease-Corrected Haematopoietic Progenitors from Fanconi Anaemia Induced Pluripotent Stem Cells.” *Nature* 460 (7251): 53–59. https://doi.org/10.1038/nature08129.

Richard, Laurence, Piotr Topilko, Laurent Magy, Anne-Valérie Decouvelaere, Patrick Charnay, Beno\^\it Funalot, and Jean-Michel Vallat. 2012. “Endoneurial Fibroblast-like Cells.” *Journal of Neuropathology and Experimental Neurology* 71 (11): 938–47.

Rosenbaum, Thorsten, Claudia Rosenbaum, Ursula Winner, Hans Werner Müller, Hans Gerd Lenard, and C. Oliver Hanemann. 2000. “Long-Term Culture and Characterization of Human Neurofibroma-Derived Schwann Cells.” *Journal of Neuroscience Research* 61 (5): 524–32. https://doi.org/10.1002/1097-4547(20000901)61:5<524::AID-JNR7>3.0.CO;2-Z.

Rowe, R. Grant, and George Q. Daley. 2019. “Induced Pluripotent Stem Cells in Disease Modelling and Drug Discovery.” *Nature Reviews Genetics* 20 (7): 377–88. https://doi.org/10.1038/s41576-019-0100-z.

Roy, Vincent, Brice Magne, Maude Vaillancourt-audet, Mathieu Blais, Stéphane Chabaud, Emil Grammond, Léo Piquet, et al. 2020. “Review Article Human Organ-Specific 3D Cancer Models Produced by the Stromal Self-Assembly Method of Tissue Engineering for the Study of Solid Tumors” 2020.

Ruiz, S., A. Panopoulos, A. Herrerías, K. Bissig, M. Lutz, W. T. Berggren, Inder M. Verma, and J. C. Izpisua-Belmonte. 2011. “A High Proliferation Rate Is Required for Cell Reprogramming and Maintenance of Human Embryonic Stem Cell Identity.” *Current Biology* 21 (1): 45–52. https://doi.org/10.1016/j.cub.2010.11.049.A.

Salzer, James L. 2015. “Schwann Cell Myelination.” *Cold Spring Harbor Perspectives in*

Biology 7 (8). https://doi.org/10.1101/cshperspect.a020529.

Saraiva, Diana P., Ana T. Matias, Sofia Braga, António Jacinto, and M. Guadalupe Cabral. 2020. "Establishment of a 3D Co-Culture With MDA-MB-231 Breast Cancer Cell Line and Patient-Derived Immune Cells for Application in the Development of Immunotherapies." *Frontiers in Oncology* 10 (August): 1–13. https://doi.org/10.3389/fonc.2020.01543.

Sauka-Spengler, Tatjana, and Marianne Bronner-Fraser. 2008. "A Gene Regulatory Network Orchestrates Neural Crest Formation." *Nature Reviews Molecular Cell Biology* 9 (7): 557–68. https://doi.org/10.1038/nrm2428.

Schepper, Sofie De, Ophélia Maertens, Tom Callens, Jean Marie Naeyaert, Jo Lambert, and Ludwine Messiaen. 2008. "Somatic Mutation Analysis in NF1 Café Au Lait Spots Reveals Two NF1 Hits in the Melanocytes." *Journal of Investigative Dermatology* 128 (4): 1050–53. https://doi.org/10.1038/sj.jid.5701095.

Serra, E., E. Ars, A. Ravella, A. Sanchez, S. Puig, T. Rosenbaum, X. Estivill, and C. Lázaro. 2001. "Somatic NF1 Mutational Spectrum in Benign Neurofibromas: MRNA Splice Defects Are Common among Point Mutations." *Human Genetics* 108 (5): 416–29.

Serra, E., B. Gel, J. Fernández-Rodríguez, and C. Lázaro. 2020. "Genomics of Peripheral Nerve Sheath Tumors Associated with Neurofibromatosis Type 1." In *Multidisciplinary Approach to Neurofibromatosis Type 1*, 117–47.

Serra, E., S. Puig, D. Otero, A. Gaona, H. Kruyer, E. Ars, X. Estivill, and C. Lázaro. 1997. "Confirmation of a Double-Hit Model for the NF1 Gene in Benign Neurofibromas." *The American Journal of Human Genetics* 63 (3): 512–19.

Serra, E, T Rosenbaum, U Winner, R Aledo, E Ars, X Estivill, H G Lenard, and C Lázaro. 2000. "Schwann Cells Harbor the Somatic NF1 Mutation in Neurofibromas: Evidence of Two Different Schwann Cell Subpopulations." *Human Molecular Genetics* 9 (20): 3055–64. https://doi.org/10.1093/HMG/9.20.3055.

Shakiba, Nika, Ahmed Fahmy, Gowtham Jayakumaran, Sophie McGibbon, Laurent David, Daniel Trcka, Judith Elbaz, et al. 2019. "Cell Competition during Reprogramming Gives Rise to Dominant Clones." *Science* 364 (6438). https://doi.org/10.1126/science.aan0925.

Shen, Ming Hong, Peter S Harper, and Meena Upadhyaya. 1996. "Review Article Molecular Genetics of Neurofibromatosis (NFl)." *Molecular Biology* 6: 2–17.

Sherman, Diane L., and Peter J. Brophy. 2005. "Mechanisms of Axon Ensheathment and Myelin Growth." *Nature Reviews Neuroscience* 6 (9): 683–90. https://doi.org/10.1038/nrn1743.

Simões-Costa, Marcos, and Marianne E. Bronner. 2015. "Establishing Neural Crest Identity: A Gene Regulatory Recipe." *Development (Cambridge, England)* 142 (2): 242–57. https://doi.org/10.1242/dev.105445.

Soldatov, Ruslan, Marketa Kaucka, Maria Eleni Kastriti, Julian Petersen, Tatiana Chontorotzea, Lukas Englmaier, Natalia Akkuratova, et al. 2019. "Spatiotemporal Structure of Cell Fate Decisions in Murine Neural Crest." *Science* 364.

https://doi.org/10.1126/science.aas9536.

Soyombo, Abigail A., Yipin Wu, Lauren Kolski, Jonathan J. Rios, Dinesh Rakheja, Alice Chen, James Kehler, Heather Hampel, Alanna Coughran, and Theodora S. Ross. 2013. "Analysis of Induced Pluripotent Stem Cells from a BRCA1 Mutant Family." *Stem Cell Reports* 1 (4): 336–49. https://doi.org/10.1016/j.stemcr.2013.08.004.

Stemple, Derek L, and David J Anderson. 1992. "Isolation of a Stem Cell for Neurons and Glia from the Mammalian Neural Crest" 71: 973–85. internal-pdf://161.171.206.56/0642657550et al. Cell(1992).pdf.

Stevenson, David A., Holly Zhou, Shadi Ashrafi, Ludwine M. Messiaen, John C. Carey, Jacques L. D'Astous, Stephen D. Santora, and David H. Viskochil. 2006. "Double Inactivation of NF1 in Tibial Pseudarthrosis." *American Journal of Human Genetics* 79 (1): 143–48. https://doi.org/10.1086/504441.

Tabar, Viviane, and Lorenz Studer. 2014. "Pluripotent Stem Cells in Regenerative Medicine: Challenges and Recent Progress." *Nature Reviews Genetics* 15 (2): 82–92. https://doi.org/10.1038/nrg3563.

Takahashi, Kazutoshi, and Shinya Yamanaka. 2006. "Induction of Pluripotent Stem Cells from Mouse Embryonic and Adult Fibroblast Cultures by Defined Factors." *Cell* 126 (4): 663–76. https://doi.org/10.1016/j.cell.2006.07.024.

Taveggia, Carla, George Zanazzi, Ashley Petrylak, Hiroko Yano, Jack Rosenbluth, Steven Einheber, Xiaorong Xu, et al. 2005. "Neuregulin-1 Type III Determines the Ensheathment Fate of Axons." *Neuron* 47 (5): 681–94. https://doi.org/10.1016/j.neuron.2005.08.017.

Tchieu, Jason, Bastian Zimmer, Faranak Fattahi, Sadaf Amin, Nadja Zeltner, Shuibing Chen, and Lorenz Studer. 2017. "A Modular Platform for Differentiation of Human PSCs into All Major Ectodermal Lineages." *Cell Stem Cell* 21 (3): 399-410.e7. https://doi.org/10.1016/j.stem.2017.08.015.

Terribas, Ernest, Carles Garcia-Linares, Conxi Lázaro, and Eduard Serra. 2013. "Probe-Based Quantitative PCR Assay for Detecting Constitutional and Somatic Deletions in the NF1 Gene: Application to Genetic Testing and Tumor Analysis." *Clinical Chemistry* 59 (6): 928–37. https://doi.org/10.1373/clinchem.2012.194217.

Theveneau, Eric, and Roberto Mayor. 2012. "Neural Crest Delamination and Migration: From Epithelium-to-Mesenchyme Transition to Collective Cell Migration." *Developmental Biology* 366 (1): 34–54. https://doi.org/10.1016/j.ydbio.2011.12.041.

Thomson, James A. 1998. "Embryonic Stem Cell Lines Derived from Human Blastocysts." *Science* 282 (5391): 1145–47. https://doi.org/10.1126/science.282.5391.1145.

Tong, Jiayuan, Frances Hannan, Yinghua Zhu, and Yi Zhong. 2002. "Neurofibromin Regulates G Protein – Stimulated Adenylyl Cyclase Activity." *Nature Neuroscience* 5 (2): 95–96. https://doi.org/10.1038/792.

Topilko, Piotr, Sylvie Schneider-Maunoury, Giovanni Levi, Anne Baron-Van Evercooren, Amina Ben Younes Chennoufi, Tania Seitanidou, Charles Babinet, and Patrick

Charnay. 1994. “Krox-20 Controls Myelination in the Peripheral Nervous System.” *Nature*. https://doi.org/10.1038/371796a0.

Upadhyaya, Meena, and David N. Cooper. 2012. *Neurofibromatosis Type 1 Molecular and Cellular Biology*.

Utikal, Jochen, Jose M. Polo, Matthias Stadtfeld, Nimet Maherali, Warakorn Kulalert, Ryan M. Walsh, Adam Khalil, James G. Rheinwald, and Konrad Hochedlinger. 2009. “Immortalization Eliminates a Roadblock during Cellular Reprogramming into IPS Cells.” *Nature* 460 (7259): 1145–48. https://doi.org/10.1038/nature08285.

Uusitalo, Elina, Jussi Leppävirta, Anna Koffert, Sakari Suominen, Jussi Vahtera, Tero Vahlberg, Minna Pöyhönen, Juha Peltonen, and Sirkku Peltonen. 2015. “Incidence and Mortality of Neurofibromatosis: A Total Population Study in Finland.” *Journal of Investigative Dermatology* 135 (3): 904–6. https://doi.org/10.1038/jid.2014.465.

Uusitalo, Elina, Matti Rantanen, Roope A. Kallionpää, Minna Pöyhönen, Jussi Leppävirta, Heli Ylä-Outinen, Vincent M. Riccardi, et al. 2016. “Distinctive Cancer Associations in Patients with Neurofibromatosis Type 1.” *Journal of Clinical Oncology* 34 (17): 1978–86. https://doi.org/10.1200/JCO.2015.65.3576.

Vaskova, E. A., A. E. Stekleneva, S. P. Medvedev, and S. M. Zakian. 2013. “‘Epigenetic Memory’ Phenomenon in Induced Pluripotent Stem Cells.” *Acta Naturae* 5 (19): 15–21. https://doi.org/10.32607/20758251-2013-5-4-15-21.

Walker, James A, and Meena Upadhyaya. 2018. “Expert Opinion on Therapeutic Targets Emerging Therapeutic Targets for Neurofibromatosis Type 1.” *Expert Opinion on Therapeutic Targets* 22 (5): 419–37. https://doi.org/10.1080/14728222.2018.1465931.

Wallace, Margaret R, Douglas A Marchuk, Lone B Andersen, Roxanne Letcher, Hana M Odeh, A N N M Saulino, Jane W Fountain, et al. 1990. “Type 1 Neurofibromatosis Gene : Identification of a Large Transcript Disrupted in Three NF1 Patients” 345 (July).

Wang, Aijun, Zhenyu Tang, In-hyun Park, Yiqian Zhu, Shyam Patel, and George Q Daley. 2011. “Biomaterials Induced Pluripotent Stem Cells for Neural Tissue Engineering” 32. https://doi.org/10.1016/j.biomaterials.2011.03.070.

Wang, Kai, Mingyao Li, and Hakon Hakonarson. 2010. “ANNOVAR: Functional Annotation of Genetic Variants from High-Throughput Sequencing Data.” *Nucleic Acids Research* 38 (16): 1–7. https://doi.org/10.1093/nar/gkq603.

Wegscheid, Michelle L., Corina Anastasaki, and David H. Gutmann. 2018. “Human Stem Cell Modeling in Neurofibromatosis Type 1 (NF1).” *Experimental Neurology* 299: 270–80. https://doi.org/10.1016/j.expneurol.2017.04.001.

Weydert, Zoe, Madhu Lal-Nag, Lesley Mathews-Greiner, Christoph Thiel, Henrik Cordes, Lars Küpfer, Patrick Guye, Jens M. Kelm, and Marc Ferrer. 2020. “A 3D Heterotypic Multicellular Tumor Spheroid Assay Platform to Discriminate Drug Effects on Stroma versus Cancer Cells.” *SLAS Discovery* 25 (3): 265–76. https://doi.org/10.1177/2472555219880194.

Wu, Jianqiang, Jon P. Williams, Tilat A. Rizvi, Jennifer J. Kordich, David Witte, Dies Meijer, Anat O. Stemmer-Rachamimov, Jose A. Cancelas, and Nancy Ratner. 2008. "Plexiform and Dermal Neurofibromas and Pigmentation Are Caused by Nf1 Loss in Desert Hedgehog-Expressing Cells." *Cancer Cell* 13 (2): 105–16. https://doi.org/10.1016/j.ccr.2007.12.027.

Yamanaka, Shinya. 2009. "Elite and Stochastic Models for Induced Pluripotent Stem Cell Generation." *Nature* 460 (7251): 49–52. https://doi.org/10.1038/nature08180.

Yang, Feng-chun, David A Ingram, Shi Chen, Cynthia M Hingtgen, Nancy Ratner, Kelly R Monk, Travis Clegg, et al. 2003. "Cells Secrete a Potent Migratory Stimulus for Nf1 + /– Mast Cells." *Journal of Clinical Investigation* 112 (12): 1851–61. https://doi.org/10.1172/JCI200319195.Received.

York, Joshua R., and David W. McCauley. 2020. "The Origin and Evolution of Vertebrate Neural Crest Cells." *Open Biology* 10 (1). https://doi.org/10.1098/rsob.190285.

Yu, Guangchuang, Li Gen Wang, Yanyan Han, and Qing Yu He. 2012. "ClusterProfiler: An R Package for Comparing Biological Themes among Gene Clusters." *OMICS A Journal of Integrative Biology* 16 (5): 284–87. https://doi.org/10.1089/omi.2011.0118.

Zheng, Huarui, Lou Chang, Neha Patel, Jiong Yang, Lori Lowe, Dennis K. Burns, and Yuan Zhu. 2008. "Induction of Abnormal Proliferation by Nonmyelinating Schwann Cells Triggers Neurofibroma Formation." *Cancer Cell* 13 (2): 117–28. https://doi.org/10.1016/j.ccr.2008.01.002.

Zhou, Yan, and Malcolm L Snead. 2008. "Derivation of Cranial Neural Crest-like Cells from Human Embryonic Stem Cells." *Biochemical and Biophysical Research Communications* 376: 542–47. https://doi.org/10.1016/j.bbrc.2008.09.032.

Zhu, Dandan, Celine Shuet Lin Kong, Julian A. Gingold, Ruiying Zhao, and Dung Fang Lee. 2018. "Induced Pluripotent Stem Cells and Induced Pluripotent Cancer Cells in Cancer Disease Modeling." *Advances in Experimental Medicine and Biology* 1119: 169–83. https://doi.org/10.1007/5584_2018_257.

Zhu, Yuan, Pritam Ghosh, Patrick Charnay, Dennis K Burns, and Luis F Parada. 2002. "Neurofibromas in NF1 : Schwann Cell Origin and Role of Tumor Environment" 296 (May): 920–23.

Ziegler, Lina, Sergei Grigoryan, In Hong Yang, Nitish V. Thakor, and Ronald S. Goldstein. 2011. "Efficient Generation of Schwann Cells from Human Embryonic Stem Cell-Derived Neurospheres." *Stem Cell Reviews and Reports* 7 (2): 394–403. https://doi.org/10.1007/s12015-010-9198-2.

Appendix 1

1. Generation of a *NF1*(-/-) iPSC line using CRISPR/Cas9 technology

1.1. Editing strategy and *NF1*(-/-) iPSC clone generation

We generated *NF1*(-/-) iPSC lines from control *NF1*(+/+) FiPS cell line using the genetic-editing clustered regularly interspaced short palindromic repeats-CRISPR associated protein 9 (CRISPR-Cas9) technology.

The Cas9 and the guided RNA (gRNA) were introduced into the cells using the ArciTect ribonucleoprotein (RNP) system from StemCell Technologies (Kim 2014).

The sgRNA was designed to guide the Cas9 to exon 2 of the *NF1* gene in the negative strand (**Table A1-1).**

Gene	Name	Exon	Strand	sgRNA
NF1	RNP1	2	-	GTTGTGCTCAGTACTGACTT

Table A1-1. gRNA used in CRISPR-Cas9 system to edit the *NF1* gene. The gRNA recognized and cut 20 bp sequences of the exon 2 in the *NF1* gene.

RNP complexes were prepared following StemCell Technologies manufacturer's instructions. Transfection of RNP complexes into iPSCs was performed using TransILT reagent (Mirus). 72 hours after transfection, cells were detached and plated in 96-well Matrigel coated plates at a density of 1-2 cells/well to generate single-cell clones. Clones were amplified and DNA from them was extracted to analyze *NF1* mutation by Sanger sequencing.

We analyzed 15 clones, and 2 of them were compound heterozygous for *NF1*. **Figure A1-1** shows the *NF1* mutations generated in the two alleles of clone D12. Both mutations consisted in deletions near the protospacer adjacent motif (PAM) of the *NF1* sgRNA**.**

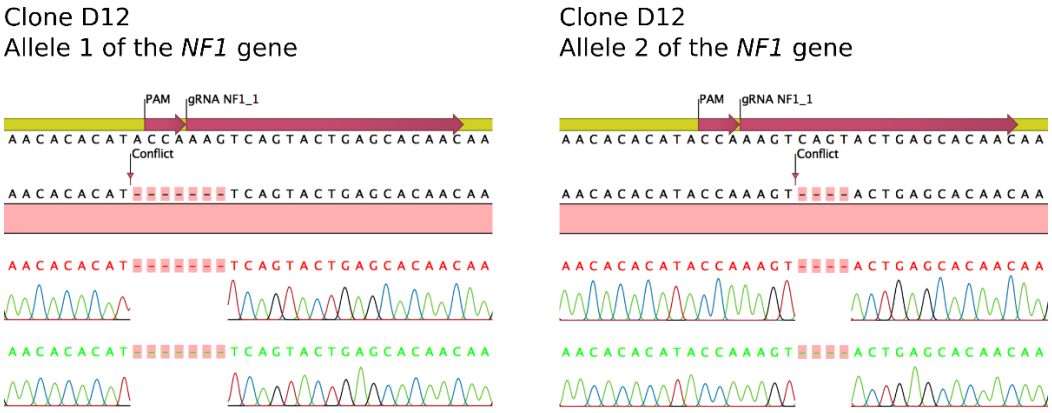

Figure A1-1. The specific *NF1* mutations in clone D12. At the top the reference sequence, below the Sanger sequencing of the specific *NF1* allele. The software pinpoints the conflict zone and

alignments the rest of the sequence. In clone D12 both mutations are deletions, a deletion of 7 nucleotides (left), and a 4-nucleotide deletion (right). Both mutations create a frameshift.

Clone allele	gDNA mutation	cDNA	Protein
Clone D12_1	g.66040_66046del	c.94_100del	p.T32_Sfs*9
Clone D12_2	g.66048_66052del	c.102_105del	p.S35_Lfs*7

Table A1-2. The specific gDNA, cDNA, and protein mutation in the two *NF1* alleles of the clone D12.

Both *NF1* mutations are deletions, a deletion of 7 nucleotides, and a 4-nucleotide deletion (**Table A1-2**). Both mutations create a frameshift, which theoretically implies a complete knock out cell line without any expression of neurofibromin.

This clone D12 is used in the thesis named as *NF1*(-/-) edited iPSC line or NF1_C.

1.2. *NF1*(-/-) edited iPSC line characterization

Clone D12 showed the typical iPSC compact colony morphology and expressed the pluripotency markers OCT3/4 and Tra1-81 by immunocytochemistry (ICC) corroborating that the *NF1*(-/-) edited iPSC line remained pluripotent (**Figure A1-2**).

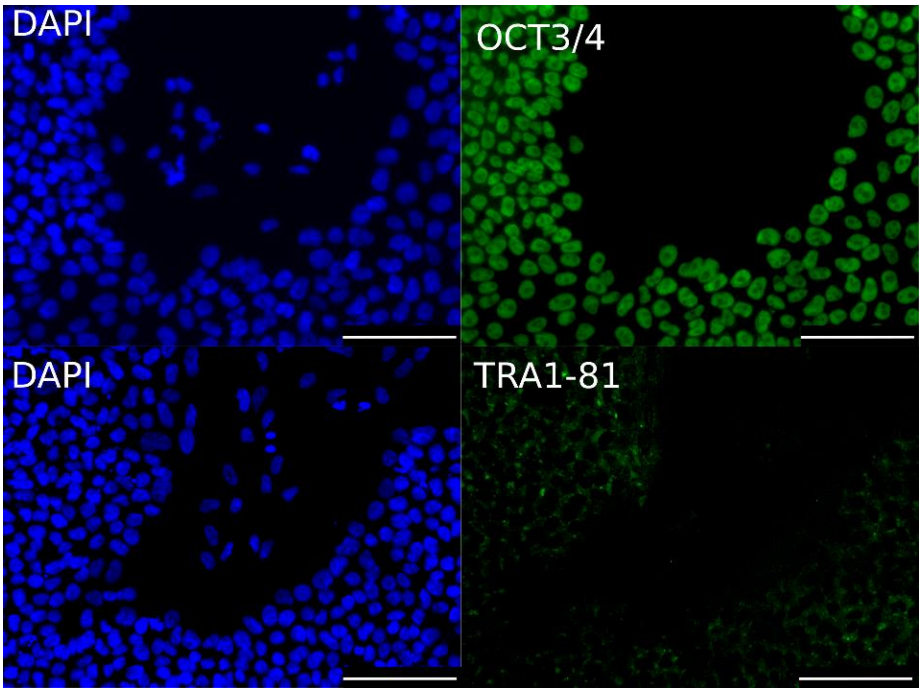

Figure A1-2. The OCT3/4 and TRA1-81 expression in clone D12 by immunocytochemistry. DAPI was used to stain nuclei. Scale bar: 100 µm

1.3. *NF1*(-/-) edited iPSC line differentiation towards neural crest cells

The *NF1*(-/-) clone D12 was differentiated into neural crest (NC) cells following the protocol previously described in the thesis.

Flow cytometry analysis confirmed the NC identity of differentiated cells showing coexpression of both p75 and Hnk1 markers (Figure A1-3A). These results were corroborated by immunocytochemistry (ICC) for SOX10, TFAP2A, and p75 (Figure A1-3B).

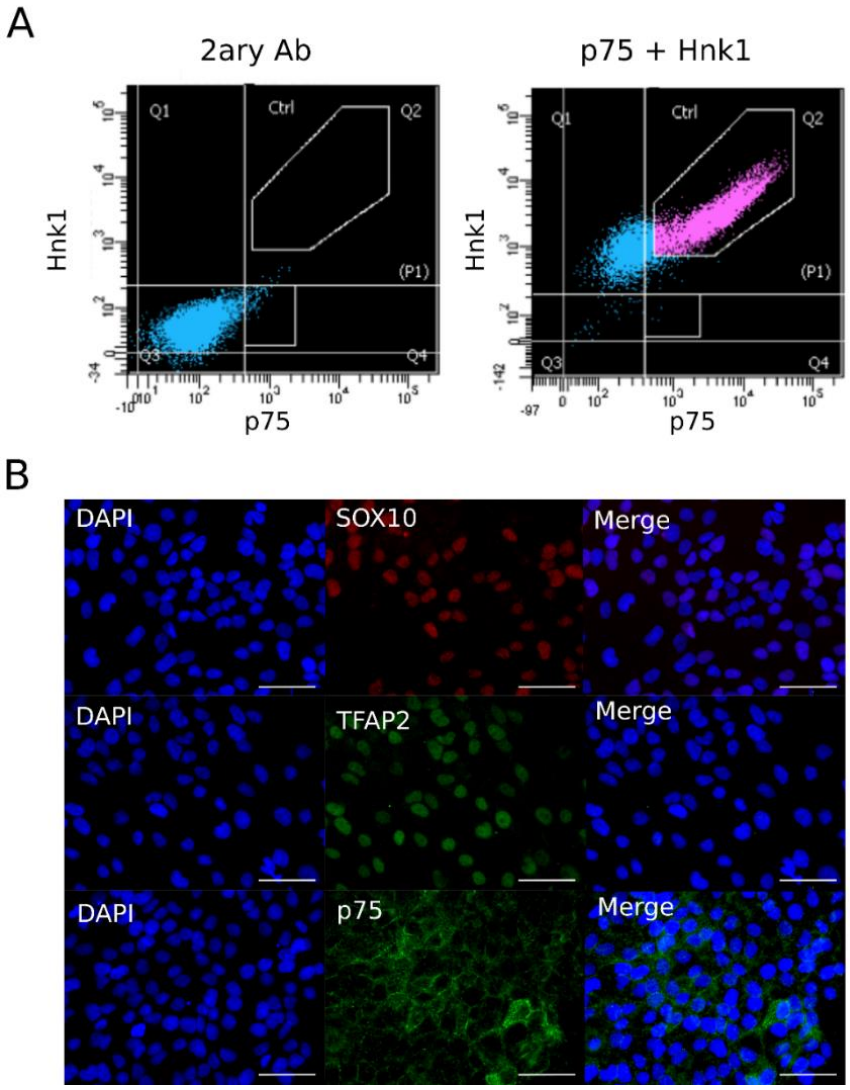

Figure A1-3. The neural crest-differentiated clone D12 expressed neural crest markers. A) Flow cytometry analysis of the expression of the p75 and Hnk-1 expression. In the x-axis the p75 expression is graphed while in the Y-axis the Hnk1. The left graph shows the distribution of cells without primary antibody. The right graph shows the distribution of the cells analyzed for p75 and Hnk1. B) ICC analysis of SOX10, TFAP2A and p75 in the NC-differentiated clone D12. Scale bar: 100 µm

1.4. *NF1*(-/-) edited iPSC line differentiation towards Schwann cells in 2D

The *NF1*(-/-) edited NC was further differentiated into Schwann cells (SCs) using the same differentiation protocol as previously described in the thesis (see Material & Methods).

The *NF1*(-/-) edited cells upon SC differentiation expressed specific NC-SC markers analyzed by RT-qPCR (**Figure A1-4**) like *SOX10*, *NGFR*, and *S100B*; although the expression was lower than control differentiating *NF1*(+/+) SCs (**Figure R6B**, **D**).

Moreover, as *NF1*(-/-) PNF-derived iPSC, *NF1*(-/-) edited differentiating SCs did not stop proliferating, naturally detached from plate surfaces and formed sphere-like structures visible to the naked eye (**Figure A1-5**).

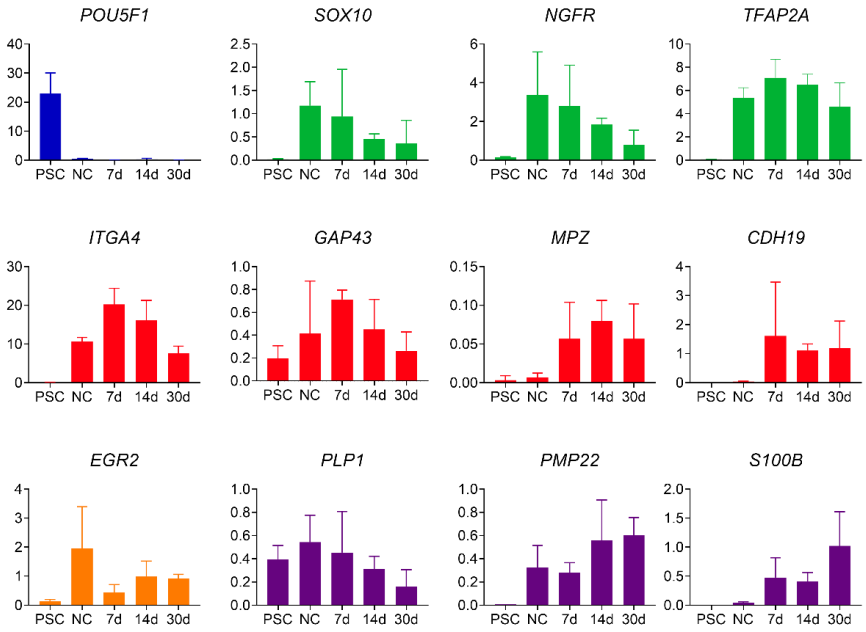

Figure A1-4. Schwann cell differentiation from differentiated neural crest *NF1*(-/-) edited iPSCs. RT-qPCR in *NF1*(-/-) edited iPSC at five different timepoints during differentiation: pluripotent stage (PSC), neural crest stage (NC) and at 7, 14, or 30 days of SC differentiation. Values are expressed as the mean of the Normalized Relative Expression (Y-axis) ± SEM from three independent differentiation experiments.

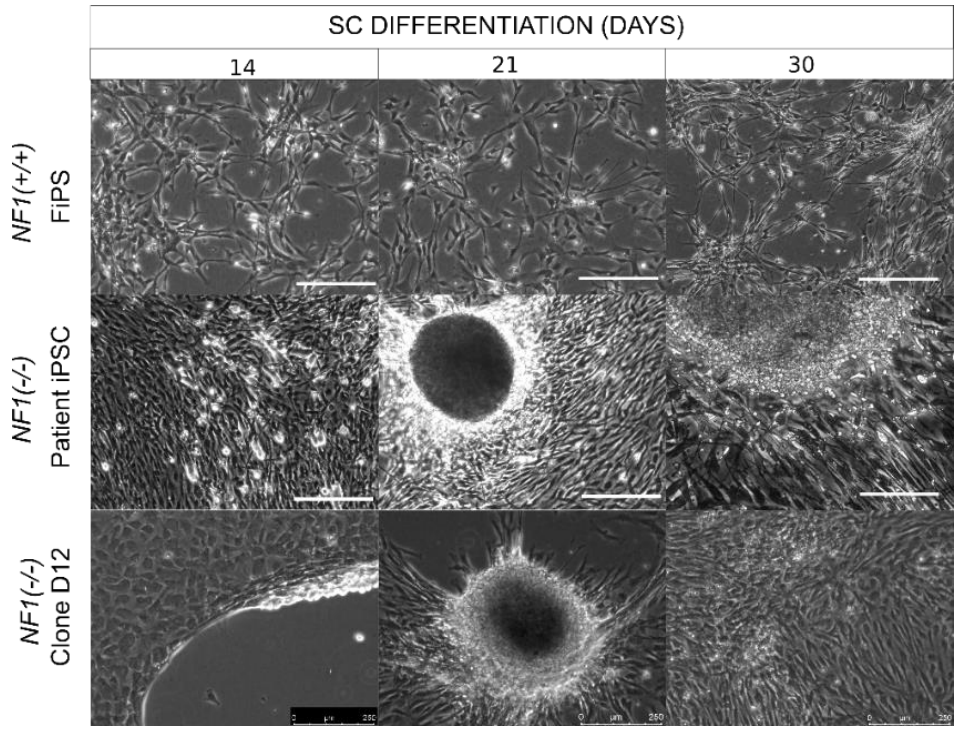

Figure A1-5. Phase contrast images from the Schwann cell differentiation process of control *NF1*(+/+) iPSC and the plexiform neurofibroma-derived iPSCs and the *NF1*(-/-) edited iPSC. Scale bar; 250 µm.

Appendix 2

1. Additional results

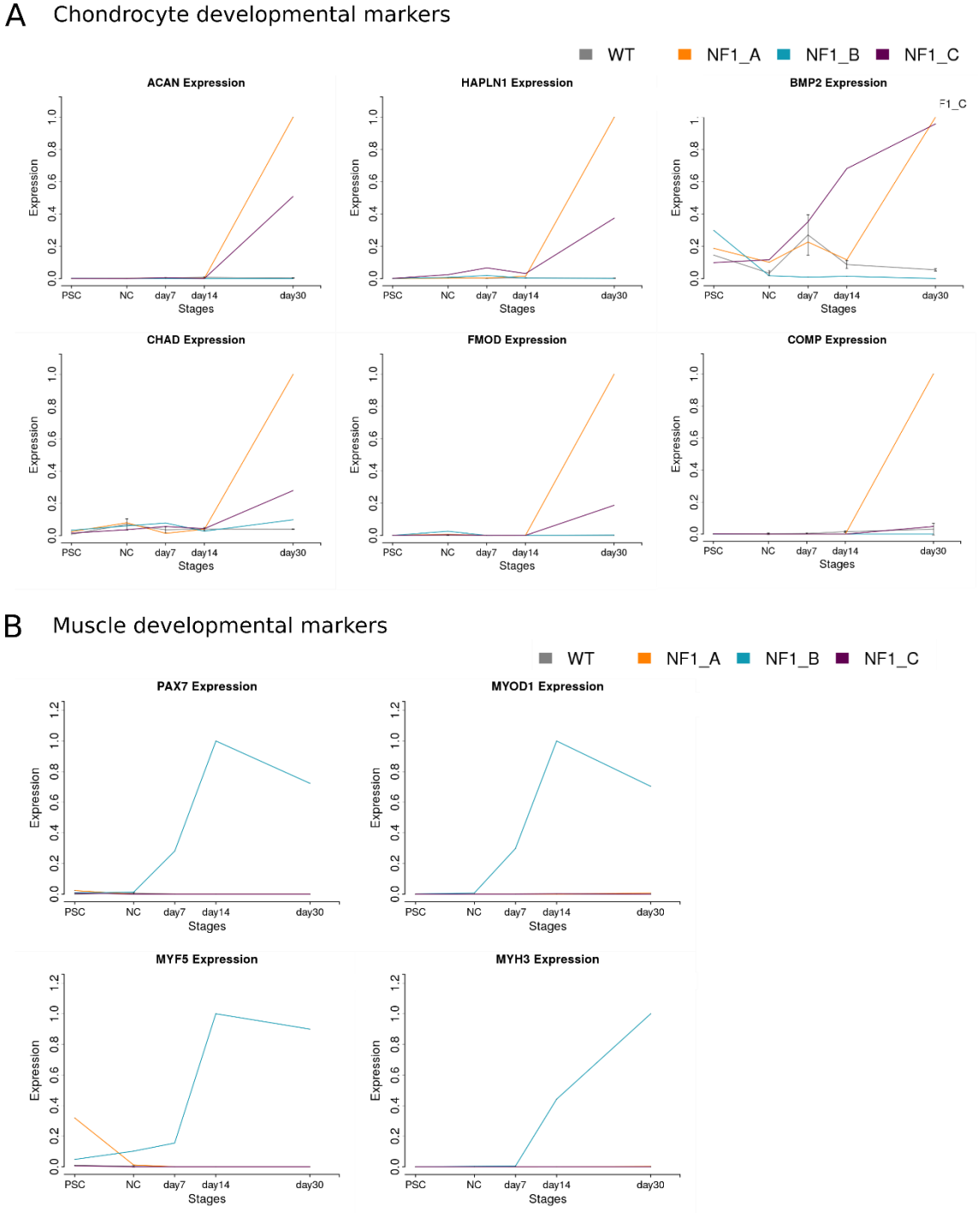

Figure A2-1. *In silico* validation of chondrocyte and muscle gene expression of *NF1*(-/-) cells in 2D cultures. Relative expression of chondrocyte developmental markers (A) and muscle developmental markers (B) using RNA-seq data of control *NF1*(+/+) iPSC line (WT) and *NF1*(-/-) iPSC lines (NF1_A, NF1_B, and NF1_C) from pluripotent stem cell stage (PSC), neural crest (NC), and 7, 14 and 30 days of the SC differentiation process.

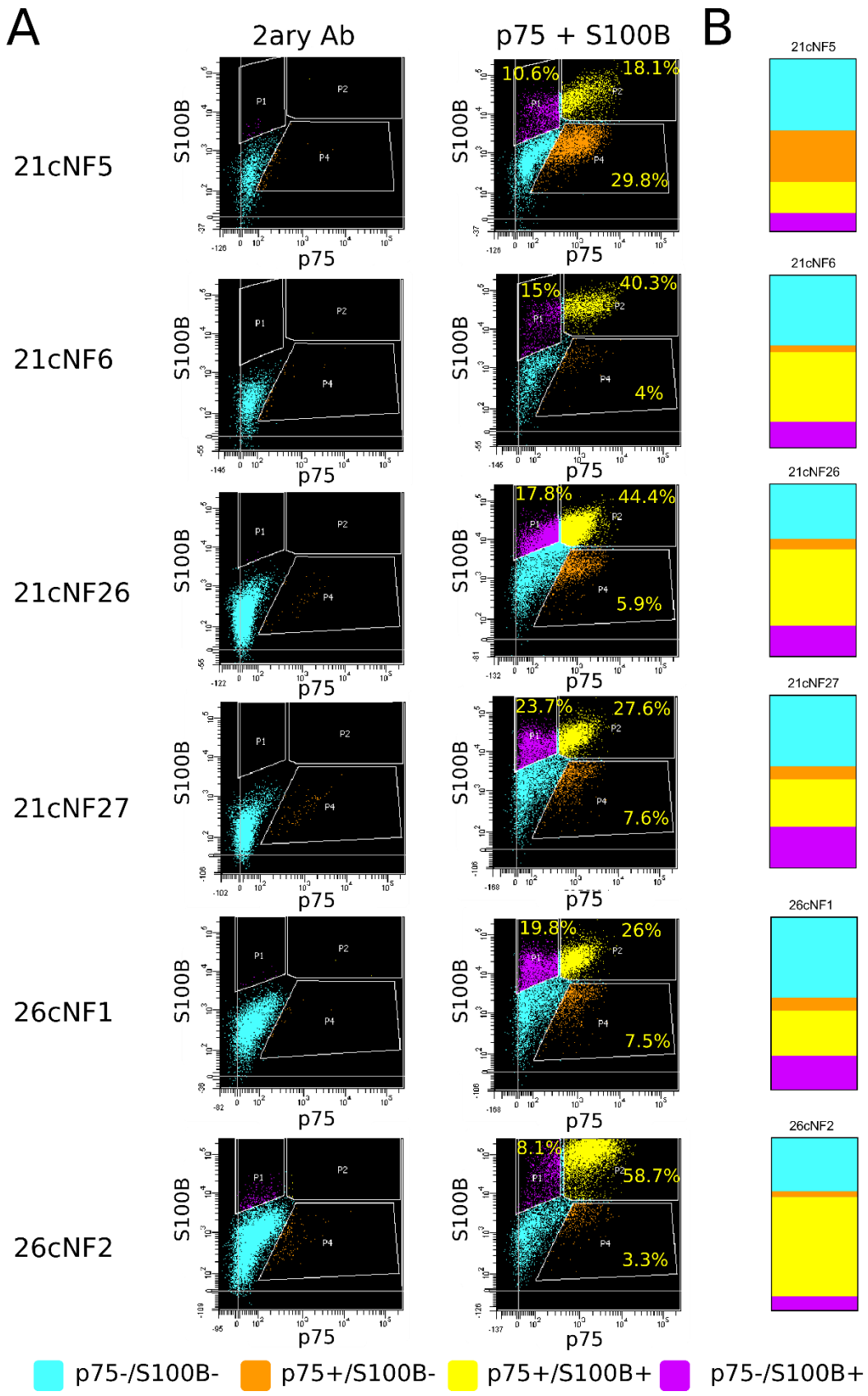

Figure A2-2. P75 and S100B double staining uncovered cell heterogeneity of the Schwann cell component within cutaneous neurofibromas A) Flow cytometry analysis of p75 and S100B of 6 cNFs (4 from patient 21 and 2 from patient 26). Left panel of cNFs reflects the signal of the secondary antibodies (2ary Ab) as controls. In the X-axis, the p75 expression is represented, while

in the Y-axis, the S100B expression. Each dot represents a cell. Each dissociated-cNF exhibited a homogenous negative population for both antibodies. Right panels, each dissociated-cNF was incubated with primary and secondary antibodies. Double-negative p75-/S100B- cells (light blue), p75+/S100B- cells (orange), double-positive p75+/S100B+ cells (yellow), and p75-/S100B+ cells (purple) are shown. **B)** Companion graphs showing the proportions of each different cell population within cNFs. The entire square represents 100% of the population, and the area of each color represents the proportion of each cell population. Some cNFs as 21cNF6, 21cNF 26 or 26cNF2 displayed a high proportion of double-positive p75+/S100B+ cells while others as 21cNF5 presented a high proportion of the p75+/S100B- cells.

Neural crest	7 days	14 days	30 days
SMOC1	FRG2DP	MGP	CFI
ZBTB16	PLPP4	ELN	KCND3
MMRN1	IL7R	PRND	LINC02735
BMP7	IL18R1	LGR5	APLNR
IGDCC3	SERPINA3	NRG3	XKR4
SCN1A	DLK1	SEPT5-GP1BB	SAMD9L
IP6K3	COL22A1	COL11A2	FCRLA
KLHL41	IL11	SLIT3	ZNF536
CCDC33	GPAT3	SSC5D	PCDH20
EDN3	ACTA1	DIO2	ABCA8
ALDH1A2	RCAN1	LTBP1	SBF1P1
PPP1R14C	FBXO32	NFIA	THBS2
COL20A1	BMP5	MN1	NFIX
NR2F1	CD93	MXRA8	PLCXD3
TFAP2B	FLJ16779	DMPK	CCN3
TXLNB	LRIG3	LOC102724488	S100B
CCL15	RASSF4	PLD3	GBP1
IGF2	GAD1	PTK7	DMTN
PRTG	PDE4D	ARMCX2	HSPA6
COL23A1	EXOC3L2	STON1	COL15A1
MEOX1	ENC1	CTDSP2	BBOX1
NOS3	SYNM		KIRREL3
CCSER1	SEMA3D		ADAMTSL1
SRRM4	CEMIP2		APOD
PRELP	SLC9A7		GABRA2
MSTN	SPP1		GBP3
VIT	SERPINE2		EMP1
VEGFD	GPAM		UNC13C
LRRK2	LRRN3		FCGR2A
RCSD1	LINC00472		RNF128
H19	IGSF3		GPR158
SPAG6	USP53		PMEPA1
HOXB9	FRMD6		TRAF1

FOXD2	ASAP2		AQP7P3
EBF2	BIRC2		MIA
RXRG	PLS3		RGS4
DUSP9	SMAD3		CCL2
LMOD3	TRIB2		LYST
CRABP2	PICALM		AQP7P1
VSIG10L2	EHBP1		SQOR
CPB2-AS1	SMURF2		AQP6
PRRT4	IGF1R		LAMA2
LOC101928058	ITPKB		KLF9
POU3F3	COTL1		PRSS12
NTRK1	GPR161		P2RX7
NKD1	SOCS6		RASGEF1C
HOTS	SOX11		ITGB8
CAMK2A	SLC26A2		FAM184B
SLC8A3	IMMP2L		MYOT
FRMD4B	TGFBR1		GFRA3
PAX3	FNDC3A		CDKN2C
NLRP14	EFR3B		PLSCR4
RIMBP2	CHSY1		CCDC102B
PCDH15	CDK2		CLIP4
COLEC12	TSPAN13		FXYD3
DUSP27	MAP4K4		SLFN11
EYA1	NCK2		IL1R1
DOCK10	KIF5B		TIMP1
FREM1	DYNC1I2		PDGFB
CT75	CTNNB1		KCNF1
ITGA9	PRDM4		ADGRG1
HOXB8	GNB4		KCNA2
ST6GALNAC5	OTUD3		ENDOD1
EYA2	PPP4R1		CRISPLD2
KCNJ12	PIK3C3		PCSK2
FBLN7	PXYLP1		AHRR
GPC3	MOCS1		EBF4
GJB1	PTPN1		FLRT1
LINC00461	RCN2		HSPA12A
C10orf90	RAB8B		MEF2C
SCN3A	ATP6V1B2		DPYD
TSPAN18	TDG		PLEKHG1
RFX4	FRYL		GAS7
SLITRK5	RRN3		SCN9A
XKR5	CDV3		IFI16
TNNI1			TDRD7
GREB1L			ARNTL
FOSB			SH3PXD2A

MGLL			TENM3-AS1
PLCB4			PKNOX2
ZAP70			SCN7A
CPED1			ST6GALNAC2
CYP1A1			LOXL3
RTN4RL1			ZBTB20
DPYSL5			TMEM47
TGFBR3			ZNF365
FIGNL2			AFAP1L2
CHN2			NFIL3
GAS2			SRCIN1
MUSTN1			PDLIM4
NR2F2			WIPF1
POU4F1			SLC5A9
VWCE			LGI4
SLC47A1			TRPV3
SRGAP3			TENM3
TMEM215			ANKRD36
MTSS1			NR3C1
LAPTM5			SYT11
PCSK6			MFSD6
TTPA			FXYD1
MYO7A			PARP9
ABCG2			ANKH
COL25A1			S100A16
RIMS3			CIITA
FOXD2-AS1			TGFBR2
TRIL			FNTB
SPSB4			ITGA6
SSUH2			TMOD2
CLGN			PLA2G4A
TWIST1			VEGFA
LINC01715			ANGPTL2
RNVU1-14			PLP1
MYH15			SCARB2
CNTFR			FAHD2B
TENM4			NEFL
LRRN4CL			MTMR9LP
C2orf91			COL6A2
BAHCC1			SHISA4
HES6			GIPC3
COL13A1			ABHD2
MECOM			DAG1
TRMT9B			CYP4V2
MEGF10			KAT2B

CELF2-AS2			FAM78B
NID2			ATP10D
ATP1A2			FUT8
NR2F2-AS1			DTX3L
DCX			SPATA6
LINC02381			RGMB
ACVRL1			ERBB3
PANTR1			RUNX1T1
ACSS1			COL6A1
MDK			MAN2A2
ARHGAP28			SPPL2A
NCALD			TAPBP
RNF157			LPAR1
GFRA1			PLPP1
EPOP			SIPA1L2
TMEM97			SEC14L2
PEAR1			KATNAL1
DAPK2			TSPAN11
TMEM150C			HMG20B
KBTBD11			BTG1
COLGALT2			LYPD6
ATP6V1B1			ARHGEF2
LOC107985770			EMP2
RAPGEF4			SHROOM4
EYA4			PTPN3
FOS			CTNNA1
GOLGA8T			MERTK
H2BU1			NBPF1
CXXC4			AOPEP
DNAH6			MINDY1
TNFSF9			BICD1
SPON1			SRGAP2B
SELENBP1			SESN3
LOC101926964			ARHGEF12
TMEM107			ADAMTS4
TMSB15A			KCTD12
ENPP2			MARCKS
CELF2-AS1			ETV3
LRRC4			TMX4
SCD5			ZNF641
FAM110B			ANKRD39
ODC1			TRPV1
HSPA4L			TRPM7
RNASE1			ST3GAL6
MT2A			ARNT2

LINC01686			SOCS5
HUNK			ATP11B
IL16			VPS13C
GREB1			LDLRAP1
CSRNP3			FBXO7
H3C2			ATG2B
CAMK2N1			ABHD6
SHC3			ELK4
CDON			TLE3
NETO2			CHD9
PRKCE			RTKN
FRZB			LRCH3
C3orf52			TRIM56
SOX9			GLTP
PEG10			SLC12A6
USP3-AS1			PPP1R12B
MDGA1			KIAA0754
H4C14			EFHC1
LINC02609			CLCN3
RADIL			NEMP2
KCNC1			RUBCN
RNF165			TRAK1
INKA1			DENND4C
H3C4			
MYLK-AS1			
PLXNA2			
EPHB2			
CNTN3			
APOLD1			
H2AC20			
HDAC9			
SNX22			
MGC16025			
DACH1			
LRP4			
ELOVL2			
MACROH2A2			
BCORL1			
H4C1			
RGS10			
C2orf72			
NRGN			
NQO1			
KCNJ8			
PLCXD2			

ADGRE5			
LPAR6			
ASIC1			
CNRIP1			
EFNB2			
MDGA2			
H2BC5			
IFIT1			
RUBCNL			
NAALAD2			
ALX1			
NCR3LG1			
SDC1			
TYMS			
ALX4			
BCL7A			
RGS20			
KIAA0895			
OBSCN			
H2BC12			
NR2F1-AS1			
LOC100289511			
USP3			
TSHZ2			
STARD5			
H2BC18			
H4C3			
HMGA2			
WDR17			
KDM4D			
GPC5			
AMOT			
ARHGAP5-AS1			
ERBB4			
HMGCS1			
GRK5			
PYGO1			
TOB1			
MBNL3			
LINC02249			
PREX1			
SCML1			
JUN			
H2BC21			
SOBP			

PIK3R1			
PBK			
CREG1			
SIM1			
CXCL11			
TIFA			
PLCD1			
RFX2			
FHOD3			
DCHS1			
TMEM170B			
AFF2			
TP53I11			
CHRFAM7A			
ZC3H12C			
CELF2			
GPR162			
ENOSF1			
MGAT3			
MAN1C1			
HS6ST2			
ARRB1			
STRA6			
MSH5			
H1-4			
BTN3A2			
E2F2			
SOCS2			
ACSF2			
SDK2			
ZNF521			
ABCA5			
MEOX2			
LOC644656			
SVIP			
TMCC1-AS1			
MSI1			
ITIH4			
PHF6			
ZNF704			
RNFT2			
MCF2L			
SHF			
UHRF1			
NSD2			

SNAI1			
NPL			
GAS1			
SPA17			
MAPK10			
SOGA3			
ARID3A			
APOBEC3B			
PIK3R3			
EFNB1			
CRNDE			
DENND2A			
TRIM9			
CHRNA7			
SKP2			
CPXM1			
SREBF2-AS1			
APBA2			
HIC2			
ZFP36L1			
LOC730101			
LRRC8C			
TLNRD1			
RRM1			
PIR			
H1-10			
TIAM1			
EFNA5			
GVINP1			
HEY2			
PPFIBP2			
GRAMD1C			
GYPC			
PRC1			
THEM6			
GSTA4			
KNL1			
DUSP7			
STARD8			
CHD7			
HADH			
KIAA1549			
EZH2			
ANP32B			
BTG2			

WDR76			
GOLGA8H			
COBLL1			
PCLO			
CALM3			
BOC			
CEP128			
HFM1			
TTC28			
CEP55			
SIRPA			
PCTP			
LOC101929479			
PRR3			
TUBA1B			
ZC3H8			
TMCC2			
LRRC4B			
SHANK3			
GPCPD1			
TCTEX1D2			
GLT8D2			
GAS2L3			
ABHD3			
ZNF618			
ZNF124			
RADX			
DERA			
XYLB			
ZNF438			
FUS			
ARHGAP33			
IQGAP3			
BTBD3			
CKAP2			
CBX5			
RACGAP1			
LINC00476			
MTMR4			
RPS4Y1			
GUSBP16			
TEDC1			
STMN1			
DPF1			
CNTRL			

MTBP			
ETS1			
ZNF516			
SH3BP1			
ABAT			
GDF11			
ACSS2			
LSS			
CORO7			
POP1			
KIF24			
FBXL14			
HMGN2			
BZW2			
SCMH1			
GOLGA2P7			
CCDC121			
SSBP2			
DYNLL2			
FXYD6			
FDPS			
GUSBP15			
CEP85L			
NFRKB			
AHDC1			
POLR3B			
CEP78			
MMAB			
CUEDC2			
CITED2			
HAUS5			
KIAA0586			
LPIN1			
SMC1A			
EVL			
CDK4			
BIN1			
HMGCR			
CDK5RAP2			
CHAMP1			
BTN2A2			
GPSM2			
SCD			
LBR			
LDAH			

CYFIP2			
RALGDS			
THEM4			
PARP16			
HNRNPA3			
DNAJC9			
PPA2			
SNX1			
TTC12			
SKA2			
RUSC1-AS1			
CHPT1			
ARHGEF25			
KLF3			
TMEM106C			
RBL1			
NAIP			
FAM53B			
APBB1			
GUSBP14			
PLIN2			
ATP6V0E2			
FIGNL1			
CDK5RAP3			
MPHOSPH9			
CBX1			
PUDP			
SNCA			
ERI2			
RASA4			
CNTNAP1			
E2F5			
DMXL2			
MCC			
VAV2			
FOXO3			
GUSBP1			
RCBTB2			
PGAP1			
SACS			
BLMH			
TMEM200C			
PLPBP			
NONO			
PHKB			

HIP1R			
DYNC2H1			
TARBP1			
HNRNPA1L2			
FSCN1			
CTNNBIP1			
KIAA1614			
NLGN2			
ZBTB10			
CRMP1			
ZBTB46			
ZNF280C			
CCDC14			
DYRK3			
SESTD1			
GPHN			
LOC284581			
ZNF608			
SLC25A40			
QDPR			
ARL3			
TMEM135			
LIN52			
TTC21B			
TMEM44			
AGPAT4			
TBL1X			
IFT81			
CSK			
ANKRD26			
PCYT2			
SGSM2			
OBI1			
SIMC1			
INTS6L			
NSDHL			
TMEM164			
SQLE			
RBFOX2			
ROBO1			
GOLGA6L9			
PTGR1			
RFX3			
PLEKHA8			
ACVR1B			

CYB5B			
ANKRD13B			
B4GALNT4			
SF1			
PRXL2A			
PC			
TJP1			
FBXO10			
ANKMY2			
DCLRE1B			
CHD1L			
DCXR			
C12orf57			
FADS1			
BCL9			
TMEM38B			
HSF2			
DYM			
SRSF5			
DET1			
INTS9			
TRIM66			
ZC3H13			
SMYD3			
JAKMIP2			
SFSWAP			
FUNDC2			
SEPTIN9			
HNRNPH1			
ZNF346			
LOC389906			
ZKSCAN2			
DCAKD			
BTBD2			
STAU2			
HSD17B11			
MTR			
PI4KAP2			
LMO4			
STARD9			
CCNL1			
CNOT6			
SREK1			
ILKAP			
ZNF354C			

RSRC1			
CHCHD2			
CEP95			
UBE2R2			
NT5C3B			
IFT52			
SMCHD1			
LRRC58			
MRPL40			
FTH1			
NFATC3			
UBE2E3			
NFYA			
GNE			
RPRD1B			
ARGLU1			
CNOT6L			
HNRNPR			
RAE1			
MYO10			
MED12			
RNPEP			
THAP12			
DCAF7			
NIT2			
MPP5			
MTCH2			
PPP1R10			
FAM239A			
SHKBP1			
ESD			
WASF2			
BAZ1B			
RPRD2			
SRSF6			
NAA40			
PIAS1			
PARD3			
JRK			
CLK2			
LUC7L2			
FOXK2			
PGD			
TENT4A			
RAPGEF6			

PRPSAP1			
ELP3			
ACAD9			
MAPRE2			
PCM1			
XPC			
SCAF8			
C11orf95			
CAMKK2			
IPO9			

Table A2-1. Neural crest-Schwann cell *in vitro* differentiation expression roadmap signature.

Neural crest	7 days	14 days	30 days
ALDH1A2	BMP5	MXRA8	ADGRG1
ALX1	CTNNB1	PTK7	APOD
BMP7	GPR161		CCL2
BTG2	SEMA3D		DAG1
CDON	SOX11		ERBB3
CITED2			GFRA3
CNTNAP1			LAMA2
DCHS1			LGI4
DCLRE1B			LPAR1
DCX			MEF2C
DCXR			NEFL
DENND2A			PLP1
DERA			S100B
DET1			SYT11
DMXL2			TRPV1
DNAH6			
DNAJC9			
DOCK10			
DPF1			
DPYSL5			
DUSP27			
DUSP7			
DUSP9			
DYM			
DYNC2H1			
DYNLL2			
DYRK3			
E2F2			
E2F5			
EBF2			
EDN3			
EFNA5			

EFNB1
EFNB2
ELOVL2
ELP3
ENOSF1
ENPP2
EPHB2
EPOP
ERBB4
ERI2
EZH2
FOXO3
FRZB
GFRA1
IFT52
INKA1
INTS6L
INTS9
IP6K3
IPO9
IQGAP3
ITGA9
ITIH4
JRK
JUN
KCNC1
KCNJ12
KCNJ8
KDM4D
KIAA0586
KIAA1614
KIF24
KLF3
KLHL41
KNL1
LAPTM5
LBR
LDAH
LIN52
LMO4
LMOD3
LPAR6
LPIN1
LRP4
LRRC4
LRRC4B

LRRC8C
LRRK2
LSS
LUC7L2
MACROH2A2
MAN1C1
MAPK10
MAPRE2
MBNL3
MCC
MCF2L
MDGA1
MDGA2
MDK
MECOM
MED12
MEGF10
MEOX1
MEOX2
MGAT3
MGLL
MMAB
MMRN1
MPP5
MRPL40
MSH5
MSI1
MSTN
MT2A
MTBP
MTCH2
MTMR4
MTR
MTSS1
MUSTN1
MYH15
MYO10
MYO7A
NAA40
NAALAD2
NAIP
NCALD
NCR3LG1
NETO2
NFATC3

NFRKB
NFYA
NIT2
NKD1
NLGN2
NLRP14
NONO
NOS3
NPL
NQO1
NR2F1
NR2F2
NRGN
NSD2
NSDHL
NT5C3B
NTRK1
OBI1
OBSCN
ODC1
PARD3
PARP16
PAX3
PBK
PC
PCDH15
PCLO
PCM1
PCSK6
PCTP
PCYT2
PEAR1
PEG10
PGAP1
PGD
PHF6
PHKB
PIAS1
PIK3R1
PIK3R3
PIR
PLCB4
PLCD1
PLCXD2
PLEKHA8
PLIN2

PLPBP
PLXNA2
POLR3B
POP1
POU4F1
SLC8A3
SNCA
SOX9
TENM4
TIAM1
TMEM107
TTC21B
TWIST1
ZFP36L1

Table A2-2. Selection of the genes in the neural crest-Schwann cell *in vitro* differentiation expression roadmap signature containing biological processes that contained any of the following terms: peripheral, glial, neural, Schwann cell, myelin, and gliogenesis

ADAMTS14	PTX3	KIT	CXCL14
PLPPR4	PSG5	BDKRB2	TGFA
SLAMF8	LIPG	PDE1A	SERPINA9
DCLK3	RASL10B	ZC3H12A	TGFB3
C3orf80	DHRS3	LOC101928985	IBSP
COL7A1	CEMIP	DES	ICOSLG
MAG	ADAMTSL3	FOXS1	IL4I1
HAPLN1	PECAM1	TARID	RGS2
ACSBG1	KRT14	PODXL	CPNE7
PTGIS	ISLR2	RGS16	SVEP1
MYH2	TMEM51	SPINT2	TNFAIP6
IGFBP5	GPR1	CHRNA9	ICAM5
MBP	DTX4	SH2D4A	IL33
AOX1	ADGRD1	RGS7BP	MAP3K5
GLI1	CD82	JAG1	LOC102723996
OXTR	TNFSF10	IL6	ARPP21
GPR68	ACAN	CCL7	KRT19
LINC02257	EFEMP1	INMT	UBE2QL1
COL6A3	POM121L9P	GREM2	LYPD6B
BDKRB1	SLC1A3	CCDC85A	LINC01592
CAVIN2	PPP1R1C	GLDN	PTGDR
PLXDC1	KCNQ5	CAPS	PSG4
WNT5A	CITED2	LINC00968	GUCY1A1
RASL12	S1PR1	SH2D2A	LRRC18
CDX1	MYPN	CD22	C1QTNF1
GGT5	IL1B	ASPN	INHBE
HEYL	NPAS1	LINC01142	C11orf87
LINC01929	OSR1	RNF152	GRIK3
DKK1	TIMP4	SUSD4	LINC02539
EDARADD	HSPB7	HSD11B1	LINC02783
PDGFRB	TMEM132E	C11orf96	FAM43B
LINC01614	NTRK1	KIF21B	SERPINB7
LINC01279	PRR15	LINC02015	F2RL1
CLIC3	COL10A1	PADI2	COL11A2
KRT3	DLX2	TDO2	TSPAN9
CLDN14	NKD2	TNFAIP3	MEGF10
ST6GAL2	DRAXIN	PLPPR5	RGS7
LINC02547	FMN2	CSF2RB	AKR1B15
POU2F2	DAPK1	ADGRD1-AS1	AREG
TNXB	TMEM26	OTOGL	ALDH1A1
ACTC1	SLC6A7	CRYBA2	CHST9
GFPT2	GJB2	SLC1A7	CLEC3B
CCL11	FRAS1	TNNI1	ELOVL3
ATOH8	IGFBP3	PTHLH	VSIR
CILP	ADH1B	LINC02511	KALRN
RPLP0P2	LINC00536	AZIN2	CCDC80

CACNA2D3	EDNRA	SAMD11	CLEC2L
SLC38A4	FAM216B	LOC101928143	LHX9
LINC01050	PRDM1	GNA15	
ICAM1	PTPRB	FST	
LRRN4CL	RAP1GAP	RIMS1	

Table A2-3. Differentially expressed genes between cutaneous neurofibroma real and virtual Schwann cell-endoneurial fibroblast co-cultures.

Appendix 3

1. Paper: Carrió et al. 2019

Please cite this article in press as: Carrió et al., Reprogramming Captures the Genetic and Tumorigenic Properties of Neurofibromatosis Type 1 Plexiform Neurofibromas, Stem Cell Reports (2019), https://doi.org/10.1016/j.stemcr.2019.01.001

Stem Cell Reports
Resource
ISSCR
OPEN ACCESS

Reprogramming Captures the Genetic and Tumorigenic Properties of Neurofibromatosis Type 1 Plexiform Neurofibromas

Meritxell Carrió,[1] Helena Mazuelas,[1,9] Yvonne Richaud-Patin,[2,3,9] Bernat Gel,[1] Ernest Terribas,[1] Imma Rosas,[1] Senda Jimenez-Delgado,[2,3] Josep Biayna,[1,7] Leen Vendredy,[1,8] Ignacio Blanco,[4] Elisabeth Castellanos,[1] Conxi Lázaro,[5] Ángel Raya,[2,3,6,*] and Eduard Serra[1,*]

[1]Hereditary Cancer Group, Germans Trias i Pujol Research Institute (IGTP)-PMPPC-CIBERONC, Can Ruti Campus, Badalona, Barcelona 08916, Spain
[2]Center of Regenerative Medicine in Barcelona (CMRB), Hospitalet de Llobregat, Barcelona 08098, Spain
[3]Center for Networked Biomedical Research on Bioengineering, Biomaterials and Nanomedicine (CIBER-BBN), Hospitalet de Llobregat, Barcelona 08098, Spain
[4]Clinical Genetics and Genetic Counseling Program, Germans Trias i Pujol University Hospital (HUGTiP), Can Ruti Campus, Badalona, Barcelona 08916, Spain
[5]Hereditary Cancer Program, Catalan Institute of Oncology (ICO-IDIBELL-CIBERONC), L'Hospitalet de Llobregat, Barcelona 08098, Spain
[6]Institució Catalana de Recerca i Estudis Avançats (ICREA), Barcelona 08010, Spain
[7]Present address: Genome Data Science Group, Institute for Research in Biomedicine (IRB), Barcelona, Spain
[8]Present address: Peripheral Neuropathy Research Group, University of Antwerp, Antwerp, Belgium
[9]These authors contributed equally
*Correspondence: araya@cmrb.eu (Á.R.), eserra@igtp.cat (E.S.)
https://doi.org/10.1016/j.stemcr.2019.01.001

SUMMARY

Neurofibromatosis type 1 (NF1) is a tumor predisposition genetic disease caused by mutations in the *NF1* tumor suppressor gene. Plexiform neurofibromas (PNFs) are benign Schwann cell (SC) tumors of the peripheral nerve sheath that develop through *NF1* inactivation and can progress toward a malignant soft tissue sarcoma. There is a lack of non-perishable model systems to investigate PNF development. We reprogrammed PNF-derived *NF1*(−/−) cells, descendants from the tumor originating cell. These *NF1*(−/−)-induced pluripotent stem cells (iPSCs) captured the genomic status of PNFs and were able to differentiate toward neural crest stem cells and further to SCs. iPSC-derived *NF1*(−/−) SCs exhibited a continuous high proliferation rate, poor myelination ability, and a tendency to form 3D spheres that expressed the same markers as their PNF-derived primary SC counterparts. They represent a valuable model to study and treat PNFs. PNF-derived iPSC lines were banked for making them available.

INTRODUCTION

Neurofibromatosis type 1 (NF1) is a tumor predisposition genetic disease (VM & Riccardi, 1992) caused by the inheritance of a mutated copy of the *NF1* gene, a negative regulator of Ras (Ratner and Miller, 2015). The major disease features involve the nervous system, the skin, and the skeletal system. There is a great variability in the clinical expressivity of the disease, but the development of different tumors of the peripheral nervous system, such as cutaneous neurofibromas (CNFs), plexiform neurofibromas (PNFs) or, less frequently, malignant peripheral nerve sheath tumors (MPNSTs), constitute one of the hallmarks of the disease (Ferner, 2007).

PNFs are mainly developed in the context of NF1 and are thought to be congenital. They are identified in around 50% of NF1 individuals if MRI is used (Mautner et al., 2008). This tumor type constitutes a major source of morbidity (Prada et al., 2012) and, in some cases, undergoes malignant transformation (McCarron and Goldblum, 1998). Surgery is still the standard therapeutic option. However, complete resection can cause important functional deficiencies and sometimes can be unfeasible because of the size or location of the tumor (Packer and Rosser, 2002). Recently, the MEK inhibitor Selumetinib has been used in children with inoperable PNFs showing confirmed partial responses (Dombi et al., 2016).

Neurofibromas are composed of different cell types, mainly Schwann cells (SCs) and endoneurial fibroblasts, as well as perineurial cells and infiltrating immune cells, all embedded in an abundant collagen-rich extracellular matrix (Krone et al., 1983; Peltonen et al., 1988). PNFs arise through a biallelic inactivation of the *NF1* gene (Däschner et al., 1997; Hirbe et al., 2015; Kluwe et al., 1999; Rasmussen et al., 2000). Only neurofibroma-derived SCs bear this *NF1* inactivation (Kluwe et al., 1999; Li et al., 2016; Maertens et al., 2006; Muir et al., 2001; Serra et al., 2000). Like CNFs, different PNFs arising in the same individual bear different somatic *NF1* mutations (Pemov et al., 2017). Also, like CNFs (Garcia-Linares et al., 2011), no recurrent gross genomic alterations or recurrent point mutations have been identified in PNFs besides the involvement of chromosome 17 in the inactivation of the *NF1* locus (Beert et al., 2011; Carrió et al., 2018; Miller et al., 2009; Pemov et al., 2017). PNF progression to malignancy often occurs through the formation of a pre-malignant lesion termed atypical neurofibroma, which involves the additional loss of the *CDKN2A/B* locus (Beert et al., 2011; Higham et al., 2018). It has been shown in one case (Hirbe et al., 2015) that somatic *NF1* inactivating mutation is shared by PNF

and their subsequent MPNST and metastasis, linking the PNF and MPNST cell of origin.

Different models for PNFs have been developed, both *in vitro* (primary cells, immortalized cells, 3D culture models) and *in vivo* (genetically modified mouse models). Primary SC cultures from PNFs have been established (Wallace et al., 2000). However, these cultures are perishable after several passages, limiting their use for molecular and cellular analyses that require large amounts of cells. To overcome this problem, immortalized cell lines have been generated (Li et al., 2016), but inextricably alter the biological status of the cells. These cells have also been used to generate 3D models (Kraniak et al., 2018) to better recapitulate the natural PNF environment of SCs. In addition, different genetically modified animal models using the Cre/lox system to ablate *NF1* in specific cell stages of the neural crest stem cells (NCs, for simplicity)-SC axis during development have been generated that develop PNFs (reviewed in Buchstaller et al., 2012). Furthermore, Chen et al. (2014) established a non-germline model of PNF, consisting of the transplantation of *Nf1*-deficient embryonic dorsal root ganglia/nerve root neurosphere cells to sciatic nerves of nude mice.

Another way of obtaining imperishable cell-based model systems is the generation of induced pluripotent stem cells (iPSCs) (Takahashi and Yamanaka, 2006). iPSCs have been generated to model hereditary cancer syndromes (Papapetrou, 2016), like Fanconi anemia (Raya et al., 2009). iPSCs for NF1n have also been developed (Anastasaki et al., 2015; Larribere et al., 2015; Wegscheid et al., 2018). However, as for most other cancer syndromes, NF1 iPSCs have been generated from patient fibroblasts and not directly from cells of the associated tumors.

iPSC technology has been used to reprogram cancer cells, encountering different obstacles, such as their chromosomal and genomic composition or the necessity of remodeling their epigenetic state. Another limiting factor is the cell type to be reprogrammed. These aspects make the efficiency of generating iPSCs from cancer cells low (Kim and Zaret, 2015). Despite the low efficiency, there are several examples of iPSCs generated from cancer cells (Pan et al., 2017), mainly from established cancer cell lines (Bernhardt et al., 2017) and much less common from primary tumors (Kim et al., 2013; Kotini et al., 2017). However, the generation of iPSCs from benign tumors or pre-malignant lesions has been less explored (Papapetrou, 2016). To generate a non-perishable cell-based model system that recapitulates the genetic content and tumorigenic properties of NF1 benign PNFs, we generated iPSCs directly from PNF-derived primary cells. These iPSCs were differentiated to NCs and further to SCs. *NF1*(−/−) SCs obtained from PNF-derived iPSCs were extensively characterized and compared with primary *NF1*(−/−) SCs derived from primary tumors.

RESULTS

Generation of PNF-Derived iPSC Lines

We obtained five different PNFs (code-named 3PNF, 5PNF, 6PNF, 7PNF, and 13PNF) from five independent patients diagnosed of NF1 according to standard diagnostic criteria (DeBella et al., 2000). For most of them, histological information is available (Carrió et al., 2018). PNFs are composed of different cell types, mainly SCs and endoneurial fibroblasts. SCs within PNFs are the only cells bearing the two *NF1* alleles inactivated, one by a constitutional mutation shared by all cells of the individual, and the other by a somatic mutation specific for each PNF. Our intention was to create an imperishable cell-based model resource by reprogramming *NF1*(−/−) cells present in PNF descendants from the cell originating them. In addition, we planned to obtain *NF1*(+/−) isogenic iPSCs from the same tumors. We first determined the *NF1* germline mutation of each patient by next-generation sequencing panel analysis (Castellanos et al., 2017) and also the *NF1* somatic mutation of each excised PNF (Table 1; Figure S1). *NF1*(−/−) iPSCs were generated either from pure cultures of PNF-derived *NF1*(−/−) SCs (Serra et al., 2000) or directly from a short culture of PNF-dissociated cells. *NF1*(+/−) iPSCs were obtained by reprogramming either cultures of PNF-derived *NF1*(+/−) endoneurial fibroblasts, directly from PNF-dissociated cells or from skin-derived fibroblast cultures of the same patients (see Table S1 for details). Reprogramming to pluripotency was induced by retrovirus- and/or Sendai virus-mediated transduction (Ban et al., 2011; Takahashi and Yamanaka, 2006) of the patient-derived cells. Table 1 summarizes information on patient (sex, age, and germline mutation), tumor (diagnostic and *NF1* somatic mutation), and iPSC (name and banking information). Further reprogramming information is summarized in Table S1.

Overall, we generated seven genetically different iPSC lines from five independent NF1 patients. We were able to isolate two independent *NF1*(−/−) iPSCs, bearing the constitutional and somatic *NF1* mutations, from five distinct PNFs. From all five patients we obtained *NF1*(+/−) iPSCs bearing only the constitutional mutation. Thus, from two different tumors, 3PNF and 5PNF, we were able to generate isogenic iPSC lines bearing two distinct *NF1* genotypes: *NF1*(+/−) and *NF1*(−/−) (Table 1).

Characterization of PNF-Derived iPSC Lines

After confirming the *NF1* genetic status, selected iPSC clones representing each patient and *NF1* genotype were further expanded and characterized. Figure 1 illustrates the characterization of the isogenic iPSC lines derived from 3PNF and 5PNF; the characterization of the remaining banked iPSC lines is shown in Figure S2. We selected

Table 1. Patient, Tumor, and iPSC Line Information

Patient Information				Tumor Information			iPSC Lines Generated	
Patient ID	Sex	Age (at PNF Resection)	NF1 Germline Mutation	Tumor ID	Diagnostic	NF1 Somatic Mutation	iPSC Line (Named in the Paper)	iPSC Line (Banking Name)
3	XX	8	c.3943C > T; p.Gln1315*	3PNF	PNF with diffuse extraneural invasion	LOH (HR) whole ch.17q	3PNFiPS(NF1+/−)	3PNF_FiPSsv_PM
							3PNFiPS(NF1−/−)	3PNF_SiPSsv_MM
5	XY	10	intragenic deletion (E16-35)	5PNF	PNF with diffuse extraneural invasion	LOH (3.8Mb del)	5PNFiPS(NF1+/−)	5PNF_TDiPSsv_PM
							5PNFiPS(NF1−/−)	5PNF_TDiPSsv_MM
6	XX	33	c.2946delT; p.Leu983*	6PNF	PNF with diffuse extraneural invasion	c.2033dupC; p.Ile679Aspfs*21	6PNFiPS(NF1+/−)	6PNF_SiPSrv_PM
7	XX	66	c.2033dupC; p.Ile679Aspfs*21	7PNF	PNF with diffuse extraneural invasion	LOH (1.4Mb del)	7PNFiPS(NF1+/−)	7PNF_TDiPSrv_PM
13	XY	14	c.1318C > T; p.Arg440*	13PNF	PNF with diffuse extraneural invasion	LOH (HR) whole ch.17q	13PNFiPS(NF1+/−)	not banked

LOH, loss of heterozygosity; HR, homologous recombination. The link below will take you to the Spanish National Stem Cell Bank-Institute of Health Carlos III, where the iPSC lines have been deposited to be able to be distributed. http://www.eng.isciii.es/ISCIII/es/contenidos/fd-el-instituto/fd-organizacion/fd-estructura-directiva/fd-subdireccion-general-investigacion-terapia-celular-medicina-regenerativa/fd-centros-unidades/fd-banco-nacional-lineas-celulares/fd-lineas-celulares-disponibles/lineas-de-celulas-iPS.shtml.

clones that displayed a compact embryonic stem cell-like morphology, were positive for alkaline phosphatase staining, and expressed high levels of pluripotency-associated transcription factors and surface markers (Figures 1A and 1B). Moreover, selected clones showed pluripotent differentiation ability *in vitro* and *in vivo* (teratoma formation), demethylation of *POU5F1* and *NANOG* promoters, and karyotype stability after more than 15 passages (Figures 1C–1F and S2). It is worth noting that 5PNFiPS(−/−) carried a chromosomal translocation (karyotype: 46,XYt(17; 22)(q11.2; q13.3)) also present in the parental reprogrammed SCs, as the cause of *NF1* somatic inactivation (Figure S2G). Finally, we confirmed by PCR-based DNA fingerprinting analysis that the iPSC lines generated genetically matched their parental tumors (Table S2). As expected, the levels of neurofibromin were reduced in *NF1*(+/−) iPSCs compared with control *NF1*(+/+) pluripotent cells, and were absent in *NF1*(−/−) iPSCs (Figure 2G). Altogether, these data demonstrated that we successfully generated iPSCs from PNF-derived *NF1*(+/−) and *NF1*(−/−) cells, and indicated that reduced levels or even absence of neurofibromin did not appear to compromise somatic cell reprogramming to pluripotency, maintenance, or differentiation capacity of iPSCs.

PNF-Derived *NF1*(−/−) iPSCs Exhibit a Higher Proliferation Rate Than Control Pluripotent Cells

It has been shown that *NF1*-deficient cells exhibit a higher proliferation rate than their cellular counterparts carrying one or two wild-type copies of the *NF1* gene (Kim et al., 1995, 1997; Rosenbaum et al., 1995). Consistent with this, we noticed that cultures of *NF1*(−/−) 3PNFiPS and 5PNFiPS needed to be split more frequently than control iPSCs or human embryonic stem cells (hESCs) maintained in parallel. To quantify the effect of the *NF1* status on iPSC proliferation rate, we used a flow cytometry-based Click-iT EdU assay. We compared PNF-derived *NF1*(+/−) or (−/−) iPSC lines with control *NF1*(+/+) pluripotent stem cells (PSCs). Control cells included iPSCs from skin fibroblasts of a healthy donor (FiPS cell line) and embryonic stem cells (ES4 cell line). On average, *NF1*(−/−) 3PNFiPS and 5PNFiPS cell lines exhibited a 10%–15% increase in cell proliferation rate compared with control PSCs (Figure 2H). *NF1*(−/−) iPSCs also exhibited a higher proliferation rate than *NF1*(+/−) iPSCs ($p < 0.05$). These results indicate that cell proliferation rate in PSCs, as is the case for somatic cells, is influenced by neurofibromin activity.

PNF-Derived iPSCs Capture the Genomic Status of Their Cell of Origin

We extensively characterized the genomic content of the different iPSC lines generated from PNFs. We performed cytogenetic karyotyping, exome sequencing, and molecular karyotyping by SNP array analysis comparing tumors, *NF1*(−/−) SC and *NF1*(+/−) fibroblast cultures and iPSCs. All samples were 2n according to the cytogenetic and molecular karyotypes (Figures 1F, 2A, S2, and S3). As previously observed in CNFs (Garcia-Linares et al., 2011), the only genomic alterations present resulted from the somatic inactivation of the *NF1* gene, in some cases affecting the structure of chromosome 17q (Figures 2 and S3) (Carrió et al., 2018). Gross somatic mutations affecting the *NF1*

Please cite this article in press as: Carrió et al., Reprogramming Captures the Genetic and Tumorigenic Properties of Neurofibromatosis Type 1 Plexiform Neurofibromas, Stem Cell Reports (2019), https://doi.org/10.1016/j.stemcr.2019.01.001

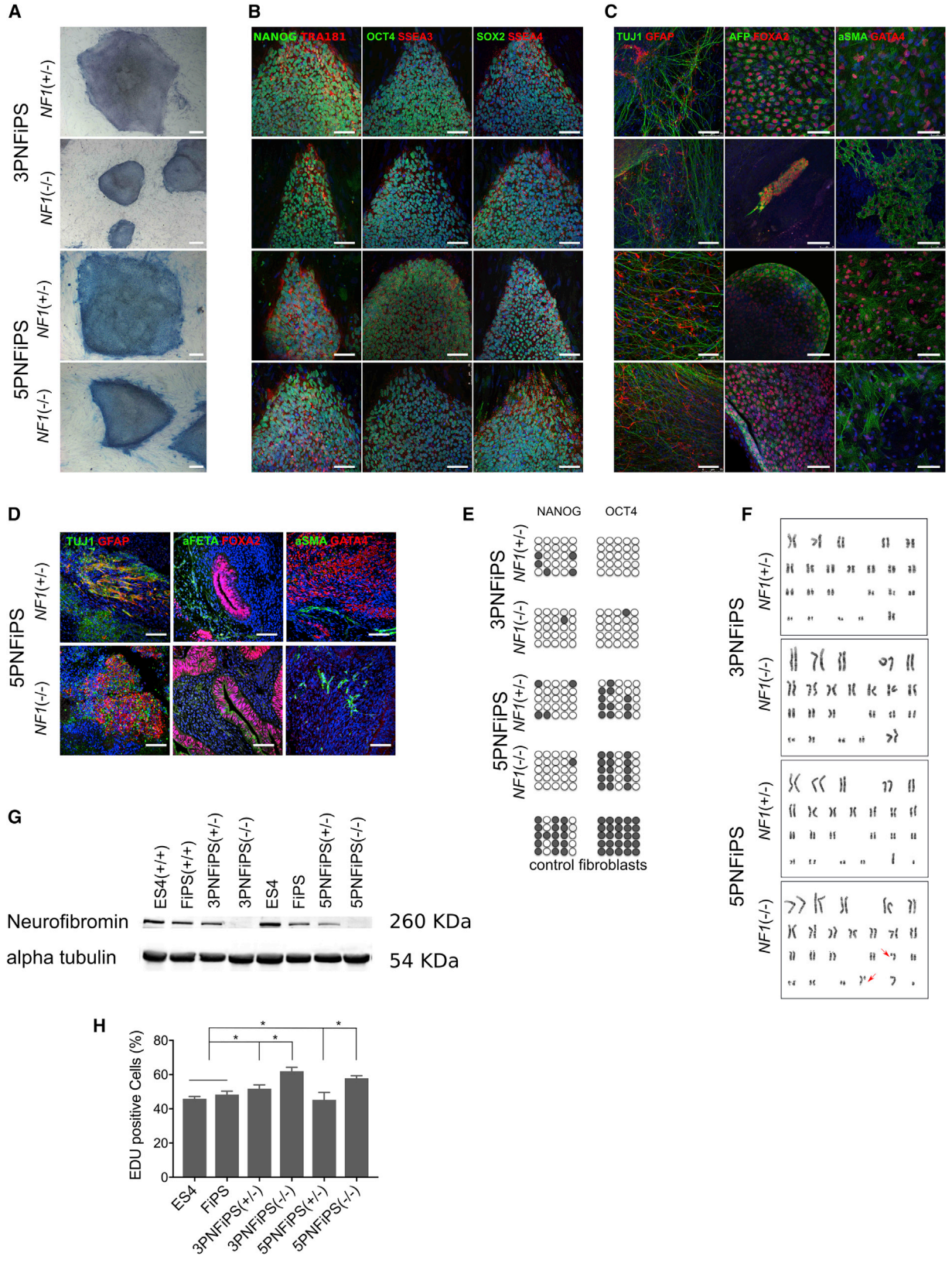

(legend on next page)

gene were found in four of the tumors and consisted in either large deletions of 1.4 Mb (7PNF) and 3.8 Mb (5PNF), both involving the *NF1* and *SUZ12* genes, or homologous recombination (3PNF and 13PNF) generating loss of heterozygosity (LOH) in almost the entire 17q arm (Figure 2B) and bringing the constitutional *NF1* mutation into homozygosity, as described previously (Serra et al., 2001; Steinmann et al., 2009). Somatic *NF1* inactivation in 6PNF was due to a point mutation (Table 1; Figure S1). The same somatic *NF1* inactivation was shared by PNF and its derived *NF1*(−/−) SC culture, but was not present in fibroblast cultures or in *NF1*(+/−) iPSCs (Figures 2 and S3). We also performed exome sequencing to identify the presence of small pathogenic variants. On average, we identified the presence of ten additional point mutations in the whole exome of PNF-derived iPSCs that were not present in PNFs or primary SC cultures (Figure 2C; Table S3). The low number of mutations is consistent with the reprogramming and clonal expansion of a cell already containing these mutations, which would not be detectable in the bulk cell population of PNFs or primary SC cultures. None of the identified somatic point mutations was recurrent among the five PNFs (data not shown for 13PNF). These results are in agreement with data from recent exome analysis of PNFs and CNFs (Gosline et al., 2017; Pemov et al., 2017).

Neural Crest Differentiation of PNF-Derived iPSCs

We posit that PNF-derived iPSCs constitute a non-perishable cell-based experimental system that should facilitate the identification of the PNF cell of origin as well as the development of therapeutic strategies against these types of tumors. Thus, we next set out to differentiate PNF-derived iPSCs toward the NC-SC axis. To generate NCs, we used a previously described differentiation protocol that employs chemically defined medium to activate Wnt signaling while inhibiting Activin/Nodal/transforming growth factor β signaling (Lee et al., 2007; Menendez et al., 2013) (see Supplemental Experimental Procedures for details).

Control PSCs, as well as all *NF1*(+/−) and *NF1*(−/−) PNF-derived iPSC lines tested, successfully differentiated toward NC cells when applying this protocol. Approximately 12 days after NC induction, cells adopted a stellate morphology typical of NCs (Figure 3A), which was maintained throughout the passages. To characterize the generated NCs we performed flow cytometry analysis using two specific NC markers, p75 (*NGFR*) and HNK1 (Lee et al., 2010), at early (7–10 days, passage 1) and late (>20 days, passage 4–5) differentiation stages (Figure 3B). Although both markers were heterogeneously expressed in early passages, NCs from both control and PNF-derived iPSCs homogeneously co-expressed high levels of p75 and HNK1 at later differentiation stages, indicating a clear NC identity. NCs cultured under these specific conditions could be maintained as a stable, self-renewing population for up to 20 passages without losing NC identity (see below), enabling the freezing and cryopreservation of NC batches for subsequent differentiation assays.

NC identity was further confirmed by immunofluorescence (Figure 3C) and qRT-PCR (Figure 3D) analyses of the NC markers SOX10, p75, and AP2. qRT-PCR analyses also showed that PSC-derived NCs did not express the pluripotency-associated marker OCT4 (*POU5F1*), or the SC lineage-specific marker S100b, present in PNF-derived SCs (Figure 3D). Moreover, we also functionally tested NC biological capacities such as migration and differentiation potential. A scratch assay showed the ability of all NCs (control and PNF derived) to start migrating already at 6 h and to be able to close the scratch in less than 24 h (Figure S4A). Furthermore, PSC-derived NCs were able to undergo further differentiation into NC-derived cell types, such as peripheral neurons and melanocytes (Figure S4B), confirming their NC multi-lineage differentiation ability.

Figure 1. Characterization of PNF-Derived iPSC Lines

(A) Morphology and alkaline phosphatase staining of 3PNF and 5PNF iPSC colonies. Scale bars, 100 μm.

(B) Characterization of pluripotency markers. Representative images of 3PNF and 5PNF iPSC colonies stained positive for the pluripotency-associated markers NANOG, OCT4, and SOX2 (in green), and TRA-1-81, SSEA3, and SSEA4 (in red). Scale bars, 100 μm.

(C) *In vitro* differentiation potential of 3PNF and 5PNF iPSC lines. Generation of cell derivatives of the three primary germ layers including ectoderm (TUJ1 in green and GFAP in red), endoderm (AFP in green and FOXA2 in red) and mesoderm (SMA in green and GATA4 in red). Scale bars, 100 μm.

(D) Teratoma formation from 5PNF iPSC, showing their differentiation toward ectoderm (TUJ1 in green and GFAP in red), endoderm (AFP in green and FOXA2 in red) and mesoderm (SMA in green and GATA4 in red). Scale bars, 100 μm.

(E) Bisulphite sequencing showing demethylation of *NANOG* and *POU5F1* promoters in the 3PNF and 5PNF iPSC lines.

(F) Karyotype of 3PNF and 5PNF iPSC lines at passage 20.

(G) Western blot analysis showing the absence of neurofibromin in 3PNFiPS(−/−) and 5PNFiPS(−/−). The human embryonic stem cell (hESC) line ES4 and a control iPSC line generated from foreskin fibroblasts (FiPS), both *NF1*(+/+), were used as control cell lines.

(H) Proliferation capacity of 3PNF and 5PNF iPSC lines assessed by Click-iT EdU Flow Cytometry Assay. Double-positive cells (in S phase) are represented in the graph. Bars represent means from three independent experiments.*$p < 0.05$ (unpaired t tests).

Please cite this article in press as: Carrió et al., Reprogramming Captures the Genetic and Tumorigenic Properties of Neurofibromatosis Type 1 Plexiform Neurofibromas, Stem Cell Reports (2019), https://doi.org/10.1016/j.stemcr.2019.01.001

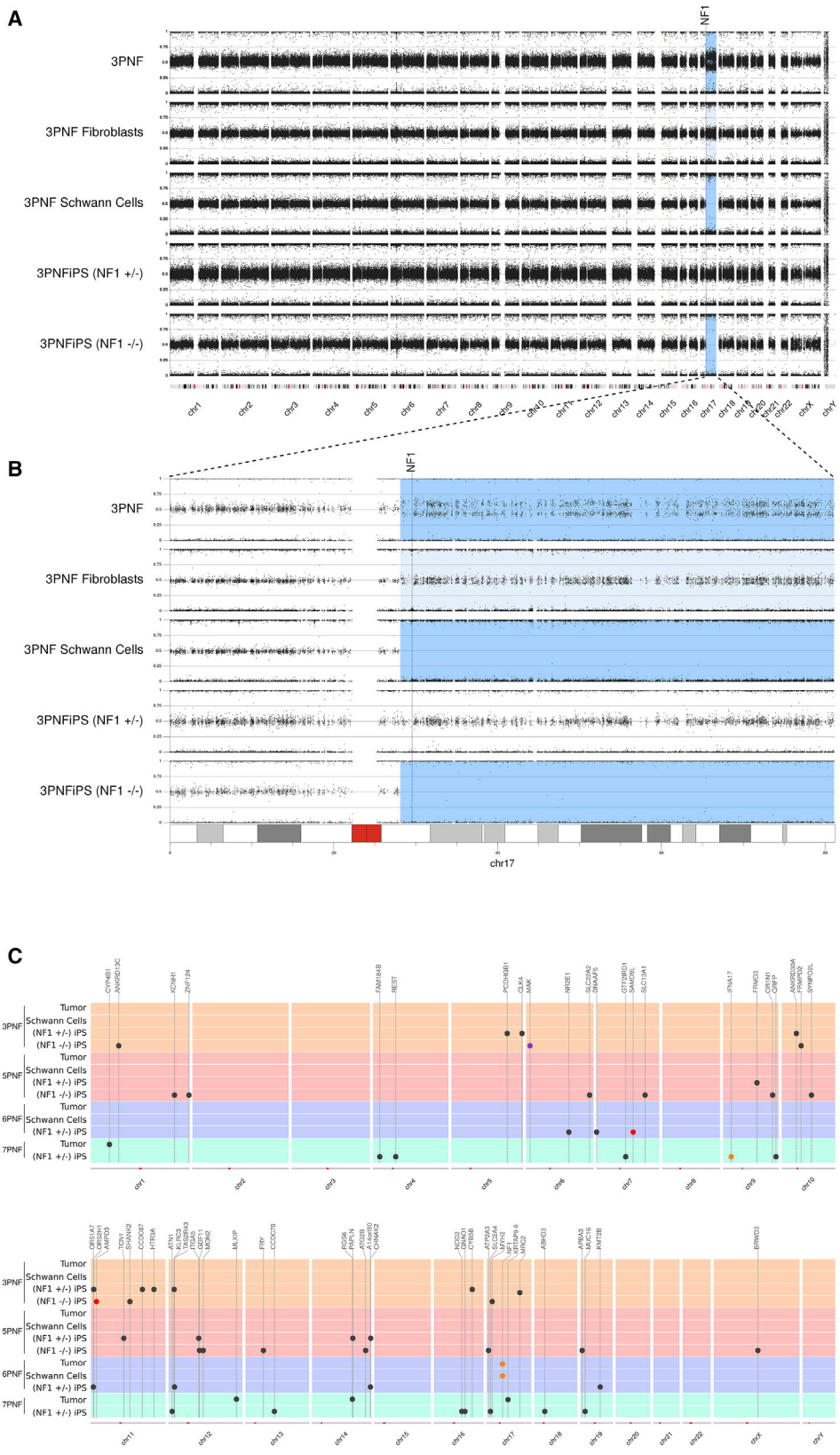

(legend on next page)

SC Differentiation of PNF-Derived NCs

We then set up an SC differentiation protocol starting from the established NCs. We differentiated NCs from control FiPS and PNF-derived iPSC lines into SCs (Figure 4A) (see Supplemental Experimental Procedures). The differentiation process was monitored by immunocytochemistry and qRT-PCR analysis of various markers of the NC-SC lineage at different time points (7, 14, and 30 days).

After 7 days under SC differentiation conditions, NCs from *NF1*(+/+) control FiPS already changed morphology, becoming more elongated. This phenotype progressed over time until reaching the typical bipolar spindle-like morphology of SCs between 14 and 30 days of differentiation (Figure 4B). SC markers such as p75 and S100b were expressed homogenously in the culture throughout the whole differentiation process (Figure 4B). qRT-PCR analysis confirmed expression of NC-SC lineage-specific markers throughout the differentiation process (Figure 4D). *NGFR* and *SOX10*, two key regulators of NC formation and SC fate determination, persisted during the entire differentiation process. Expression of SC precursor markers such as *CDH19*, *ITG4A*, and *MPZ* had a remarkable increase after 7 days of differentiation. *GAP43* was also highly expressed. SC markers such as *PLP*, *PMP22*, and S100b were already detected after 1 week of differentiation and reached maximum expression by day 30. *EGR2* (*KROX20*), a master regulator for myelinating SC was detected already in NCs and had a peak at 30 days of differentiation, as reported previously (Jessen and Mirsky, 2005; Reiprich et al., 2010) (Figure 4D).

At 7 days of differentiation *NF1*(−/−) NCs resembled control *NF1*(+/+) cells, both morphologically and according to SC marker expression (p75 and S100b) (Figure 4C). After 14 days of differentiation, *NF1*(−/−) cells already acquired the slender, elongated morphology of SCs. However, whereas control *NF1*(+/+) cultures progressively stopped proliferation, maintaining a homogeneous expression of SC markers, *NF1*(−/−) cells continued to exhibit a high proliferation capacity and heterogeneously expressed some of the markers, such as S100b (Figure 4C). This altered differentiation process of *NF1*(−/−) SCs was also observed by qRT-PCR analysis (Figure 4E). While markers of the NC-SC lineage were expressed in differentiation *NF1*(−/−) SC cultures, those markers related to SC maturation were not maintained through the differentiation process compared with control *NF1*(+/+).

NF1(−/−) Differentiating SCs Exhibited a Continuous High Proliferation Rate and a Lack of Myelination Capacity

NF1(−/−) differentiating SCs proliferated so much during differentiation experiments that cultures were generated with a high cell density and a natural tendency to form sphere-like structures visible to the naked eye. Spheres grew either attached to the plate surface or as free-floating cultures resembling 3D spheroids (Figures 5A and 5B). We quantified the proliferation capacity of differentiating SCs by Ki-67 immunostaining (Figure 5C), confirming a statistically significant higher proliferation rate in *NF1*(−/−) cells, both at 7 and at 30 days of SC differentiation, compared with control *NF1*(+/+) and *NF1*(+/−) cell lines (Figure 5D).

In addition to the proliferation rate of differentiating SCs, we also tested their ability to myelinate axons. *NF1*(+/+) FiPS-derived SCs, co-cultured with rat dorsal root ganglion (DRG) neurons in the presence of myelinating medium, were capable of associating and myelinating peripheral neuron axons, as demonstrated by the co-localization of S100b/myelin protein zero (MPZ)-positive cells with neuron-specific tubulin (TUJ1)-positive axons (Figure 5E). We identified fragments of myelinated axons longer than 400 μm in three independent experiments (Figure S5). These functional assays confirmed the myelinating capacity of FiPS-derived SCs and validated the protocol used to differentiate NCs into SCs. However, when we co-cultured *NF1*(−/−) iPSC-derived SCs with DRG neurons, they kept proliferating during the assay and were not able to properly associate and form myelinating axons, neither cells growing in monolayer nor sphere-forming cells, as happens in PNFs (Figure 5F). *NF1*(−/−) differentiating SCs generated either spheres or wide lanes of organized cells. In addition, *NF1*(−/−) cells expressed the

Figure 2. Genomic Characterization of PNFs, Primary Cells, and Generated iPSCs

(A) B allele frequency (BAF) data from SNP array analysis characterizing the genomic structure of five samples associated with 3PNF tumor; fibroblasts; PNF-derived Schwann cells; 3PNFiPS(+/−) and 3PNFiPS(−/−). The genome of all samples was mostly 2n, denoted by a BAF signal around 0.5. A blue shaded region indicates somatic copy neutral (CN)-loss of heterozygosity (LOH).

(B) A detailed view of BAF for chromosome 17. Somatic *NF1* inactivation was produced by mitotic recombination generating CN-LOH in 17q and the reduction to homozygosity for the constitutional *NF1* mutation. LOH is observed in 3PNF and in 100% of cells in 3PNF-derived Schwann cells and in 3PNFiPS(−/−). Fibroblast primary culture (3PNF fibroblasts) is an early passage and still exhibit a residual LOH due to the presence of "contaminating" tumor SCs.

(C) Summary of somatic exonic variants identified by exome sequencing. All samples associated with a PNF are represented by wide horizontal line of the same color covering all chromosomes. Color dots indicate the type of genetic variant: missense (black), frameshift (orange), in-frame deletion (purple), and non-sense (red). Position of genes containing the variants is marked with vertical lines.

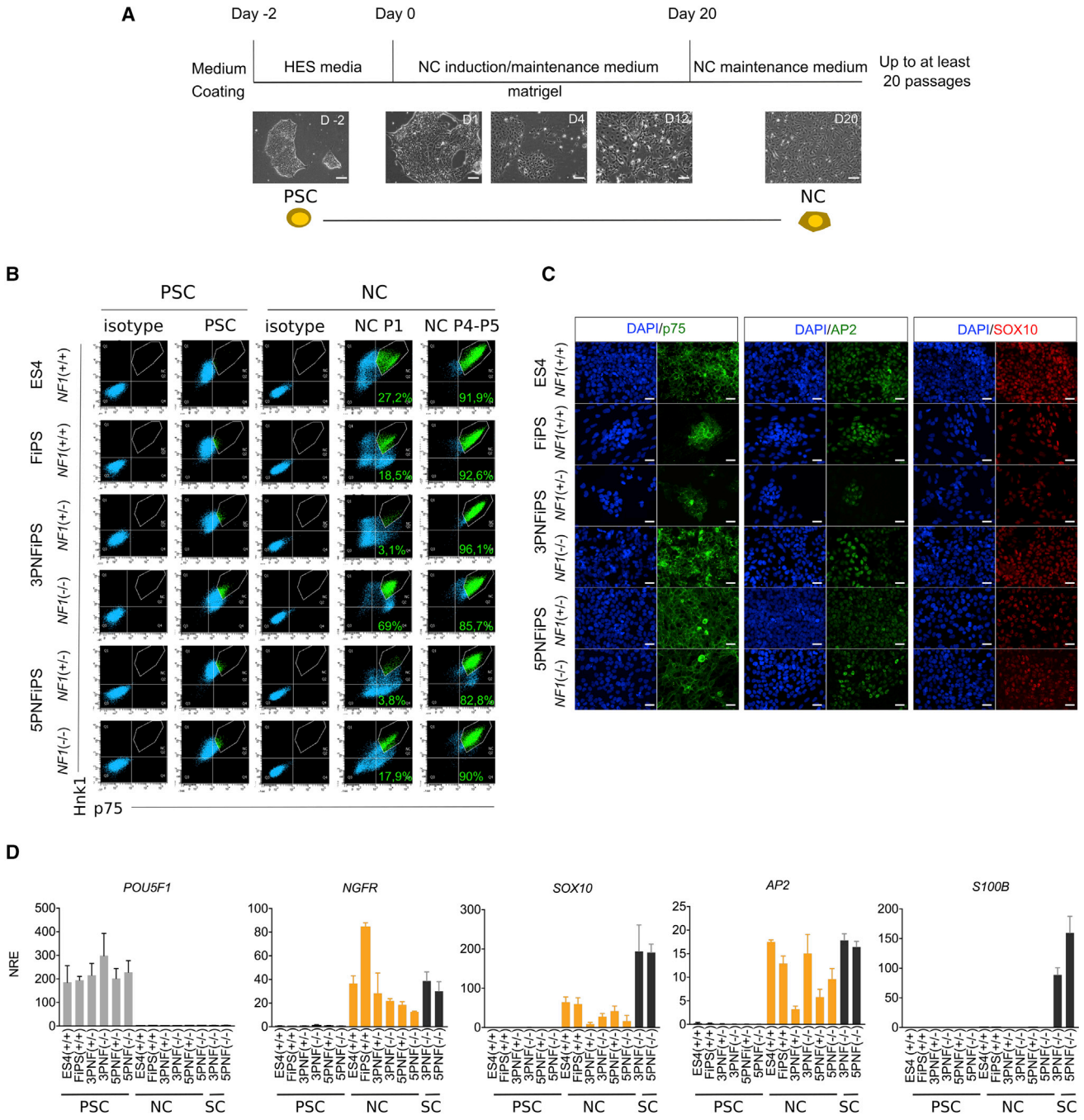

Figure 3. PNF-Derived iPSCs Correctly Differentiate into NCs

(A) Schematic representation of the protocol used for differentiating iPSCs into NCs. Control (ES4 and FiPS) and PNF-derived iPSCs were seeded on Matrigel and cultured in NC induction medium for 20 days (see Supplemental Experimental Procedures). Representative bright-field images during the differentiation process over time (in days, D) are shown. PSC, pluripotent stem cell. Scale bar, 50 μm.

(B) Flow cytometry analysis for p75 and Hnk1 before and after NC differentiation. The percentage of double p75 and Hnk1-positive cells is shown inside the graph. P1, passage 1; P4-5, passages 4–5.

(legend continued on next page)

neuronal marker TUJ1, complicating the analysis. Since TUJ1 was not expressed by *NF1*(+/+) differentiating SCs in the co-culture assay, we analyzed PNF-derived primary SC cultures and found that they also expressed TUJ1 (Figure 5G).

Sphere-Forming SCs from *NF1*(−/−) iPSCs Recapitulate the Expression Pattern of Their PNF-Derived Primary SC Counterparts

To have a better idea to which extent sphere-forming *NF1*(−/−) differentiating SCs from PNF-derived iPSCs recapitulated the expression of their primary PNF counterparts, we compared the expression of SC markers in *NF1*(−/−) spheres at 30 days of differentiation with the expression of their parental PNF-derived primary SCs (Figure 6A). In contrast to the heterogeneous expression of SC markers (s100b) exhibited by differentiating SCs growing in monolayer (Figure 4C), sphere-forming SCs homogeneously expressed all markers tested. When we analyzed the expression of p75, s100b, SOX10, GAP43, and PLP by immunofluorescence, the expression pattern of PNF-derived SCs and sphere-forming SCs were strikingly similar (Figure 6A).

Sphere-forming SCs bore the same genetic and genomic content as their primary SC counterparts and recapitulated both a high proliferation rate and the same expression pattern in a homogeneous manner. Taking everything together, *NF1*(−/−) iPSC-derived spheres represent a valuable experimental model to study PNF formation, and to test potential therapeutic options *in vitro* (Figure 6B).

DISCUSSION

There exists a lack of imperishable cell-based systems to model benign tumor progression and assay therapeutic strategies. PNFs are benign SC tumors of the peripheral nervous system associated to NF1 that can progress toward a malignant soft tissue sarcoma. We have generated *NF1*(−/−) iPSC lines directly from PNFs, sharing the same constitutional and somatic *NF1* mutations as the cell originating them. We also generated five independent *NF1*(+/−) iPSCs from five PNFs, two being isogenic to the *NF1*(−/−) iPSC lines established. These cells have the genetic and genomic content of their parental primary cells, and can be differentiated toward NCs and further to SCs. SCs derived from *NF1*(−/−) iPSCs exhibit a high proliferation rate, show poor ability to myelinate, and show a tendency to form spheres in culture that resemble PNFs and preserve the same expression marker profile of the NC-SC axis as their parental *NF1*(−/−) primary SCs.

iPSC technology has been used to reprogram cancer cells, encountering different obstacles, like the chromosomal and genomic composition of cancer cells or the necessity of remodeling their epigenetic state. The *NF1*(−/−) iPSCs described here may have overcome these problems since they have been generated from benign tumors. Reprogramming technology has been previously used to model hereditary cancer syndromes (Papapetrou, 2016), NF1 among them (Anastasaki et al., 2015; Larribere et al., 2015; Wegscheid et al., 2018), but never from cells of the associated tumors. PNFs have the potential to progress to malignancy. In this regard, we believe that these iPSCs could constitute an excellent model for investigating tumor progression when combined with existing DNA-editing tools (CRISPR-Cas9) to better identify the genetic and epigenetic changes required for malignant transformation.

Even though the relatively low number of samples complicates drawing strong conclusions, we noticed that the efficiency of generating *NF1*(−/−) iPSC lines from PNFs (also *NF1*(+/−)) varied depending on the tumor and on the starting cell type. Different factors could be involved, such as the culture conditions used, the different reprogramming efficiency of distinct cell types (reviewed in Ebrahimi, 2015) or the age of the PNF donor, although all these aspects would need to be further explored.

Whereas *NF1*(+/+) differentiating SCs progressively stopped proliferation, maintained a homogeneous expression of SC markers, and had the capacity to myelinate axons, *NF1*(−/−) cells continued exhibiting a high proliferation capacity and heterogeneously expressed S100b during differentiation, and exhibit a poor ability to myelinate axons. These results are consistent with the biological status of SCs within PNFs. The exact mechanism and role of the *NF1* gene in relation to the altered SC differentiation is an exciting topic for further research.

The PNF-resembling spheres generated by the high proliferation capacity of differentiating SCs from PNF-derived *NF1*(−/−) iPSCs constitute a very promising non-perishable model for PNFs, even more so taking into account that currently there is no tumoroid model generated directly from primary PNF cells. An *in vitro* 3D PNF model

(C) Immunocytochemistry analysis showing that both control (ES4 and FiPS) and PNF-derived iPSCs differentiated to NCs (passage 5) express p75 (green), AP2 (green), and SOX10 (red). DAPI was used to stain cell nuclei. Scale bar, 50 μm.
(D) qRT-PCR expression analysis of pluripotent (*POU5F1*), NC (*NGFR, SOX10, AP2*), and SC (*S100B*) markers, in pluripotent cells (PSCs), PSCs differentiated to NCs and PNF-derived SCs. qRT-PCR values are expressed as the mean normalized relative expression (NRE) ± SEM from three independent differentiation experiments.

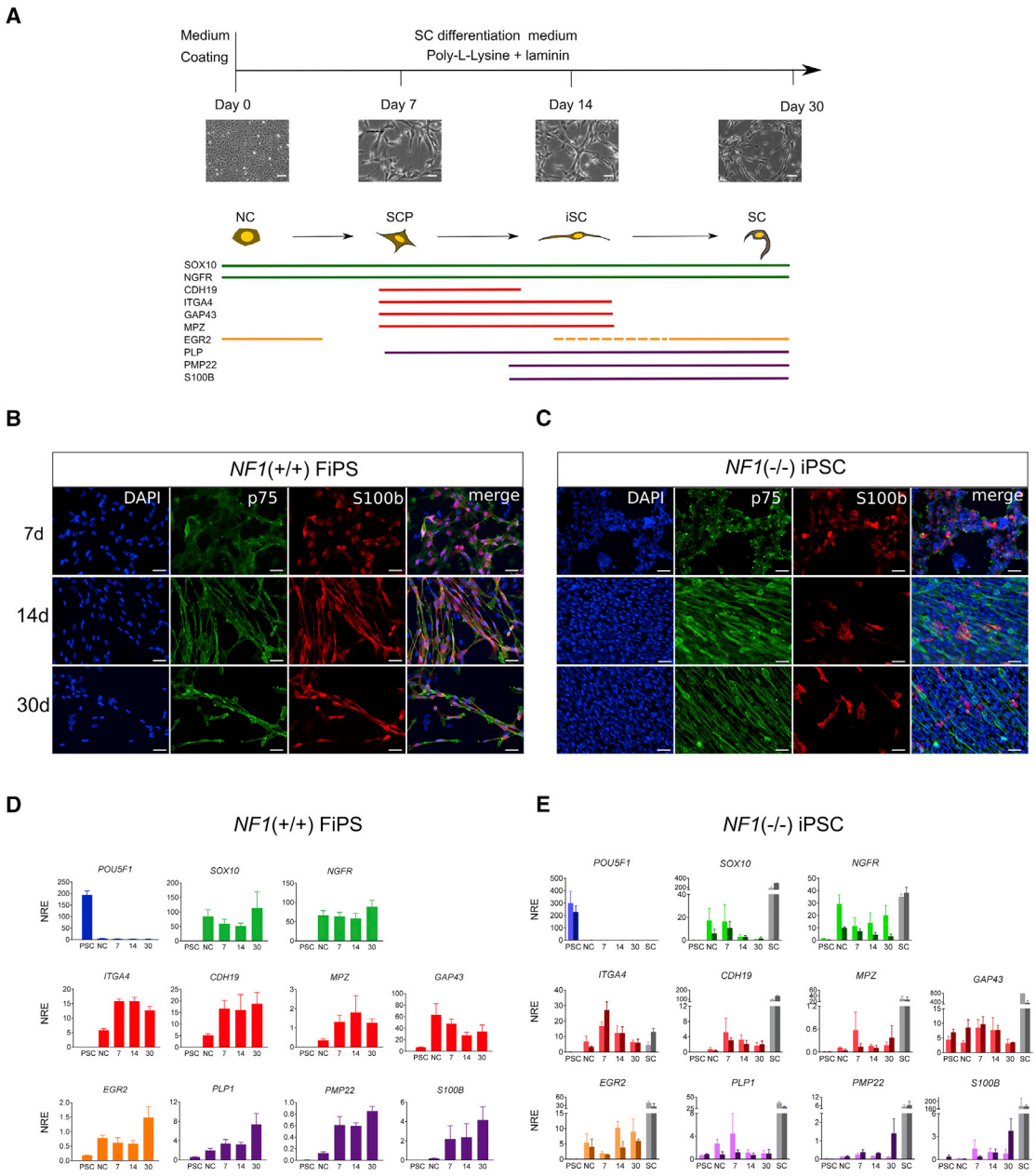

Figure 4. Schwann Cells Differentiation of iPSC-Derived NCs

(A) Top: schematic representation of the protocol used for differentiating NCs to Schwann cells (SCs). NCs were seeded on poly-L-lysine and laminin-coated plates and cultured in SC differentiation medium (see Supplemental Experimental Procedures). After 7, 14, and 30 days, SC differentiation was monitored by qRT-PCR and immunocytochemistry analysis. Representative bright-field images during the differentiation process from a control cell line are shown. Scale bars, 50 μm. Bottom: diagram showing the expression of markers associated with the NC-SC lineage. The colored horizontal bars represent the temporal window during differentiation when the corresponding marker is expressed *in vivo*, according to the literature (Jessen and Mirsky, 2005). SCP, Schwann cell precursor; iSC, immature Schwann cells (iSCs).
(B and C) Immunocytochemical analysis for S100b and p75 at different stages of SC differentiation (7, 14, and 30 days) in control *NF1*(+/+) FiPS (B) and 3PNFiPS(−/−) cells (C). DAPI was used to stain cell nuclei. Scale bars, 50 μm.
(D and E) qRT-PCR in control *NF1*(+/+) FiPS (D) and *NF1*(−/−) iPSCs (E) at five different time points during differentiation: pluripotent stage (PSC), neural crest stage (NC) and at 7, 14, or 30 days of SC differentiation. For *NF1*(−/−) iPSC graphs (E): light bar represents SC differentiation for 3PNF and dark bar for 5PNF. As control cells for marker expression, primary SC cultures (gray bars) from 3PNF (light gray) and 5PNF (dark gray) were used. Values are expressed as the mean NRE ± SEM from three independent differentiation experiments.

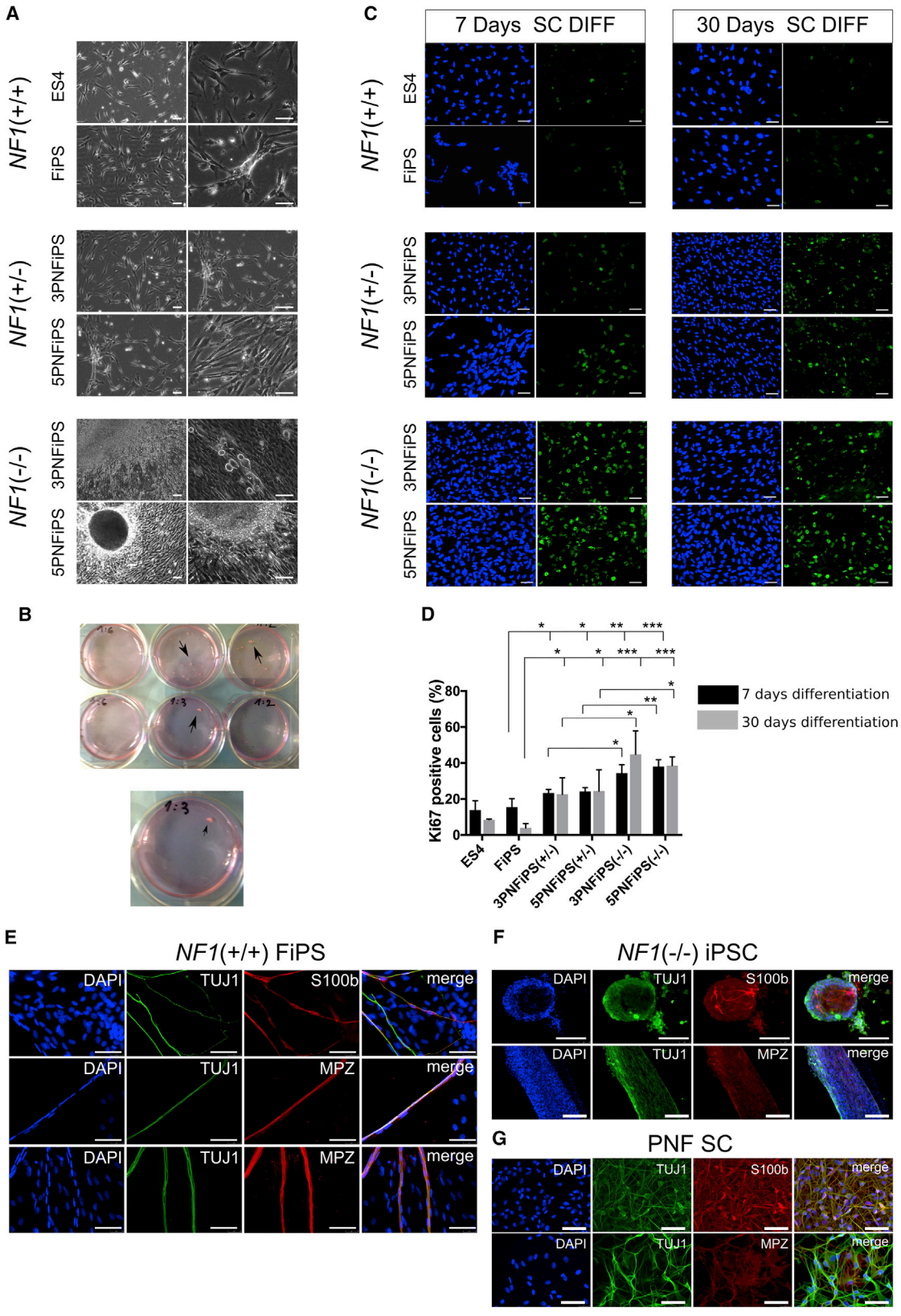

(legend on next page)

will facilitate the testing of therapeutic agents in a PNF-resembling environment before jumping to an *in vivo* model, although further development will be necessary.

In the field of NF1 research, there is still an open debate regarding the cell of origin of neurofibromas (Buchstaller et al., 2012). PNFs are thought to be congenital but the identity and biological capacity of the cell type that receives the inactivation of *NF1* is still not completely understood. Essential information has been obtained from the different genetically modified mouse models that develop PNFs in which *NF1* ablation is driven by Cre recombinase expressed under promoters active along the NC-SC differentiation axis. The ability to differentiate PNF-derived iPSCs toward NCs and SCs could complement the information coming from genetically modified mice.

In summary, we have generated *NF1*(−/−) iPSCs directly from PNFs. They represent an iPSC-based non-perishable cell model system for a benign tumor. *NF1*(−/−) iPSCs contain the same naturally occurring mutations as their primary counterparts and preserve their proliferative properties when differentiated from NCs toward SCs. SCs differentiated from PNF-derived iPSCs have a high tendency to form spheres. This cell-based model system constitutes a great tool to investigate the PNF cell of origin, the genetic and epigenetic changes required for progression toward MPNSTs and finally, a model to test new therapeutic strategies before pre-clinical *in vivo* models.

EXPERIMENTAL PROCEDURES

Patients, Plexiform Neurofibromas, and Tumor Processing

Tumor samples were kindly provided by NF1 patients after giving written informed consent for iPSC generation and genomic analysis studies. The study was approved by our Institutional Review Board and local ethical commitees. The patients were diagnosed according to standard diagnostic criteria (DeBella et al., 2000). Tumor specimens were obtained after surgery of five PNFs from five independent patients (two males, three females; ages 8–66 years). Immediately after excision, tumor samples were placed in DMEM medium (Gibco) containing 10% FBS (Gibco) + 1× Glx (Gibco) + 1× normocin antibiotic cocktail (InvivoGene), and shipped at room temperature to our laboratory. Tumors were processed as follows: surrounding fat tissue and skin were removed and tumors were cut into 1-mm pieces and cryopreserved in 10% DMSO (Sigma) + 90% FBS until used.

PNF-Derived SCs and Fibroblasts Cultures

PNF-derived SCs and fibroblasts were isolated as described previously (Serra et al., 2000). In brief, PNF pieces that were preserved in liquid nitrogen were thawed and digested with 160 U/mL collagenase type 1 and 0.8 U/mL dispase (Worthington, Lakewood, NJ) for 16 h at 37°C. Dissociated cells were washed and seeded onto 0.1 mg/mL poly-L-lysine (Sigma) and 4 μg/mL laminin (Gibco)-coated dishes in Schwann cell medium (SCM) and maintained at 37°C under a 10% CO_2 atmosphere. SCM is DMEM (Gibco) with 10% FBS, 500 U/mL penicillin/500 μg/mL streptomycin (Gibco), 0.5 mM 3-iso-butyl-1-methilxantine (Sigma), 2.5 mg/mL insulin (Sigma), 10 nM heregulin-β1 (PeproTech), and 0.5 μM forskolin (Sigma). One day after plating, culture medium was replaced by SCM without forskolin for an additional 2–3 days. This process was repeated in cycles and cells were passaged as needed with trypsin 0.05% (Gibco). SC purity was assessed by performing S100β staining as described previously (Serra et al., 2000). To isolate fibroblasts, dissociated cells were plated in DMEM 10% FBS media and passaged when necessary.

Reprogramming of SCs, Fibroblasts, and Digested Tumors

Between 1 × 10^4 and 2 × 10^4 cells were reprogrammed through the retroviral delivery of human cDNA coding for OCT4, SOX2, KLF4, and cMYC transcription factors as described previously (Raya et al., 2009). For non-integrative reprogramming, a Cytotune-iPS 2.0 Sendai Reprogramming Kit (Thermo Fisher Scientific) was used according to the manufacturer's protocol. Approximately 3 or 4 weeks after transduction, colonies displaying embryonic stem cell-like morphology and behavior were selected for further characterization and genotyping. iPSC established lines were grown on dishes coated with growth factor-reduced Matrigel (BD Biosciences) in mTESR1 medium (STEMCELL Technologies). See Supplemental Information for a detailed description of iPSC characterization.

Figure 5. *NF1*(−/−) Differentiating SCs Exhibited a Continuous High Proliferation Rate and a Lack of Myelinating Capacity

(A) Representative bright-field images after 20 days of differentiation from NC to SC for different *NF1* genotypes. 3PNFiPS(−/−) and 5PNFiPS(−/−) cells exhibited a high cell density and the formation of 3D spheres. Scale bars, 50 μm.

(B) Macroscopic detail of sphere formation in 3PNiPS(−/−) and 5PNFiPS(−/−) cells during SC differentiation.

(C) Proliferation capacity of differentiating SCs. Representative immunofluorescence images of Ki-67 (green) at 7 and 30 days of differentiation. DAPI was used to stain cell nuclei. Scale bars, 50 μm.

(D) Quantification of Ki-67-positive cells (percentage over total DAPI-positive nuclei) expressed as the mean ± SE (n = 3 independent differentiation experiments). At least 300 nuclei were counted per time point and sample. *p < 0.05, **p < 0.01, ***p < 0.001 (unpaired t test).

(E and F) Myelination capacity of control *NF1*(+/+) FiPS (E) and *NF1*(−/−) iPSCs (F). Myelination was assessed by co-culturing differentiated SCs (at 7 days) with rat DRG neurons for 30 days. SC myelination capacity was measured by immunostaining for TUJ1, S100b, and MPZ. Scale bars, 50 μm.

(G) PNF-derived SC immunostained with TUJ1, S100b, and MPZ. Scale bars, 50 μm.

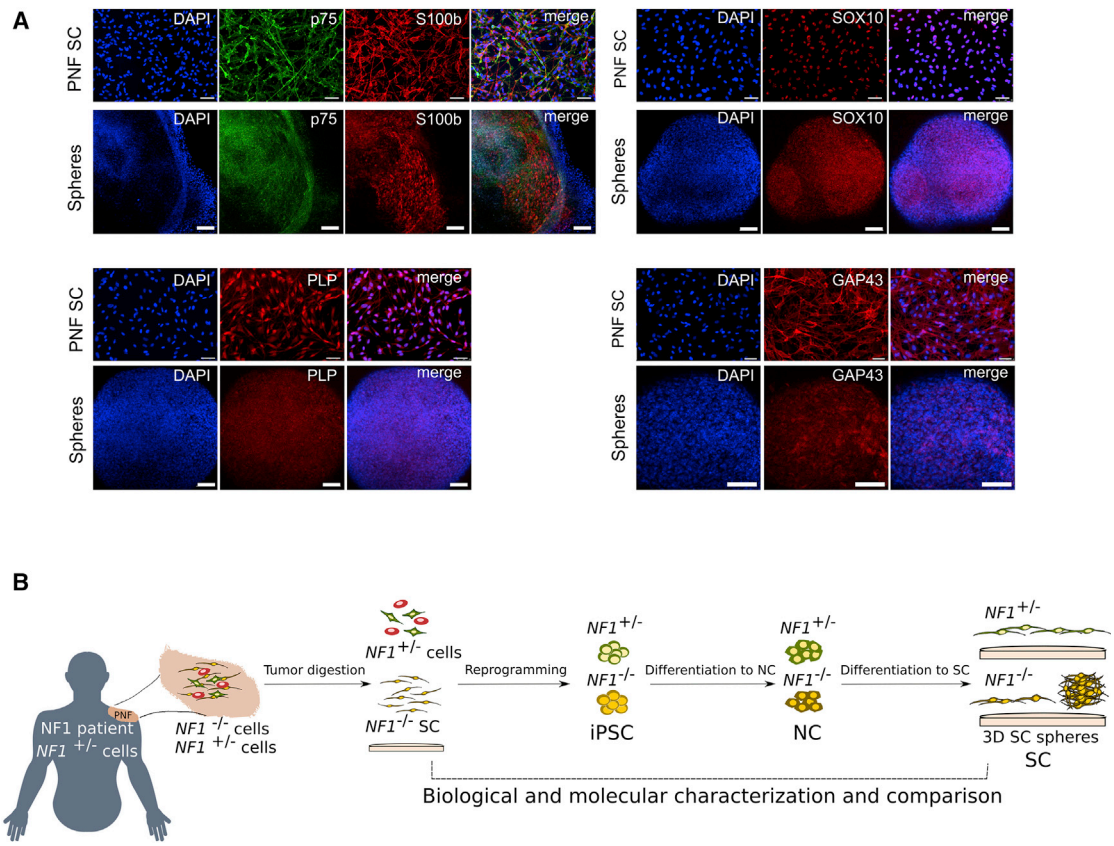

Figure 6. Sphere-Forming SCs from *NF1*(−/−) iPSCs Recapitulate the Expression Pattern of their PNF-Derived Primary SC Counterparts

(A) Representative immunofluorescence images showing expression of S100b, p75, SOX10, GAP43, and PLP, in 5PNF primary SCs (PNF SC) compared with sphere-forming 5PNFiPS(−/−) differentiating SCs, at 30 days of differentiation. Scale bars, 100 μm.

(B) Schematic representation of the generated PNF model.

Differentiation toward NCs and SCs

Neural crest differentiation was performed as described by Menendez et al. (2013) with some modifications. In brief, 9 × 10^4 cells/cm^2 were plated onto Matrigel-coated plates in mTESR medium. The following day, the medium was replaced with hESC maintenance medium: DMEM:F12 (Gibco) 1:1; 5 mg/mL BSA (Sigma); 500 U/mL penicillin/500 μg/mL streptomycin (Gibco); 2 mM GlutaMAX (Gibco); 1× MEM non-essential amino acids (Gibco); 1× trace elements A; 1× trace elements B; 1× trace elements C (Corning); 2-mercaptoethanol (Gibco); 10 μg/mL transferrin (Sigma); 50 μg/mL sodium L-ascorbate (Sigma); 10 ng/mL heregulin-β1 (PeproTech); 10 ng/mL activin A (PeproTech); 200 μg/mL LONG R3 IGFR (PeproTech); 8 ng/mL basic fibroblast growth factor 2 (PeproTech). Next day, the medium was replaced with neural crest induction/differentiation medium: hESC medium without activin and supplemented with 2 μM CHIR9902 (STEMCELL Technologies) and 20 μM SB432542 (STEMCELL Technologies), and was replaced every day. NCs were maintained in this medium and split with Accutase (Thermo Fischer Scientific) when necessary.

For SC differentiation NCs were plated onto 0.1 mg/mL poly-L-lysine (Sigma) and 4 μg/mL laminin (Gibco)-coated plates and cultured in SC differentiation medium: DMEM:F12 (3:1); 500 U/ml penicillin/500 μg/mL streptomycin antibiotics (Gibco); 5 μM forskolin (Sigma); 50 ng/mL heregulin-β1; 2% N2 supplement (Gibco); 1% FBS (Gibco). The medium was replaced twice a week.

Additional Experimental Procedures

Additional experimental procedures can be found in Supplemental Information.

REPOSITORIES

The iPSC lines generated have been banked banked and are currently distributed by the Spanish National Stem Cell Bank-Institute of Health Carlos III in compliance with the informed consent signed by the patient (see Table 1).

ACCESSION NUMBERS

Data are available at the Synapse repository with accession number syn17413894 (DOI: 10.7303/syn17413894.1) (https://www.synapse.org/#!Synapse:syn17413894/tables/).

SUPPLEMENTAL INFORMATION

Supplemental Information includes Supplemental Experimental Procedures, five figures, and five tables and can be found with this article online at https://doi.org/10.1016/j.stemcr.2019.01.001.

AUTHOR CONTRIBUTIONS

E.S. conceived the study. M.C., Y.R.-P., A.R., and E.S. designed the study and wrote the manuscript that was revised, corrected, and improved by all authors. M.C., H.M., and Y.R.-P. performed most of the experimental work. B.G. performed bioinformatic analysis. I.R. and E.C. performed NF1 genetic analysis. E.T., S.J.-D., J.B., and L.V. performed experimental work. I.B. and C.L. provided scientific input. M.C. and B.G. generated the figures for the paper. All authors approved the final version of the manuscript.

ACKNOWLEDGMENTS

This work has mainly been supported by an agreement from the Johns Hopkins University School of Medicine and the Neurofibromatosis Therapeutic Acceleration Program (NTAP). Its contents are solely the responsibility of the authors and do not necessarily represent the official views of the Johns Hopkins University School of Medicine. The work has also been partially supported by the Spanish Ministry of Science and Innovation, Carlos III Health Institute (ISCIII) (PI14/00577; PI17/00524; RD16/0011/0024; and PIE14/00061) Plan Estatal de I. D. i 2013–16; co-financed by the FEDER program; and by the Government of Catalonia (2017-SGR-899) and CERCA Program/Generalitat de Catalunya. We thank the patients and their physicians who contributed the original samples. We would like to specially thank the Asociación de Afectados de Neurofibromatosis for their constant support and coordination with patients. We also give thanks for the support of ACNefi and the Spanish Association Against Cancer (AECC) for recognizing our group with one of its awards. We thank the IGTP core facilities and their staff for their contribution and technical support: Translational Genomics Core Facility; High Content Genomics and Bioinformatics Core Facility; Flow Cytometry (Gerard Requena and Marco A. Fernández); Microscopy Core facility (Gerard Requena). We also thank the National Center for Genomic Analysis (CNAG). Finally, we would like to thank Dr. Jaishri Blakeley, Dr. Sharad Verma, and people at NTAP for their constant support and appreciate insightful discussions of the different PIs funded by the NTAP Cell Culture Initiative.

Received: June 11, 2018
Revised: December 31, 2018
Accepted: January 1, 2019
Published: January 31, 2019

REFERENCES

Anastasaki, C., Woo, A.S., Messiaen, L.M., and Gutmann, D.H. (2015). Elucidating the impact of neurofibromatosis-1 germline mutations on neurofibromin function and dopamine-based learning. Hum. Mol. Genet. *24*, 3518–3528.

Ban, H., Nishishita, N., Fusaki, N., Tabata, T., Saeki, K., Shikamura, M., Takada, N., Inoue, M., Hasegawa, M., Kawamata, S., and Nishikawa, S. (2011). Efficient generation of transgene-free human induced pluripotent stem cells (iPSCs) by temperature-sensitive Sendai virus vectors. Proc. Natl. Acad. Sci. U S A *108*, 14234–14239.

Beert, E., Brems, H., Daniels, B., De Wever, I., Van Calenbergh, F., Schoenaers, J., Debiec-Rychter, M., Gevaert, O., De Raedt, T., Van Den Bruel, A., et al. (2011). Atypical neurofibromas in neurofibromatosis type 1 are premalignant tumors. Genes Chromosomes Cancer *50*, 1021–1032.

Bernhardt, M., Novak, D., Assenov, Y., Orouji, E., Knappe, N., Weina, K., Reith, M., Larribere, L., Gebhardt, C., Plass, C., et al. (2017). Melanoma-derived iPCCs show differential tumorigenicity and therapy response. Stem Cell Rep. *8*, 1379–1391.

Buchstaller, J., Clapp, D.W., Parada, L.F., and Zhu, Y. (2012). Cell of origin and the contribution of microenvironment in NF1 tumorigenesis and therapeutic implications. In Neurofibromatosis Type 1:Molecular and Cellular Biology, M. Upadhyaya and D.N. Cooper, eds. (Springer Berlin Heidelberg), pp. 549–568.

Carrió, M., Gel, B., Terribas, E., Carolina Zucchiatti, A., Moliné, M., Rosas, I., Teulé, A., Ramón y Cajal, S., López-Gutiérrez, J.C., Blanco, I., et al. (2018). Analysis of intra-tumor heterogeneity in neurofibromatosis type 1 plexiform neurofibromas and neurofibromas with atypical features: correlating histological and genomic findings. Hum. Mutat. *39*, 1112–1125.

Castellanos, E., Gel, B., Rosas, I., Tornero, E., Santín, S., Pluvinet, R., Velasco, J., Sumoy, L., Del Valle, J., Perucho, M., et al. (2017). A comprehensive custom panel design for routine hereditary cancer testing: preserving control, improving diagnostics and revealing a complex variation landscape. Sci. Rep. *7*, 39348.

Chen, Z., Liu, C., Patel, A.J., Liao, C.-P., Wang, Y., and Le, L.Q. (2014). Cells of origin in the embryonic nerve roots for NF1-associated plexiform neurofibroma. Cancer Cell *26*, 695–706.

Däschner, K., Assum, G., Eisenbarth, I., Krone, W., Hoffmeyer, S., Wortmann, S., Heymer, B., and Kehrer-Sawatzki, H. (1997). Clonal origin of tumor cells in a plexiform neurofibroma with LOH in NF1 intron 38 and in dermal neurofibromas without LOH of the NF1 gene. Biochem. Biophys. Res. Commun. *234*, 346–350.

DeBella, K., Szudek, J., and Friedman, J.M. (2000). Use of the National Institutes of Health criteria for diagnosis of neurofibromatosis 1 in children. Pediatrics *105* (3 Pt 1), 608–614.

Dombi, E., Baldwin, A., Marcus, L.J., Fisher, M.J., Weiss, B., Kim, A., Whitcomb, P., Martin, S., Aschbacher-Smith, L.E., Rizvi, T.A., et al. (2016). Activity of selumetinib in neurofibromatosis type 1-related plexiform neurofibromas. N. Engl. J. Med. *375*, 2550–2560.

Ebrahimi, B. (2015). Reprogramming barriers and enhancers: strategies to enhance the efficiency and kinetics of induced pluripotency. Cell Regen. (Lond) *4*, 10.

Ferner, R.E. (2007). Neurofibromatosis 1 and neurofibromatosis 2: a twenty-first century perspective. Lancet Neurol. *6*, 340–351.

Garcia-Linares, C., Fernández-Rodríguez, J., Terribas, E., Mercadé, J., Pros, E., Benito, L., Benavente, Y., Capellà, G., Ravella, A., Blanco, I., et al. (2011). Dissecting loss of heterozygosity (LOH) in neurofibromatosis type 1-associated neurofibromas: importance of copy neutral LOH. Hum. Mutat. *32*, 78–90.

Gosline, S.J.C., Weinberg, H., Knight, P., Yu, T., Guo, X., Prasad, N., Jones, A., Shrestha, S., Boone, B., Levy, S.E., et al. (2017). A high-throughput molecular data resource for cutaneous neurofibromas. Sci. Data *4*, 170045.

Higham, C.S., Dombi, E., Rogiers, A., Bhaumik, S., Pans, S., Connor, S.E.J., Miettinen, M., Sciot, R., Tirabosco, R., Brems, H., et al. (2018). The characteristics of 76 atypical neurofibromas as precursors to neurofibromatosis 1 associated malignant peripheral nerve sheath tumors. Neuro. Oncol. *20*, 818–825.

Hirbe, A.C., Dahiya, S., Miller, C.A., Li, T., Fulton, R.S., Zhang, X., McDonald, S., DeSchryver, K., Duncavage, E.J., Walrath, J., et al. (2015). Whole exome sequencing reveals the order of genetic changes during malignant transformation and metastasis in a single patient with NF1-plexiform neurofibroma. Clin. Cancer Res. *21*, 4201–4211.

Jessen, K.R., and Mirsky, R. (2005). The origin and development of glial cells in peripheral nerves. Nat. Rev. Neurosci. *6*, 671–682.

Kim, H.A., Ling, B., and Ratner, N. (1997). *Nf1*-deficient mouse Schwann cells are angiogenic and invasive and can be induced to hyperproliferate: reversion of some phenotypes by an inhibitor of farnesyl protein transferase. Mol. Cell. Biol. *17*, 862–872.

Kim, H.A., Rosenbaum, T., Marchionni, M.A., Ratner, N., and DeClue, J.E. (1995). Schwann cells from neurofibromin deficient mice exhibit activation of p21ras, inhibition of cell proliferation and morphological changes. Oncogene *11*, 325–335.

Kim, J., Hoffman, J.P., Alpaugh, R.K., Rhim, A.D., Reichert, M., Stanger, B.Z., Furth, E.E., Sepulveda, A.R., Yuan, C.-X., Won, K.-J., et al. (2013). An iPSC line from human pancreatic ductal adenocarcinoma undergoes early to invasive stages of pancreatic cancer progression. Cell Rep. *3*, 2088–2099.

Kim, J., and Zaret, K.S. (2015). Reprogramming of human cancer cells to pluripotency for models of cancer progression. EMBO J. *34*, 739–747.

Kluwe, L., Friedrich, R.E., and Mautner, V.F. (1999). Allelic loss of the NF1 gene in NF1-associated plexiform neurofibromas. Cancer Genet. Cytogenet. *113*, 65–69.

Kotini, A.G., Chang, C.-J., Chow, A., Yuan, H., Ho, T.-C., Wang, T., Vora, S., Solovyov, A., Husser, C., Olszewska, M., et al. (2017). Stage-specific human induced pluripotent stem cells map the progression of myeloid transformation to transplantable leukemia. Cell Stem Cell *20*, 315–328.e7.

Kraniak, J.M., Chalasani, A., Wallace, M.R., and Mattingly, R.R. (2018). Development of 3D culture models of plexiform neurofibroma and initial application for phenotypic characterization and drug screening. Exp. Neurol. *299*, 289–298.

Krone, W., Jirikowski, G., Mühleck, O., Kling, H., and Gall, H. (1983). Cell culture studies on neurofibromatosis (von Recklinghausen). II. Occurrence of glial cells in primary cultures of peripheral neurofibromas. Hum. Genet. *63*, 247–251.

Larribere, L., Wu, H., Novak, D., Galach, M., Bernhardt, M., Orouji, E., Weina, K., Knappe, N., Sachpekidis, C., Umansky, L., et al. (2015). NF1 loss induces senescence during human melanocyte differentiation in an iPSC-based model. Pigment Cell Melanoma Res. *28*, 407–416.

Lee, G., Kim, H., Elkabetz, Y., Al Shamy, G., Panagiotakos, G., Barberi, T., Tabar, V., and Studer, L. (2007). Isolation and directed differentiation of neural crest stem cells derived from human embryonic stem cells. Nat. Biotechnol. *25*, 1468–1475.

Lee, G., Chambers, S.M., Tomishima, M.J., and Studer, L. (2010). Derivation of neural crest cells from human pluripotent stem cells. Nat. Protoc. *5*, 688–701.

Li, H., Chang, L.-J., Neubauer, D.R., Muir, D.F., and Wallace, M.R. (2016). Immortalization of human normal and NF1 neurofibroma Schwann cells. Lab. Invest. *96*, 1105–1115.

Maertens, O., Brems, H., Vandesompele, J., De Raedt, T., Heyns, I., Rosenbaum, T., De Schepper, S., De Paepe, A., Mortier, G., Janssens, S., et al. (2006). Comprehensive NF1 screening on cultured Schwann cells from neurofibromas. Hum. Mutat. *27*, 1030–1040.

Mautner, V.-F., Asuagbor, F.A., Dombi, E., Funsterer, C., Kluwe, L., Wenzel, R., Widemann, B.C., and Friedman, J.M. (2008). Assessment of benign tumor burden by whole-body MRI in patients with neurofibromatosis 1. Neuro. Oncol. *10*, 593–598.

McCarron, K.F., and Goldblum, J.R. (1998). Plexiform neurofibroma with and without associated malignant peripheral nerve sheath tumor: a clinicopathologic and immunohistochemical analysis of 54 cases. Mod. Pathol. *11*, 612–617.

Menendez, L., Kulik, M.J., Page, A.T., Park, S.S., Lauderdale, J.D., Cunningham, M.L., and Dalton, S. (2013). Directed differentiation of human pluripotent cells to neural crest stem cells. Nat. Protoc. *8*, 203–212.

Miller, S.J., Jessen, W.J., Mehta, J., Hardiman, A., Sites, E., Kaiser, S., Jegga, A.G., Li, H., Upadhyaya, M., Giovannini, M., et al. (2009). Integrative genomic analyses of neurofibromatosis tumours identify SOX9 as a biomarker and survival gene. EMBO Mol. Med. *1*, 236–248.

Muir, D., Neubauer, D., Lim, I.T., Yachnis, A.T., and Wallace, M.R. (2001). Tumorigenic properties of neurofibromin-deficient neurofibroma Schwann cells. Am. J. Pathol. *158*, 501–513.

Packer, R.J., and Rosser, T. (2002). Therapy for plexiform neurofibromas in children with neurofibromatosis 1: an overview. J. Child Neurol. *17*, 638–641.

Pan, X.-Y., Tsai, M.-H., Wuputra, K., Ku, C.-C., Lin, W.-H., Lin, Y.-C., Kishikawa, S., Noguchi, M., Saito, S., Lin, C.-S., and Yokoyama, K.K. (2017). Application of cancer cell reprogramming technology to human cancer research. Anticancer Res. *37*, 3367–3377.

Papapetrou, E.P. (2016). Patient-derived induced pluripotent stem cells in cancer research and precision oncology. Nat. Med. *22*, 1392–1401.

Peltonen, J., Jaakkola, S., Lebwohl, M., Renvall, S., Risteli, L., Virtanen, I., and Uitto, J. (1988). Cellular differentiation and expression of matrix genes in type 1 neurofibromatosis. Lab. Invest. *59*, 760–771.

Pemov, A., Li, H., Patidar, R., Hansen, N.F., Sindiri, S., Hartley, S.W., Wei, J.S., Elkahloun, A., Chandrasekharappa, S.C., Boland, J.F., et al. (2017). The primacy of NF1 loss as the driver of tumorigenesis in neurofibromatosis type 1-associated plexiform neurofibromas. Oncogene *36*, 3168–3177.

Prada, C.E., Rangwala, F.A., Martin, L.J., Lovell, A.M., Saal, H.M., Schorry, E.K., and Hopkin, R.J. (2012). Pediatric plexiform neurofibromas: impact on morbidity and mortality in neurofibromatosis type 1. J. Pediatr. *160*, 461–467.

Rasmussen, S.A., Overman, J., Thomson, S.A., Colman, S.D., Abernathy, C.R., Trimpert, R.E., Moose, R., Virdi, G., Roux, K., Bauer, M., et al. (2000). Chromosome 17 loss-of-heterozygosity studies in benign and malignant tumors in neurofibromatosis type 1. Genes. Chromosomes Cancer *28*, 425–431.

Ratner, N., and Miller, S.J. (2015). A RASopathy gene commonly mutated in cancer: the neurofibromatosis type 1 tumour suppressor. Nat. Rev. Cancer *15*, 290–301.

Raya, Á., Rodríguez-Pizà, I., Guenechea, G., Vassena, R., Navarro, S., Barrero, M.J., Consiglio, A., Castellà, M., Río, P., Sleep, E., et al. (2009). Disease-corrected haematopoietic progenitors from Fanconi anaemia induced pluripotent stem cells. Nature *460*, 53–59.

Reiprich, S., Kriesch, J., Schreiner, S., and Wegner, M. (2010). Activation of Krox20 gene expression by Sox10 in myelinating Schwann cells. J. Neurochem. *112*, 744–754.

Rosenbaum, T., Boissy, Y.L., Kombrinck, K., Brannan, C.I., Jenkins, N.A., Copeland, N.G., and Ratner, N. (1995). Neurofibromin-deficient fibroblasts fail to form perineurium in vitro. Development *121*, 3583–3592.

Serra, E., Rosenbaum, T., Winner, U., Aledo, R., Ars, E., Estivill, X., Lenard, H.G., and Lázaro, C. (2000). Schwann cells harbor the somatic NF1 mutation in neurofibromas: evidence of two different Schwann cell subpopulations. Hum. Mol. Genet. *9*, 3055–3064.

Serra, E., Rosenbaum, T., Nadal, M., Winner, U., Ars, E., Estivill, X., and Lázaro, C. (2001). Mitotic recombination effects homozygosity for NF1 germline mutations in neurofibromas. Nat. Genet. *28*, 294–296.

Steinmann, K., Kluwe, L., Friedrich, R.E., Mautner, V.-F., Cooper, D.N., and Kehrer-Sawatzki, H. (2009). Mechanisms of loss of heterozygosity in neurofibromatosis type 1-associated plexiform neurofibromas. J. Invest. Dermatol. *129*, 615–621.

Takahashi, K., and Yamanaka, S. (2006). Induction of pluripotent stem cells from mouse embryonic and adult fibroblast cultures by defined factors. Cell *126*, 663–676.

VM, and Riccardi. (1992). Neurofibromatosis: Phenotype, Natural History, and Pathogenesis, Second Edition (Johns Hopkins University Press).

Wallace, M.R., Rasmussen, S.A., Lim, I.T., Gray, B.A., Zori, R.T., and Muir, D. (2000). Culture of cytogenetically abnormal Schwann cells from benign and malignant NF1 tumors. Genes. Chromosomes Cancer *27*, 117–123.

Wegscheid, M.L., Anastasaki, C., and Gutmann, D.H. (2018). Human stem cell modeling in neurofibromatosis type 1 (NF1). Exp. Neurol. *299*, 270–280.

Stem Cell Reports, Volume *12*

Supplemental Information

Reprogramming Captures the Genetic and Tumorigenic Properties of Neurofibromatosis Type 1 Plexiform Neurofibromas

Meritxell Carrió, Helena Mazuelas, Yvonne Richaud-Patin, Bernat Gel, Ernest Terribas, Imma Rosas, Senda Jimenez-Delgado, Josep Biayna, Leen Vendredy, Ignacio Blanco, Elisabeth Castellanos, Conxi Lázaro, Ángel Raya, and Eduard Serra

FIGURE S1

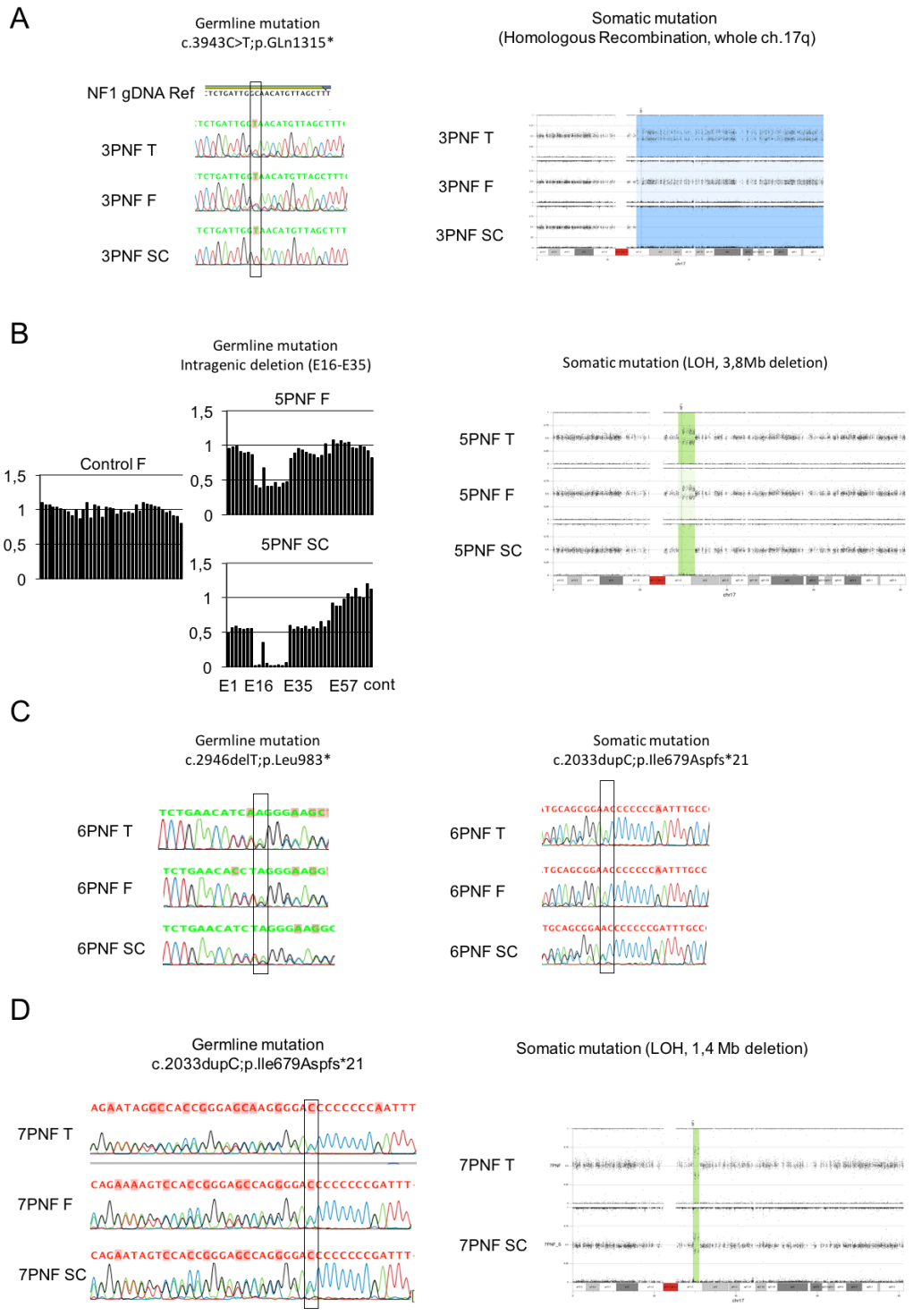
A
Germline mutation
c.3943C>T;p.GLn1315*
NF1 gDNA Ref
3PNF T
3PNF F
3PNF SC
Somatic mutation
(Homologous Recombination, whole ch.17q)
3PNF T
3PNF F
3PNF SC
B
Germline mutation
Intragenic deletion (E16-E35)
Control F
5PNF F
5PNF SC
1,5
1
0,5
0
E1 E16 E35 E57 cont
Somatic mutation (LOH, 3,8Mb deletion)
5PNF T
5PNF F
5PNF SC
C
Germline mutation
c.2946delT;p.Leu983*
6PNF T
6PNF F
6PNF SC
Somatic mutation
c.2033dupC;p.Ile679Aspfs*21
6PNF T
6PNF F
6PNF SC
D
Germline mutation
c.2033dupC;p.Ile679Aspfs*21
7PNF T
7PNF F
7PNF SC
Somatic mutation (LOH, 1,4 Mb deletion)
7PNF T
7PNF SC

Figure S1. *NF1* germline and somatic mutation analysis in the four PNFs used to generate the banked iPSC lines.

A) 3PNF *NF1* mutational analysis. Left: Sanger sequencing showing the germline mutation c.3943C>T;p.GLn1315* in the *NF1* gene. The germline mutation is present in the tumor (3PNF T), in tumor fibroblasts (3PNF F) and in tumor SC (3PNF SC). Right: B-allele frequency (BAF) data (a detailed view from chromosome 17) from SNP-array analysis showing the somatic mutation of 3PNF. Somatic *NF1* inactivation is produced by mitotic recombination generating CN-LOH in 17q and the reduction to homozygosity for the constitutional *NF1* mutation. LOH is observed in 3PNF and in 100% of cells in 3PNF SC. Fibroblast culture (3PNF F) is an early passage and still exhibit a residual LOH due to the presence of tumor SCs.
B) 5PNF *NF1* mutational analysis. Left: MLPA analysis showing an intragenic deletion in the *NF1* gene, from exon 16 (E16) to exon 57 (E57). The deletion is detected in tumor fibroblasts (5PNF F) and in tumor SC (5PNF SC). Right: detailed view of BAF for chromosome 17. Somatic *NF1* inactivation is produced by a deletion generating CN-LOH in 17q and the reduction to homozygosity for the constitutional *NF1* mutation. LOH is observed in 5PNF and in 100% of cells in 5PNF SC.
C) 6PNF *NF1* mutational analysis. Left: Sanger sequencing showing the germline mutation c.2946delT;p.Leu983* present in the tumor (6PNF T), tumor fibroblasts (6PNF F) and tumor SCs (6PNF SC). Right: sanger sequencing showing the somatic mutation c.2033dupC;p.ile679Aspf*21 only present 6PNF SC and not in 6PNF F.
D) 7PNF *NF1* mutational analysis. Left: Sanger sequencing showing the germline mutation c.2033dupC;p.ile679Aspf*21 present in the tumor (7PNF T), tumor fibroblasts (7PNF F) and tumor SC (7 PNF SC). Right: detailed view of BAF for chromosome 17. Somatic *NF1* inactivation is produced by a deletion generating CN-LOH in 17q. LOH is observed in 7PNF and in 7PNF SC.

FIGURE S2

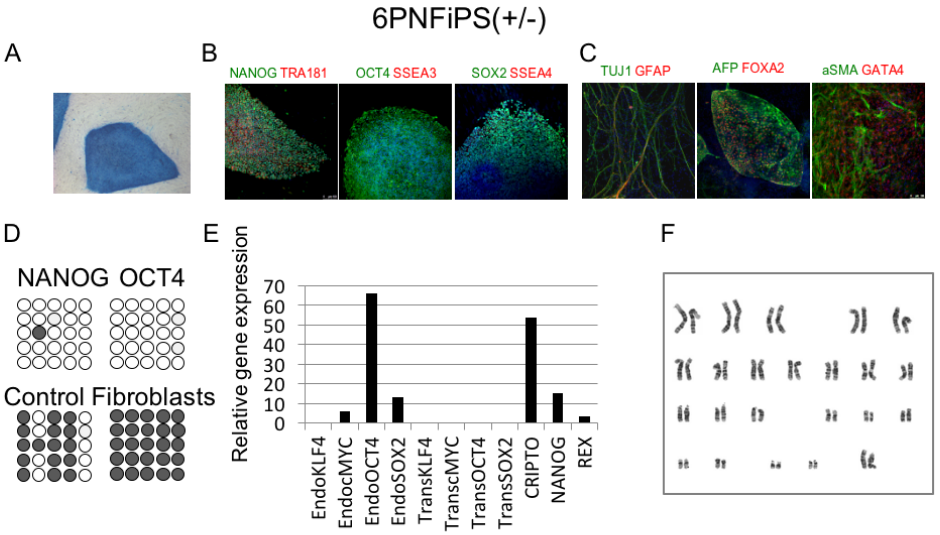

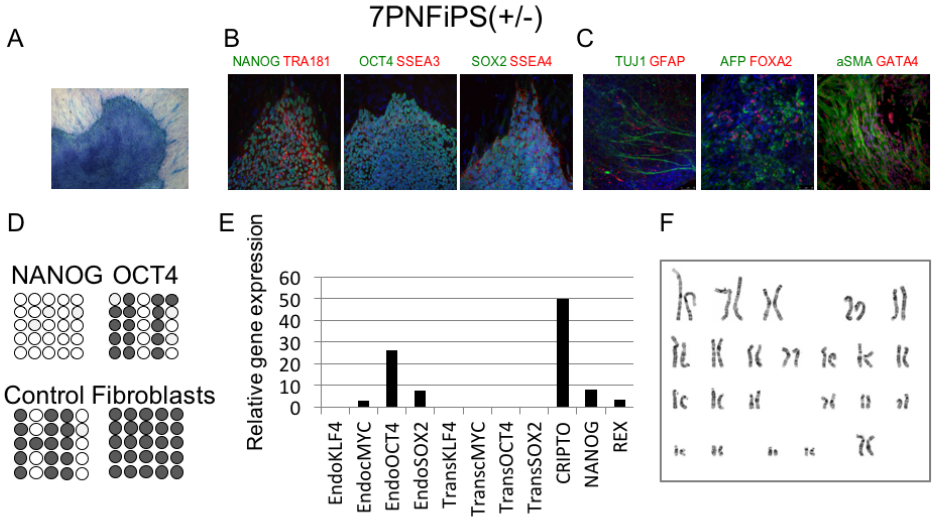

G

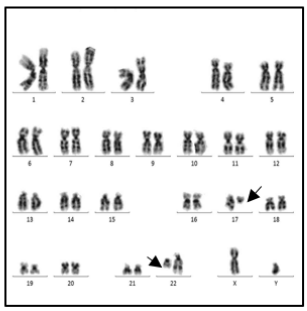

5PNF SC passage 3
46,XY,t(17;22)(q10;q13.3)

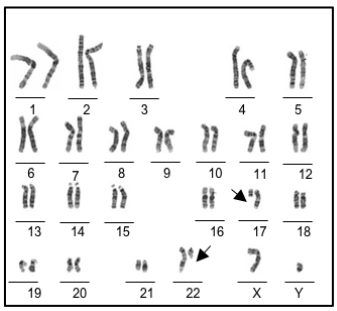

5PNFiPS (NF1-/-) passage 20
46,XY,t(17;22)(q10;q13.3)

Figure S2. iPSC Characterization of the additional banked NF1 iPSCs lines.

A) Morphology and alkaline phosphatase staining of a representative colony. Scale bar: 100µm
B) Pluripotency markers. Scale bar: 100µm
C) *In vitro* differentiation potential. Scale bar: 100µm
D) Bisulphite sequencing showing demethylation of the *NANOG and POU5F1(*OCT4*)* promoters.
E) RT-qPCR analysis characterizing the expression levels of reprogramming genes either endogenous. (iPSC) or retroviral-derived (transgenes). Expression of pluripotency markers (CRIPTO, NANOG, REX) are also shown.
F) karyotypes at passage 20.
G) Karyotype of the 5PNF-derived SCs (5PNF SC) showing the presence of the same translocation t(17;22) as in the 5PNFiPS N(-/-) cell line that causes the somatic *NF1* mutation.

FIGURE S3

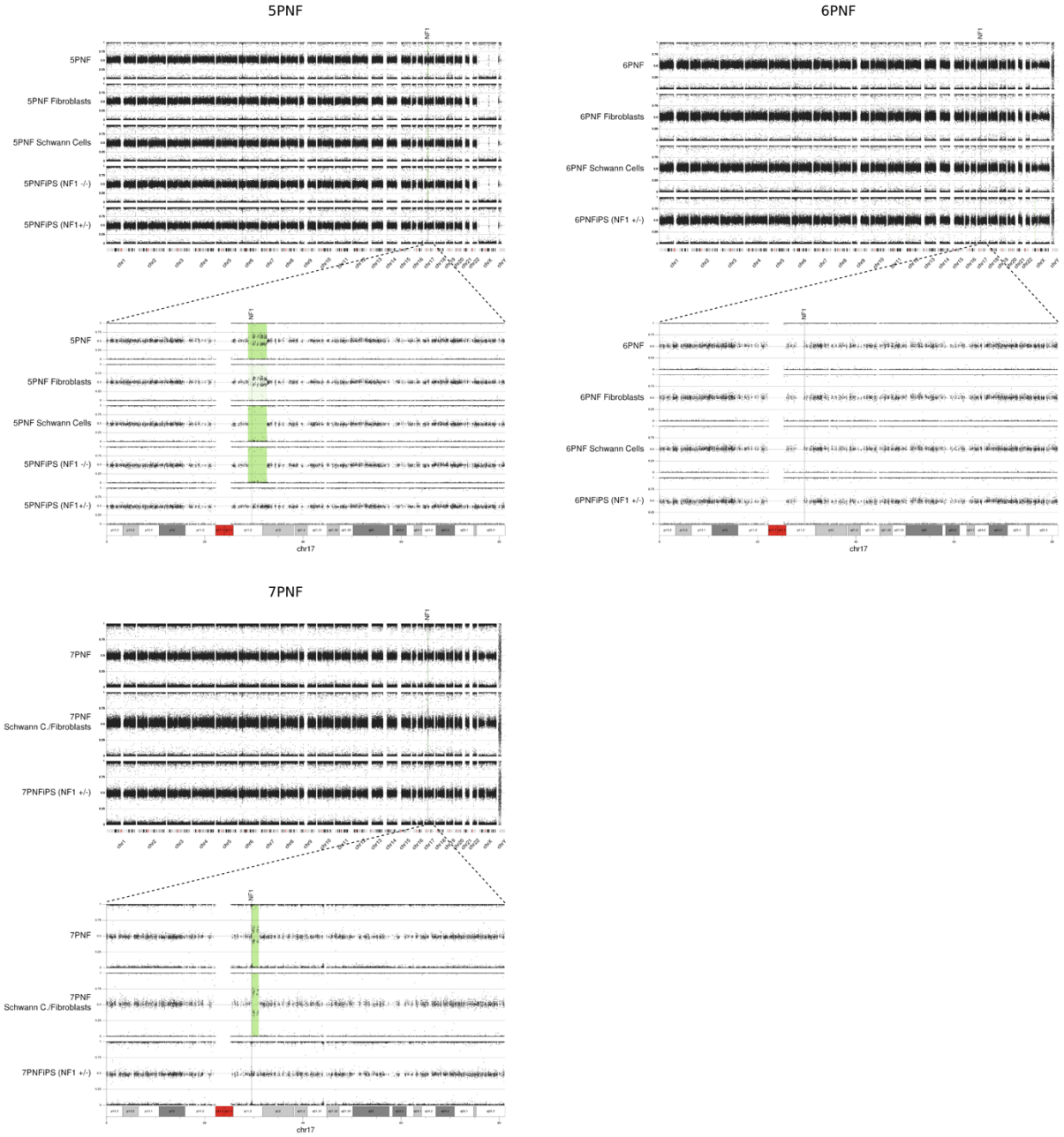

Figure S3. Genomic characterization of tumors, tumor isolated cells and corresponding iPSC lines.

B-allele frequency (BAF) data along the genome is plotted for all samples associated to each PNF. Green shaded regions denote somatic LOH due to genomic loss. Fibroblast cultures from tumor 5PNF are early passages in which LOH can still be detected due to the presence of *NF1*(-/-) Schwann cells. 7PNF Schwann cells/Fibroblasts is a heterogeneous cell culture (60% SC and 40% fibroblasts). The position of *NF1* is marked with a vertical black line.

FIGURE S4

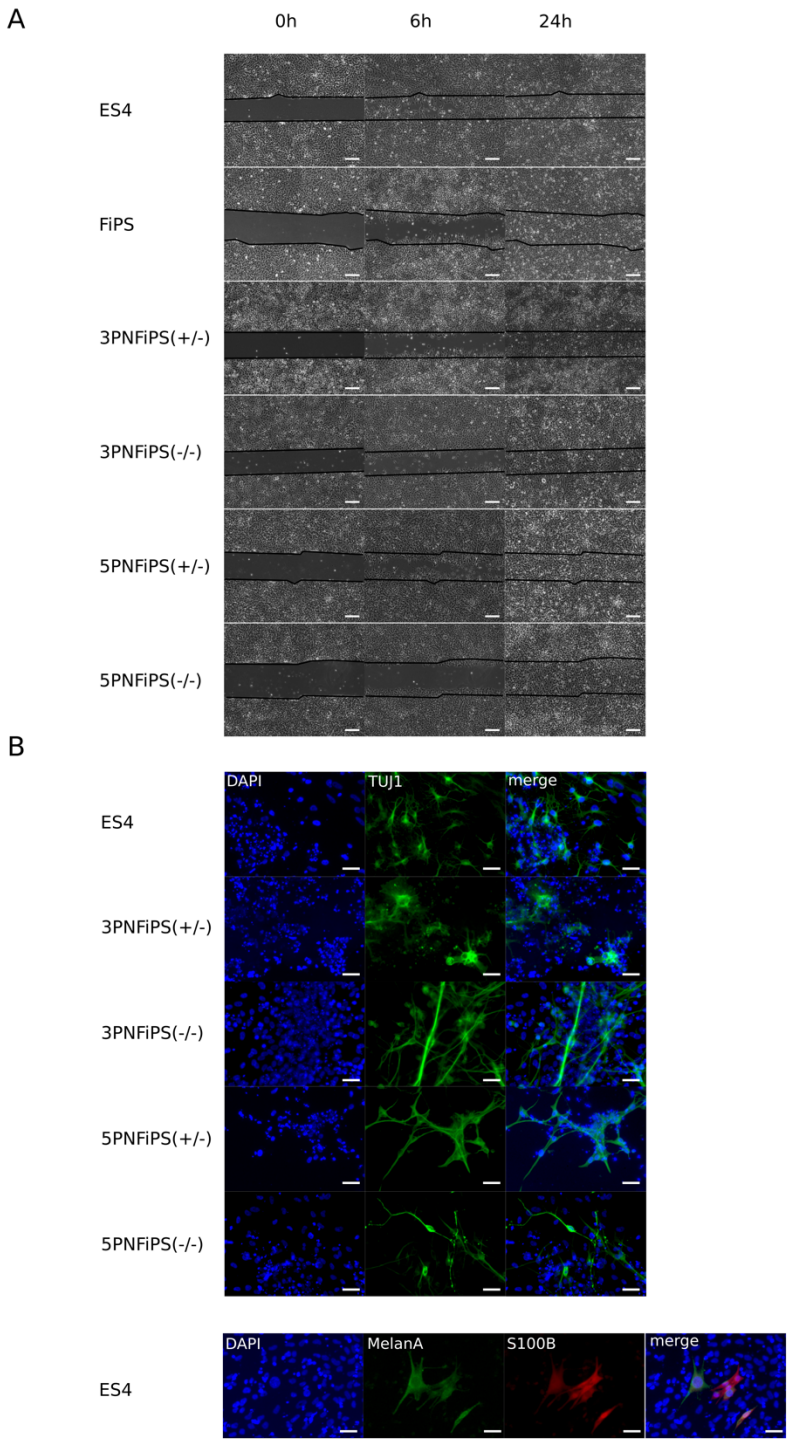

Figure S4. iPSC-derived NCSC lines have the capacity to migrate and differentiate into different NC-derivatives.

A) Scratch assay. A cell free-free gap was created using a pipette tip and migration capacity was measured by taking images of the same region at 6 and 24 hours after gap creation. Scale bar= 150µM. **B)** Differentiation capacity of generated NC towards peripheral neurons (Tuj1+) and melanocytes (MelanA+ and S100B+). Scale bar= 50µM.

FIGURE S5

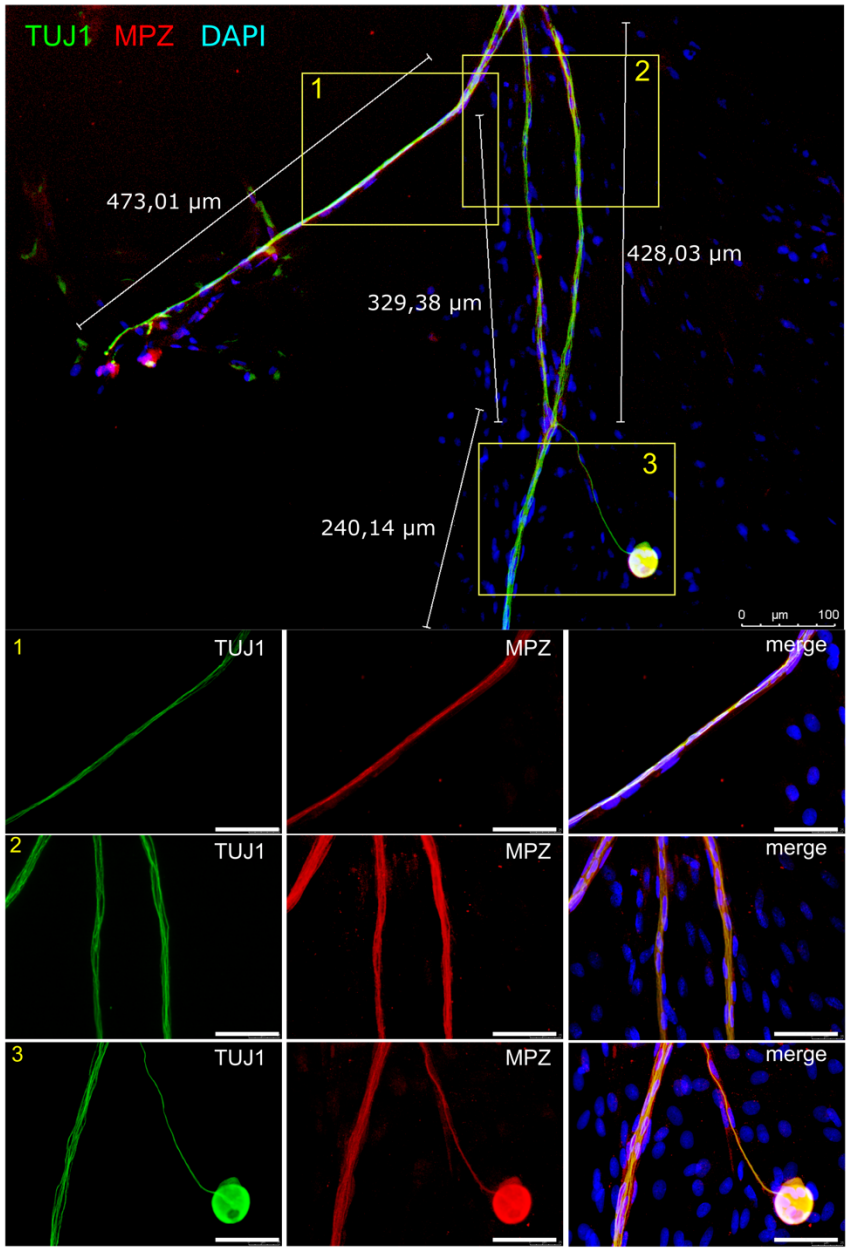

FIGURE S5. Myelin quantification of FiPS-differentiated SC.

The myelination capacity of FiPS-differentiated SCs was assessed by co-culturing cells at 7 days of differentiation with rat DRG neurons for 30 days. SC specification and myelination was measured by immunostaining for TUJ1 (green) andMPZ (red). The length of myelinated axons was measured using LEICA LASAF software and are marked by a white line. Scale bar: 50µm.

TABLE S1. Reprogramming information

TUMOR INFORMATION	REPROGRAMMING INFORMATION						
Tumor ID	Method	Reprogrammed cell	Num. of clones	NF1 mutation			iPSC LINE BANKING NAME
				Germline	Somatic		
					yes	No	
3PNF	Rv	PNF skin fibroblasts*	7	7	7*		
		PNF Schwann cells	10	10	10		
	Sv	PNF skin fibroblasts*	9	9		2	3PNFiPS(+/-) 3PNF_FiPSsv_PM
					7*		
		PNF Schwann cells	12	12	12		3PNFiPS(-/-) 3PNF_SiPSsv_MM
5PNF	Rv	PNF endoneurial fibroblasts	0				
		PNF Schwann cells	2	2	2		5PNFiPS(-/-)_Rv
	Sv	Digested PNF	12	12		1	5PNFiPS(+/-) 5PNF_TDiPSsv_PM
					11		5PNFiPS(-/-) 5PNF_TDiPSsv_MM
6PNF	Rv	PNF endoneurial fibroblasts	1	1	0	1	6PNFiPS(+/-)_Rv
		PNF Schwann cells	10	10	0	10	6PNFiPS(+/-) 6PNF_SiPSrv_PM
	Sv	Digested PNF	10	10	0	10	
7PNF	Rv	PNF endoneurial fibroblasts	1	1	0	1	
		Mix population T(40% PNF Schwann cell, 60% endoneurial fibroblasts)	12	12	0	12	7PNFiPS(+/-) 7PNF_TDiPSrv_PM
13PNF	Sv	PNF endoneurial fibroblasts	11	11	0	11	13PNFiPS(+/-)
		PNF Schwann cells	40	40	0	40	13PNFiPS(+/-)
		Digested PNF	27	27	0	27	

*The skin used was covering the PNF. When skin was separated, part of the tumor was still left.

TABLE S2. Sample authentication.

AmpFISTR Identifiler loci	3PNF	5PNF	6PNF	7PNF
CSF1PO	11,14	10	10,12	11,13
D2S1338	17,24	17,19	17,23	24
D3S1358	15,16	15,16	16,18	15,17
D5S818	10,11	12,13	11,13	10,12
D7S820	10	10,13	11	8,12
D8S1179	10,14	8,13	10,12	13,14
D13S317	8,13	8,12	11,14	8,13
D16S539	9,12	12,13	9,13	11,12
D18S51	13,15	15,16	11,13	12,15
D19S433	12,14.2	14,15	13,14	13,15
D21S11	30,32.2	29	29,30.2	29,30
FGA	21,24	21,23	21,27	20,25
THO1	8,9.3	9,3	7,9.3	6,9.3
TPOX	8	10,11	9,11	10,11

TABLE S3. List of somatic mutations.
The list includes all somatic mutations identified in each sample, meeting the following criteria: exonic or present in canonical splice sites, passing manual validation and excluding synonymous mutations. The list includes only non-*NF1* mutations.
See attached Supplemental_Table_S3.xls

TABLE S4. Primers for RT-qPCR.

Gene	Sequence(5′-3′)		UPL
POU5F1	*Forward*	cttcgcaagccctcatttc	60
	Reverse	gagaaggcgaaatccgaag	
POU3F1	*Forward*	ttctcaagtgccccaagc	78
	Reverse	ccggttgcagaaccagac	
NGFR	*Forward*	ccttccacgctgtctcca	60
	Reverse	cctaggcaagcatcccatc	
SOX10	*Forward*	gacacggttttccacttccta	25
	Reverse	gtcctcgcaaagagtccaac	
TFAP2A	*Forward*	ggtgaaccccaacgaagtc	73
	Reverse	accgtgaccttgtacttcgag	
S100B	*Forward*	ggaaggggtgagacaagga	73
	Reverse	ggtggaaaacgtcgatgag	
CDH19	*Forward*	tgtaccagaggaaatgaatacgac	78
	Reverse	catatatgtcacctgttctttcatca	
ITGA4	*Forward*	atgcaggatcggaaagaatc	78
	Reverse	ccacaaggttctccattaggg	
PLP1	*Forward*	cttcaacacctggaccacct	60
	Reverse	ccatgggagaacaccataca	
GAP43	*Forward*	gctccaagcctgatgagc	12
	Reverse	gctctgtggcagcatcac	
EGR2	*Forward*	gctgctacccagaaggcata	60
	Reverse	ggatgaggctgtggttgaa	
PMP22	*Forward*	ctgtcgatcatcttcagcattc	29
	Reverse	agcactcatcacgcacagac	
MPZ	*Forward*	ttcccatctcctgcatcc	55
	Reverse	ctgggccacctggtagag	
EndoKLF4	*Forward*	agcctaaatgatggtgcttggt	68
	Reverse	ttgaaaactttggcttccttgtt	
EndoMYC	*Forward*	cgggcgggcactttg	55
	Reverse	ggagagtcgcgtccttgct	
EndoOCT4	*Forward*	gggtttttgggattaagttcttca	63
	Reverse	gcccccacccttttgtgtt	
EndoSOX2	*Forward*	caaaaatggccatgcaggtt	63
	Reverse	agttgggatcgaacaaaagctatt	
TransKLF4	*Forward*	tggactacaaggacgacgatga	60
	Reverse	cgtcgctgacagccatga	
TransMYC	*Forward*	tggactacaaggacgacgatga	77
	Reverse	gttcctgttggtgaagctaacgt	
TransOCT4	*Forward*	tggactacaaggacgacgatga	58
	Reverse	caggtgtcccgccatga	
TransSOX2	*Forward*	gctcgaggttaacgaattcatgt	57
	Reverse	gcccggcggcttca	
CRIPTO	*Forward*	cggaactgtgagcacgatgt	66
	Reverse	gggcagccaggtgtcatg	
NANOG	*Forward*	acaactggccgaagaatagca	63
	Reverse	ggttcccagtcgggttcac	
REX	*Forward*	cctgcaggcggaaatagaac	61
	Reverse	gcacacatagccatcacataagg	

TABLE S5. Antibody list.

Antibody	Supplier	Reference	Dilution
Rabbit anti-NF1	Bethyl laboratories	A300-140A	1:1000 (WB)
Mouse IgG anti-OCT3/4	Santa Cruz Biotechnology	Sc-5279	1:60
Rabbit IgG anti-SOX2	Pierce Antibodies	PA1-16968	1:100
Goat IgG anti-NANOG	R&D Systems	AF1997	1:25
Rat IgM anti-SSEA3	Hybridoma Bank	MC-631	1:3
Mouse IgG anti-SSEA4	Hybridoma Bank	MC-813-70	1:3
Mouse IgM anti TRA-1-81	Millipore	MAB4381	1:200
Rabbit IgG anti-alpha-1-fetoprotein	Dako	A0008	1:400
Goat IgG anti-FOXA2	R&D Systems	AF2400	1:50
Rabbit IgG anti-GATA4	Santa Cruz Biotechnology	sc-9053	1:50
Mouse IgG anti SMA	Sigma	A5228	1:400
Mouse IgM anti-ASA	Sigma	A2172	1:400
Mouse IgG anti-TUJ1	Bio Legend	MMS-435P	1:500
Rabbit IgG anti GFAP	Dako	Z0334	1:500
Rabbit IgG anti NF200	Sigma	N4142	1:100
Mouse IgG anti-Nerve growth factor (p75) receptor (ME20.4)	Advanced targeting System	AB-N07	1:100 (IF) 1:1000 (FACS)
Rabbit IgG anti-S100B	Dako	Z0311	1:1000
Mouse IgG anti-AP2	Thermo Scientific	MA1-872	1:50
Rabbit IgG anti-Sox10	Abcam	ac108408	1:50
Mouse IgG anti-MelanA	Ventana	790-2990	1:100
Rabbit IgG anti-MPZ	Abcam	Ab31851	1:500
Rabbit IgG anti-PLP	Abcam	ab28486	1:100
Rabbit IgG anti-GAP43	Novus Biologicals	NB300-143SS	1:500
Mouse IgG anti-Ki67	Santa Cruz Biotechnology	sc-23900	1:50
Mouse IgG anti-HNK1	SIGMA	C6680	1:1000 (FACS)

Extended Methodology

iPSC characterization

Alkaline phosphatase activity was demonstrated using the Alkaline Phosphatase Blue Membrane Substrate Solution (Sigma). Briefly, iPSC were grown on top of mitotically inactivated human foreskin fibroblasts (HFF) during one week. Cells were fixed during 2 min in 3.7% paraformaldehyde and exposed to the substrate solution. After 20 min incubation in the dark, blue staining was evident in iPS colonies. Detection of pluripotency-associated markers (nuclear: OCT4, SOX2 and NANOG; cytoplasmic: SSEA3, SSEA4 and Tra-1-81) was performed on iPSC cultured on HFF for 8 days and fixed with 4% paraformaldehyde (PFA). Then, samples were processed for immunocytochemistry. *In vitro* differentiation ability to the three germ layers was carried out through embryoid body (EB) formation. For endoderm, EBs were plated on 0.1% gelatin (Millipore) coated coverslips and cultured 3 weeks in KODMEM (Gibco) supplemented with 20% fetal bovine serum (Hyclone), 1x penicillin/streptomycin (Gibco), 1x Glutamax (Gibco), 0.05 mM 2-mercaptoethanol (Gibco), non essential aminoacids (Lonza). For mesoderm induction the same medium was used as before mentioned with the addition of 0.5 mM L-ascorbic acid (Sigma). Ectoderm differentiation was done culturing the EBs in suspension in N2B27 medium (Neurobasal:DMEM:F12 50:50 v/v, 1x N2 supplement, 1x B27 supplement, 1x Glutamax) supplemented with b-FGF as described (Sánchez-Danés, 2012). After 10 days in culture, EBs were plated on Matrigel (Corning) coated coverslips and cultured for additional three weeks in N2B27 medium without b-FGF. Differentiated cells were fixed with 4% PFA. Immunocytochemistry was performed by standard methods as previously reported (Martí, 2013). Primary antibodies used are listed in table S5. Secondary antibodies were of the Alexa Fluor series from Jackson Immuno Research and used between 1:250 and 1:500 dilution. Cell nuclei were counterstained with 0.5 µg/ml DAPI (Invitrogen). Images were acquired with an SP5 Leica confocal microscope. For karyotyping, iPSC were cultured on matrigel in the absence of HFF and treated with colcemide (Gibco) at a final concentration of 0.1 µg/mL and processed as described (Campos, 2009).

In the case of retroviral reprogrammed cell lines qPCR was performed to confirm the silencing of the transgenes. Sendai virus reprogrammed iPSC lines were subjected to qualitative PCR to check that they were vector-free at passage 10. The genetic expression of endogenous pluripotency-associated genes (*OCT4*, *NANOG*, *CRIPTO* and *Rex1*) were confirmed by qPCR. Primers employed are listed in Table S4.

For DNA methylation analysis, genomic DNA was extracted from cell pellets using QIAamp DNA Mini Kit (Qiagen 51304). DNA methylation analysis was performed with Methylamp DNA Modification kit (Epigentek P-1001-1) according to manufacturer's specifications. Oct4 and Nanog promoters were amplified by PCR using primers previously described in Freberg et al (2007), amplified in DH5a cells, purified and sequenced. Severe combined immunodeficient (SCID) beige mice (Charles River Laboratories) were used to generate teratomas from two iPSC line, 5PNFiPS(+/-) and 5PNFiPS(-/-). Animal assays were conducted following experimental procedures previously approved by the Institutional Ethics Committee on Experimental Animals, in full compliance with Spanish and European laws and regulations. Teratomas were stained with hematoxylin eosin and also the detection of the three germ layers was done by immunocytochemistry. Antibodies used are included in Table S5.

DNA extraction

Genomic DNA from tumors was extracted using the Gentra Puregene Kit (Qiagen, Chatsworth, CA) following manufacturer's instructions, after tissue homogenization using Tissue Lyser (Qiagen). Genomic DNA from primary cells and iPSCs was extracted using Promega Maxwell 16 system following manufacturer's instructions.

NF1 genetic analysis

NF1 germline and somatic mutations were detected by *NF1* cDNA Sanger sequencing, by gDNA sequencing using the I2HCP NGS custom panel (Castellanos *et al*, 2017) and MLPA from cultured PNF-derived Schwann cells treated with 250 µg/ml puromycin (Sigma) or PNFs DNA following Genetic Diagnostics for Hereditary Cancer Unit protocols. Germline mutations were confirmed by DNA Sanger sequencing from cultured PNF-derived fibroblast cells. Loss of heterozigosity of NF1 locus was detected by Microsatellite multiplex PCR analysis (MMPA) of chromosome 17 (Garcia-Linares *et al*, 2012). Reference sequence used was GeneBank: NG_009018_1, NM_000267_3, NP_000258.1. For intragenic deletions we used GeneBank: NM_001042492.2.

SNP-array analysis

SNP-array analysis was performed on selected samples using Illumina HumanOmniExpress v1 BeadChips (730,525 SNPs). Raw data was processed with Illumina Genome Studio v2011.1 with the Genotyping module v1.9.4 to extract B Allele frequency (BAF) and log R ratio (LRR) and then analyzed with the R package ASCAT (Van Loo *et al*, 2010) to obtain loss of heterozygosity (LOH) and allele specific copy

number (CN) profiles. All samples were analyzed independently and treated as unpaired samples, using the germline genotype prediction functionality from ASCAT.

Exome sequencing

Exome was captured using Agilent SureSelect Human All Exon V5 kit (Agilent, Santa Clara, CA, US) according to the manufacturer's instructions and sequenced in a HiSeq instrument (Illumina) producing 100-base long paired-end reads. Reads were aligned to the hs37d5 reference genome using BWA MEM (Li H 2013) (bwa-0.7.13). After that, duplicates were marked using Picard (v2.0.1) and the Genome Analysis Toolkit (GATK) (McKenna *et al*, 2010) (v.3.4.46) was used for local realignment around indels. GATK's Mutect2 (Cibulskis *et al*, 2013) was used to detect somatic variants specific to primary tumors, SC and iPSC with respect to their associated fibroblasts. Variants were annotated using annovar (Wang *et al*, 2010)(v20160201), filtered using custom R scripts and further validated by manual inspection.

Data visualization

Genomic plots were created with the R/Bioconductor package karyoploteR (Gel & Serra, 2017) and additional custom R scripts. Graphs were created with Graphpad Prism 7.0.

RT-qPCR analysis

Total RNA was extracted from cultured cells using the 16 LEV simplyRNA Purification Kit, from Maxwell technology following manufacturer's instructions. RNA (0,5 µg) was reverse-transcribed using the Superscript III reverse transcriptase enzyme (Life technologies) according to manufacturer's instructions. Quantitative polymerase chain reaction (qPCR) was performed with Roche Universal Probe Library (UPL) technology and analyzed using the Light-Cycler® 480 Real-Time PCR System (Roche Diagnostics). Gene expression was normalized to two selected reference genes (*EP300* and *TBP*) and expressed as Normalized Relative Expression (NRE). Primer sequences used are listed in Table S4. A Microsoft Excel spreadsheet was used to analyze qPCR data for relative expression calculations (Terribas *et al*, 2013).

Western Blotting

Cells were washed with chilled PBS twice and lysed with RIPA buffer (50 mM Tris-HCl (pH 7.4), 150 mM NaCl, 1mM EDTA, 0.5% Igepal CA-630) supplemented with 3mM DTT (Roche), 1mM PMSF (Fluka), 1mM sodium orthovanadate (Sigma), 5mM NaF (Honeywell), 10 ug/ml leupeptin (Sigma), 5ug/ml aprotinin (Sigma) and 1xPhosSTOP (Roche). Lysates were boiled with 1X Laemmli buffer and 90 µg of protein was subjected to SDS-PAGE and transfered onto PVDF membranes (18 hours 90mA at 4ºC). Membranes were blocked with Odyssey Blocking Buffer (PBS)(LI-COR) and incubated with rabbit anti-NF1 Antibody (Bethyl laboratories) at 4ºC overnight; and with mouse anti-αtubulin (Sigma-Aldrich) 1 h at room temperature. Membranes were then incubated with IRDye 680LT and IRDye 800CW secondary antibodies (1:25,000 and 1:15,000, respectively; LI-COR) for 1 h at room temperature and scanned using the Odyssey Infrared Imaging System (LI-COR).

Immunocytochemistry and flow cytometry

For immunofluorescence, cells were fixed in 4% para-formaldehyde in PBS for 15min at RT, permeabilized with 0.1%Triton-X 100 in PBS for 10 min at RT, blocked in 10% FBS in PBS for 15 min at RT and stained with the primary antibodies (Table S4) overnight at 4ºC. Secondary antibodies were Alexa Fluor 488- and Alexa Fluor 568- (Invitrogen). Nuclei were stained with DAPI and images captured using LEICA DMIL6000 and LASAF software. Confocal images from spheres were captured using AxioObserver Z1 Confocal LSM 710, and ZEN Black 2012 software. For flow cytometry assays, cells were dissociated with accutase, resuspended in 0.1% BSA in PBS, incubated for 30 min on ice with unconjugated primary antibody p75 and detected with Alexa Fluor 568-conjugated secondary antibodies, following incubation for 30 min on ice with unconjugated primary antibody Hnk1 and detected with Alexa Fluor 488-conjugated secondary antibodies Cells were analyzed by flow cytometry using BD LSR Fortessa SORP and BD FACSDiva 6.2 software.

Proliferation Assay (Click-iT Edu assay)

Two hundred thousand iPSCs (ES4, FiPS and iPSC) were plated on matrigel-coated 6-well plates, and feeded daily with mTESR medium. After 72h cells were treated with 20 µM EdU for 2 hours, fixed, permeabilized and click labeled with Alexa Fluor 488 azide using Click-iT Plus EdU Flow Cytometry Assay Kits (Thermo Fisher) according to the manufacturer protocol. Cells were also stained with propidium iodide to detect DNA content. Data was collected and analyzed using an BD LSR Fortessa SORP and BD FACSDiva 6.2 software.

Scratch assay

$0.5x10^6$ NC cells were plated onto matrigel–coated 6-well dishes. When cells reached confluence a scratch area was created using a sterile tip. Medium was replaced and migration was measured after 6 and 24 hours. To obtain data in cell migration 9 fields covering the scratch were imaged with a 10x lens at 0, 6 and 24 hours after the scratch. The 9 images were joined using tilescan tool from the LASAF software (Leica).

In vitro Myelination assay

In vitro myelination assay was performed as described in Kim H-S et al (Kim *et al*, 2017) co-culturing Rat Dorsal Root Ganglion (DRG) neurons (Innoprot, Spain) with SCP (7 days differentiation)-FiPS, for 30 days.

Statistical Analyses

Statistical analysis was carried out using GraphPad Prism software v7. For multiple group comparisons, a two-tailed unpaired t test was performed. The number of biological replicates (n) for each experiment and average ± SEM are indicated when applicable, and statistical significance is indicated by *p < 0.05, **p < 0.01, and ***p < 0.001.

References

Campos PB , Sartore RC, Abdalla SN, Rehen SK. Chromosomal spread preparation of human embryonic stem cells for karyotyping E J Vis Exp. 2009 Sep 4;(31)

Castellanos E, Gel B, Rosas I, Tornero E, Santín S, Pluvinet R, Velasco J, Sumoy L, del Valle J, Perucho M, Blanco I, Navarro M, Brunet J, Pineda M, Feliubadaló L, Capellá G, Lázaro C & Serra E (2017) A comprehensive custom panel design for routine hereditary cancer testing: preserving control, improving diagnostics and revealing a complex variation landscape. *Sci. Rep.* **7:** 39348

Cibulskis K, Lawrence MS, Carter SL, Sivachenko A, Jaffe D, Sougnez C, Gabriel S, Meyerson M, Lander ES & Getz G (2013) Sensitive detection of somatic point mutations in impure and heterogeneous cancer samples. *Nat. Biotechnol.* **31:** 213–219

Freberg CT, Dahl JA, Timoskainen S, Collas P. Epigenetic reprogramming of OCT4 and NANOG regulatory regions by embryonal carcinoma cell extract. Mol Biol Cell. 2007 May;18(5):1543-53. Epub 2007 Feb 21.

Garcia-Linares C, Mercadé J, Gel B, Biayna J, Terribas E, Lázaro C & Serra E (2012) Applying microsatellite multiplex PCR analysis (MMPA) for determining allele copy-number status and percentage of normal cells within tumors. *PLoS One* **7:** e42682

Gel B & Serra E (2017) karyoploteR: an R/Bioconductor package to plot customizable genomes displaying arbitrary data. *Bioinformatics***:** 31–33

Kim H-S, Lee J, Lee DY, Kim Y-D, Kim JY, Lim HJ, Lim S & Cho YS (2017) Schwann Cell Precursors from Human Pluripotent Stem Cells as a Potential Therapeutic Target for Myelin Repair. *Stem Cell Reports* **8:** 1714–1726

Martí M, Mulero L, Pardo C, Morera C, Carrió M, Laricchia-Robbio L, Esteban CR, Izpisua Belmonte JC. Characterization of pluripotent stem cells. Nat. Protoc. 2013 Feb;8(2):223-53. doi: 10.1038/nprot.2012.154. Epub 2013 Jan 10.

McKenna A, Hanna M, Banks E, Sivachenko A, Cibulskis K, Kernytsky A, Garimella K, Altshuler D, Gabriel S, Daly M & DePristo MA (2010) The Genome Analysis Toolkit: A MapReduce framework for analyzing next-generation DNA sequencing data. *Genome Res.* **20:** 1297–1303

Sánchez-Danés A, Richaud-Patin Y, Carballo-Carbajal I, Jiménez-Delgado S, Caig C, Mora S, Di Guglielmo C, Ezquerra M, Patel B, Giralt A, Canals JM, Memo M, Alberch J, López-Barneo J, Vila M, Cuervo AM, Tolosa E, Consiglio A, Raya A. Disease-specific phenotypes in dopamine neurons from human iPS-based models of genetic and sporadic Parkinson's disease EMBO Mol Med. 2012 May;4(5):380-95. doi: 10.1002/emmm.201200215. Epub 2012 Mar 8.

Terribas E, Garcia-Linares C, Lázaro C & Serra E (2013) Probe-based quantitative PCR assay for detecting constitutional and somatic deletions in the NF1 gene: application to genetic testing and tumor analysis. *Clin. Chem.* **59:** 928–37

Van Loo P, Nordgard SH, Lingjaerde OC, Russnes HG, Rye IH, Sun W, Weigman VJ, Marynen P, Zetterberg A, Naume B, et al. (2010) Allele-specific copy number analysis of tumors. *Proc. Natl. Acad. Sci.* **107:** 16910–16915

Wang K, Li M & Hakonarson H (2010) ANNOVAR: functional annotation of genetic variants from high-throughput sequencing data. *Nucleic Acids Res.* **38:** e164–e164

Appendix 4

1. Review: Mazuelas et al., 2020

Stem Cell Research 49 (2020) 102068

Contents lists available at ScienceDirect

Stem Cell Research

journal homepage: www.elsevier.com/locate/scr

Review

Modeling tumors of the peripheral nervous system associated with Neurofibromatosis type 1: Reprogramming plexiform neurofibroma cells

Helena Mazuelas, Meritxell Carrió *, Eduard Serra *

Hereditary Cancer Group, Germans Trias i Pujol Research Institute (IGTP), Can Ruti Biomedical Campus, Badalona, Barcelona, Spain

ARTICLE INFO

Keywords:
Cancer predisposition syndrome
Neurofibromatosis
Plexiform neurofibroma
iPSC
Neural crest
Schwann cell
Spheroid

ABSTRACT

Plexiform neurofibromas (pNFs) are benign tumors of the peripheral nervous system (PNS) that can progress towards a deadly soft tissue sarcoma termed malignant peripheral nerve sheath tumor (MPNST). pNFs appear during development in the context of the genetic disease Neurofibromatosis type 1 (NF1) due to the complete loss of the *NF1* tumor suppressor gene in a cell of the neural crest (NC) – Schwann cell (SC) axis of differentiation. *NF1*(−/−) cells from pNFs can be reprogrammed into induced pluripotent stem cells (iPSCs) that exhibit an increased proliferation rate and maintain full iPSC properties. Efficient protocols for iPSC differentiation towards NC and SC exist and thus NC cells can be efficiently obtained from *NF1*(−/−) iPSCs and further differentiated towards SCs. In this review, we will focus on the iPSC modeling of pNFs, including the reprogramming of primary pNF-derived cells, the properties of pNF-derived iPSCs, the capacity to differentiate towards the NC-SC lineage, and how well iPSC-derived *NF1*(−/−) SC spheroids recapitulate pNF-derived primary SCs. The potential uses of *NF1*(−/−) iPSCs in pNF modeling and a future outlook are discussed.

1. Neurofibromatosis type 1

Neurofibromatosis type 1 (NF1) is a tumor predisposition genetic disease affecting about 1 in 3500 people worldwide and caused by the inheritance of a mutated copy of the *NF1* tumor suppressor gene (Riccardi, 1992). The major clinical manifestations of the disease involve the nervous system, the skin, and the skeletal system, implicating cells derived from the neural crest (NC). There is a great variability in the clinical expressivity of the disease, but the development of different tumors of the peripheral nervous system (PNS) constitutes one of the hallmarks of the disease (Ferner, 2007). The *NF1* gene encodes for a protein termed neurofibromin, a GTPase activating protein that catalyzes the inactivation of Ras. In NF1 tumors, loss of neurofibromin results in activated Ras and its downstream signaling pathways, like the MAPK/ERK kinase cascade. Neurofibromin is also involved in the regulation of cAMP-dependent pathways (Cichowski and Jacks, 2001; Ratner and Miller, 2015).

2. Peripheral nervous system tumors in NF1

One of the major clinical complications of NF1 patients is the development of different tumors of the PNS which arise both in childhood and adulthood, such as cutaneous neurofibromas (cNFs), plexiform neurofibromas (pNFs) or, less frequently, malignant peripheral nerve sheath tumors (MPNSTs). cNFs originate in the PNS that resides in the skin, forming discrete and well-circumscribed non-encapsulated nodules that never progress to malignancy. cNFs normally appear during puberty and are present in more than 95% of NF1 patients (Ortonne et al., 2018). Their number increases with age, ranging from tens to thousands (Huson et al., 1988). Neurofibromas are composed of different cell types, mainly Schwann cells (SCs) and endoneurial fibroblasts, but also perineurial cells, infiltrating immune cells, axons, and others that are embedded in an abundant collagen-rich extracellular matrix (Krone et al., 1983; Peltonen et al., 1986). cNFs arise due to the double inactivation of the *NF1* tumor suppressor gene in SCs (Kluwe et al., 1999; Maertens et al., 2006; Serra et al., 2000). All other cellular components are *NF1*(+/−) and their interaction with *NF1*(−/−) SCs facilitates neurofibroma formation (Buchstaller et al., 2012).

pNFs are big neurofibroma lesions that appear during development and grow along large nerves. A pNF may be visible or may lie internally and are normally diagnosed in early childhood when they grow most rapidly. They are identified in around 50% of NF1 individuals by combining physical examination and MRI (Mautner et al., 2008). Each pNF arises from an independent biallelic inactivation of the *NF1* gene

* Corresponding authors.
E-mail addresses: mcarriol@igtp.cat (M. Carrió), eserra@igtp.cat (E. Serra).

https://doi.org/10.1016/j.scr.2020.102068
Received 18 May 2020; Received in revised form 16 October 2020; Accepted 20 October 2020
Available online 29 October 2020

(Pemov et al., 2017). Besides the complete *NF1* loss, no recurrent gross genomic alterations or recurrent point mutations have been identified in pNFs (Carrió et al., 2018; Pemov et al., 2017). pNFs constitute a major source of morbidity (Prada et al., 2012) and in some cases undergo malignant transformation towards an MPNST (McCarron and Goldblum, 1998). The MEK inhibitor Selumetinib has been used in children with inoperable pNFs in Phase 1 (Dombi et al., 2016) and Phase 2 (Gross et al., 2020) trials showing tumor volume decrease in about 70% of the cases, most of them with a durable response, lowering pain and improving their quality of life. Selumetinib has been approved by the FDA as the first ever treatment for NF1.

A common path to malignancy in the context of NF1, involves the generation of an atypical neurofibroma (aNF), a distinct growing nodular lesion that exhibits atypical histological features considered pre-malignant lesions (Beert et al., 2011; Higham et al., 2018; Miettinen et al., 2017). In addition to the biallelic *NF1* inactivation, loss of the *CDKN2A/B* locus drives aNFs formation (Beert et al., 2011; Carrió et al., 2018; Pemov et al., 2019; Rhodes et al., 2019; Röhrich et al., 2016). There are no prognostic markers to determine whether an aNF will progress into an MPNSTs or not, but resection by surgery is recommended when possible. MPNSTs are aggressive and highly metastatic soft tissue sarcomas with limited sensitivity to chemotherapy and radiation. Half of them appear in patients with NF1, who have a lifetime risk of about 10–15% of developing an MPNST (Evans et al., 2002; Uusitalo et al., 2016). NF1-associated MPNSTs have the same cellular origin as pNFs and aNFs, since histological progressions containing benign and malignant components share the same somatic *NF1* mutation (Beert et al., 2011; Hirbe et al., 2015). Like other sarcomas, these tumors contain hyperploid and highly rearranged genomes with a low mutation burden (Abeshouse et al., 2017). However, in addition to *NF1* and *CDKN2A/B*, other tumor suppressors such as components of the histone methyltransferase polycomb repressive complex 2 (*PRC2*) and the *TP53* gene are frequently mutated.

3. Model systems for plexiform neurofibromas

pNFs have the same complex cellular composition as cNFs, with *NF1*(−/−) SCs and *NF1*(+/−) endoneurial fibroblasts being the main cell types. Different models for cNFs and pNFs have been developed, both *in vitro* cell-based, like primary cells, immortalized cells, and 3D culture models; and *in vivo*, like genetically modified mouse models (GEMMs). Primary SC cultures from neurofibromas have been established (Rosenbaum et al., 2000; Serra et al., 2000; Wallace et al., 2000) and very incipient neurofibroma-like growths have formed when these SCs have been engrafted in the sciatic nerve of immunodeficient mice (Muir et al., 2001). However, these primary cultures are perishable after several passages, limiting their use in mid- large-scale molecular and cellular analyses. To overcome this problem, immortalized cell lines have been established (Li et al., 2016), and their 3D growth has been used to better recapitulate the natural pNF environment of SCs (Kraniak et al., 2018). But the process of immortalization invariably alters the biological status of the cells.

Different GEMMs have been generated that develop pNFs. In these animals, the Cre-loxP system has been used to ablate the *NF1* gene in specific developmental cell stages of the NC-SC axis (Joseph et al., 2008; Wu et al., 2008; Zheng et al., 2008; Zhu et al., 2002) (see below). The transplantation of *Nf1*-deficient embryonic DRG/nerve root neurosphere cells to sciatic nerves of nude mice also forms pNFs (Chen et al., 2014). Altogether these models point to a Schwann Cell Precursor (SCP) as the most probable pNF cell of origin (Buchstaller et al., 2012; Le et al., 2011). Moreover, since pNFs and cNFs appear in patients at distinct moments in life, it is not known whether both neurofibroma types share the same cell type of origin. Two recently generated GEMMs in which *NF1* is ablated in cells expressing either *Hoxb7* (Chen et al., 2018) or *Prss56* (Radomska et al., 2019) in the developing mouse, generated both cNF and pNF tumors. Furthermore, transplantation of *Nf1*-deficient skin-derived precursors (SKPs) can give rise to either dermal or plexiform neurofibromas when grafted in the dermis and the sciatic nerve, respectively (Le et al., 2009). These results support a common cell of origin for both types of neurofibromas.

Finally, patient-derived xenograft (PDX) models have also been established by grafting human MPNSTs to the sciatic nerve of nude mice (Castellsagué et al., 2015). However, using the same methodology, neither pNFs nor aNFs have been able to grow as PDXs (Conxi Lazaro, Juana Fernandez-Rodriguez, Alberto Villanueva, personal communication).

4. NF1 iPSC models

Induced pluripotent stem cells (iPSCs) have been generated to model NF1 disease (for a review see (Wegscheid et al., 2018). Anastasaki and Gutmann (2014) were the first to reprogram primary skin fibroblasts from NF1 patients into iPSCs, generating several *NF1*(+/−) iPSC lines harboring distinct *NF1* constitutional mutations with the goal to study the learning, attention and cognitive deficits affecting NF1 individuals. They differentiated iPSCs into neural progenitor cells (NPCs) to study the involvement of neurofibromin in the regulation of cAMP signaling and its crosstalk with Ras (Anastasaki and Gutmann, 2014), as well as the impact of different constitutional *NF1* mutations on NPC signaling and dopamine production (Anastasaki et al., 2015). The group has recently further explored the importance of *NF1* mutation on the heterogeneity of clinical presentation by expanding the iPSC-modeling palette. They generated different isogenic *NF1*(+/−) iPSC lines by editing specific constitutional mutations present in NF1 patients in the same iPS cell line. They explored the effect of constitutional mutation on phenotype by differentiating them towards astrocytes, 3D embryoid bodies and cerebral organoids (Anastasaki et al., 2020).

Larribere L et al. (2015) used reprogrammed *NF1* patient-derived fibroblasts to gain insight into cafe-au-lait macules (CALMs), melanocytic lesions present in almost all NF1 patients and a hallmark of the disease. This group showed that *NF1*(+/−) patient-derived iPSCs undergo abnormal melanocyte differentiation and that *NF1* loss induces senescence during melanocyte differentiation, as well as in patient-derived CALMs (Larribere et al., 2015).

These studies used patient-derived fibroblasts bearing the constitutional *NF1* mutation but did not address the possibility of reprogramming *NF1*(−/−) cells, particularly those present in neurofibromas. Recently, our group has demonstrated that pNF-derived *NF1*(−/−) cells can be reprogrammed and we successfully generated isogenic *NF1*(+/−) and *NF1*(−/−) iPSC lines from different pNFs (Carrió et al., 2019). Our results indicate that the absence of neurofibromin does not compromise somatic cell reprogramming to pluripotency, maintenance, or differentiation capacity of *NF1*(−/−) iPSCs towards the three embryonic germ layers. These cells represent an endless iPSC-based model system for the study of these benign tumors.

5. iPSC generation for modeling pNFs

5.1. Reprogramming pNF cells versus generating NF1-edited iPSCs

As mentioned earlier, pNFs are complex benign tumors composed of an admixture of *NF1*(−/−) and *NF1*(+/−) cells. These tumors start forming during development, when a progenitor cell completely inactivates the *NF1* gene. In this context, the use of iPSCs is a reasonable strategy to obtain the precise cell type to recreate pNF initiation, combining iPSC differentiation potential with the correct *NF1* genotype. There are at least two ways of generating these iPSC lines: reprogramming pNF cells with distinct *NF1* genotypes or editing the *NF1* gene in already established iPSC lines. The reprogramming approach allows the preservation of the entire genetic background, both the *NF1* status and also any potential patient or pNF-specific genetic variants. The persistence of gene expression and differentiation propensity of the starting

cell has been described in iPSCs (Feng et al., 2010; Ghosh et al., 2010; Hu et al., 2010; Marchetto et al., 2009). These observations led to speculation that iPSCs possess epigenetic and transcriptomic remnants of the donor tissue, which was termed "epigenetic memory" (Bar-Nur et al., 2011; Firas et al., 2014; Vaskova et al., 2013). This idea is controversial, as subsequent studies did not find evidence of any epigenetic memory. Furthermore, the reprogramming of pNF cells, as opposed to genome editing, overcomes any potential off-target effects related to genome editing. On the other hand, the editing approach allows the generation of isogenic *NF1*(+/−) and *NF1*(−/−) iPSCs, with the advantage of having in addition the isogenic *NF1*(+/+) cell line. Although not required for pNF modeling, *NF1*(+/+) cells can provide an additional control to study the effects of specific *NF1* mutations. Furthermore, any reprogramming bottleneck related to culture conditions of pNF-derived cells, to cell type specificities, or to the lack of *NF1*, could be overcome with this approach.

The reprogramming approach was used in Carrió et al. (2019). Our group has also recently edited the *NF1* gene in control *NF1*(+/+) iPSC cells by CRISPR/Cas9 to evaluate to which extent *NF1*(−/−) edited iPSCs have the same behavior and properties compared to pNF-derived *NF1*(−/−) iPSCs. Our results indicate that differentiating *NF1*(−/−) SCs from edited iPSCs also recapitulate the same proliferation capacity, tendency to form spheroids and SC marker expression identity (see below) as pNF-derived primary SCs and as differentiating SCs from pNF-derived iPSCs (Mazuelas et al. unpublished results). These results demonstrate that these cell properties are mainly conferred by the loss of *NF1* function, indicating the validity of both strategies to generate iPSCs for pNF modeling.

5.2. Strategies for reprogramming pNF-derived cells

pNFs are composed of different cell types with distinct *NF1* genotypes, mainly *NF1*(−/−) SCs and *NF1*(+/−) endoneurial fibroblasts (FBs). This cellular and genetic diversity represents a technical challenge when trying to generate *NF1*(−/−) iPSC lines from pNF cells. Thus, before pNF reprogramming, there is the need to determine the *NF1* constitutional and somatic mutations present in these tumors. Constitutional *NF1* mutation is the one inherited and present in all cells of the NF1 patient. Since the *NF1* gene is a large gene composed of 60 exons, mutation detection in genetic diagnostic units is normally performed through either cDNA Sanger sequencing and multiplex ligation-dependent probe amplification, for DNA copy-number analysis

BOX 1
Reprogramming pNF cells. Two different strategies can be used to obtain *NF1*(+/−) and *NF1*(−/−) pNF iPSCs.

Strategy 1

1. Digest pNF tumor tissue enzymatically
2. Establish primary cultures of SCs and FBs
3. Check for cell culture purity using specific lineage markers
4. Check for cell culture purity according to somatic *NF1* mutation
5. Reprogram SC and FB cultures at early passages
6. Grow several iPSC clones
7. Genotype iPSC clones for *NF1* somatic mutation
8. Grow, expand and characterize chosen *NF1*(+/−) and *NF1*(-/-) iPSC clones for pluripotency and differentiation capacity

Advantages

- Cells prepared for reprogramming according to *NF1* genotype: *NF1*(+/−) or *NF1*(-/-)

Limitations

- Highly pure SC cultures might require several passages
- SC proliferation decreases throughout passages, affecting reprogramming efficiency
- For certain tumors *NF1*(+/−) fibroblast contamination persist in SC cultures

Strategy 2

1. Digest pNF tumor tissue enzymatically
2. Plate digested cells in SC media
3. Reprogram plated cells after 48h
4. Grow several iPSC clones
5. Genotype iPSC clones for *NF1* somatic mutation
6. Grow, expand and characterize chosen *NF1*(+/−) and *NF1*(-/-) iPSC clones for pluripotency and differentiation capacity

Advantages

- Minimization of culture conditions affecting reprogramming efficiency
- Faster procedure, not requiring long cell culturing

Limitations

- Necessity of genotyping large number of iPSC clones.

(Messiaen and Wimmer, 2008) or by DNA NGS panel sequencing (Castellanos et al., 2017). The somatic *NF1* mutation is restricted to the descendants of the originating pNF cell. It can be detected in pNFs or pNF-derived SC cultures by loss of heterozygosity (LOH) analysis comparing blood and tumor DNA (Garcia-Linares et al., 2011) or by point mutation detection in DNA from *NF1*(−/−) SC cultures (Maertens et al., 2006; Serra et al., 2001).

After identification of both *NF1* mutations, pNF cells can be reprogrammed. In order to optimize obtaining *NF1*(−/−) iPSC clones, two different strategies can be used to prepare tumor cells for reprogramming. The first one consists of the establishment of selective *NF1*(−/−) SC and *NF1*(+/−) FB cultures from digested tumors, followed by their reprogramming. The second consists of performing a tumor digestion and then directly reprogramming of pNF digested cells without establishing primary cultures (Box 1). In both approaches, isogenic *NF1*(−/−) and *NF1*(+/−) iPSCs from the same pNFs can be identified by genetic *NF1* analysis and further characterized for pluripotency and differentiation capacity.

in specific cells during development. Our group has attempted to reprogram 5 pNFs from 5 independent NF1 patients. We obtained *NF1*(+/−) iPSCs from all of them but *NF1*(−/−) iPSCs only from 2, suggesting a lower reprogramming efficiency of *NF1*(−/−) cells. Despite the low number of reprogrammed tumors, which does not allow us to draw any definitive conclusions, we identified several factors potentially influencing the reprogramming efficiency of pNF-derived *NF1*(+/−) and *NF1*(−/−) cells worth mentioning. In addition to the possibility that the complete loss of *NF1* reduces reprogramming efficiency, other identified factors were: the age of the pNF donor, the cell type and culture conditions.

Independently of the reprogramming strategy used (Box 1), we obtained *NF1*(−/−) iPSC clones from two pNFs belonging to children of 10 years or younger. Most rapidly growing pNFs are observed in young children (Akshintala et al., 2020). This could influence the number of elite or progenitor cells present within pNFs and their replicative capacity, two factors known to influence reprogramming efficiency (Eminli et al., 2009; Utikal et al., 2009).

Another interesting observation is the lower reprogramming efficiency obtained in *NF1*(+/−) endoneurial fibroblast primary cultures (Table 1). In contrast, using the same culture conditions, fibroblast-enriched cultures derived from skin produced many *NF1*(+/−) clones, indicating that fibroblasts of different origin may have different reprogramming efficiencies.

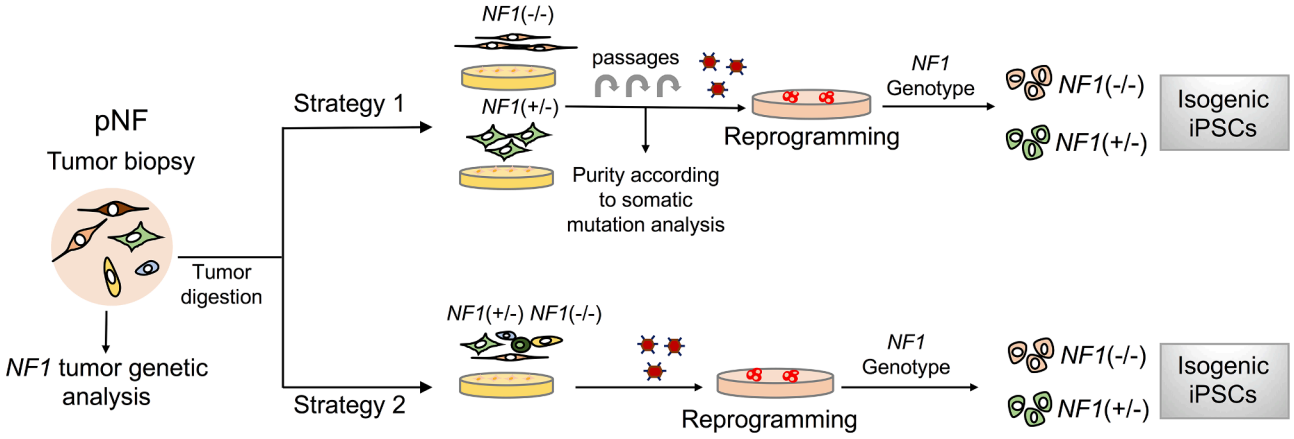

5.3. Efficiency of reprogramming pNF cells

Reprogramming to pluripotency is a complex process involving different stages, in which multiple players synergistically converge to remodel transcriptional and epigenetic programs. Different factors have been identified to affect the efficiency of reprogramming, like cell cycle regulators, chromatin remodelers and facilitators of the mesenchymal-to-epithelial transition (Buganim et al., 2013). Most somatic cell types reprogram to pluripotency with a very low efficiency and Yamanaka (Yamanaka, 2009) proposed two alternative explanations for this. In the elite-cell model, reprogramming takes place only in a few predisposed cells within a population (Shakiba et al., 2019). On the contrary, in the stochastic model most or all cells are competent for reprogramming at low probabilities (Hanna et al., 2009). Are all cells equally capable of reprogramming? Recent technical developments that allow identifying and following single cells in heterogeneous populations do not seem to indicate so. By combining cellular barcoding, mathematical modeling and lineage tracing approaches, Shakiba et al. (2019) demonstrated that reprogramming dynamics in heterogeneous populations of mouse embryonic fibroblasts were driven by dominant elite clones expressing Wnt1.

To model pNFs both *NF1*(+/−) and *NF1*(−/−) iPSCs are required, but especially the latter, since pNFs are initiated upon *NF1* inactivation

Table 1
pNF Reprogramming strategies.

Reprogramming Strategy		Tumor	Clones	NF1 genotype	
				NF1(+/−)	NF1(−/−)
DIGESTED		3PNF	–		
		5PNF	12	1	11
		13PNF	27	27	0
		6PNF	10	10	0
		7PNF	–		
CULTURED	SC	3PNF	22	0	22
		5PNF	2	0	2
		13PNF	40	40	0
		6PNF	10	10	0
		7PNF	12	12	0
	Endo FB	3PNF	–		
		5PNF	0		
		13PNF	11	11	0
		6PNF	1	1	0
		7PNF	1	1	0
	Skin FB*	3PNF	16	14	2

*The skin used was covering the pNF. When skin was separated, part of the tumor was still left; - Not reprogrammed; In grey: tumors from children younger than 12 years old. SC: Schwann cells; FB: Fibroblasts.

To our experience, *NF1*(−/−) reprogramming efficiency was increased when selective culturing was avoided and digested tumor cells were directly reprogrammed, as more *NF1*(−/−) clones were obtained from the same pNFs (Box 1, Table 1). This strategy may reduce selection pressure imposed by culture conditions and minimize loss of cell heterogeneity during *in vitro* passaging. Nonetheless, when we used the selective culturing strategy to reprogram primary *NF1*(−/−) SC, in one case we established SC primary cultures that were >95% enriched in *NF1*(−/−) SCs and still only obtained *NF1*(+/−) iPSC clones, suggesting that those *NF1*(−/−) cultures had very low (if any) reprogramming capacity.

We confirmed the pluripotency and differentiation capacity of pNF-derived *NF1*(+/−) and *NF1*(−/−) iPSCs and showed that reduced levels or absence of neurofibromin do not compromise somatic cell reprogramming to pluripotency, maintenance, or differentiation capacity of iPSCs. Despite the rapid cell cycle of iPSCs, *NF1*(−/−) iPSC lines exhibit a 10–15% higher proliferation rate than control *NF1*(+/+) iPSC lines, indicating that neurofibromin function influences iPSC proliferation capacity (Carrió et al., 2019).

6. iPSC differentiation towards the neural crest-Schwann cell lineage

6.1. Development of the neural crest – Schwann cell axis

During early vertebrate development, the neural plate folds and fuses to form the neural tube. A population of cells called neural crest (NC) cells undergo an epithelial-to-mesenchymal transition, delaminate from the dorsal surface of the neural tube and migrate dispersing throughout the embryo (Bronner and Simões-costa, 2016; Etchevers et al., 2019). NC cells are multipotent and give rise to a variety of cell types including SCs and neurons from the PNS, connective tissue components of the head, cardiac cells, melanocytes, and many others, in a series of sequential decisions of activating and repressing competing fate programs (Baggiolini et al., 2015; Bronner-Fraser and Fraser, 1988; Morrison et al., 1999; Soldatov et al., 2019).

In addition to the glial and neuronal components of the PNS, NCs also form a stem cell-like population of cells termed the boundary cap (BC) cells, transiently localized at the interface between the central and peripheral nervous system, at the nerve root entry/exit points along the neural tube (Katarzyna and Topilko, 2017). A secondary source of SCs and neurons of the PNS also arise from BC cells. BC derivatives migrate along the nerves to provide the major glial component of nerve roots and cutaneous nerve terminals (Gresset et al., 2015; Marol et al., 2004). As stated earlier, ablation of the *NF1* gene in Prss56 expressing BC cells can generate both plexiform and cutaneous neurofibromas in a GEMM (Radomska et al., 2019).

During embryo development, NC cells differentiate into SCs in a multistep differentiation process, involving the generation of an intermediate cell population termed Schwann cell precursors (SCPs), which can differentiate into immature SCs (iSCs) that will finally form myelinating (mSCs) or non-myelinating (nmSCs) SCs (Jessen and Mirsky, 2005; Kastriti and Adameyko, 2017; Monk et al., 2015). SCPs are also considered multipotent migrating embryonic progenitors covering all developing peripheral nerves that can detach from nerves and generate different cell types such as SCs, melanocytes, endoneurial fibroblasts, parasympathetic/enteric neurons, Chromaffin cells, tooth pulp cells and other cell types (Furlan and Adameyko, 2018; Jessen and Mirsky, 2019). Committed SCPs differentiate into iSCs that stop migrating, deposit, and organize extra-cellular matrix components to produce the basal lamina. Around birth, iSCs contribute to nerve morphogenesis by separating axons destined to become myelinated from those that will remain nonmyelinated in a process called radial sorting. iSCs acquire myelinating capacity and can establish a 1:1 ratio with large-caliber axons that will be myelinated by mSCs, or can associate with multiple small-caliber axons in a non-myelinated form (nmSC) constituting Remake bundles (Jessen and Mirsky, 2005; Kastriti and Adameyko, 2017; Monk et al., 2015).

6.2. Generation of NCs and SCs from iPSCs

pNF modeling using *NF1*(−/−) iPSCs requires differentiation to the NC-SC axis. NC differentiation protocols have been established from different laboratories (Chambers et al., 2009; Hackland et al., 2017; Lee et al., 2010, 2007; Menendez et al., 2011; Mica et al., 2013; Pomp et al., 2005; Tchieu et al., 2017). During the last decade, these protocols have evolved towards better-defined conditions, moving from co-culture with feeder cells, serum and purification steps, to a simpler version using chemically defined media. One of the most efficient and most used procedures combines activation of the canonical Wnt signaling simultaneously with suppression of TGFβ-dependent signaling (Menendez et al., 2013). Wnt signaling activation can be achieved using recombinant Wnt or a GSK3 inhibitor, such as CHIR 99021. TGFβ signaling suppression is accomplished through inhibitors such as SB432542. NC production using this method is highly efficient, achieving over 90% efficiency. Moreover, NCs can be maintained as a stable, self-renewing population and can be expanded, frozen, and thawed without loss of self-renewing potential. Thus, NC batches can be produced and cryopreserved for multiple subsequent differentiation assays. This population can be further differentiated to a variety of different cell types such as SCs, melanocytes, peripheral neurons, and others.

Phenotypic analysis of differentiated cells is usually performed by morphologic characterization together with the detection of lineage-specific markers. Defined transcription factors, such as SOX10, SOX9 and TFAP2A, as well as cell membrane markers, such as p75 and HNK1, are usually used to identify NCs by immunocytochemistry, RT-qPCR and flow cytometry analyses. Functional validation of embryonic stem cell (ESC)- or iPSC-derived NC is based on its natural capacity to migrate and its multipotency. Thus, classical migration scratch assays (or wound healing assay) might be used to evaluate their migration capacity and distinct differentiation protocols can be applied to produce different cell types that in turn need to be evaluated with cell type-specific markers. In this case, differentiation protocols might be used to generate melanocytes, peripheral nervous system lineages such as peripheral neurons or SCs, or mesenchymal lineages, like chondrocytes, osteoblasts, adipocytes, or smooth muscle (Lee et al., 2010; Menendez et al., 2013).

Different protocols to differentiate SCs from either iPSCs or NCs have also been developed (Lee et al., 2007; Liu et al., 2012; Ma et al., 2015; Wang et al., 2011; Ziegler et al., 2011). Most of them rely on the dual activation of ERBB2/ERBB3 receptors and cAMP signaling pathways. ERBB2/ERBB3 receptors and downstream signaling pathways, like the MAPK/ERK pathway, are activated by using exogenous type III neuregulin, such as neuregulin 1. cAMP-dependent signaling is stimulated either by the addition of cAMP analogs together with phosphodiesterase inhibitors, or the use of adenylate cyclase activators such as forskolin. SCs are highly responsive to these signals, and SC survival, lineage specification, proliferation, and differentiation into myelin-forming cells require fine regulation of the degree of pathway activation and balance among activation of different pathways (Arthur-Farraj et al., 2011).

In vitro SC differentiation is a dynamic process, in which differentiating cells go through various stages. To monitor the progression along the SC differentiation process, the expression of stage-specific markers (e.g.: CDH19; GAP43, PLP1, S100b, MPZ and PMP22) can be analyzed at different time points. Analysis of terminally differentiated SC markers can also be performed at the end point (Jessen and Mirsky, 2005). In addition to morphology and marker characterization, functional validation is desirable. For SCs it could be based on their biological capacity to myelinate axons, usually performed through an *in vitro* myelination assay (Liu et al., 2012; Ziegler et al., 2011). This assay consists of co-culturing the differentiating SCs together with rat or mouse dorsal root ganglia neurons and evaluating the resultant myelin production by SCs. Another functional assay is the sciatic nerve injury model, in which

the sciatic nerve of mice or rats is damaged, and differentiating SCs are injected to evaluate their capacity to repopulate and myelinate the injured axons (Geuna et al., 2016).

6.3. *NF1*(−/−) iPSC-derived SCs recapitulate pNF SC properties

Results from our laboratory showed that control and pNF iPSCs could be differentiated with high efficiency towards NC, expressed homogenously NC lineage markers, and were able to undergo further differentiation into NC-derived cell types (peripheral neurons and melanocytes), indicating a clear NC identity, independently of the iPSC *NF1* genotype.

It is worth noting that, while at the pluripotent stage *NF1*(−/−) and *NF1*(+/−) iPSCs exhibited a higher proliferation rate compared to control *NF1*(+/+) iPSCs, this was not the case at the NC stage, in which all NC genotypes showed similar proliferation capacity, suggesting a different role of *NF1* at these two differentiation stages. On the other hand, SCs derived from *NF1*(−/−) NCs exhibited higher proliferation rate compared to control *NF1*(+/+) iPSCs, poor ability to myelinate, and a natural tendency to form sphere-like structures visible to the naked eye. These spheres grew either attached to the plate surface or as free-floating cultures resembling incipient tumors and recapitulated the same expression marker profile of the NC-SC axis as their parental primary *NF1*(−/−) SC (Fig. 1). These results highlight the validity of the pNF-derived iPSCs as a source of cells to model these benign tumors and emphasize the importance of *NF1* function throughout the NC-SC differentiation process.

7. Future outlook and potential uses of *NF1*(−/−) iPSCs in pNF modeling

iPSCs have been generated from patients with different familial cancer predisposition syndromes carrying germline mutations. Li-Fraumeni syndrome patients carry constitutional *TP53* mutations and are at risk of osteosarcoma development. Patient-derived iPSCs showed defective osteoblastic differentiation that recapitulated osteosarcoma features at a phenotype and gene expression level, demonstrating the value of iPSC technology to develop models of hereditary cancer (Lee et al., 2015). Our results with NF1 pNFs build up on this line of research and support the generation of iPSCs from benign tumors developing in hereditary cancer predisposition syndrome patients as promising models to investigate tumorigenesis.

The natural tendency of *NF1*(−/−) differentiating SCs to form spheroids that recapitulate the marker expression of primary pNF SCs forms the basis for developing an iPSC-based 3D pNF model system. This model system could be used to study neurofibromagenesis, tumor progression towards malignancy and constitute a platform for drug screening (Fig. 2).

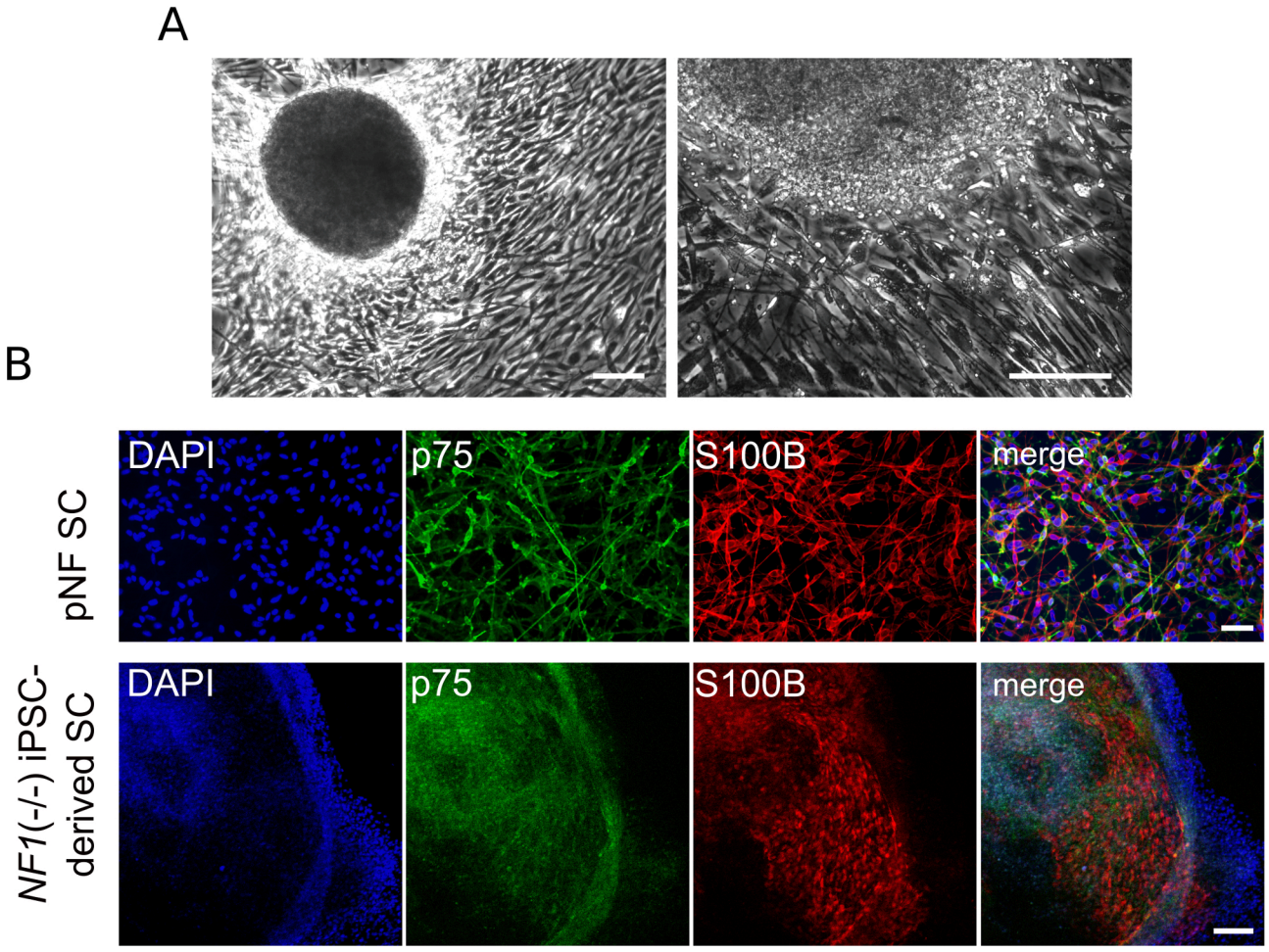

Fig. 1. Spheres from *NF1*(−/−) iPSC-derived SCs recapitulate the expression pattern of their pNF-derived SCs counterparts. A) Bright-field images showing the formation of spheres from *NF1*(−/−) iPSC-derived SCs at 20 days of differentiation. B) Representative immunofluorescent images showing expression of S100b and p75 in primary SCs (pNF SC) compared to sphere-forming *NF1*(−/−) iPSC-derived SCs at 30 days of differentiation. Scale bars, 100 μm. Images have been extracted and adapted from Carrió M. et al 2019.

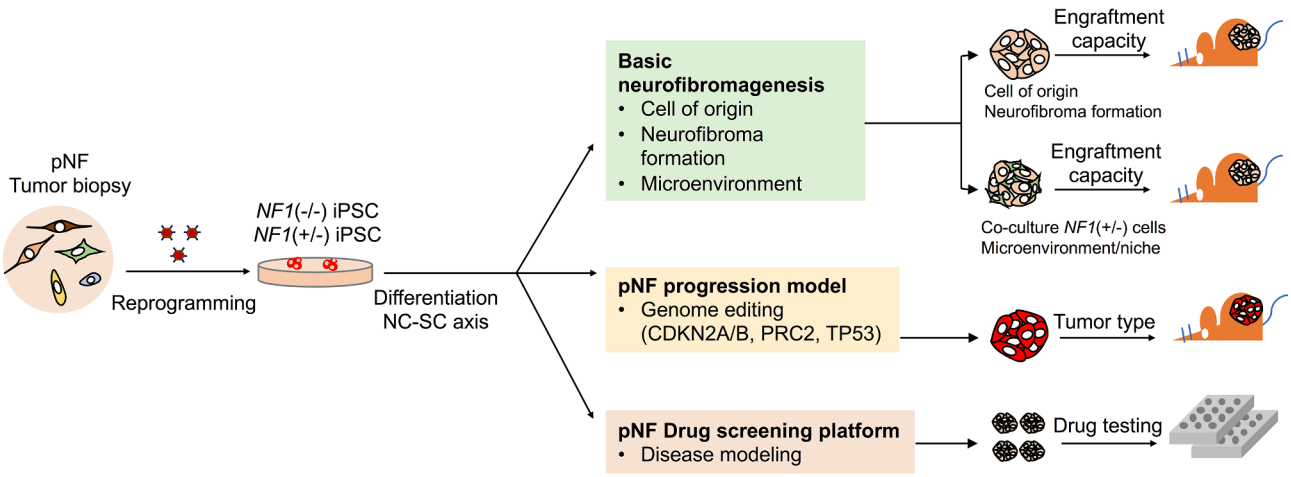

Fig. 2. An overview of pNF-derived iPSC modeling. pNF cells are reprogrammed and *NF1*(+/−) and *NF1*(−/−) iPSC clones are established and characterized. *NF1*(−/−) pNF-derived iPSC are then differentiated towards the NC-SC lineage. These differentiated cells can be used to generate tumor spheroids to study basic neurofibromagenesis either alone or after adding microenvironment components, or to study pNF progression to malignancy by incorporating specific mutations using genome editing. Either of these can then be transplanted into xenograft models. pNF-derived differentiated spheroids can also serve as a drug screening platform to identify and validate therapeutic targets.

7.1. Neurofibromagenesis and microenvironment

pNFs originate during development and iPSCs are ideal to reproduce cell states present along embryo development. The generation of spheroids from differentiating SCs at different time points of differentiation combined with their capacity to engraft in the sciatic nerve of nude mice and form neurofibroma-like tumors is a powerful strategy to capture the exact identity of pNF-originating cells (Fig. 2). These cells could be isolated and their transcriptome and epigenome extensively analyzed. Furthermore, pNF are complex cellular tumors, and microenvironment components can be easily incorporated in 3D models (Weydert et al., 2020). In this regard, we have recently established a multiplexed heterotypic spheroid 3D culture system using iPSC-derived *NF1*(−/−) SCs co-cultured with primary tumor *NF1*(+/−) endoneurial fibroblasts, to incorporate niche elements from the tumor microenvironment (Mazuelas et al. unpublished results). Changes in gene expression of spheroid-composing cells and spheroid *in vivo* engraftment capacity could be analyzed to evaluate the role of specific cells of microenvironment on tumor formation. Spheroids with progressive cellular complexity to mimic pNFs can be envisioned.

7.2. Modeling neurofibroma progression towards malignancy

The molecular pathogenesis of pNF-aNF-MPNST progression is well established. While pNFs bear the complete inactivation of *NF1*, aNFs in addition inactivate the *CDKN2A* locus. The most frequent genetic alteration found in MPNSTs, in addition to the preceding inactivation of the two tumor suppressors, is the functional loss of PRC2 by mutations in the *SUZ12* or *EED* genes. Alterations in these three tumor suppressors constitute a core signature of MPNST development (Serra et al., 2020). iPSCs are especially amenable to CRISPR/Cas9 genome editing (Hockemeyer and Jaenisch, 2016). Thus, *NF1*(−/−) iPSCs constitute a starting point, in which specific mutations of the core signature involved in progression towards MPNST could be introduced in a step-wise manner. An alternative way of modeling progression would be the editing of NCs, due to their amenability. In both scenarios, tumor formation capacity and tumor type generation could be tested and analyzed by engrafting spheroids formed with the edited cells into the sciatic nerve of nude mice (Fig. 2).

7.3. pNF drug development platform

Spheroid and 3D technology have greatly improved. One example is the growing number of available microplate systems for producing large quantities of individualized spheroids. These multiplex systems allow reading fluorescence and luminescence-based signals without the need for transfer to other platforms, allowing the collection of different physiological readouts, like viability and apoptosis. 3D assay systems are being explored to create more clinically relevant models of tumors for drug development (Weydert et al., 2020). Our developed multiplexed heterotypic spheroid 3D culture system (Mazuelas et al. unpublished results) is amenable to mid and high throughput drug testing and could be used to speed up the testing of new compounds on 3D pNF models (Fig. 2).

8. Conclusions

The development of benign and malignant tumors is common in hereditary cancer syndromes. Neurofibromatosis type 1 patients frequently develop benign pNFs that can progress towards MPNST. pNF cells can be reprogrammed to generate *NF1*(+/−) and *NF1*(−/−) iPSCs. *NF1*(−/−) SCs differentiated from iPSCs exhibit higher proliferation rate, poor myelination capacity and a natural tendency to form spheroids that recapitulate the marker expression of primary pNF SCs. These spheroids constitute an excellent model system to study neurofibroma origin, formation and tumor progression, as well as a platform for drug screening. pNF-derived iPSCs constitute a paradigm for modeling benign tumors that develop in the context of cancer predisposition syndromes.

Declaration of Competing Interest

The authors declare that they have no known competing financial interests or personal relationships that could have appeared to influence the work reported in this paper.

Acknowledgements

We would like to thank all members of the Hereditary Cancer Lab and Conxi Lazaro's lab. This work has mainly been supported by an agreement from the Johns Hopkins University School of Medicine and the Neurofibromatosis Therapeutic Acceleration Program (NTAP). Its

contents are solely the responsibility of the authors and do not necessarily represent the official views of the Johns Hopkins University School of Medicine. The work has also been supported by the Spanish Ministry of Science and Innovation, Carlos III Health Institute (ISCIII) (PI14/00577; PI17/00524) Plan Estatal de I + D + I 2013– 2016, co-financed by the FEDER program; and by the Government of Catalonia (2014-SGR338; 2017-SGR-496) and CERCA Program/Generalitat de Catalunya. We also would like to specially thank the Fundación Proyecto Neurofibromatosis, the Asociación de Afectados de Neurofibromatosis (AANF) and the Catalan Neurofibromatosis Association (ACNefi) for their constant support.

References

Abeshouse, A., Adebamowo, C., Adebamowo, S.N., Akbani, R., Akeredolu, T., Ally, A., Anderson, M.L., Anur, P., Appelbaum, E.L., Armenia, J., Auman, J.T., Bailey, M.H., Baker, L., Balasundaram, M., Balu, S., Barthel, F.P., Bartlett, J., Baylin, S.B., Behera, M., Belyaev, D., Bennett, J., Benz, C., Beroukhim, R., Birrer, M., Bocklage, T., Bodenheimer, T., Boice, L., Bootwalla, M.S., Bowen, J., Bowlby, R., Boyd, J., Brohl, A.S., Brooks, D., Byers, L., Carlsen, R., Castro, P., Chen, H.-W., Cherniack, A. D., Chibon, F., Chin, L., Cho, J., Chuah, E., Chudamani, S., Cibulskis, C., Cooper, L.A. D.D., Cope, L., Cordes, M.G., Crain, D., Curley, E., Danilova, L., Dao, F., Davis, I.J., Davis, L.E., Defreitas, T., Delman, K., Demchok, J.A., Demetri, G.D., Demicco, E.G., Dhalla, N., Diao, L., Ding, L., DiSaia, P., Dottino, P., Doyle, L.A., Drill, E., Dubina, M., Eschbacher, J., Fedosenko, K., Felau, I., Ferguson, M.L., Frazer, S., Fronick, C.C., Fulidou, V., Fulton, L.A., Fulton, R.S., Gabriel, S.B., Gao, J., Gao, Q., Gardner, J., Gastier-Foster, J.M., Gay, C.M., Gehlenborg, N., Gerken, M., Getz, G., Godwin, A.K., Godwin, E.M., Gordienko, E., Grilley-Olson, J.E., Gutman, D.A., Gutmann, D.H., Hayes, D.N., Hegde, A.M., Heiman, D.I., Heins, Z., Helsel, C., Hepperla, A.J., Higgins, K., Hoadley, K.A., Hobensack, S., Holt, R.A., Hoon, D.B., Hornick, J.L., Hoyle, A.P., Hu, X., Huang, M., Hutter, C.M., Iacocca, M., Ingram, D.R., Ittmann, M., Iype, L., Jefferys, S.R., Jones, K.B., Jones, C.D., Jones, S.J.M.M., Kalir, T., Karlan, B. Y., Karseladze, A., Kasaian, K., Kim, J., Kundra, R., Kuo, H., Ladanyi, M., Lai, P.H., Laird, P.W., Larsson, E., Lawrence, M.S., Lazar, A.J., Lee, S., Lee, D., Lehmann, K.-V., Leraas, K.M., Lester, J., Levine, D.A., Li, I., Lichtenberg, T.M., Lin, P., Liu, J., Liu, W., Liu, E.M., Lolla, L., Lu, Y., Ma, Y., Madan, R., Maglinte, D.T., Magliocco, A., Maki, R. G., Mallery, D., Manikhas, G., Mardis, E.R., Mariamidze, A., Marra, M.A., Martignetti, J.A., Martinez, C., Mayo, M., McLellan, M.D., Meier, S., Meng, S., Meyerson, M., Mieczkowski, P.A., Miller, C.A., Mills, G.B., Moore, R.A., Morris, S., Mose, L.E., Mozgovoy, E., Mungall, A.J., Mungall, K., Nalisnik, M., Naresh, R., Newton, Y., Noble, M.S., Novak, J.E., Ochoa, A., Olvera, N., Owonikoko, T.K., Paklina, O., Parfitt, J., Parker, J.S., Pastore, A., Paulauskis, J., Penny, R., Pereira, E., Perou, C.M., Perou, A.H., Pihl, T., Pollock, R.E., Potapova, O., Radenbaugh, A.J., Ramalingam, S.S., Ramirez, N.C., Rathmell, W.K., Raut, C.P., Riedel, R.F., Reilly, C., Reynolds, S.M., Roach, J., Robertson, A.G., Roszik, J., Rubin, B.P., Sadeghi, S., Saksena, G., Salner, A., Sanchez-Vega, F., Sander, C., Schein, J.E., Schmidt, H.K., Schultz, N., Schumacher, S.E., Sekhon, H., Senbabaoglu, Y., Setdikova, G., Shelton, C., Shelton, T., Shen, R., Shi, Y., Shih, J., Shmulevich, I., Sica, G.L., Simons, J.V., Singer, S., Sipahimalani, P., Skelly, T., Socci, N., Sofia, H.J., Soloway, M.G., Spellman, P., Sun, Q., Swanson, P., Tam, A., Tan, D., Tarnuzzer, R., Thiessen, N., Thompson, E., Thorne, L.B., Tong, P., Torres, K.E., van de Rijn, M., Van Den Berg, D.J., Van Tine, B.A., Veluvolu, U., Verhaak, R., Voet, D., Voronina, O., Wan, Y., Wang, Z., Wang, J., Weinstein, J.N., Weisenberger, D.J., Wilkerson, M.D., Wilson, R.K., Wise, L., Wong, T., Wong, W., Wrangle, J., Wu, Y., Wyczalkowski, M., Yang, L., Yau, C., Yellapantula, V., Zenklusen, J.C., Zhang (Julia), J., Zhang, H.H., Zhang, H.H., Zmuda, E., 2017. Comprehensive and integrated genomic characterization of adult soft tissue sarcomas. Cell 171, 950–965.e28. https://doi.org/10.1016/j.cell.2017.10.014.

Akshintala, S., Baldwin, A., Liewehr, D.J., Goodwin, A., Blakeley, J.O., Gross, A.M., Steinberg, S.M., Dombi, E., Widemann, B.C., 2020. Longitudinal evaluation of peripheral nerve sheath tumors in neurofibromatosis type 1: growth analysis of plexiform neurofibromas and distinct nodular lesions. Neuro. Oncol. d 1–11. https://doi.org/10.1093/neuonc/noaa053.

Anastasaki, C., Gutmann, D.H., 2014. Neuronal NF1/RAS regulation of cyclic AMP requires atypical PKC activation. Hum. Mol. Genet. 23, 6712–6721. https://doi.org/10.1093/hmg/ddu389.

Anastasaki, C., Woo, A.S., Messiaen, L.M., Gutmann, D.H., 2015. Elucidating the impact of neurofibromatosis-1 germline mutations on neurofibromin function and dopamine-based learning. Hum. Mol. Genet. 24, 3518–3528. https://doi.org/10.1093/hmg/ddv103.

Anastasaki, C., Wegscheid, M.L., Hartigan, K., Papke, J.B., Kopp, N.D., Chen, J., Cobb, O., Dougherty, J.D., Gutmann, D.H., 2020. Human iPSC-derived neurons and cerebral organoids establish differential effects of germline NF1 gene mutations. Stem Cell Rep. 14, 541–550. https://doi.org/10.1016/j.stemcr.2020.03.007.

Arthur-Farraj, P., Wanek, K., Hantke, J., Davis, C.M., Jayakar, A., Parkinson, D.B., Mirsky, R., Jessen, K.R., 2011. Mouse schwann cells need both NRG1 and cyclic AMP to myelinate. Glia 59, 720–733. https://doi.org/10.1002/glia.21144.

Baggiolini, A., Varum, S., Mateos, J.M., Bettosini, D., John, N., Bonalli, M., Ziegler, U., Dimou, L., Clevers, H., Furrer, R., Sommer, L., 2015. Premigratory and migratory neural crest cells are multipotent in vivo. Cell Stem Cell 16, 314–322. https://doi.org/10.1016/j.stem.2015.02.017.

Bar-Nur, O., Russ, H.A., Efrat, S., Benvenisty, N., 2011. Epigenetic memory and preferential lineage-specific differentiation in induced pluripotent stem cells derived from human pancreatic islet beta cells. Cell Stem Cell 9, 17–23. https://doi.org/10.1016/j.stem.2011.06.007.

Beert, E., Brems, H., Daniëls, B., De Wever, I., Van Calenbergh, F., Schoenaers, J., Debiec-Rychter, M., Gevaert, O., De Raedt, T., Van Den Bruel, A., de Ravel, T., Cichowski, K., Kluwe, L., Mautner, V., Sciot, R., Legius, E., 2011. Atypical neurofibromas in neurofibromatosis type 1 are premalignant tumors. Genes. Chromosom. Cancer 50, 1021–1032. https://doi.org/10.1002/gcc.20921.

Bronner, M.E., Simões-costa, M., 2016. The neural crest migrating into the 21st century Marianne. Curr. Top. Dev. Biol. 116, 115–134. https://doi.org/10.1016/bs.ctdb.2015.12.003.The.

Bronner-Fraser, M., Fraser, S.E., 1988. Application of new technologies to studies of neural crest migration and differentiation. Am. J. Med. Genet. Suppl. 4, 23–39. https://doi.org/10.1002/ajmg.1320310509.

Buchstaller, J., Clapp, D.W., Parada, L.F., Zhu, Y., 2012. Cell of Origin and the Contribution of Microenvironment in NF1 Tumorigenesis and Therapeutic Implications. In: Upadhyaya, M., Cooper, D.N. (Eds.), Neurofibromatosis Type 1: Molecular and Cellular Biology. Springer, Berlin Heidelberg, pp. 549–568. https://doi.org/10.1007/978-3-642-32864-0_36.

Buganim, Y., Faddah, D.A., Jaenisch, R., 2013. Mechanisms and models of somatic cell reprogramming. Nat. Rev. Genet. https://doi.org/10.1038/nrg3473.

Carrió, M., Gel, B., Terribas, E., Zucchiatti, A.C., Moliné, T., Rosas, I., Teulé, Á., Ramón y Cajal, S., López-Gutiérrez, J.C., Blanco, I., Castellanos, E., Lázaro, C., Stemmer-Rachamimov, A., Romagosa, C., Serra, E., 2018. Analysis of intratumor heterogeneity in Neurofibromatosis type 1 plexiform neurofibromas and neurofibromas with atypical features: correlating histological and genomic findings. Hum. Mutat. 39 https://doi.org/10.1002/humu.23552.

Carrió, M., Mazuelas, H., Richaud-Patin, Y., Gel, B., Terribas, E., Rosas, I., Jimenez-Delgado, S., Biayna, J., Vendredy, L., Blanco, I., Castellanos, E., Lázaro, C., Raya, Á., Serra, E., 2019. Reprogramming captures the genetic and tumorigenic properties of neurofibromatosis type 1 plexiform neurofibromas. Stem Cell Rep. 12 https://doi.org/10.1016/j.stemcr.2019.01.001.

Castellanos, E., Gel, B., Rosas, I., Tornero, E., Santín, S., Pluvinet, R., Velasco, J., Sumoy, L., del Valle, J., Perucho, M., Blanco, I., Navarro, M., Brunet, J., Pineda, M., Feliubadaló, L., Capellá, G., Lázaro, C., Serra, E., 2017. A comprehensive custom panel design for routine hereditary cancer testing: preserving control, improving diagnostics and revealing a complex variation landscape. Sci. Rep. 7, 39348. https://doi.org/10.1038/srep39348.

Castellsagué, J., Gel, B., Fernández-Rodríguez, J., Llatjós, R., Blanco, I., Benavente, Y., Pérez-Sidelnikova, D., García-Del Muro, J., Viñals, J.M., Vidal, A., Valdés-Mas, R., Terribas, E., López-Doriga, A., Pujana, M.A., Capellá, G., Puente, X.S., Serra, E., Villanueva, A., Lázaro, C., 2015. Comprehensive establishment and characterization of orthoxenograft mouse models of malignant peripheral nerve sheath tumors for personalized medicine. EMBO Mol. Med. 7, 608–627. https://doi.org/10.15252/emmm.201404430.

Chambers, S.M., Fasano, C.A., Papapetrou, E.P., Tomishima, M., Sadelain, M., Studer, L., 2009. Highly efficient neural conversion of human ES and iPS cells by dual inhibition of SMAD signaling. Nat. Biotechnol. 27, 275–280. https://doi.org/10.1038/nbt.1529.

Chen, Z., Liu, C., Patel, A.J., Liao, C.-P., Wang, Y., Le, L.Q., 2014. Cells of origin in the embryonic nerve roots for NF1-associated plexiform neurofibroma. Cancer Cell 26, 695–706. https://doi.org/10.1016/j.ccell.2014.09.009.

Chen, Z., Mo, J., Brosseau, J.-P., Shipman, T., Wang, Y., Liao, C.-P., Cooper, J.M., Allaway, R.J., Gosline, S.J.C., Guinney, J., Carroll, T.J., Le, L.Q., 2018. Spatiotemporal loss of *NF1*in schwann cell lineage leads to different types of cutaneous neurofibroma susceptible to modification by the hippo pathway. Cancer Discov. 9 https://doi.org/10.1158/2159-8290.CD-18-0151.

Cichowski, K., Jacks, T., 2001. NF1 tumor suppressor gene function. Cell 104, 593–604. https://doi.org/10.1016/s0092-8674(01)00245-8.

Dombi, E., Baldwin, A., Marcus, L.J., Fisher, M.J., Weiss, B., Kim, A., Whitcomb, P., Martin, S., Aschbacher-Smith, L.E., Rizvi, T.A., Wu, J., Ershler, R., Wolters, P., Therrien, J., Glod, J., Belasco, J.B., Schorry, E., Brofferio, A., Starosta, A.J., Gillespie, A., Doyle, A.L., Ratner, N., Widemann, B.C., 2016. Activity of selumetinib in neurofibromatosis type 1–related plexiform neurofibromas. N. Engl. J. Med. 375, 2550–2560. https://doi.org/10.1056/NEJMoa1605943.

Eminli, S., Foudi, A., Stadtfeld, M., Maherali, N., Ahfeldt, T., Mostoslavsky, G., Hock, H., Hochedlinger, K., 2009. Differentiation stage determines reprogramming potential of hematopoietic cells into iPS cells. Nat. Genet. 41, 968–976. https://doi.org/10.1038/ng.428.

Etchevers, H.C., Dupin, E., Le Douarin, N.M., 2019. The diverse neural crest: from embryology to human pathology. Development 146. https://doi.org/10.1242/dev.169821.

Evans, D.G.R., Baser, M.E., McGaughran, J., Sharif, S., Howard, E., Moran, A., 2002. Malignant peripheral nerve sheath tumours in neurofibromatosis 1. J. Med. Genet. 39, 311–314. https://doi.org/10.1136/jmg.39.5.311.

Feng, S., Jacobsen, S.E., Reik, W., 2010. Epigenetic reprogramming in plant and animal development. Science (80-.) 330, 622–627. https://doi.org/10.1126/science.1190614.

Ferner, R.E., 2007. Neurofibromatosis 1 and neurofibromatosis 2: a twenty first century perspective. Lancet Neurol. 6, 340–351. https://doi.org/10.1016/S1474-4422(07)70075-3.

Firas, J., Liu, X., Polo, J.M., 2014. Epigenetic memory in somatic cell nuclear transfer and induced pluripotency: evidence and implications. Differentiation 88, 29–32. https://doi.org/10.1016/j.diff.2014.09.001.

Furlan, A., Adameyko, I., 2018. Schwann cell precursor: a neural crest cell in disguise? Dev. Biol. 444, S25–S35. https://doi.org/10.1016/j.ydbio.2018.02.008.
Garcia-Linares, C., Fernández-Rodríguez, J., Terribas, E., Mercadé, J., Pros, E., Benito, L., Benavente, Y., Capellà, G., Ravella, A., Blanco, I., Kehrer-Sawatzki, H., Lázaro, C., Serra, E., 2011. Dissecting loss of heterozygosity (LOH) in neurofibromatosis type 1-associated neurofibromas: Importance of copy neutral LOH. Hum. Mutat. 32, 78–90. https://doi.org/10.1002/humu.21387.
Geuna, S., Raimondo, S., Fregnan, F., Grothe, C., 2016. In vitro models for peripheral nerve regeneration. Eur. J. Neurosci. 43, 287–296. https://doi.org/10.1111/ejn.13054.
Ghosh, S., Yates, A.J., Frühwald, M.C., Miecznikowski, J.C., Plass, C., Smiraglia, D., 2010. Tissue specific DNA methylation of CpG islands in normal human adult somatic tissues distinguishes neural from non-neural tissues. Epigenetics 5, 527–538.
Gresset, A., Coulpier, F., Gerschenfeld, G., Jourdon, A., Matesic, G., Richard, L., Vallat, J. M., Charnay, P., Topilko, P., 2015. Boundary caps give rise to neurogenic stem cells and terminal Glia in the skin. Stem Cell Rep. 5, 278–290. https://doi.org/10.1016/j.stemcr.2015.06.005.
Gross, A.M., Wolters, P.L., Dombi, E., Baldwin, A., Whitcomb, P., Fisher, M.J., Weiss, B., Kim, A., Bornhorst, M., Shah, A.C., Martin, S., Roderick, M.C., Pichard, D.C., Carbonell, A., Paul, S.M., Therrien, J., Kapustina, O., Heisey, K., Clapp, D.W., Zhang, C., Peer, C.J., Figg, W.D., Smith, M., Glod, J., Blakeley, J.O., Steinberg, S.M., Venzon, D.J., Doyle, L.A., Widemann, B.C., 2020. Selumetinib in children with inoperable plexiform neurofibromas. N. Engl. J. Med. 382, 1430–1442. https://doi.org/10.1056/NEJMoa1912735.
Hackland, J.O.S., Frith, T.J.R., Thompson, O., Marin Navarro, A., Garcia-Castro, M.I., Unger, C., Andrews, P.W., 2017. Top-down inhibition of BMP signaling enables robust induction of hPSCs into neural crest in fully defined, xeno-free conditions. Stem Cell Rep. 9, 1043–1052. https://doi.org/10.1016/j.stemcr.2017.08.008.
Hanna, J., Saha, K., Pando, B., Van Zon, J., Lengner, C.J., Creyghton, M.P., Van Oudenaarden, A., Jaenisch, R., 2009. Direct cell reprogramming is a stochastic process amenable to acceleration. Nature 462, 595–601. https://doi.org/10.1038/nature08592.
Higham, C.S., Dombi, E., Rogiers, A., Bhaumik, S., Pans, S., Connor, S.E.J., Miettinen, M., Sciot, R., Tirabosco, R., Brems, H., Baldwin, A., Legius, E., Widemann, B.C., Ferner, R.E., 2018. The characteristics of 76 atypical neurofibromas as precursors to neurofibromatosis 1 associated malignant peripheral nerve sheath tumors. Neuro. Oncol. https://doi.org/10.1093/neuonc/noy013.
Hirbe, A.C., Dahiya, S., Miller, C.A., Li, T., Fulton, R.S., Zhang, X., McDonald, S., DeSchryver, K., Duncavage, E.J., Walrath, J., Reilly, K.M., Abel, H.J., Pekmezci, M., Perry, A., Ley, T.J., Gutmann, D.H., 2015. Whole exome sequencing reveals the order of genetic changes during malignant transformation and metastasis in a single patient with NF1-plexiform neurofibroma. Clin. Cancer Res. 21, 4201–4211. https://doi.org/10.1158/1078-0432.CCR-14-3049.
Hockemeyer, D., Jaenisch, R., 2016. Induced pluripotent stem cells meet genome editing. Cell Stem Cell. https://doi.org/10.1016/j.stem.2016.04.013.
Hu, B.-Y., Weick, J.P., Yu, J., Ma, L.-X., Zhang, X.-Q., Thomson, J.A., Zhang, S.-C., 2010. Neural differentiation of human induced pluripotent stem cells follows developmental principles but with variable potency. Proc. Natl. Acad. Sci. 107, 4335–4340. https://doi.org/10.1073/pnas.0910012107.
Huson, S.M., Harper, P.S., Compston, D.A., 1988. Von Recklinghausen neurofibromatosis. A clinical and population study in south-east Wales. Brain 111 (Pt 6), 1355–1381.
Jessen, K.R., Mirsky, R., 2005. The origin and development of glial cells in peripheral nerves. Nat. Rev. Neurosci. 6, 671–682. https://doi.org/10.1038/nrn1746.
Jessen, K.R., Mirsky, R., 2019. Schwann cell precursors; multipotent glial cells in embryonic nerves. Front. Mol. Neurosci. 12 https://doi.org/10.3389/fnmol.2019.00069.
Joseph, N.M., Mosher, J.T., Buchstaller, J., Snider, P., McKeever, P.E., Lim, M., Conway, S.J., Parada, L.F., Zhu, Y., Morrison, S.J., 2008. The loss of Nf1 transiently promotes self-renewal but not tumorigenesis by neural crest stem cells. Cancer Cell 13, 129–140. https://doi.org/10.1016/j.ccr.2008.01.003.
Kastriti, M.E., Adameyko, I., 2017. Specification, plasticity and evolutionary origin of peripheral glial cells. Curr. Opin. Neurobiol. 47, 196–202. https://doi.org/10.1016/j.conb.2017.11.004.
Katarzyna, K.J., Topilko, P., 2017. Boundary cap cells in development and disease. Curr. Opin. Neurobiol. 47, 209–215. https://doi.org/10.1016/j.conb.2017.11.003.
Kluwe, L., Friedrich, R., Mautner, V.F., 1999. Loss of NF1 allele in Schwann cells but not in fibroblasts derived from an NF1-associated neurofibroma. Genes Chromosomes Cancer 24, 283–285.
Kraniak, J.M., Chalasani, A., Wallace, M.R., Mattingly, R.R., 2018. Development of 3D culture models of plexiform neurofibroma and initial application for phenotypic characterization and drug screening. Exp. Neurol. 299, 289–298. https://doi.org/10.1016/j.expneurol.2017.10.012.
Krone, W., Jirikowski, G., Mühleck, O., Kling, H., Gall, H., 1983. Cell culture studies on neurofibromatosis (von Recklinghausen). II. Occurrence of glial cells in primary cultures of peripheral neurofibromas. Hum. Genet. 63, 247–251.
Larribere, L., Wu, H., Novak, D., Galach, M., Bernhardt, M., Orouji, E., Weina, K., Knappe, N., Sachpekidis, C., Umansky, L., Beckhove, P., Umansky, V., De Schepper, S., Kaufmann, D., Ballotti, R., Bertolotto, C., Utikal, J., 2015. NF1 loss induces senescence during human melanocyte differentiation in an iPSC-based model. Pigment Cell Melanoma Res. 28, 407–416. https://doi.org/10.1111/pcmr.12369.
Le, L.Q., Shipman, T., Burns, D.K., Parada, L.F., 2009. Cell of origin and microenvironment contribution for NF1-associated dermal neurofibromas. Cell Stem Cell 4, 453–463. https://doi.org/10.1016/j.stem.2009.03.017.
Le, L.Q., Liu, C., Shipman, T., Chen, Z., Suter, U., Parada, L.F., 2011. Susceptible stages in Schwann cells for NF1-associated plexiform neurofibroma development. Cancer Res. 71, 4686–4695. https://doi.org/10.1158/0008-5472.CAN-10-4577.
Lee, G., Kim, H., Elkabetz, Y., Al Shamy, G., Panagiotakos, G., Barberi, T., Tabar, V., Studer, L., 2007. Isolation and directed differentiation of neural crest stem cells derived from human embryonic stem cells. Nat. Biotechnol. 25, 1468–1475. https://doi.org/10.1038/nbt1365.
Lee, G., Chambers, S.M., Tomishima, M.J., Studer, L., 2010. Derivation of neural crest cells from human pluripotent stem cells. Nat. Protoc. 5, 688–701. https://doi.org/10.1038/nprot.2010.35.
Lee, D.-F., Su, J., Kim, H.S., Chang, B., Papatsenko, D., Zhao, R., Yuan, Y., Gingold, J., Xia, W., Darr, H., Mirzayans, R., Hung, M.-C., Schaniel, C., Lemischka, I.R., 2015. Modeling familial cancer with induced pluripotent stem cells. Cell 161, 240–254. https://doi.org/10.1016/j.cell.2015.02.045.
Li, H., Chang, L.-J., Neubauer, D.R., Muir, D.F., Wallace, M.R., 2016. Immortalization of human normal and NF1 neurofibroma Schwann cells. Lab. Investig. 96, 1105–1115. https://doi.org/10.1038/labinvest.2016.88.
Liu, Q., Spusta, S.C., Mi, R., Lassiter, R.N.T., Stark, M.R., Höke, A., Rao, M.S., Zeng, X., 2012. Human neural crest stem cells derived from human ESCs and induced pluripotent stem cells: induction, maintenance, and differentiation into functional schwann cells. Stem Cells Transl. Med. 1, 266–278. https://doi.org/10.5966/sctm.2011-0042.
Ma, M.S., Boddeke, E., Copray, S., 2015. Pluripotent stem cells for schwann cell engineering. Stem Cell Rev. Rep. 11, 205–218. https://doi.org/10.1007/s12015-014-9577-1.
Maertens, O., Brems, H., Vandesompele, J., De Raedt, T., Heyns, I., Rosenbaum, T., De Schepper, S., De Paepe, A., Mortier, G., Janssens, S., Speleman, F., Legius, E., Messiaen, L., 2006. ComprehensiveNF1 screening on cultured Schwann cells from neurofibromas. Hum. Mutat. 27, 1030–1040. https://doi.org/10.1002/humu.20389.
Marchetto, M.C.N., Yeo, G.W., Kainohana, O., Marsala, M., Gage, F.H., Muotri, A.R., 2009. Transcriptional signature and memory retention of human-induced pluripotent stem cells. PLoS One 4, e7076. https://doi.org/10.1371/journal.pone.0007076.
Marol, G.S., Vermeren, M., Voiculescu, O., Melton, L., Cohen, J., Charnay, P., Topilko, P., 2004. Neural crest boundary cap cells constitute a source of neuronal and glial cells of the PNS. Nat. Neurosci. 7, 930–938. https://doi.org/10.1038/nn1299.
Mautner, V.-F., Asuagbor, F.A., Dombi, E., Funsterer, C., Kluwe, L., Wenzel, R., Widemann, B.C., Friedman, J.M., 2008. Assessment of benign tumor burden by whole-body MRI in patients with neurofibromatosis 1. Neuro. Oncol. 10, 593–598. https://doi.org/10.1215/15228517-2008-011.
McCarron, K.F., Goldblum, J.R., 1998. Plexiform neurofibroma with and without associated malignant peripheral nerve sheath tumor: a clinicopathologic and immunohistochemical analysis of 54 cases. Mod. Pathol. 11, 612–617.
Menendez, L., Yatskievych, T.A., Antin, P.B., Dalton, S., 2011. Wnt signaling and a Smad pathway blockade direct the differentiation of human pluripotent stem cells to multipotent neural crest cells. Proc. Natl. Acad. Sci. U.S.A. 108, 19240–19245. https://doi.org/10.1073/pnas.1113746108.
Menendez, L., Kulik, M.J., Page, A.T., Park, S.S., Lauderdale, J.D., Cunningham, M.L., Dalton, S., 2013. Directed differentiation of human pluripotent cells to neural crest stem cells. Nat. Protoc. 8, 203–212. https://doi.org/10.1038/nprot.2012.156.
Messiaen, L., Wimmer, K., 2008. NF1 mutational spectrum. Monogr. Hum. Genet. 63–77. https://doi.org/10.1159/000126545.
Mica, Y., Lee, G., Chambers, S.M., Tomishima, M.J., Studer, L., 2013. Modeling neural crest induction, melanocyte specification, and disease-related pigmentation defects in hescs and patient-specific iPSCs. Cell Rep. 3, 1140–1152. https://doi.org/10.1016/j.celrep.2013.03.025.
Miettinen, M.M., Antonescu, C.R., Fletcher, C.D.M., Kim, A., Lazar, A.J., Quezado, M.M., Reilly, K.M., Stemmer-Rachamimov, A., Stewart, D.R., Viskochil, D., Widemann, B., Perry, A., 2017. Histopathologic evaluation of atypical neurofibromatous tumors and their transformation into malignant peripheral nerve sheath tumor in patients with neurofibromatosis 1—a consensus overview. Hum. Pathol. 67, 1–10. https://doi.org/10.1016/j.humpath.2017.05.010.
Monk, K.R., Feltri, M.L., Taveggia, C., 2015. New insights on schwann cell development. Glia 63, 1376–1393. https://doi.org/10.1002/glia.22852.
Morrison, S.J., White, P.M., Zock, C., Anderson, D.J., 1999. Prospective identification, isolation by flow cytometry, and in vivo self-renewal of multipotent mammalian neural crest stem cells. Cell 96, 737–749. https://doi.org/10.1016/S0092-8674(00)80583-8.
Muir, D., Neubauer, D., Lim, I.T., Yachnis, A.T., Wallace, M.R., 2001. Tumorigenic properties of neurofibromin-deficient neurofibroma schwann cells. Am. J. Pathol. 158, 501–513. https://doi.org/10.1016/S0002-9440(10)63992-2.
Ortonne, N., Wolkenstein, P., Blakeley, J.O., Korf, B., Plotkin, S.R., Riccardi, V.M., Miller, D.C., Huson, S., Peltonen, J., Rosenberg, A., Carroll, S.L., Verma, S.K., Mautner, V., Upadhyaya, M., Stemmer-Rachamimov, A., 2018. Cutaneous neurofibromas. Neurology 91, S5–S13. https://doi.org/10.1212/WNL.0000000000005792.
Peltonen, J., Penttinen, R., Larjava, H., Aho, H.J., 1986. Collagens in neurofibromas and neurofibroma cell cultures. Ann. N. Y. Acad. Sci. 486, 260–270.
Pemov, A., Li, H., Patidar, R., Hansen, N.F., Sindiri, S., Hartley, S.W., Wei, J.S., Elkahloun, A., Chandrasekharappa, S.C., Boland, J.F., Bass, S., Mullikin, J.C., Khan, J., Widemann, B.C., Wallace, M.R., Stewart, D.R., Wallace, M.R., Stewart, D. R., 2017. The primacy of NF1 loss as the driver of tumorigenesis in neurofibromatosis type 1-associated plexiform neurofibromas. Oncogene 36, 3168–3177. https://doi.org/10.1038/onc.2016.464.
Pemov, A., Hansen, N.F., Sindiri, S., Patidar, R., Higham, C.S., Dombi, E., Miettinen, M. M., Fetsch, P., Brems, H., Chandrasekharappa, S.C., Jones, K., Zhu, B., Wei, J.S.,

Mullikin, J.C., Wallace, M.R., Khan, J., Legius, E., Widemann, B.C., Stewart, D.R., 2019. Low mutation burden and frequent loss of CDKN2A/B and SMARCA2, but not PRC2, define premalignant neurofibromatosis type 1–associated atypical neurofibromas. Neuro. Oncol. 21, 981–992. https://doi.org/10.1093/neuonc/noz028.

Pomp, O., Brokhman, I., Ben-Dor, I., Reubinoff, B., Goldstein, R.S., 2005. Generation of peripheral sensory and sympathetic neurons and neural crest cells from human embryonic stem cells. Stem Cells 23, 923–930. https://doi.org/10.1634/stemcells.2005-0038.

Prada, C.E., Rangwala, F.A., Martin, L.J., Lovell, A.M., Saal, H.M., Schorry, E.K., Hopkin, R.J., 2012. Pediatric plexiform neurofibromas: impact on morbidity and mortality in neurofibromatosis type 1. J. Pediatr. 160, 461–467. https://doi.org/10.1016/j.jpeds.2011.08.051.

Radomska, K.J., Coulpier, F., Gresset, A., Schmitt, A., Debbiche, A., Lemoine, S., Wolkenstein, P., Vallat, J.M., Charnay, P., Topilko, P., 2019. Cellular origin, tumor progression, and pathogenic mechanisms of cutaneous neurofibromas revealed by mice with Nf1 knockout in boundary cap cells. Cancer Discov. 9, 130–147. https://doi.org/10.1158/2159-8290.CD-18-0156.

Ratner, N., Miller, S.J., 2015. A RASopathy gene commonly mutated in cancer: the neurofibromatosis type 1 tumour suppressor. Nat. Rev. Cancer 15, 290–301. https://doi.org/10.1038/nrc3911.

Rhodes, S.D., He, Y., Smith, A., Jiang, L., Lu, Q., Mund, J., Li, X., Bessler, W., Qian, S., Dyer, W., Sandusky, G.E., Horvai, A.E., Armstrong, A.E., Clapp, D.W., 2019. Cdkn2a (Arf) loss drives NF1-associated atypical neurofibroma and malignant transformation. Hum. Mol. Genet. 28, 2752–2762. https://doi.org/10.1093/hmg/ddz095.

Riccardi, V.M., 1992. Neurofibromatosis: Phenotype, Natural History, and Pathogenesis, 2nd ed. Johns Hopkins University Press, Baltimore.

Röhrich, M., Koelsche, C., Schrimpf, D., Capper, D., Sahm, F., Kratz, A., Reuss, J., Hovestadt, V., Jones, D.T.W., Bewerunge-Hudler, M., Becker, A., Weis, J., Mawrin, C., Mittelbronn, M., Perry, A., Mautner, V.-F., Mechtersheimer, G., Hartmann, C., Okuducu, A.F., Arp, M., Seiz-Rosenhagen, M., Hänggi, D., Heim, S., Paulus, W., Schittenhelm, J., Ahmadi, R., Herold-Mende, C., Unterberg, A., Pfister, S. M., von Deimling, A., Reuss, D.E., 2016. Methylation-based classification of benign and malignant peripheral nerve sheath tumors. Acta Neuropathol. 131, 877–887. https://doi.org/10.1007/s00401-016-1540-6.

Rosenbaum, T., Rosenbaum, C., Winner, U., Müller, H.W., Lenard, H.G., Hanemann, C. O., 2000. Long-term culture and characterization of human neurofibroma-derived Schwann cells. J. Neurosci. Res. 61, 524–532. https://doi.org/10.1002/1097-4547(20000901)61:5<524::AID-JNR7>3.0.CO;2-Z.

Serra, E., Rosenbaum, T., Winner, U., Aledo, R., Ars, E., Estivill, X., Lenard, H.G., Lázaro, C., 2000. Schwann cells harbor the somatic NF1 mutation in neurofibromas: evidence of two different Schwann cell subpopulations. Hum. Mol. Genet. 9, 3055–3064.

Serra, E., Ars, E., Ravella, A., Sánchez, A., Puig, S., Rosenbaum, T., Estivill, X., Lázaro, C., 2001. Somatic NF1 mutational spectrum in benign neurofibromas: mRNA splice defects are common among point mutations. Hum. Genet. 108, 416–429.

Serra, E., Gel, B., Fernández-Rodríguez, J., Lázaro, C., 2020. Genomics of peripheral nerve sheath tumors associated with neurofibromatosis type 1. In: Multidisciplinary Approach to Neurofibromatosis Type 1. Springer International Publishing, pp. 117–147. https://doi.org/10.1007/978-3-319-92450-2_9.

Shakiba, N., Fahmy, A., Jayakumaran, G., McGibbon, S., David, L., Trcka, D., Elbaz, J., Puri, M.C., Nagy, A., van der Kooy, D., Goyal, S., Wrana, J.L., Zandstra, P.W., 2019. Cell competition during reprogramming gives rise to dominant clones. Science (80.-) 364. https://doi.org/10.1126/science.aan0925.

Soldatov, R., Kaucka, M., Kastriti, M.E., Petersen, J., Chontorotzea, T., Englmaier, L., Akkuratova, N., Yang, Y., Häring, M., Dyachuk, V., Bock, C., Farlik, M., Piacentino, M.L., Boismoreau, F., Hilscher, M.M., Yokota, C., Qian, X., Nilsson, M., Bronner, M.E., Croci, L., Hsiao, W.Y., Guertin, D.A., Brunet, J.F., Consalez, G.G., Ernfors, P., Fried, K., Kharchenko, P.V., Adameyko, I., 2019. Spatiotemporal structure of cell fate decisions in murine neural crest. Science (80.-) 364. https://doi.org/10.1126/science.aas9536.

Tchieu, J., Zimmer, B., Fattahi, F., Amin, S., Zeltner, N., Chen, S., Studer, L., 2017. A modular platform for differentiation of human PSCs into all major ectodermal lineages. Cell Stem Cell 21, 399–410.e7. https://doi.org/10.1016/j.stem.2017.08.015.

Utikal, J., Polo, J.M., Stadtfeld, M., Maherali, N., Kulalert, W., Walsh, R.M., Khalil, A., Rheinwald, J.G., Hochedlinger, K., 2009. Immortalization eliminates a roadblock during cellular reprogramming into iPS cells. Nature 460, 1145–1148. https://doi.org/10.1038/nature08285.

Uusitalo, E., Rantanen, M., Kallionpää, R.A., Pöyhönen, M., Leppävirta, J., Ylä-Outinen, H., Riccardi, V.M., Pukkala, E., Pitkäniemi, J., Peltonen, S., Peltonen, J., 2016. Distinctive cancer associations in patients with neurofibromatosis type 1. J. Clin. Oncol. 34, 1978–1986. https://doi.org/10.1200/JCO.2015.65.3576.

Vaskova, E.A., Stekleneva, A.E., Medvedev, S.P., Zakian, S.M., 2013. "Epigenetic memory" phenomenon in induced pluripotent stem cells. Acta Naturae 5, 15–21.

Wallace, M.R., Rasmussen, S.A., Lim, I.T., Gray, B.A., Zori, R.T., Muir, D., 2000. Culture of cytogenetically abnormal schwann cells from benign and malignant NF1 tumors. Genes. Chromosomes Cancer 27, 117–123.

Wang, A., Tang, Z., Park, I.H., Zhu, Y., Patel, S., Daley, G.Q., Li, S., 2011. Induced pluripotent stem cells for neural tissue engineering. Biomaterials 32, 5023–5032. https://doi.org/10.1016/j.biomaterials.2011.03.070.

Wegscheid, M.L., Anastasaki, C., Gutmann, D.H., 2018. Human stem cell modeling in neurofibromatosis type 1 (NF1). Exp. Neurol. 299, 270–280. https://doi.org/10.1016/j.expneurol.2017.04.001.

Weydert, Z., Lal-Nag, M., Mathews-Greiner, L., Thiel, C., Cordes, H., Küpfer, L., Guye, P., Kelm, J.M., Ferrer, M., 2020. A 3D heterotypic multicellular tumor spheroid assay platform to discriminate drug effects on stroma versus cancer cells. SLAS Discov. 25, 265–276. https://doi.org/10.1177/2472555219880194.

Wu, J., Williams, J.P., Rizvi, T.A., Kordich, J.J., Witte, D., Meijer, D., Stemmer-Rachamimov, A.O., Cancelas, J.A., Ratner, N., 2008. Plexiform and dermal neurofibromas and pigmentation are caused by Nf1 loss in desert hedgehog-expressing cells. Cancer Cell 13, 105–116. https://doi.org/10.1016/j.ccr.2007.12.027.

Yamanaka, S., 2009. Elite and stochastic models for induced pluripotent stem cell generation. Nature. https://doi.org/10.1038/nature08180.

Zheng, H., Chang, L., Patel, N., Yang, J., Lowe, L., Burns, D.K., Zhu, Y., 2008. Induction of abnormal proliferation by nonmyelinating schwann cells triggers neurofibroma formation. Cancer Cell 13, 117–128. https://doi.org/10.1016/j.ccr.2008.01.002.

Zhu, Y., Ghosh, P., Charnay, P., Burns, D.K., Parada, L.F., 2002. Neurofibromas in NF1: schwann cell origin and role of tumor environment. Science (80-.) 296, 920–922. https://doi.org/10.1126/science.1068452.

Ziegler, L., Grigoryan, S., Yang, I.H., Thakor, N.V., Goldstein, R.S., 2011. Efficient generation of schwann cells from human embryonic stem cell-derived neurospheres. Stem Cell Rev. Rep. 7, 394–403. https://doi.org/10.1007/s12015-010-9198-2.

Appendix 5

1. Directors’ report

Eduard Serra Arenas and Meritxell Carrió Llach, as co-directors of the doctoral thesis of Helena Mazuelas Gallego entitled "*Modeling Neurofibromatosis type 1 neurofibroma composition and formation"*, certify that the doctoral candidate has actively participated in designing experimental work included in this thesis and conducting the main experimental part of it, including the analysis and presentation of results, discussion and drawing conclusions, and preparing publications.

The experimental work performed by the candidate has been extensive and involving expertise in many different techniques. Below is a summary of the experimental work developed by the candidate:

- The candidate performed all the experimental procedures to set up the NC and SC differentiation protocols including setting up cell culture conditions, cellular and molecular characterization of the processes, and functional NC and SC assays.
- She performed all experimental procedures to perform RNAseq analysis from iPSC lines, NC and SC differentiating cells both in 2D and 3D: set up differentiation experiments, RNA extraction and sample preparation.
- The candidate performed all the experimental procedures to set up the 3D SC differentiation protocol including setting up cell culture conditions and characterization of the model both at the cellular and molecular level. She also performed the differentiation experiments, prepared the cells for injection, help dissecting the mice and prepared biological samples for processing.
- Helena also established SC and Fb primary cultures, performed immunofluorescence and cytometry analysis. She set up the experimental design for co-culturing Sc and Fb, characterized LOH in cNF tumors, selected candidates and performed co-cultures experiment. She also performed flow cytometry analysis, RNA extraction and analysis of supernatants using Luminex technology.
- The candidate set up experimental conditions to prepare tumors for scRNA-seq

Despite the main contribution of the candidate in all the work presented here, due to the numerous techniques and expertise required for the developed work, this thesis also benefited from the collaboration with other individuals and groups, and the help of core facilities, as follows:

Bioinformatic analysis were basically performed by Miriam Magallon and Bernat Gel, Hereditary Cancer Lab-IGTP

The generation of the CRISPR/Cas9 edited *NF1*(-/-) iPS cell line was performed by Itziar Uriarte, Hereditary Cancer Lab-IGTP

Generation and main characterization of iPSCs was performed by Yvonne Richaud at Ángel Raya's lab, now at the CMRB-IDIBELL

Mice manipulation and cell injection was performed by Juana Fernández-Rodriguez at Conxi Lázaro's lab, IDIBELL-IGTP

Paraffin embedding, H&E and IHC were performed at the Pathology Department of the Vall d'Hebron Hospital (*in vivo* experiment 1) and at the Banc de Tumors and Pathology Department of the Germans Trias i Pujol Hospital (*in vivo* engraftment 2).

Single-cell RNA-seq analysis was performed by the Single Cell Genomics Group, at CNAG, led by Holger Heyn

Different techniques were performed at distinct IGTP Core Facilities, benefiting from their expertise: Cytometry; High Content Genomics and Bioiformatics; Microscopy, Translational Genomics.

Article contribution of the candidate:

Article 1 (Appendix 3)

Reprogramming Captures the Genetic and Tumorigenic Properties of Neurofibromatosis Type 1 Plexiform Neurofibromas

Meritxell Carrió, **Helena Mazuelas**, Yvonne Richaud-Patin, Bernat Gel, Ernest Terribas, Imma Rosas, Senda Jimenez-Delgado, Josep Biayna, Leen Vendredy, Ignacio Blanco, Elisabeth Castellanos, Conxi Lázaro, Ángel Raya, and Eduard Serra

Stem Cell Reports Vol. 12 411–426, 2019

Impact factor (2019 JCR Science Edition): 5.60

Contribution of the PhD candidate: set up NC and SC differentiation protocol including characterization by RT-qPCR analysis; Flow cytometry, immunofluorescence as well as functional assays (migration assay, myelination assay). Participation in the analysis of the data; presentation of results and figures; revising the manuscript.

Article 2 (Appendix 4)

Modeling tumors of the peripheral nervous system associated to Neurofibromatosis type 1: reprogramming plexiform neurofibroma cells

Helena Mazuelas, Meritxell Carrió, Eduard Serra

Stem Cell Research. Review article (2019 JCR Science Edition): 4.48 Accepted for publication

Contribution of the PhD candidate: active participation of the writing of the review article, preparation of figures and tables.

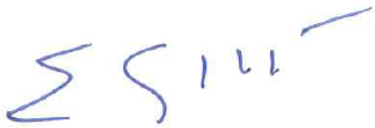

Meritxell Carrió Llach, Co-director

Eduard Serra Arenas, Co-director

Badalona (Barcelona), November 2020